KINETIC PROCESSES AND PLASMA REMEDIATION OF TOXIC GASES

BY

ANN CATHERINE GENTILE

B.S., Carnegie-Mellon University, 1988
M.S., University of Illinois, 1992

THESIS

Submitted in partial fulfillment of the requirements
for the degree of Doctor of Philosophy in Chemical Physics
in the Graduate College of the
University of Illinois at Urbana-Champaign, 1995

Urbana, Illinois

KINETIC PROCESSES AND PLASMA REMEDIATION OF TOXIC GASES

Ann Catherine Gentile, Ph.D.
Department of Chemistry
University of Illinois at Urbana-Champaign, 1995
M. J. Kushner, Advisor

Regulations on the allowable emissions of toxic gases have resulted in increasing industrial interest in the development of energy efficient methods for remediation. In this work we computationally study the application of Dielectric Barrier Discharges to the remediation of perchloroethylene (C_2Cl_4 or PCE) and N_xO_y. We determine the kinetic processes that occur in remediation in order to devise methods for improving the energy efficiency of remediation.

PCE remediation progresses by a chain chemistry. Removal is efficient in humid gas streams since reactions of H_2O initiate the production of radicals necessary for remediation. The end products can be further treated by conventional methods and then exhausted.

Processes during N_xO_y remediation can be considered in terms of three time regimes. During the pulse, radicals are produced. NO and N_xO_y are then remediated. At long times NO is converted to NO_2 with no net change in N_xO_y. Remediation of NO is largely due to reduction by N. Removal is more efficient with higher applied voltage, faster rising pulses, more H_2O in the gas stream, and more pulses of lower energy.

Spatial dependencies can affect the energy efficiencies of remediation. Localized energy deposition in the streamer can result in high temperatures facilitating production of NO. Diffusion of NO into the streamer region and advective transport of N outward into the bulk gas increase remediation. At very high energy depositions, transport decreases the instantaneous rate of change of efficiency with energy deposition despite the increased temperature.

TABLE OF CONTENTS

1. INTRODUCTION

Oxides of nitrogen (N_XO_y) in the atmosphere have been shown to be detrimental to human health and the environment [1]. Exposure to high concentrations of nitrogen oxides can result in irritation of the respiratory tract and tissue damage. Additionally, nitrogen oxides can react with the environment to produce smog as well as other toxic substances such as ozone and peroxoacetyl nitrate (PAN). As a result, the United States Environmental Protection Agency has established stringent limits on the allowable levels of N_XO_y emissions from the combustion of fossil fuels. For example, in the emission of N_XO_y (primarily NO and NO_2) from diesel exhaust, the allowable concentration of N_XO_y in California will decrease to less than 50% of its present value in 1998. Such restrictions have resulted in increasing economic and regulatory interest in developing energy efficient processes for the removal of N_XO_y from atmospheric pressure gas streams.

Various methods of plasma based removal have been studied to efficiently remove N_XO_y from gas streams [2]. Perhaps the most extensively studied application of this type is remediation of SO_2 and N_XO_y from the effluent of coal fired electrical power plants. Electron-beam [3-6] and electrical discharge processing, such as dielectric barrier discharges (DBDs) [7] and pulsed corona reactors [8] have been researched in this regard.

In electron beam processing [6] the gas is irradiated by a beam of high-energy (100s keV) electrons. These electrons collide with the gas, resulting in ionization and, to a lesser extent, dissociation of the gas. Secondary electrons produced from these ionizations are also significant in processing the gas [9]. Reactions of the ions with the background gas are the major producer of radicals in the plasma. Remediation of toxins in the gas results primarily from ion-produced radicals reacting with the toxins.

DBDs [10] are compact, efficient plasma sources originally developed in the 1850’s for use as ozonizers. DBDs have previously been investigated for remediation of

volatile organic compounds [11, 12] from atmospheric pressure gas streams. A schematic of a DBD is shown in Fig. 1.1. DBDs are composed of two parallel (or concentric) electrodes, at least one of which is covered by a dielectric. The gap in which the plasma is produced is typically 2-5 mm wide. An alternating voltage (100s Hz to many kHz) is applied to the electrodes. When the applied voltage exceeds the breakdown value, electron avalanches occur, resulting in a "forest" of microstreamers that function as conducting channels between the plates. Charge buildup on the dielectric during the current pulse reduces the net voltage across the gap. Eventually the electric field in the plasma is unable to sustain the microstreamer, and the plasma at that location is extinguished. Typically, the microstreamers are 10s-100s of μms in diameter and 10s of ns in duration. The area density of the randomly distributed microstreamers (10s - many hundred/cm^2) is sufficiently large that on the average, the entire gas is processed. Electron impact reactions largely result in vibrational excitation and dissociation of the background gas. Remediation of toxins occurs predominantly through reactions of the toxins with the radicals produced through dissociation. Radical production and remediation chemistry will be discussed in more detail in Chapters 3-5.

Like the DBD, pulsed corona reactors [13, 14] also process the gas through the production of microstreamers. A common configuration of the reactor involves a wire-plate arrangement of the electrodes. Unlike the DBD, however, the lifetime of the streamer is determined by the duration of the voltage pulse. The pulse is typically short (100 ns) and of high voltage (10s to 100s kV). Despite the high applied voltage, the characteristic electron energy may reach small enough values for dissociative reactions as opposed to ionization with the background gas to dominate [9]. Thus, the corona discharge has the potential to produce radicals for remediation either through direct dissociation, as in the DBD, or by ion-molecule reactions, as in the electron-beam.

Experimental difficulties in measuring the energy deposition to the gas due to the stochastic nature of the current pulses lead to inexact values for the energy efficiencies obtained from such studies. However, a few general comments can be made about the amounts of removal and trends seen in remediation of N_XO_y and SO_2.

Electron-beam studies [2-6] have shown over 85% removal of NO_X from initial values of 100s of ppm. The inclusion of SO_2 in the initial gas is believed [3] to increase the amount of NO_X removal through the production of nitrogen-sulfur compounds. Theoretical studies [15] predict high energy efficiencies for electron-beam processing, as a result of efficient radical production from the ions formed, with little input energy wasted in vibrational excitation of the background gas.

Pulsed corona studies [2, 8, 14] have shown varying amounts of removal of NO_X ranging from 50-60 % [16] to over 90 % [17]. Hydrocarbon additives [14] have been considered as a way to improve energy efficiency, but appear to be effective only for low initial amounts of NO_X.

Significant amounts of removal have been achieved in DBD processing [7, 18], although some theoretical studies have suggested that DBD removal is less energy efficient than corona or electron-beam treatments [14, 15]. Additives and combined methods of processing have been considered as ways to improve energy efficiency. Ammonia addition and combining a surface discharge reactor and a DBD [19] have been demonstrated to be effective in the remediation of NO_X from mixtures not containing SO_2, with the energy efficiency increasing with increasing ammonia concentration. However, ammonia did not change the amount of removal of NO in a study where SO_2 was present in the stream [7]. UV irradiation combined with DBD processing has been seen to be less effective than DBD processing alone due to the photolysis to HNO_3 and NO_2 to NO [7].

Although large amounts of removal have been demonstrated in many of these studies using electron beam and corona processing, and high energy efficiencies predicted for these processes, efficient removal is, however, not the only requirement for effective plasma remediation of N_XO_y from mobile emission sources, such as diesel trucks. The plasma sources must be lightweight, use low voltage, require minimum maintenance and be easily scalable as the rate of N_XO_y emission varies with vehicle speed and road conditions. Also, the energy efficiencies required for these devices is determined by the available engine power. For example, consider a 100 hp diesel engine (flow rate 1 liter/s/hp) whose exhaust initially contains 500 ppm of NO. In order for the remediation process to consume less than 10% of the engine power, the maximum energy allowance is 51 eV/N_XO_y molecule removed. This efficiency must be realized without generating significant amounts of other unwanted species such as other N_XO_y or O_3.

For mobile sources, DBDs are potentially a more attractive technology for plasma remediation than either electron-beams or coronas. They are compact and can operate stably at atmospheric pressures, with high average power and with low voltages (a few - 10kV) compared to coronas or electron beams. They also have lower capital costs than electron-beam processing, which requires an accelerator, and are not subject to the associated x-ray hazards.

A DBD applied to plasma remediation of atmospheric pressure gas streams from mobile sources such as diesel exhaust will need to process large flowrates of gas in a small volume. A conceptual design of such a device is shown in Fig. 1.2. The DBD consists of concentric or “stacked” discharges. The voltage is applied to alternating electrodes. The intervening electrodes are covered by dielectric. This arrangement provides a large cross sectional area of the discharge in a compact volume. A similar apparatus has been implemented by Rosocha et. al. for the plasma remediation of volatile organic compounds [20].

Given the advantages in size, cost, and safety of the DBD over other plasma technologies, the successful application of DBDs to plasma remediation of N_xO_y from diesel exhaust will largely depend on the ability to meet the goals of obtaining high efficiency of remediation (low eV/molecule removed) and low production of undesirable compounds. In order to determine the practicality of using DBDs for such remediation we have developed computer models for DBD processing of atmospheric pressure gas streams that allow for a detailed analysis of the reaction mechanisms that occur in remediation. By understanding the processes that occur in remediation, strategies for optimization can be proposed.

We discuss the models for the DBD in Chapter 2. Although the case of primary interest is N_xO_y remediation from $N_2/O_2/H_2O/CO_2$ mixtures, we first present a brief study of perchloroethlylene (PCE) processing in $Ar/O_2/H_2O$ mixtures in Chapter 3. We determine the reaction mechanisms that occur both during PCE remediation and at long times, after the initial PCE has been removed. We use this information to determine the effects of H_2O content on remediation. Results from an in-depth analysis of N_xO_y remediation are contained in Chapters 4-6. The reaction mechanisms and end products from uniform processing of the gas are presented in Chapter 4. We use these results to determine ways to optimize operating parameters for efficient remediation of N_xO_y. The results from a non-uniform processing of the gas considering the effects of radial dependence of the streamer are presented in Chapters 5 and 6. Transport is limited to the effects due to only diffusive transport in Chapter 5. This simplification is appropriate for cases of low energy deposition. Higher energy deposition cases for which both diffusive and advective transport must be considered are discussed in Chapter 6. In these chapters, we show the spatial dependencies of remediation and how they affect the chemistry and energy efficiency of DBD processing. We end, in Chapter 7, with concluding remarks.

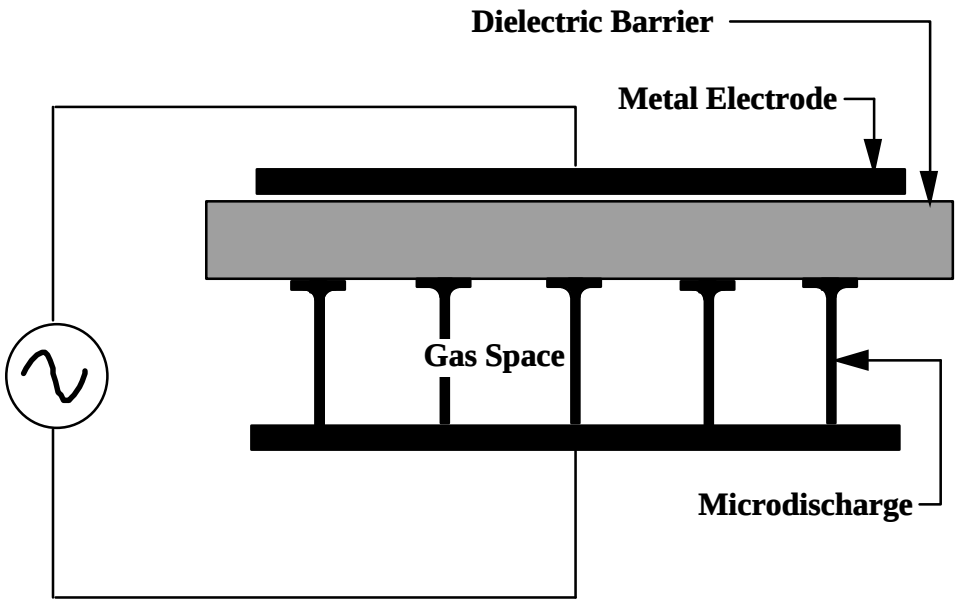

Fig 1.1. Schematic of a Dielectric Barrier Discharge. The DBD is composed of two parallel electrodes. One electrode is covered by a dielectric. When the applied voltage exceeds the breakdown voltage, electron avalanches occur, resulting in the formation of a “forest” of microstreamers.

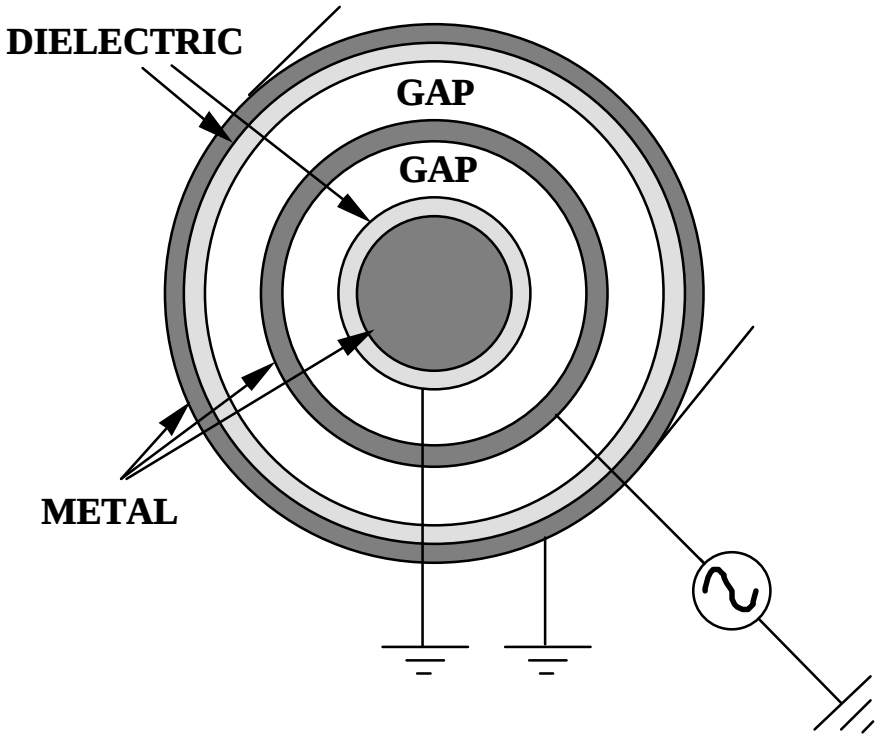

Fig 1.2. Cross section of a conceptual design for a device for the remediation of vehicle exhaust consisting of concentric Dielectric Barrier Discharges. The voltage is applied to alternating electrodes. The intervening electrodes are covered by dielectric. This design provides a compact device capable of processing large volumes of gas.

1.1 References

1. J. D. Splenger, M. Brauer, and P. Koutrakis, Environ. Sci. Technol. **24**, 946 (1990), *Industrial Toxicology*, L. T. Fairhall (Hafner Publishing Company, New York, 1969), *Hazardous and Toxic Effects of Industrial Chemicals*, M. Sittig (Noyes Data Corporation, Park Ridge, NJ, 1979), *Enivironment and Man, Vol. 6: The Chemical Environment*, J. Lenihan and W. Fletcher, Eds. (Academica Press, New York, 1977).
2. A collection of papers on various plasma technologies being investigated for plasma remediation of toxic gases appears in *Proceedings of the NATO Advanced Research Workshop on Non-Thermal Plasma Techniques for Pollution Control*, B. Penetrante and S. Schulthesis, Eds. (Springer-Verlag, Berlin, 1993).
3. D. J. Helfritch in *Proceedings of the NATO Advanced Research Workshop on Non-Thermal Plasma Techniques for Pollution Control, Part B*, B. Penetrante and S. Schulthesis, Eds. (Springer-Verlag, Berlin, 1993) pp. 33-46.
4. I. Gallinberti, Pure Appl. Chem.. **60**, 663 (1998).
5. K. Kawamura and V. H. Sui, Radiat. Phys. Chem. **24**, 117 (1984).
6. H. Matzing in *Proceedings of the NATO Advanced Research Workshop on Non-Thermal Plasma Techniques for Pollution Control, Part B*, B. Penetrante and S. Schulthesis, Eds. (Springer-Verlag, Berlin, 1993) pp. 59-64.
7. M. B. Chang, M. J. Kushner, and M. J. Rood, Environ. Sci. and Tech., **26** 777 (1992), M. B. Chang, M. J. Kushner, and M. J. Rood, Plasma Chem. and Plasma Proc. **12**, 565 (1992), M. B. Chang, *Simultaneous Removal of SO_2 and NO from Gas Streams Via Combined Plasma Photolysis*, Ph.D. Thesis, University of Illinois at Urbana-Champaign, Urbana, IL (1992).
8. S. Masuda, Pure Appl. Chem. **60**, 727 (1988).
9. Y. L. M. Creyghton, E. M. van Veldhuizen, and W. R. Rutgers in *Proceedings of the NATO Advanced Research Workshop on Non-Thermal Plasma Techniques for*

Pollution Control, Part A, B. Penetrante and S. Schulthesis, Eds. (Springer-Verlag, Berlin, 1993) pp. 205-230.

10. B. Eliasson, M, Hirth, and U. Kogelschatz, J. Phys D **20**, 1421 (1987), B. Eliasson and U. Kogelschatz, Appl. Phys. B **46**, 299 (1988).
11. L. A. Rosocha, G. K. Anderson, L. A. Bechtold, J. J. Coogan, H. G. Heck, M. Kang, W. H. McCulla, R. A. Tenant, and P. J. Wantuck in *Proceedings of the NATO Advanced Research Workshop on Non-Thermal Plasma Techniques for Pollution Control, Part B*, B. Penetrante and S. Schulthesis, Eds. (Springer-Verlag, Berlin, 1993) pp. 281-308.
12. D. Evans, L. A. Rosocha, G. K. Anderson, J. J. Coogan, and M. J. Kushner, J. Appl. Phys. **74**, 5378 (1993).
13. G. Kirkman, N. Reinhardt, B. Jiang, J. Hur, and J. Yampolski in *Proceedings of the NATO Advanced Research Workshop on Non-Thermal Plasma Techniques for Pollution Control, Part A,* B. Penetrante and S. Schulthesis, Eds. (Springer-Verlag, Berlin, 1993) pp. 379-386.
14. G. E. Vogtlin and B. M. Penetrante in *Proceedings of the NATO Advanced Research Workshop on Non-Thermal Plasma Techniques for Pollution Control, Part B*, B. Penetrante and S. Schulthesis, Eds. (Springer-Verlag, Berlin, 1993) pp. 187-197.
15. B. M. Penetrante in *Proceedings of the NATO Advanced Research Workshop on Non-Thermal Plasma Techniques for Pollution Control, Part A,* B. Penetrante and S. Schulthesis, Eds. (Springer-Verlag, Berlin, 1993) pp. 65-90.
16. G. Dinelli, L. Civitano, and M. Rea, IEEE Trans. Indst. Appl., **26**, 535 (1990).
17. R. H. Amirov, E. I. Asinovsky, I. S. Samoilov, and A. V. Sheplin and M. Izutsu in *Proceedings of the NATO Advanced Research Workshop on Non-Thermal Plasma Techniques for Pollution Control, Part B,* B. Penetrante and S. Schulthesis, Eds. (Springer-Verlag, Berlin, 1993) pp. 149-164.

18. A short summary of results of DBD application to flue gas is presented by J-S. Chang in *Proceedings of the NATO Advanced Research Workshop on Non-Thermal Plasma Techniques for Pollution Control, Part A*, B. Penetrante and S. Schulthesis, Eds. (Springer-Verlag, Berlin, 1993), pp. 1-32.
19. K. Urshima, T. Ito, and J-S. Chang, 1994 Electrostatics and Heat Transfer Societies of Japan Joint Workshop on the Applications of Discharge Plasmas (1994).
20. L. A. Rosocha, J. J. Coogan, and M. Kang, IEEE Conference on Plasma Science, Santa Fe, NM, June 6-8, 1994.

2. DESCRIPTIONS OF THE MODELS

2.1 Introduction

In order to investigate the volumetric plasma kinetics and transport phenomena in plasma remediation, we have developed both zero dimensional (0-D) and 1-D (radially dependent) models for DBD processing of gases. We describe the 0-D model that is used in Chapter 3 to investigate PCE processing and in Chapter 4 for N_xO_y processing in Section 2.2. We describe the 1-D model that is used in Chapters 5 and 6 for N_xO_y processing in Sections 2.3.1 and 2.3.2. The basic structure and implementation of the model including only the effects of diffusive transport are described in Section 2.3.1. The results from consideration of diffusion only are discussed in Chapter 5. We describe the enhancements to the 1-D model by including advection in Section 2.3.2. Results from inclusion of both diffusion and advection are discussed in Chapter 6. Remarks on the expected accuracy of the models are in Section 2.4.

2.2 Description of the 0-D Model

In the 0-D model, the gas is uniformly processed with each pulse. A schematic of the modules in the model and their inputs and outputs is shown in Fig 2.1. The simulation consists of a circuit model, a solution of Boltzmann's equation for the electron energy distribution, and a plasma chemistry model.

The circuit model provides E/N (electric field/number density) in the plasma which is used as input to the solution of Boltzmann's equation. Boltzmann's equation is solved using a two-term spherical harmonic expansion to determine the electron energy distributions from which electron impact rate coefficients are generated [1]. For the study of PCE in $Ar/O_2/H_2O$ mixtures, there are 63 electron impact processes considered. For the study of NO in $N_2/O_2/H_2O$ there are 43 electron impact processes, and in $N_2/O_2/H_2O/CO_2$ there are 56. The species used in the model are listed in Appendix A.

Electron impact reactions and sample rates for typical values of E/N are listed in Appendix B.

The plasma chemistry model uses the rate coefficients obtained from solving Boltzmann's equation along with temperature dependent heavy particle reaction rate coefficients to produce species densities as a function of time. The plasma chemistry model for PCE uses 445 temperature dependent rates and includes 90 species. The model for NO in mixtures without CO_2 uses 331 temperature dependent rates and includes 56 species. The model for NO in mixtures with CO_2 uses 404 temperature dependent rates and includes 74 species. Temperature dependent reactions and corresponding rate coefficients are listed in Appendix B. The density of species "i", symbolized by N_i, changes through reactions of two forms:

$$\text{producing } N_i: \quad \Sigma_j N_j \rightarrow N_i + \Sigma_m N_m \text{ , rate} = k_l \qquad (2.1a)$$

$$\text{consuming } N_i: N_i + \Sigma_j N_j \rightarrow \Sigma_m N_m \text{ , rate} = k_n. \qquad (2.1b)$$

In these expressions, the N_j denote the reactants and the N_m denote the products. N_i is explicitly listed as a reactant or a product as appropriate. The magnitude of the contribution to the time rate of change of N_i from a given reaction is equal to the product of the concentrations of the reactants multiplied by the rate of that reaction. This contribution is, of course, positive for those reactions producing N_i and negative for those consuming N_i so that species derivatives as a function of time are therefore determined by the following:

$$\partial N_i/\partial t = \Sigma_l (k_l \Pi_j N_j) - \Sigma_n (N_i k_n \Pi_j N_j). \qquad (2.2)$$

The time rate of change in species density are integrated using a third-order Runga Kutta scheme. This rate of change is compared to that that would be obtained by a first-order

update. If the rate of change is not linear, the timestep is chosen such that the change in density for each of the species will be less than or equal to 2.5 % of the density of that species. This change is estimated by the rate of change obtained from the previous timestep. If the rate of change is linear, the maximum allowable timestep, and thus density change, is increased. Once the species densities are updated, the conductivity is calculated and cycled back into the circuit model for updating the circuit parameters.

In actual DBDs, remediation is accomplished by a large number of discharge pulses, each of which removes a small fraction of the total gas to be remediated. We capture this behavior by running the model for a series of current pulses and afterglow periods, each lasting the inverse of the specified repetition rate. The initial species densities for a given current pulse are provided by the densities at the end of the afterglow of the previous pulse. Although the DBD operates in a filimentary mode, the 0-D model treats all quantities as volume averaged. The resistance of the plasma is then represented in the circuit model by a single resistor. The circuit model is shown in Fig. 2.2. Typical values for the circuit parameters are:

$$\text{Applied Voltage} = 9\text{-}15 \text{ kV} \tag{2.3a}$$

$$C_a = 5\text{x}10^{-8} \text{ F} \tag{2.3b}$$

$$C_b = 5\text{x}10^{-9} \text{ F} \tag{2.3c}$$

$$L_a = 5\text{x}10^{-8} \text{ H} \tag{2.3d}$$

$$L_b = 2.5\text{x}10^{-8} \text{ H} \tag{2.3e}$$

Although in actual devices the streamer is extinguished by charge build-up on the dielectric, as discussed in Section 1.2, in all cases we will be considering the streamer is shut off after a fixed amount of energy deposition determined from the circuit current and voltage. This enables comparison of cases based upon energy deposition. The capacitor representing the dielectric is therefore not included in the results discussed here and,

hence, effects of charge build-up on the dielectric are not considered. In general, however, the model is capable of including the capacitor.

Most major scaling laws are captured by the 0-D model. These will be discussed in Chapter 4. Changes in the reaction chemistry and spatial dependencies in remediation are considered in Chapters 5 and 6 using the 1-D model described below.

2.3 Description of the 1-D Model

In the 1-D model, we include the radial dependence of the streamers and the surrounding area. Species densities are now subject to change as a result of kinetics, diffusive transport, and advective transport. In order to study the effects of diffusion alone, we first consider a model in which advection is not included. This will adequately approximate the behavior of systems for low energy depositions. The basic structure of the 1-D model and the implementation of diffusive transport is discussed in Section 2.3.1. Results from this version of the model will be presented in Chapter 5. Enhancements to the model by including advective transport will be discussed in Section 2.3.2. Results from the full 1-D model, including both diffusion and advection, will be presented in Chapter 6.

2.3.1 Basics of the Model and Implementation of Diffusive Transport

In the 1-D model, the gas is processed by a matrix of radially symmetric streamers. The streamers are equally spaced and identical, so that the total discharge area is then divided up into a number of equivalent blocks with each block being processed by 1 streamer as shown in Fig. 2.3. The streamers are coincident in time at either regular or irregular intervals. They occur at the same locale each time. In actual devices, the streamers will have axial variations [2-4], are not radially identical, and will not be equally spaced. The streamers will occur at approximately the same voltage, however, and this can occur close enough in time for the streamers to begin nearly simultaneously.

Also, defects in the surface can lead to electric field enhancements that will cause the streamers to occur preferentially in the same location at each time.

For computational purposes, each streamer and its surrounding volume within a block are discretized into a set of concentric cylinders. The streamer center coincides with the cylinders' center. The mesh spacing between the centers of consecutive cylinders increases with increasing overall radius as shown in Fig. 2.4. Species densities, electron and gas temperatures, and circuit values are calculated for each individual cylindrical shell as described below. Since the streamers are identical, fluxes of all quantities across the boundaries of the blocks are zero.

The time rate of change of species densities and gas temperature due to diffusion are calculated by the following:

$$\partial N_i/\partial t = \nabla\cdot(D_i \nabla N_i) + \text{0-D kinetics (Eq. 2.3)} \qquad (2.4)$$

$$\partial(\rho c_V T)/\partial t = j\cdot E + \nabla\cdot\kappa\nabla T \qquad (2.5)$$

D_i is the diffusion constant for species "i", ρ is the mass density, c_V is the heat capacity at constant volume, j is the current density, E is the electric field, and κ is the thermal conductivity. Diffusion constants were estimated by

$$D_i = (\Sigma_j (D_{ij})^{-1})^{-1} \qquad (2.6)$$

where D_{ij} is the binary diffusion coefficient and i and j are species indices. Binary diffusion coefficients were calculated from the Lennard-Jones parameter σ for individual species using approximate formulas given in Ref. 5. Species for which σ was not available were estimated. These values are listed in Table 2.1. The value of the thermal conductivity used was that of N_2 at 400 K.

The species densities are updated in two stages. First, the plasma chemistry model calculates the species densities due to the 0-D kinetics for each cylindrical shell independently. This is done for the time interval of t to t + Δt. A number of kinetic timesteps Δt_{kin} less than Δt are used. Following integration of the local kinetics, the densities for all species at all locations are updated due to diffusive transport. This update is done in one timestep, $\Delta t_{diff} = \Delta t$. Thus, the changes in species densities due to kinetics and diffusion are done sequentially, not concurrently, with Δt_{kin} frequently much smaller than Δt_{diff}. Density updates can be implemented in this fashion without significantly altering the dynamics since significant changes in species densities due to kinetics occur on a much shorter timescale than changes in densities due to diffusion. The advantage of this technique is that the local kinetics in each region can be independently calculated. Therefore, the kinetic timesteps may vary from region to region until all regions reach the common time t + Δt.

The timestep between diffusive updates is chosen such that either the maximum change in density for any species due to diffusion will be less than or equal to 10 % of its density or the change in circuit element values will be less than or equal to 2 % of that circuit element's value, whichever is shorter.

The contribution to the species densities from the diffusive term in Eq. 2.4 for species "i" in region "k", can be written as

$$\partial N_{ik}/\partial t = A_k (N_{ik} - N_{ik-1}) (D_{ik}+D_{ik-1})/2 + B_k (N_{ik+1} - N_{ik}) (D_{ik+1}+D_{ik})/2 \qquad (2.7)$$

where A_k and B_k are geometrical constants. This can be regrouped as:

$$\partial N_{ik}/\partial t = A_{ik}' N_{ik-1} + B_{ik}' N_{ik} + C_{ik}' N_{ik+1} \qquad (2.8)$$

with A_{ik}', B_{ik}', and C_{ik}' now expressions involving the diffusion coefficients and the geometrical constants for each region. In this way, the equations for updating a species in all regions can be written in the form of a tridiagonal matrix. This matrix formulation is solved in the model using an algorithm from Ref. 7.

The temperature updates due to the thermal conductivity (Eq. 2.6), are calculated in a manner similar to the diffusion with κ mapped on to D, and T mapped on to N.

A schematic of the modules for the 1-D, diffusion-only model is shown in Fig. 2.5. It differs from the 0-D in two respects. First, in the circuit model, shown in Fig. 2.6, each individual cylindrical shell is represented as a resistor. Thus, the plasma is now represented as a set of resistors in parallel, rather than by a single resistor. As in the 0-D model, each streamer is shut off after a fixed energy deposition rather than being extinguished by the charge build-up on the dielectric. Secondly, the species densities are updated in two stages as described above. First, the plasma chemistry model updates the species densities in each region independently. Then, the diffusive update for densities in all regions is done in the transport section of the model. After the diffusive update, the conductivity is cycled back into the circuit model as before.

Typical values for the circuit parameters in Fig. 2.6 are:

$$\text{Applied Voltage} = 10 \text{ kV} \tag{2.9a}$$

$$C_a = 10^{-6} \text{ F} \tag{2.9b}$$

$$C_b = 10^{-8} \text{ F} \tag{2.9c}$$

$$L_a = 10^{-6} \text{ H} \tag{2.9d}$$

$$L_b = 5 \times 10^{-8} \text{ H} \tag{2.9e}$$

with C_a and C_b initially charged up to the applied voltage.

2.3.2 Implementation of Advective Transport

In order to examine the procceses that occur at high energy depositions, it is necessary to include a more complete description of the hydrodynamics than the merely diffusive effects discussed above. In this section, we discuss the additions to the model due to the inclusion of advective transport.

Species densities are now determined by:

$$\partial N_i/\partial t = \nabla\cdot(D_i\rho\nabla(N_i/\rho) - N_i\,\mathbf{v}) + \text{0-D kinetics (Eq. 2.3)} \qquad (2.10)$$

where ρ is the mass density and $\mathbf{v}$ is the advective velocity in the radial direction. The advective velocity is determined from solution of the Navier-Stokes equations:

$$\partial\rho/\partial t = -\nabla\cdot\rho\mathbf{v} \qquad (2.11)$$

$$\partial(\rho\mathbf{v})/\partial t = -\nabla P - \nabla\cdot(\rho\mathbf{v}\mathbf{v}) + \mu\nabla\cdot(\nabla\mathbf{v}) \qquad (2.12)$$

$$\partial(\rho c_V T)/\partial t = j\cdot E - \nabla\cdot\rho\mathbf{v}c_V T - P\nabla\cdot\mathbf{v} + \nabla\cdot\kappa\nabla T + 2\mu\,(\nabla\cdot\mathbf{v})^2 \qquad (2.13)$$

where P is the thermodynamic pressure and μ is the viscosity.

In updating the species densities, the contributions from the kinetic, advective, and diffusive terms in Eq. 2.10 are all calculated separately. First, the densities are indepedently updated in each region due the kinetics from t to t + Δt. Next, the densities obtained at the end of the kinetic updates are further updated over Δt due to advection. A single advective velocity is used for all species. Finally, these densities are updated, again over Δt, by diffusion. Thus, the advective calculation comprises a separate module, taking place between the kinetics and the diffusion. This is shown schematically in Fig. 2.7.

The kinetic updates proceed as described in Section 2.3.1. The diffusive update proceeds similarly to that described previously, with $D_i\rho$ now mapped on to D_i and N_i/ρ mapped on to N_i, thus accounting for the change in the form of the contribution from the

diffusive term between Eqs. 2.4 and 2.10. Changes in density due to advection are implemented as described below.

Equations 2.11 - 2.13 are solved iteratively. ρ, $\rho\mathbf{v}$, and $\rho c_V T$ are updated by a first-order update in time, with a fixed timestep, Δt_{adv}, of 10^{-9} s. From these equations the gas temperature and the advective velocity are determined. Using the resultant $\mathbf{v}$, the species densities are updated. ρ, $\rho\mathbf{v}$, $\rho c_V T$, T, and the species densities (through c_V) are cycled back into Eqs. 2.11-2.13 for the next update. Changes in density due to advection will be large only during and slightly after the pulse when the pressure gradients are greatest. During these times the timesteps between kinetic and diffusive updates are also small so that the changes in density due to the advection can be separated from those due to kinetics without incurring large errors. At times greater than 10^{-3} s, changes in densities and temperature due to advection are small enough so that densities and temperatures are updated by the diffusion only methods described in Section 2.3.1.

2.4 Accuracy of the Models

The major sources of inaccuracy in the models come from the simplifications in the model in the streamer behavior and inherent uncertainties in the reaction rates and electron impact cross-sections. The simplifications in the streamer behavior have been discussed in Sections 2.2 and 2.3.1. Uncertainties in the reaction rates and cross sections are of more importance since significant errors in the rates for the major processes can change which kinetic processes are important in remediation.

The accuracies of rates and completeness of reaction sets is variable [8]. For certain classes of reactions that exhibit consistent behavior, there exist some standard methods to estimate the entropies and pre-exponential factors. For other reactions, rates are obtained experimentally by measuring the loss of a certain species and attributing this loss to a given reaction or reactions. In these cases, the products may, in fact, be ill-

defined, and reactions with surfaces may confuse the issue. Conflicting processes are of particular concern in less saturated hydrocarbons which are highly reactive.

Since it is impossible to determine the extent of error in the reaction rates and reaction sets, it would be idle to place a numerical estimate on the accuracy of the values of energy efficiencies and amounts of remediation obtained. It is possible, however, to pinpoint the reactions that figure largely in the kinetics. Errors in these reactions will therefore most significantly affect the accuracy of the results.

The study of PCE remediation is more subject to incompleteness in the reaction set than the study of N_xO_y since the N_xO_y reactions have been extensively investigated in the context of combustion. Barring any significant omissions in the reaction set that would change the kinetic pathways, then, the reactions that are of the most significance in the kinetics will be shown in Chapter 3 to be

$$C_2Cl_4 + ClO \rightarrow CCl_3 + COCl_2 \quad (2.14)$$

$$CCl_3 + O \rightarrow Cl + COCl_2 \quad (2.15)$$

$$Cl + O_3 \rightarrow ClO + O_2 \quad (2.16)$$

$$C_2Cl_4 + OH \rightarrow CHCl_2COCl + Cl \quad (2.17)$$

$$OH + ClO \rightarrow HCl + O_2. \quad (2.18)$$

Eq. 2.14 is the major remediative pathway. Eqs. 2.15 and 2.16 subsequently produce ClO to make this pathway self-propagating. Eq. 2.17 initiates production of Cl, and thus ClO, starting the pathway. Eq. 2.18 consumes ClO, making it unavailable for remediation. Significant inaccuracies in these reactions would directly affect the major remediation pathway.

Under the conditions of Chapters 4 - 6, N_xO_y remediation primarily progresses through the reduction reaction

$$NO + N \rightarrow N_2 + O. \quad (2.19)$$

Thus, remediation is particularly sensitive to the production of N, which is determined by the cross sections for N_2 dissociation. Varying production of N for mixtures of low water concentration, could shift the major pathway from N_2 production to N_xO_y production, in the form of NO_2 by reaction with O. Therefore reactions producing NO_2 are also of importance, such as

$$NO + O + M \rightarrow NO_2 + M \quad (2.20)$$

$$NO + O_3 \rightarrow NO_2 + O_2. \quad (2.21)$$

The latter reaction is also significant in that it is the major reaction for NO at long times.

In Chapters 5 and 6, it will be shown that additional reactions that largely determine the energy efficiency of remediation are

$$N + N + M \rightarrow N_2 + M \quad (2.22)$$

$$N + O_2 \rightarrow NO + O. \quad (2.23)$$

Eq. 2.22 consumes N that would otherwise be used in the reduction reaction. Eq. 2.23 produces NO at high temperatures. At low NO concentrations

$$NO_2 + N \rightarrow NO + NO \quad (2.24)$$

is also important since it consumes N and produces NO.

In the study of N_xO_y remediation in the presence of CO_2 (Chapter 5) the production of CO and the various cyanides are of interest. These are determined by the CO_2 dissociation cross section and the CN and HCN producing reactions.

Given the uncertainties in the reaction rates and reaction sets, the results presented in this work are not intended to be used as precise figures but as estimates. More importantly, the model allows for a detailed analysis of the kinetics and dynamics of remediation that is difficult or impractical to achieve experimentally. This analysis can indicate general guidelines for improving efficiency and suggest chemical pathways that can possibly be controlled to decrease production of undesirable end products.

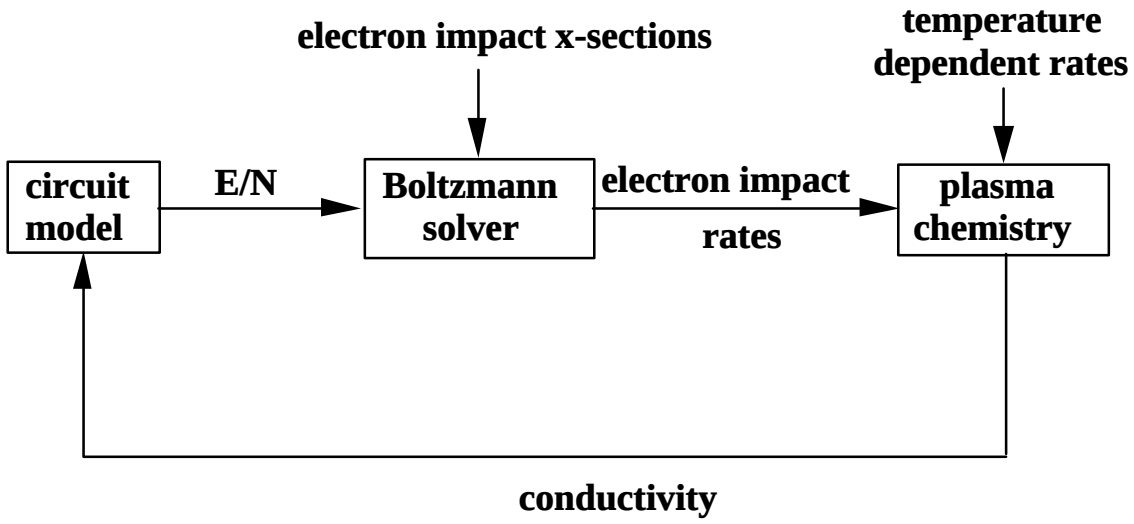

Fig. 2.1. Schematic of the modules in the 0-D model of the DBD.

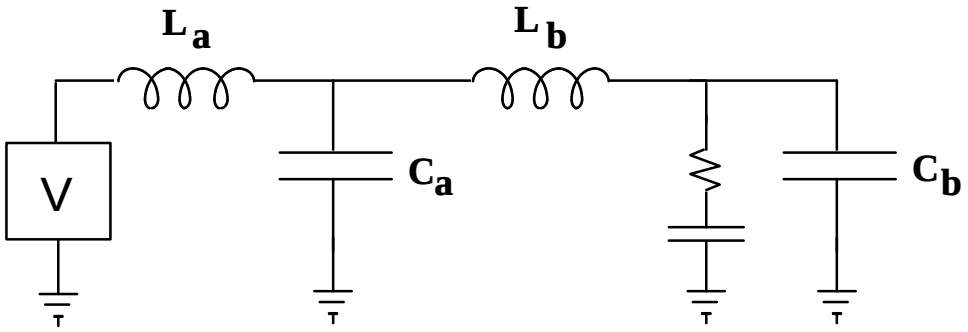

Fig. 2.2. Diagram of the circuit used in the 0-D model. The plasma is represented by the resistor. Although the model is in general capable of including the effects of the dielectric by the capacitor in series with the resistor, in all cases discussed here it is not included since the discharge is shut off after a fixed energy deposition.

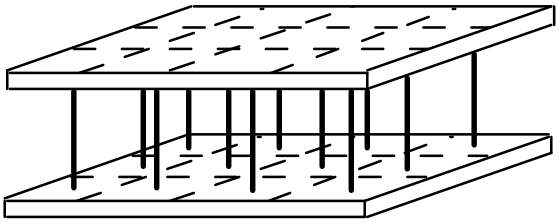

Fig. 2.3. Division of the discharge in the 0-D model. The discharge is divided up into a number of equivalent blocks, each containing one streamer.

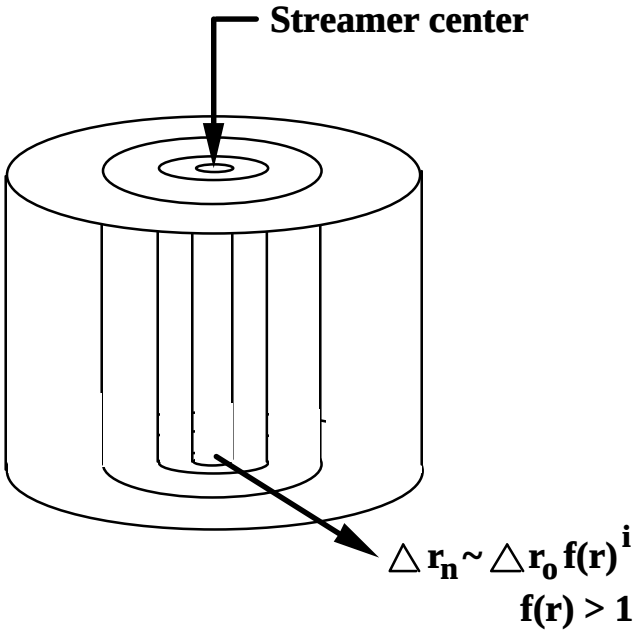

Fig. 2.4. Division of the block and streamer into computational regions. Each streamer and its surrounding area are divided up into concentric cylinders. The streamer center corresponds to the cylinder center. The difference in radii of concentric cylinders increases with increasing overall radius.

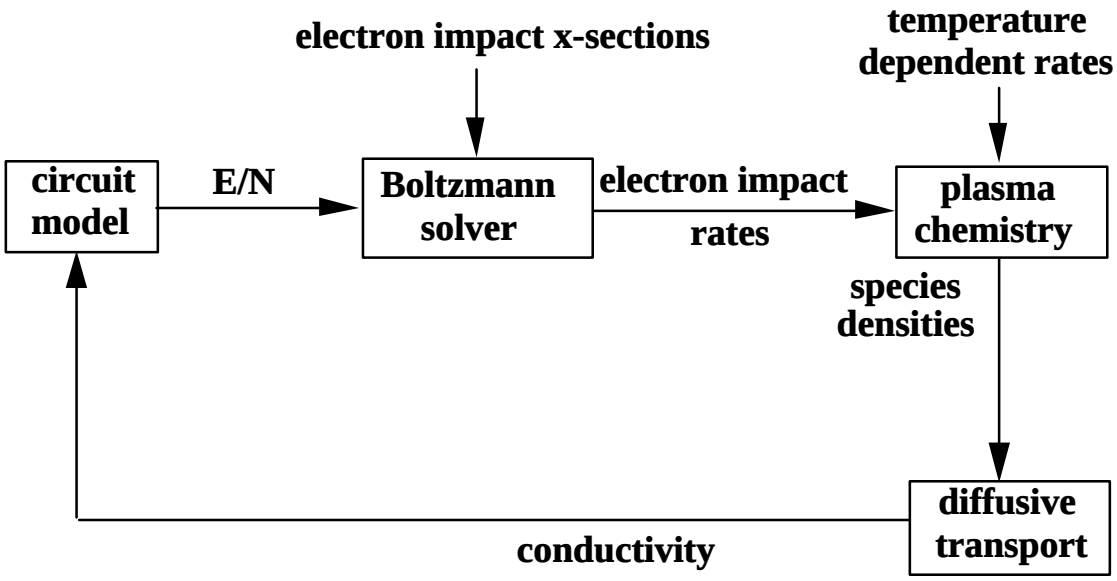

Fig. 2.5. Schematic of the modules in the 1-D, diffusion-only model of the DBD.

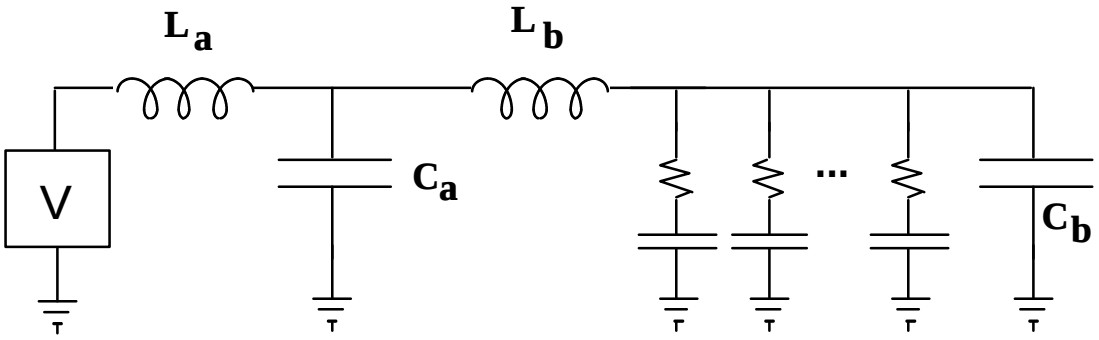

Fig. 2.6. Diagram of the circuit used in the 1-D model. Each cylindrical region in the plasma is represented by a resistor. Although the model is in general capable of including the effects of the dielectric by the regional capacitors, in all cases discussed here they are not included since the discharge is shut off after a fixed energy deposition.

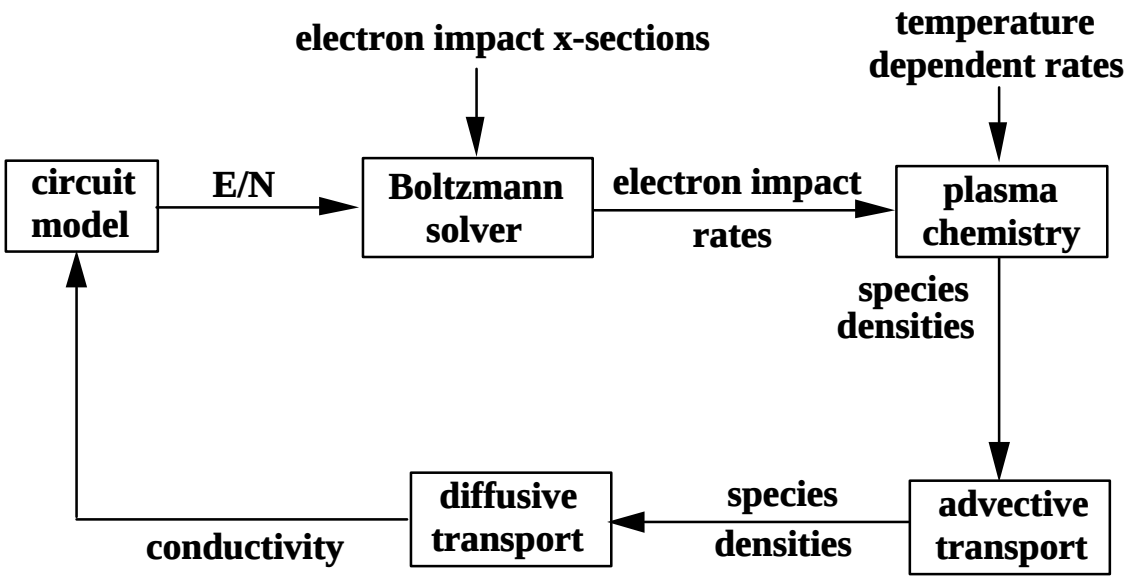

Fig. 2.7. Schematic of the modules in the full 1-D model of the DBD.

Species	σ	Ref.	Species	σ	Ref.
C	3.385	6	N^+	3.3	6[a]
C^+	3.385	6[a]	NCCN	4.5	a
CCN	4.2	a	NCO	4.1	a
C_2O	4.0	a	NH	3.31	6
CH_2O	3.9	a	NH_3	3.75	a
CN	3.856	6	NH_3^+	3.75	a
CNN	4.2	a	NH_4^+	3.75	a
CO	3.690	6	N_2	3.8	5
CO_2	3.94	6	N_2^+	3.8	6[a]
CO_2^+	3.94	6[a]	$N_2(A)$	3.8	6[a]
H	2.71	6	N_3	3.8	6[a]
H^+	2.71	a	N_3^+	3.8	a
H^-	2.71	6[a]	N_4	3.8	a
HCN	3.630	6	N_4^+	3.8	a
HCO	3.5	a	N_2O	3.83	6
HCOOH	4.5	a	N_2O_4	4.8	a
H_2	2.94	a	N_2O_5	5.2	a
H_2^+	2.94	a	NO	3.492	6
H_3O	4.1	a	NO^+	3.492	6[a]
H_3O^+	4.1	a	$NO^+ \cdot H_2O$	5.5	a
$H_3O^+ \cdot H_2O$	5.5	a	$NO^+ \cdot (H_2O)_2$	5.5	a
$H_3O+ \cdot (H_2O)_2$	5.5	a	$NO^+ \cdot (H_2O)_3$	5.5	a
H_2NO	4.1	a	$NO^+ \cdot O_2$	5.5	a
H_2NO^+	4.1	a	NO_2	3.8	a
H_2O	2.64	6	NO_2^+	3.8	a
H_2O^+	2.64	6[a]	NO_2-	3.8	a
$(H_2O)_3$	5.5	a	NO_3	4.2	a
H_2O_2	4.196	6	NO_3-	4.2	a
HNCO	4.3	a	O	3.05	6
HNO	3.7	a	O^+	3.05	6[a]
HNO_2	4.2	a	O^-	3.05	6[a]
HNO_3	4.5	a	$O(^1D)$	3.050	6[a]
HOCN	4.3	a	OH	3.147	6
$HOCO^*$	4.1	a	O_2	2.44	a
HO_2	3.9	a	O_2^+	2.44	a
HO_2NO_2	5.2	a	$O_2^+ \cdot H_2O$	5.5	a
N	3.3	6	O_2^-	2.44	a
$N(^2D)$	3.8	a	O_3	3.75	a

[a] Estimated, X[a] Estimated based on Ref. X.

Table 2.1. Lennard-Jones sigma parameter used in determining diffusion constants.

2.5 References

1. S. D. Rockwood, Phys. Rev. A. **6**, 2348 (1973).
2. B. Eliasson and U. Kogelschatz, IEEE Trans. Plasma Sci. **19**, 309 (1991).
3. P. A. Vitello, B. M. Penetrante, and J. N. Bardsley in *Proceedings of the NATO Advanced Research Workshop on Non-Thermal Plasma Techniques for Pollution Control*, B. Penetrante and S. Schulthesis, Eds. (Springer-Verlag, Berlin, 1993) pp. 249-272, P. A. Vitello, B. M. Penetrante, and J. N. Bardsley, Phys. Rev. E. **49**, 5574 (1994).
4. G. J. Pietch, D. Braun, and V. I. Gibalov in *Proceedings of the NATO Advanced Research Workshop on Non-Thermal Plasma Techniques for Pollution Control*, B. Penetrante and S. Schulthesis, Eds. (Springer-Verlag, Berlin, 1993) pp. 273-286.
5. J. O. Hirschfelder, C. F. Curtiss, and R. B. Bird, *Molecular Theory of Gases and Liquids* (John Wiley and Sons, New York, 1954).
6. R. A. Svehla, *Estimated Viscosities and Thermal Conductivities of Gases at High Temperatures*, National Aeronautics and Space Administration Technical Report R-132 (1962).
7. W. H. Press, B. P. Flannery, S. A. Teukolsky, W. T. Vetterling, *Numerical Recipes: The Art of Scientific Computing* (Cambridge University Press, Cambridge, 1986).
8. C. Melius, private communication, 1995.

3. REMEDIATION OF PCE

3.1 Introduction

In Chapter 1 it was stated that the model for DBD processing can be used to analyze reaction mechanisms and that such an analysis can be used to determine strategies for optimizing remediation. Before we give an in depth examination of the case of greatest interest, i.e., N_xO_y in diesel exhaust, we first introduce the model by briefly examining the results from the 0-D model for remediation of percholoroethylene, C_2Cl_4, more commonly known as PCE.

PCE [1-3] is primarily used as a dry-cleaning and industrial degreasing agent. Exposure to large amounts of PCE can cause a variety of symptoms ranging from nausea to coma. PCE is difficult to dispose of since it is nearly insoluble in water, nonflammable, and miscible with alcohol, ether, and other organic solvents.

As will be described in this chapter, DBD treatment can convert PCE into products that while still toxic, can, after further conventional treatments, be more easily disposed. Knowledge of the reaction mechanisms of PCE can be used to determine operating parameters that optimize remediation of PCE and production of such end products. The model has been used to elucidate the chemistry of PCE remediation to determine the effects of H_2O content on the chemistry. In Section 3.2 we present the reaction mechanisms and products during and after remediation of PCE with particular attention to the effects of H_2O in the gas stream. Concluding remarks are in Section 3.3.

3.2 Reaction Mechanisms in Remediation of PCE

Using the 0-D model described in Section 2.2, we studied processes in the processing of PCE. For purposes of discussion, we consider two timescales in the processing of PCE: remediation and post-remediation. Remediation refers to times during

which chemical reactions with PCE reduce its density from its initial amount to 1 ppm. Post-remediation refers to times after the initial concentration of PCE has been reduced to 1 ppm. Chemical reactions during this time further process the products from PCE remediation. The initial gas mixture was $Ar/O_2/H_2O$ = 80-x/20/x (x = 0 -1) at 300 K and 1 atm with an initial PCE concentration of 500 ppm. Under these conditions 1 ppm is equivalent to 2.5 x 10^{13} cm^{-3}. The DBD was pulsed at a repetition rate of 10 Hz with a volume averaged energy deposition of 5 mJ/cm^3/pulse. The applied E/N had a maximum value of 260 Td.

For a mixture containing 1% H_2O, removal of PCE to amounts less than 1 ppm was achieved with a total energy deposition of 45 mJ/cm^3 as shown in Fig. 3.1. Significant removal of PCE occurs during and immediately after the short current pulse (10 ns in length and not resolved in the figure) as a result of direct reactions of PCE with the O and OH radicals produced by electron impact dissociation of O_2 and H_2O. Remediation continues, however, during the majority of the interpulse period (0.1 s) due to chain reaction chemistry, discussed below.

The reaction scheme for the dominant remediative and post-remediative processes of PCE is shown in Fig. 3.2. Products of remediation are indicated by bold lettering, products of post-remediation are boxed, and products for both time periods are both in bold and boxed. Reactions of physically smaller species (such as CO + ClO —> CO_2 + Cl) are not indicated on the diagram, but are discussed in the text.

Remediation of PCE proceeds largely through its reactions with OH, O, and ClO. These species react with PCE as follows :

$$C_2Cl_4 + O \rightarrow COCl_2 + CCl_2 \quad (3.1)$$

$$C_2Cl_4 + OH \rightarrow CHCl_2 + COCl_2 \quad (3.2)$$

$$\rightarrow HOCl + C_2Cl_3 \quad (3.3)$$

$$\rightarrow CHCl_2COCl + Cl \quad (3.4)$$

$$C_2Cl_4 + ClO \rightarrow CCl_3 + COCl_2 \quad (3.5)$$

$$\rightarrow CCl_3COCl + Cl \quad (3.6)$$

O and OH are easily produced by electron impact reactions with O_2 and H_2O, respectively . Details of these processes are considered in Section 4.3 where they are more germane to the discussion. ClO is produced on a later timescale by the subsequent plasma chemistry. Thus, O and OH are important not only in that they remediate PCE but also in that they initiate production of ClO.

Eqs. 3.1-3.4 lead to ClO production through reactions of their products either producing ClO directly or producing Cl. Cl then easily forms ClO by

$$Cl + O_3 \rightarrow ClO + O_2. \quad (3.7)$$

This is the primary route to ClO production. O_3 is formed in significant quantities by the discharge by

$$O + O_2 + M \rightarrow O_3 + M. \quad (3.8)$$

Other reactions forming ClO or Cl, and thus subsequently ClO, are

$$COCl_2 + O(^1D) \rightarrow ClO + COCl \quad (3.9)$$

$$CCl_2 + O_2 \rightarrow ClO + COCl \quad (3.10)$$

$$COCl + O_2 \rightarrow ClO + CO_2 \quad (3.11)$$

$$Cl_2 + O \rightarrow ClO + Cl \quad (3.12)$$

$$CHCl_2 + O \rightarrow Cl + CHOCl \quad (3.13)$$

$$COCl + O \rightarrow Cl + CO_2 \quad (3.14)$$

The excited state $O(^1D)$ is produced by electron impact dissociative excitation of O2, and so reactions with it are only important during the short current pulse. Small amounts of ClO are also produced by $CHCl_2COCl$ and C_2Cl_3.

Once enough ClO is produced by OH and O remediation and subsequent reactions, remediation by ClO (Eqs. 3.5 and 3.6) can take place. Eq. 3.5 then becomes the major pathway for remediation since it regenerates ClO from production of CCl_3 by

$$CCl_3 + O \rightarrow Cl + COCl_2 \qquad (3.15)$$

followed by Eq. 3.7. Thus remediation by ClO becomes self-propagating, unlike remediation by O and OH.

Although the major role of Cl is the production of ClO, it does react with PCE by

$$C_2Cl_4 + Cl \rightarrow C_2Cl_5. \qquad (3.16)$$

It is not a major contributor to the remediation of PCE since C_2Cl_5 quickly back reacts to regenerate PCE by

$$C_2Cl_5 \rightarrow C_2Cl_4 + Cl \qquad (3.17)$$

$$C_2Cl_5 + Cl \rightarrow C_2Cl_4 + Cl_2 \qquad (3.18)$$

The rates for these reactions are sufficiently fast that C_2Cl_5 does not accumulate in the discharge. However, the flux of reactants through these reactions is large enough so that significant densities of Cl_2 are produced during remediation.

The production of ClO in these reactions constitutes a chain chemistry. The initial reactions of PCE with O and OH generate ClO, either directly or through Cl. ClO subsequently reacts with PCE, forming ClO in the process to continue the chain. A potential chain breaking process is the reaction of ClO with OH

$$OH + ClO \rightarrow HCl + O_2 \qquad (3.19)$$

which prevents ClO from assisting in further remediation. However, the effectiveness of OH in remediating PCE and in leading to the production of ClO, far outweighs any loss of efficiency due to the ClO lost by this reaction. Therefore, remediation of PCE is greatly increased by the presence of water, and is slow without it (Fig. 3.1). Although remediation is more efficient with larger amounts of H_2O, this effect is small for the values shown. Only a small amount of OH is necessary to initiate the production of ClO. Additional production of ClO by the chain is quite efficient, especially as the major remediation reaction, Eq. 3.5, produces ClO and is thus self-propagating. In fact, for later pulses, remediation continues throughout the duration of the interpulse period (Fig. 3.1) due to the fact that ClO is still existent by the onset of the next pulse. This shown in Fig. 3.3 for pulse 9 of the case of 1% H_2O. Thus, enough ClO is produced by the chain that any additional production of OH, either by additional energy deposition or increasing H_2O percentage, is superfluous.

The enhancement of PCE remediation with the inclusion of water is in direct contrast to DBD remediation of TCE [4, 5], for which removal in dry mixtures is more efficient than in humid mixtures. In that system, ClO is a major reactant with TCE, but reactions of OH with TCE are slow. Water addition thus produces no significant benefits and, through the consumption of ClO, reduces the total removal efficiency.

The dominant species formed by the remediation of PCE are $CHCl_2COCl$, CHOCl, $COCl_2$, Cl_2, HCl, HOCl, CO, and CO_2. At the end of PCE remediation approximately 90% of the Cl atoms of PCE are in $COCl_2$, with the remainder primarily in CHOCl and Cl_2. These species and PCE during remediation and post-remediation (which will be discussed below) are shown in Fig. 3.4. The products can be traced to one or more of the initial remediation reactions of PCE with O, OH, or ClO (Eqs. 3.1-3.6) as indicted in Table 3.1. Physically smaller products, such as HCl and CO_2, are also produced by smaller species reactions such as Eq. 3.19 as well as

$$CO + OH \rightarrow CO_2 + H \quad (3.20)$$

$$CO + ClO \rightarrow CO_2 + Cl. \quad (3.21)$$

O_3 is also formed in significant quantities by the discharge process (Eq. 3.8), rather than by remediation.

In a closed cycle system, the endproducts, while still toxic can be further treated by more conventional methods and then disposed. Those endproducts containing -COCl, can be further treated by some combination of mixing with soda and slaked lime as well as mixing with a large amount of water [1]. Cl_2 can be combined with a concentrated solution of a reducing agent and neutralized with soda ash or dilute HCl [1].

The final products change somewhat if the device is continued to be run after PCE is remediated. Under these conditions, $CHCl_2COCl$ and CHOCl are consumed while the density of $COCl_2$ remains relatively constant. Densities of Cl_2, HCl, HOCl, CO_2, and CO increase and ClO now accumulates. PCE and the products of remediation that remain relatively constant during post-remediation are shown in Fig. 3.4a. Products of remediation only or post-remediation only are shown in Fig. 3.4b. Products of both remediation and post-remediation are shown in Fig. 3.4c.

$CHCl_2COCl$ is primarily converted into $COCl_2$ by channels indicted in Fig. 3.2. Since the reactions which consume $CHCl_2COCl$ are slow, $CHCl_2COCl$ accumulates during remediation and only decreases on the longer, post-remediative, time period. CHOCl generally decreases in density due to its continuing consumption by channels indicated in Fig. 3.2 while its production has been eliminated by the removal of PCE. It largely produces HCl, HOCl, ClO, CO_2 and CO.

Once PCE, which is a major reactant for ClO, is remediated, the densities of ClO and Cl_2 increase. ClO continues to be produced by the previously described channels. It is now primarily destroyed by reactions with O atoms by

$$ClO + O \rightarrow Cl + O_2 \qquad (3.22)$$

accounting for the sawtooth appearance in Fig. 3.4. Cl_2 increases as a result of reactions with the products from the processing of $CHCl_2COCl$ and $COCl_2$, as indicted in Fig. 3.2, as well as reaction of the accumulated ClO with itself

$$ClO + ClO \rightarrow Cl_2 + O_2. \qquad (3.23)$$

The increase in the density of ClO also partially accounts for increases in HCl and CO_2. The remainder of the increases in these species, HOCl, and CO are due to the continuance of their production by the pathways indicted in Fig. 3.2.

From a disposal standpoint there is no greater desirability of the products obtained post-remediation as opposed to those generated during remediation. Additionally, the increase in non-COCl toxic endproducts such as CO that are not treatable by the previously mentioned methods makes the post-DBD treatment more complex and possibly more costly.

This, combined with the increased energy input required to run the discharge for a longer time, seems to indicate that post-PCE remediation processing may not be advantageous.

3.3 Concluding Remarks

Dielectric Barrier Discharges can be effective in the removal of PCE from $Ar/O_2/H_2O$ mixtures. Remediation of PCE by DBD processing results in products that can be further treated and removed by channels not available to PCE itself. Removal is achieved through reactions of PCE with OH, O, and ClO. Remediation reactions with OH are primarily responsible for the initiation of production of ClO. Remediation by ClO is self propagating and becomes the dominant pathway. The large amount of O_3 produced by the discharge aids in the production of ClO by reaction with Cl. The inefficiency of initiating ClO production in the absence of the OH remediation reactions leads to negligible remediation in dry mixtures. Once PCE reaches significantly small levels after many pulses, enough OH, O, and ClO are produced by the pulse and subsequent remediation to produce substantial or complete remediation without any further energy input. Dominant products of remediation only are $CHCl_2COCl$ and CHOCl; the product of post-remediation only is ClO; products of both remediation and post remediation are $COCl_2$, Cl_2, HCl, HOCl, CO, and CO_2. O_3 is also a product of the DBD operation. From a disposal standpoint, running the discharge post-PCE remediation is not advantageous.

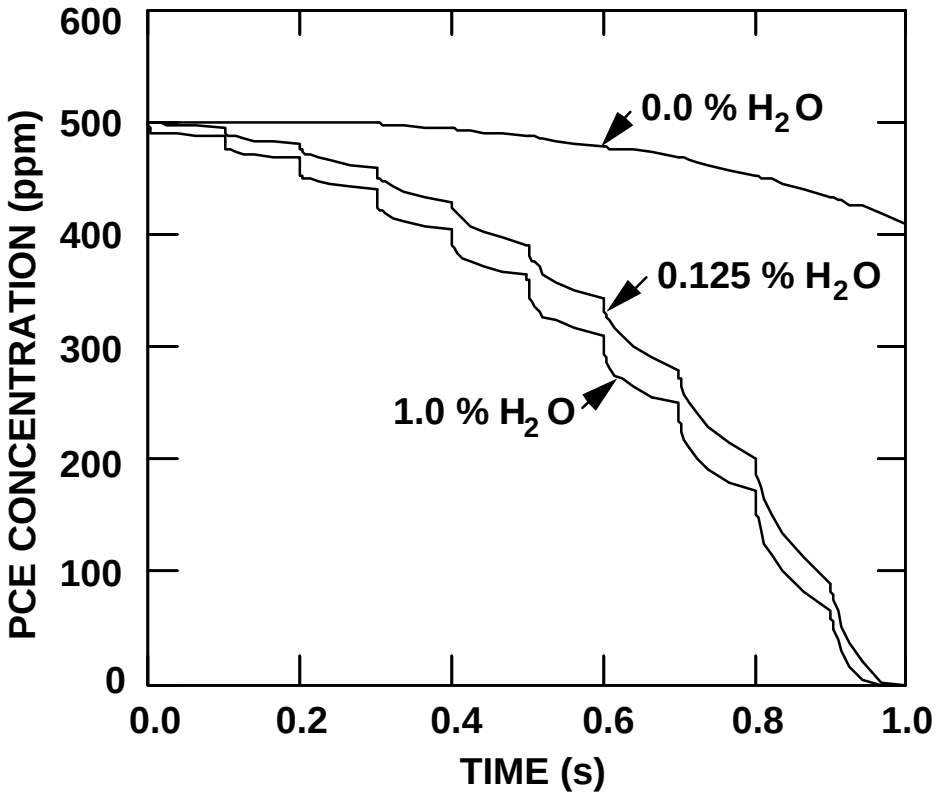

Fig. 3.1. Removal of PCE for initial gas mixtures of $Ar/O_2/H_2O$ = 80-X/20/X with 500 ppm PCE at 1 atm and 300 K. Remediation is slow without H_2O and improves slightly with increasing H_2O over the range shown. Remediation reactions with OH initiate production of ClO. Remediation of PCE by ClO is self-propagating and progresses rapidly. The behavior of later pulses indicates that once PCE reaches sufficiently small levels enough OH, O, and ClO are produced by the pulse and subsequent reactions to produce substantial or complete remediation without any further energy input required.

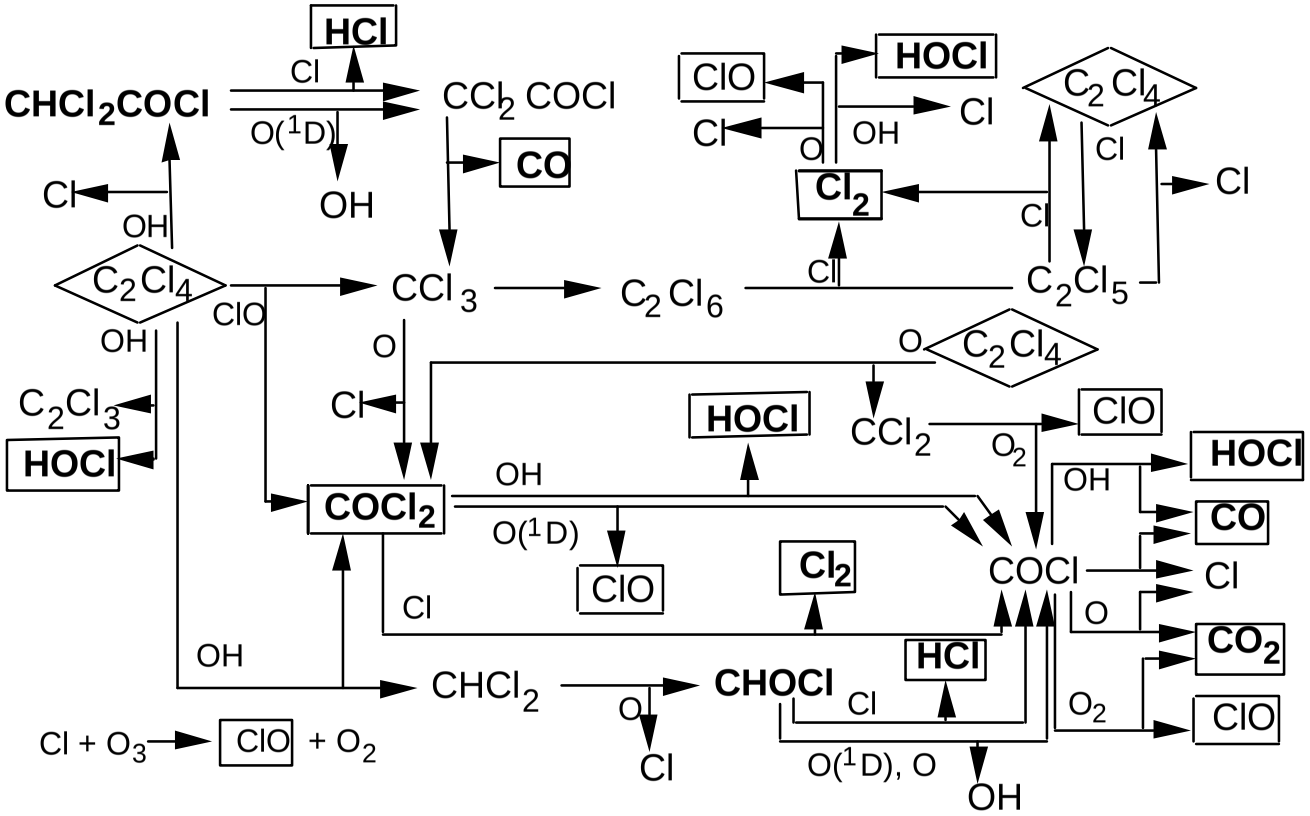

Fig. 3.2. Dominant reaction pathways for the plasma remediation of PCE. The initial toxin, PCE, is indicated by a diamond. For clarity, this initial point has been separated into several locations in the figure. The dominant products of remediation are in bold. The dominant products of post-remediation are boxed. Dominant products of both periods are both in bold and boxed.

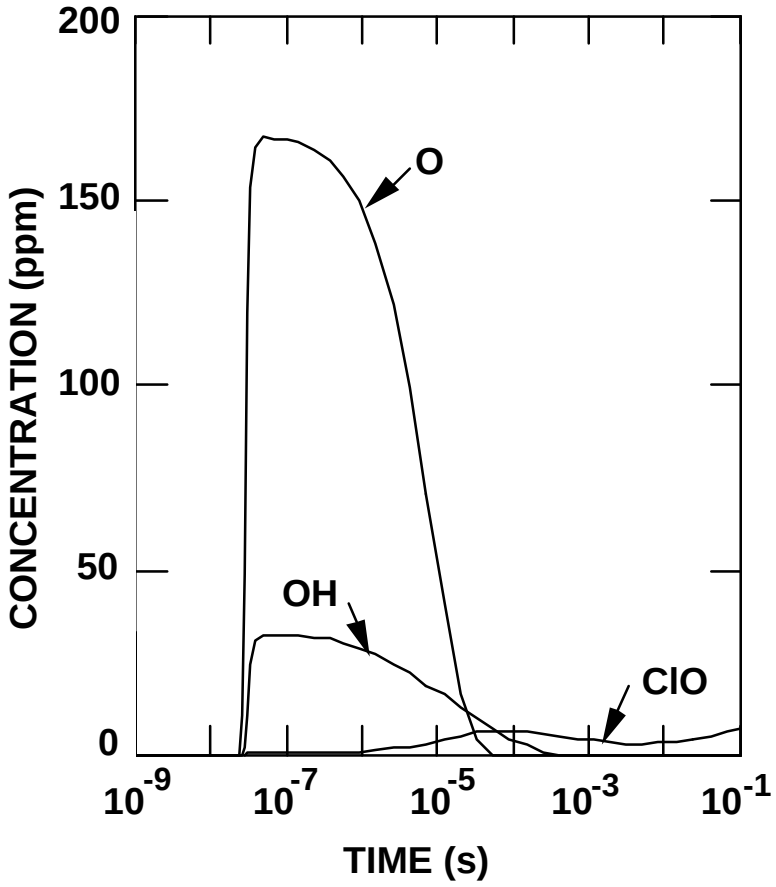

Fig. 3.3. Radicals responsible for remediation of PCE for pulse 9 of the case of 1% H_2O in Fig. 3.1. At long times, remediation occurs primarily through reaction of PCE with ClO since OH and O are depleted at these times. For late pulses, ClO is not depleted by the onset of the next pulse, and thus remediation would continue to occur without subsequent energy deposition .

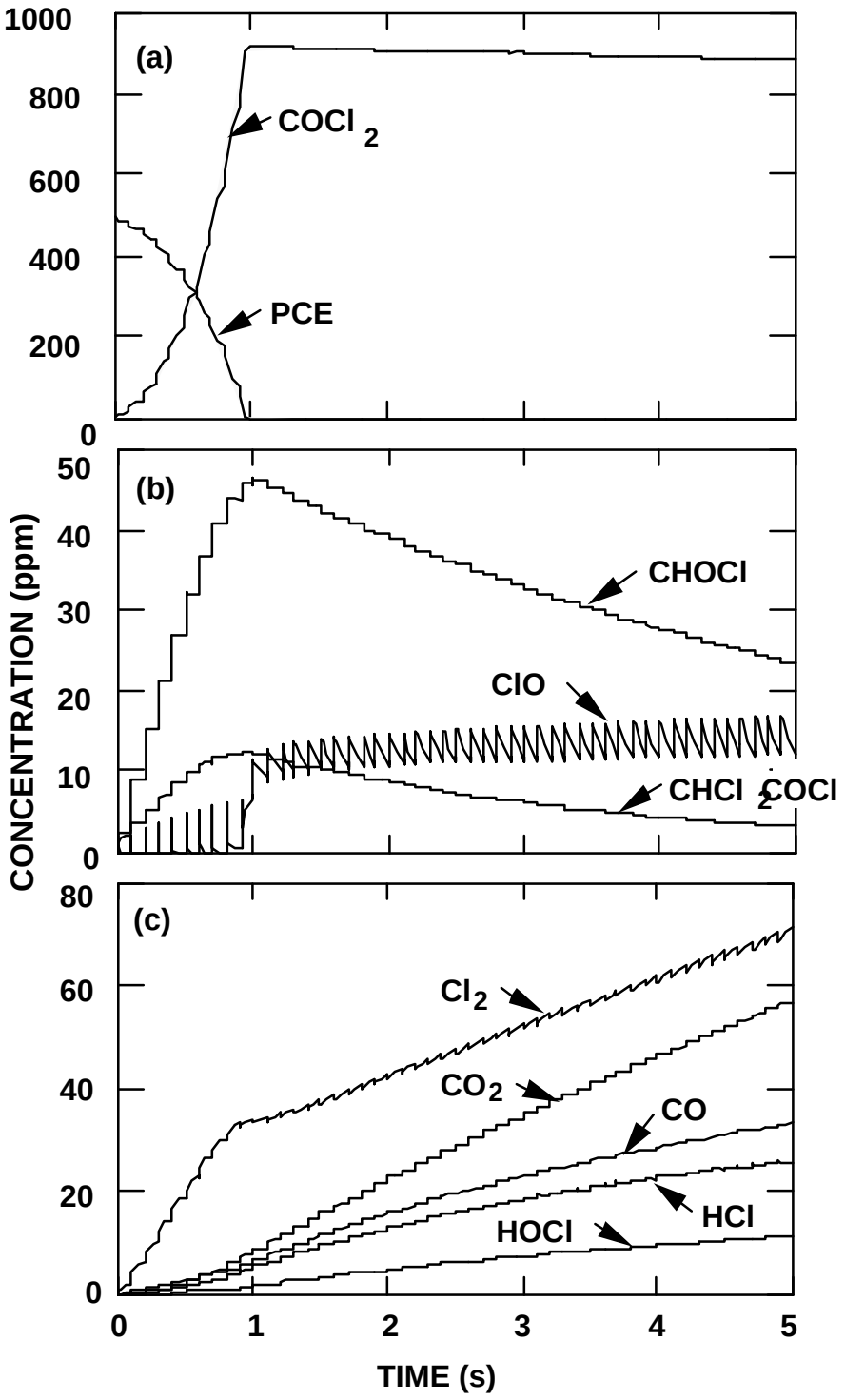

Fig. 3.4. Dominant products in the remediation and post-remediation of PCE for the case of 1% H_2O. a) PCE and the products of remediation that remain relatively constant during post-remediation; b) products of remediation only (CHOCl and $CHCl_2COCl$) or post-remediation only (ClO); c) products of both remediation and post-remediation.

	Eq. 3.1	Eq. 3.2	Eq. 3.3	Eq 3.4	Eq. 3.5	Eq. 3.18
$CHCl_2COCl$				X		
CHOCl		X				
Cl_2						X
$COCl_2$	X	X			X	
HCl				X		
HOCl	X	X	X	X	X	
CO	X	X		X	X	
CO_2	X	X			X	

Table 3.1. End products from the remediation of PCE. Equation numbers from the text of reactions directly remediating PCE are listed across the top of the table. Major products are listed in the left hand column. Products produced either directly or subsequently from a given reaction are X'ed off under the appropriate reaction heading. The pathways leading to the production of these products from these initial reactions are shown explictily in Fig. 3.2.

3.4 References

1. *Industrial Toxicology*, L. T. Fairhall (Hafner Publishing Company, New York, 1969).
2. *The Merck Index, Eleventh Edition*, S. Budavari, Ed. (Merck & Co., Inc., Rahway, New Jersey, 1989).
3. *Toxic and Hazardous Industrial Chemicals Safety Manual for Handling and Disposal with Toxicity and Hazard Data* (The International Technical Information Institute, Japan, 1978).
4. D. Evans, L. A. Rosocha, G. K. Anderson, J. J. Coogan, and M. J. Kushner, J. Appl. Phys. 74, 5378 (1993).
5. L. A. Rosocha, J. J. Coogan, and M. Kang, *Proceedings of the 1994 IEEE International Conference on Plasma Science* (IEEE, New Jersey, 1994).

4. REMEDIATION OF N_XO_Y : VOLUME AVERAGED KINETICS

4.1 Introduction

In this chapter and the following two, we present the results of an in depth study of the remediation of N_xO_y by DBDs. This chapter contains results obtained from the 0-D model, while Chapters 5 and 6 involve results from the 1-D. As was shown in Chapter 3 for PCE, knowledge of the processes that occur in remediation can be used to determine ways to optimize remediation. Thus, in this chapter, we begin with a detailed study of the reaction mechanisms that occur in remediation. Section 4.2 is an overview of remediation, discussing the general reaction mechanisms. Section 4.3 is a detailed study of the processes that occur on various time scales during and after a single current pulse. The information gained from the details of the reaction mechanisms is used in Section 4.4 to develop ways to optimize remediation. Finally, concluding remarks are in Section 4.5.

4.2 Reaction Mechanisms in Remediation of N_xO_y

A schematic of the dominant reaction pathways for plasma remediation of N_xO_y is shown in Fig. 4.1. Reaction rate coefficients for these and other processes are listed in Appendix A. The initial toxin, NO, is highlighted by a diamond in Fig. 4.1. The six major end products, N_2, NO_2, N_2O, N_2O_5, HNO_2, and HNO_3, are boxed. Plasma remediation for operating conditions typical for DBDs progresses through radical assisted reactions and these radicals are listed next to the corresponding reaction arrow. The are two main pathways for the remediation of NO :

Reduction :	$NO + N \rightarrow N_2 + O$	(4.1a)
Oxidation :	$NO + O \rightarrow NO_2$	(4.1b)
	$NO_2 + OH \rightarrow HNO_3$	(4.1c)

The preferred pathway depends on the desired end product. For stationary sources, the production of the acidic waste product may be acceptable since the acid can be readily collected and disposed of. For mobile sources, reduction is preferred over oxidation since the end products are N_2 and O. The former can be exhausted to the atmosphere and the latter generates radicals, primarily ozone, which can be beneficial to the remediation process under certain circumstances (see Section 4.3). The pathway which dominates is largely determined by the gas mixture and power deposition. Since, however, water is a product of the combustion process, it is difficult to completely eliminate the oxidation channel without drying the exhaust stream. This would be an energetically expensive procedure and impractical for mobile sources.

The predicted removal of NO in a DBD and the generation of the major end products are shown in Fig 4.2 for an initial gas mixture of $N_2/O_2/H_2O$ = 85/5/10 at 400 K and 1 atm, with an initial concentration of NO of 500 ppm (parts-per-million). At the reference temperature and pressure, 1 ppm is equivalent to 1.83×10^{13} cm^{-3}. The DBD is pulsed at a repetition rate of 10 Hz with an energy deposition of 3 mJ/cm^3/pulse. The applied E/N (electric field/number density) has a peak value of 300 Td (1 Td = 10^{-17} V-cm^2). The duration of the pulse, 10 ns, cannot be resolved in the figure. The densities of NO, the incremental change in the density of N_2 ($\Delta N_2 = N_2(t) - N_2(0)$), and the density of restricted N_xO_y products (NO_2, N_2O_5, N_2O) are shown in Fig. 4.2a. ΔN_2 is an approximate measure of the amount of NO which is removed by the reduction channel since N_2 is primarily a product of that process. The densities of NO and its oxidation products HNO_2 and HNO_3 are shown in Fig. 4.2b. The majority of the removal of NO occurs rapidly compared to the time between pulses. The densities of the reaction products generally incrementally increase with each pulse as the products accumulate in the gas stream. An exception is the reaction product NO_2 which itself reacts with plasma

generated radicals and is ultimately remediated. For these conditions, the total removal of NO (defined as achieving a density of < 1ppm) is obtained with a total energy deposition of 105 mJ/cm3, or approximately 72 eV/molecule. NO is primarily converted to N_2 through the reduction channel (indicated by the increase in ΔN_2). Approximately 10% is converted to HNO_3 through the oxidation channel. Only a small amount of the restricted oxides of nitrogen are formed.

The radicals which assist in the remediation are primarily N, OH, O, H, HO_2, NO_3, and O_3. The primary radicals N, OH, and O are created by electron impact reactions during the current pulse and are rapidly consumed by reactions in the remediation pathway. They are regenerated during the next current pulse. This general behavior is shown in Fig. 4.3 for N and OH. There is some small pulse-to-pulse variation in the peak density of these species, but in general constant amounts of N and OH are produced by each current pulse. HO_2, NO_3, and O_3 are secondary radicals in that they are not formed by direct electron impact events, but rather by reactions involving the primary radicals. They are produced and consumed on longer time scales than the primary radicals and their densities are more sensitive to plasma conditions. Detailed accounts of the behaviors of both types of radicals as well as NO and its major products will be given in the next section.

4.3 Details of the Remediation Process

We now describe the reaction chemistry that occurs during remediation in more detail by considering the chemistry that occurs during different time periods during and after the current pulse. An individual current pulse and its subsequent intrapulse period can be characterized by three time scales, each making a different contribution to the total remediation. The three periods are: the current pulse itself, having a duration of 10 ns; the Post Pulse Remediative Period (PPRP), spanning from 10 ns to 100s of μs; and the Interpulse Period (IP), spanning from 100s of μs to the start of the next current pulse,

typically 100s of ms. The primary processes during the current pulse produce radicals by electron impact collisions. During the PPRP, radical assisted remediation produces a net decrease in the concentration of N_xO_y molecules. During the IP, the total N_xO_y inventory does not significantly change, however the apportioning between the various N_xO_y products does change.

During the current pulse, the primary radicals N, OH, O, and H are produced by electron impact dissociation of the feedstock gases. N and OH, whose densities are shown in Fig 4.4, have major direct roles in the remediation process through the reduction and oxidation channels. They are primarily produced by the reactions

$$e + N_2 \rightarrow N + N + e \quad (4.2)$$

$$e + H_2O \rightarrow H + OH + e \quad (4.3)$$

The densities of N and OH increase during the current pulse as a result of these reactions. Following the current pulse they monotonically decrease owing to their removal by remediation reactions and the lack of significant sources of N and OH in the absence of electron impact processes. O atoms created during the current pulse are dominantly produced in their ground state, $O(^4S)$, and in the first excited state, $O(^1D)$,

$$e + O_2 \rightarrow O + O \quad (4.4a)$$

$$\rightarrow O + O(^1D) \quad (4.4b)$$

Reactions of $O(^1D)$ with water produce additional OH radicals

$$O(^1D) + H_2O \rightarrow OH + OH \quad (4.5)$$

however the singlet state is not otherwise particularly important to the remediation process. Significant amounts of additional O(^{4}S) are also produced during the PPRP by the reduction reaction for NO (Eq. 4.1a) and to a lesser degree by reduction of NO_2

$$NO_2 + N \rightarrow N_2O + O \quad (4.6)$$

These secondary sources of O atoms after the current pulse exceed those by electron impact collision. This results in an increase in the density of O atoms early during the PPRP, as shown in Fig. 4.4b. Ground state O directly assists in the remediation process by oxidizing NO to NO_2, which is a necessary step in the oxidation channel. O, however, more importantly produces secondary radicals, O_3 in particular, which further assist in the remediation process. H atoms, produced by electron impact processes (Eq. 4.3), also generate secondary radicals (e.g., HO_2), but have no important direct contribution to remediation.

Secondary radicals HO_2, NO_3, and O_3, whose densities are shown in Fig. 4.5, also assist in the remediation. These radicals are formed by reactions involving the primary radicals H and O, and are necessarily produced on a later time scale than the current pulse (10's of ns). The production of HO_2 and NO_3 peak at approximately 10 μs, while that of O_3 peaks at approximately 200 μs. The more significant of the reactions which produce secondary radicals are

$$H + O_2 + M \rightarrow HO_2 + M \quad (4.7)$$

$$O + OH + M \rightarrow HO_2 + M \quad (4.8)$$

$$NO_2 + O + M \rightarrow NO_3 + M \quad (4.9)$$

$$NO_2 + O_3 \rightarrow NO_3 + O2 \quad (4.10)$$

$$O + O_2 + N_2 \rightarrow O_3 + N_2 \quad (4.11)$$

HO_2 is an intermediate in the oxidation of NO to NO_2. NO_3 also assists in the oxidation of NO, but more importantly oxidizes NO_2 to make the unwanted end product N_2O_5,

$$NO_2 + NO_3 \rightarrow N_2O_5 \qquad (4.12)$$

Note that the production of NO_3 will vary with the number of the current pulse since the concentration of NO_2, its precursor reactant, depends of the number of the current pulse as shown in Fig 4.2a.

Since the radicals are responsible for the remediation of N_xO_y, their lifetimes following the current pulse will determine the duration of such remediation. The primary radicals N and OH are largely responsible for total N_xO_y remediation (as opposed to reapportioning the various nitrogen oxides) and hence set its duration. The lifetime of O radicals is less tightly tied to the duration of remediation since the major role of O atoms is to produce secondary radicals. The lifetimes of the radicals are determined primarily by radical-radical reassociation reactions, with the more important of these being

$$N + N + M \rightarrow N_2 + M \qquad (4.13)$$

$$N + O + M \rightarrow NO + M \qquad (4.14)$$

$$H + OH + M \rightarrow H_2O + M \qquad (4.15)$$

$$O + OH \rightarrow O_2 + H. \qquad (4.16)$$

Direct remediation reactions and reactions which produce secondary radicals set the lifetime to a lesser extent, with the exception of

$$N + O_2 \rightarrow NO + O \qquad (4.17)$$

which is important when the density of NO is small and at high temperatures as will be discussed in Section 5.4. As opposed to total N_xO_y remediation, the long time scale for solely NO remediation is largely determined by the depletion time of the secondary radical O_3, and will be discussed further later in this section.

The details of the reaction chemistry and species densities during the PPRP and IP depend on the number of previous current pulses since the initial conditions for each pulse are determined by its previous history and the accumulation of products. For this reason, we will examine two pulses in detail: one early during the remediation of NO while the concentration of NO_2 is increasing (pulse 4 of Fig. 4.2) and one late during the remediation (pulse 17 of Fig. 4.2) when the density of NO_2 is decreasing. The concentrations N_xO_y, NO, NO_2, and ΔN_2 for the early and late pulses are shown in Figs. 4.6 and 4.7, respectively. (In these and the following figures, densities labeled N_xO_y are the sum of the densities of all nitrogen oxides.)

In either case, remediation of N_xO_y does not begin until after the end of the current pulse, once a significant density of radicals has been produced. Then the density of N_xO_y decreases during the PPRP due to conversion of NO and NO_2 to the following products :

$$NO \rightarrow N_2, HNO_2, NO_2 \qquad (4.18a)$$

$$NO_2 \rightarrow HNO_3, N_2O, N_2O_5 \qquad (4.18b)$$

These processes are indicated by the bold solid arrows in Fig 4.1. During the PPRP, then, the individual products N_2, N_2O, N_2O_5, HNO_3, and HNO_2 are generated by these processes and reach saturation values. Their production ends when the radicals responsible for their generation are depleted as marked in Figs. 4.6 and 4.7 (ΔN_2) and 4.8 (other products in the early pulse case). Total N_xO_y removal ends when the radicals

responsible for net removal and production of N_xO_y species are depleted. Processes which change the net amount of N_xO_y are primarily reduction (Eq. 4.1a) and oxidation (Eq. 4.1b). Since reduction dominates over oxidation for the conditions studied, most of the N_xO_y remediation occurs by the depletion time of N, with the remainder occurring by the OH depletion time (Although O is longer lived than OH or N, its major role is generation of secondary radicals rather than direct assistance in the remediation.). Thus, the end of N_xO_y remediation and, by definition, the end of the PPRP coincide with the OH depletion time as shown in Figs 4.6 and 4.7.

NO continues to be remediated during the IP in both cases as well. This decrease results from NO being largely converted to NO_2 by O_3 by the reaction (indicated by the dashed line in Fig 4.1)

$$NO + O_3 \rightarrow NO_2 + O_2 \qquad (4.19)$$

This process continues until O_3 is depleted, setting the end of NO remediation. This reaction accounts for approximately 1/3 of the removal of NO for the early pulse case. Note, however, that the density of N_xO_y does not change during the IP in spite of the decrease in NO since the reaction with O_3 reapportions the densities of the nitrogen oxides as opposed to reducing their net density. Thus NO removal during the IP is misleading from the standpoint of net remediation. This process is important, though, because it does prevent the build-up of O_3 which is itself a restricted species with respect to emission.

The behavior of NO_2 significantly varies between the two pulses. For the earlier pulse NO_2 remains relatively constant during the PPRP as its creation and destruction processes balance. Its density then increases during the IP as a consequence of the reaction of NO with ozone (Eq. 4.19). This results in a net increase in NO_2 during the early pulse. For the late pulse, however, there is a net decrease in NO_2. Unlike the early pulse, in the

late pulse case NO_2 decreases during the PPRP. This change can be attributed to an additional major reaction during the PPRP. Following early pulses, N radicals were predominantly consumed by radical recombination and the reduction reaction (Eq. 4.1a). During later pulses, however, NO_2 also becomes a major reactant for the N radicals. This difference results from the increase in density of NO_2 and the decrease in density of NO which would otherwise consume N atoms. This reaction of NO_2 with N (indicated by the gray line in Fig 4.1)

$$NO_2 + N \rightarrow NO + NO \qquad (4.20)$$

causes the density of NO_2 to decrease during the PPRP of the late pulse, as opposed to its relatively constant behavior during the PPRP of the earlier pulse.

This reduction reaction of NO_2 (Eq. 4.20) replenishes NO, thus acting as a "back reaction" in the remediation scheme. The additional NO primarily enters the reduction channel. As a consequence ΔN_2 is increased during the later pulse by reduction reactions not only with the NO present at the beginning of the pulse but also with the NO created by the back reaction. This is in contrast to the earlier pulse where the majority of ΔN_2 can be attributed to decreases in NO from its initial value for that pulse. The reaction sequence $NO_2 \varnothing NO \varnothing N_2$ (Eqs. 4.20 and 4.1a) continues until N is depleted. At that time the concentration of NO briefly increases due to the lack of N. Both NO and NO_2 then achieve quasi-steady state densities as the other PPRP reactions come to an end. As in the earlier pulse, the dominant process during the IP exchanges NO for NO_2 (Eq. 4.19). Despite this additional source of NO_2 during the IP, there is a net decrease in the density of NO_2 during the later pulses due to the back reaction with N during the PPRP (Eq. 4.20).

These reactions during the later pulse suggest that operation of the DBD after the depletion of NO can result in the build-up of restricted species. For example, once NO is

depleted, the reaction of Eq. 4.19 (the major destruction mechanism for O_3) is no longer important. As a consequence, the density of O_3 increases on a pulse-to-pulse basis. This trend is shown in Fig 4.9. Similarly, once NO and NO_2 are depleted, the reaction sequence $NO_2 \varnothing NO \varnothing N_2$ which consumes N atoms does not occur. At this junction, N atoms serve as reactants which form additional N_xO_y (reactions initiated by Eq. 4.17), rather than reducing NO_2 or NO. Concentrations of the major end products during remediation and at long times (many current pulses beyond that required to removed the initial NO) are shown in Fig. 4.10. At long times the concentrations of undesirable N_xO_y are 10s-100 ppm, and are comparable to the desired products, specifically ΔN_2 and HNO_3. The density of HNO_2 stops increasing after NO is depleted since its source ($NO + OH \varnothing HNO_2$) is removed. Reactions with OH to produce NO_2 then deplete its density. The rate of production of HNO_3 decreases as the oxidation channel is slowed down due to the small amount of NO_2 which survives.

Due to the likelihood that restricted species will be produced in plasma remediation devices after the NO is depleted, a practical device should include an NO sensor that adjusts the DBD power level according to the concentration of NO in the exhaust. Power should be decreased or terminated to reduce or prevent the creation of the radicals N and O that lead to the formation of O_3 and N_xO_y as described above. Since the power deposition in a DBD can be varied from one cycle to the next, a feedback control loop is, in principal, straightforward.

Although ions do play important roles with regard to the characteristics of the plasma, they are not particularly chemically active with regard to N_xO_y remediation. The major ions consist of N_4^+, N_2O^+, N_2^+, O_2^+, H^-, O_2^-, NO_2^-, NO_3^-, and the cluster ions $H_3O^+H_2O$ and $H_3O^+(H_2O)_2$. Since in the DBD the electrons are accelerated from low energies, they most often lose energy by low energy threshold processes (e.g., vibrational excitation, molecular dissociation). Very few electrons reach energies high enough to

participate in high threshold processes such as ionization. Thus, ion densities are small. the maximum density of charged species is approximately 10^{13} cm^{-3}, with typical individual ions having maximum densities of 10^{11}-10^{12} cm^{-3}. Total ion, electron, representative positive, and representative negative ions are shown in Fig 4.11 as a function of time for typical conditions. Positive non-cluster ion densities are negligibly small at the onset of remediation after the current pulse. Such ions are chemically important only in that they may generate neutral radicals by dissociative recombination (e.g., $e + N_2^+ \rightarrow N + N$). However, even this contribution is small compared to the generation of radicals by direct electron impact dissociation of the feedstock gases. In general, positive and negative ions react to form their corresponding neutral species, or in the case of the cluster ions, neutral water clusters or molecules. Since ion densities are small, however, these species are not created to any significant extent and so, again, do not contribute significantly to the remediation.

4.4 Optimization of Remediation Conditions

Strategies for optimizing remediation of NO can be formulated in light of the chemical processes discussed in the prior section. We found that remediation is achieved primarily through neutral radical assisted reactions with ions playing a minor chemical role. Radicals are produced primarily during the current pulse (10s ns) and are depleted by remediation reactions. A multipulse format is thus required to replenish the radicals. We also found that a significant intrapulse time is required to take advantage of the radical assisted remediation reactions. The optimum pulse repetition frequency is determined by the durations of these reactions (100 μs - many ms) which are dictated by the radical lifetimes. Therefore, in deriving an optimal remediation strategy, it is important to consider the effects of parameters that affect radical formation, concentration, and lifetime, and that optimize radical usage.

To examine these dependencies we parameterized the model over intrapulse time, voltage, water content in the gas stream, and energy deposition/pulse. To evaluate the efficiency of remediation, we define ε = (energy deposition in eV) / (NO or N_xO_y molecule removed). Thus, lower ε is more efficient. By defining ε in this manner we hope to capture the detrimental effects of merely converting NO to other nitrogen oxides, or producing additional nitrogen oxides. Although virtually total removal of NO can be achieved using DBDs, we will consider the effect of these parameters on remediation at a total energy deposition of 60 mJ/cm^3 as a point of comparison. Typically 20 pulses are required to achieve the desired energy deposition. In general, the conditions for each case will be those of Section 4.2 with the exception of the parameter being varied.

Concentrations and remediation efficiencies of NO and N_xO_y are shown in Fig. 4.12 as a function of intrapulse time or repetition rate. As might be anticipated from the single pulse chemistry, N_xO_y remediation and efficiency are independent of the intrapulse period for times longer than the PPRP which, for these conditions is approximately 100 μs (10^4 Hz). NO remediation and efficiency improve until O_3 is depleted, which, for these conditions is approximately 10 ms (10^2 Hz). Therefore the net removal of N_xO_y is independent of repetition rate for practical devices (operating at less than many kHz). However to minimize production of O_3, the repetition rate should be less than 100s Hz. The optimum intrapulse time for both the removal of N_xO_y and minimizing the production of the undesirable end product O_3 is at least the depletion time of approximately 1 ms.

The time scales for these processes can be varied by operating at different pressures. Although this is not a viable option for open remediation systems such as diesel exhaust, it may be an option for closed cycle industrial processes. In general, higher pressures produce shorter time scales since reactions occur more frequently with increasing reactant density. This change in time scale with pressure is shown in Fig 4.13 where species densities for NO, N_xO_y, OH as a representative radical, and N_2O_5 as a

representative product are shown for operating at 1 and 1.7 atm. the onset and end time of remediation, the radical formation and depletion times, and the onset and end time of product formation all occur earlier for the higher pressure case. (Note that the absolute concentration values for these cases are misleading as the higher pressure case has higher initial densities and therefore less energy deposited per molecule.) The shortened time scale for higher pressure will lead to a higher optimum repetition frequency.

For a given energy deposition, remediation and ε improve at higher applied voltage, and thus, E/N, as shown in Fig. 4.14. This scaling results form the fact that the fractional power deposition producing dissociation and ionization increases with increasing E/N relative to those processes which are non-dissociative. This scaling is shown in Fig 4.15 where the fractional power deposition by electron impact processes is shown as a function of E/N. Power deposition is dominated by electron impact at E/N < 100 Td. In the operating range of interest (approximately 300 Td), the fraction of power deposition producing dissociation of N_2 is largest. At higher E/N, power deposition is dominated by ionization. At lower E/N, power deposition is dominated by vibrational excitations. This also indicates that faster rising pulses will be more efficient, since E/N values where dissociation dominates will be reached sooner and less energy will be wasted in exciting vibrational modes.

Significant improvement in remediation and ε can be obtained with increasing water content in the gas stream, as shown in Fig 4.16. This trend is due to the increased removal of NO and NO_2 by oxidation. The large range for the efficiencies obtained while varying the water content indicates that the availability of the oxidation channel is a major leverage in remediation.

Remediation and ε generally improve when using a larger number of current pulses delivering a smaller specific energy/pulse to achieve a desired total energy deposition. This scaling is shown in Fig. 4.17. Although higher specific power deposition produces a

higher density of radicals, increased radical densities enhance radical-radical recombination reactions (e.g., Eq. 4.19) which are non-linear in radical concentration relative to the linear remediation reactions (e.g., Eq. 4.13). Therefore lower specific power deposition results in fewer radical-radical reassociation reactions, and therefore a more effective use of the radicals in direct remediation.

4.5 Concluding Remarks

Dielectric barrier discharges are potentially and effective technology for the remediation of N_xO_y. NO can be removed from atmospheric gas streams from concentrations of 500 ppm to < 1 ppm with an energy expenditure of < 72 eV/molecule. For typical diesel engines, this efficiency corresponds to 15 % of the engine power output. Remediation of NO to concentrations below statutory amounts (<100 ppm) requires energy expenditures of < 60 eV/molecule. The end products of remediation are primarily N_2 and HNO_3. Only small amounts of restricted nitrogen oxides or ozone are formed as long as the device is not operated at power levels beyond that required for total NO remediation.

There are three timescales in the remediation process during a single pulse: the Pulse, during which primary radical N, O, and OH are created by electron impact reactions; the Post Pulse Remediative Period (PPRP), during which NO and N_xO_y are remediated; and the Interpulse Period (IP) during which NO is converted to NO_2 with no change in the net N_xO_y. Remediation occurs due to radical assisted reactions, with the ions largely uninvolved.

The optimum intrapulse time for remediation is at least as long as the O_3 depletion time. In closed cycle systems, these time scales can be varied to fit constraints on repetition rate by adjusting the total gas pressure. Removal efficiency is higher when using larger applied voltage, faster rising pulses, larger H_2O percentage in the gas stream, and more pulses of lower energy. Our results indicate that even for mobile applications, it may

be worthwhile to take advantage of the oxidation pathway which leads to the acidic waste product because of the significantly improved efficiency.

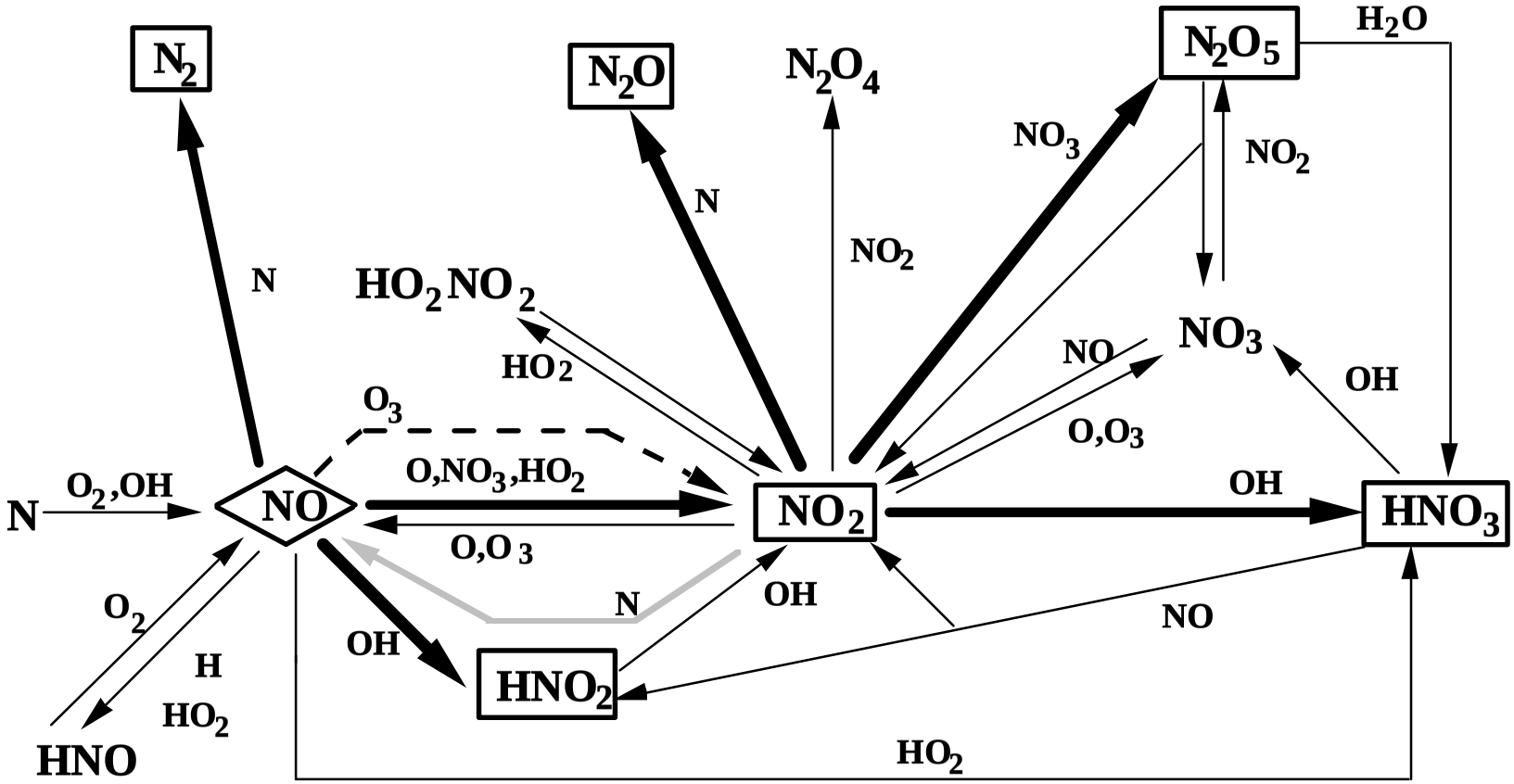

Fig. 4.1. Dominant reaction pathways, shown by arrows for plasma remediation of N_xO_y. The initial toxin, NO, is shown by the diamond. The dominant end products are boxed. The radicals assisting in the reactions are noted adjacent to the corresponding reaction arrow.

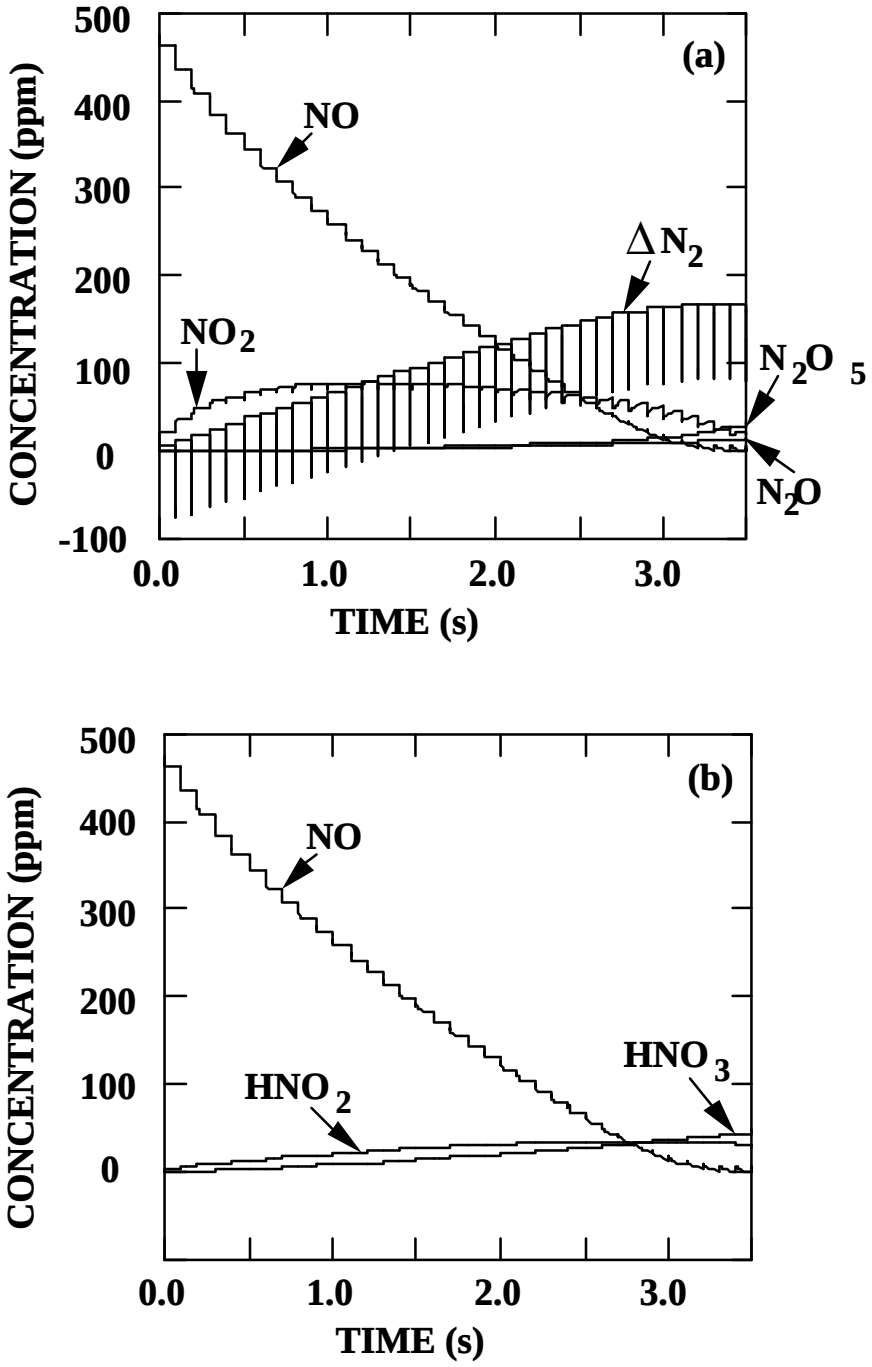

Fig. 4.2. Removal of NO and generation of end products. a) NO, ΔN_2, and N_xO_y products; b) NO and oxidation products HNO_2 and HNO_3. The initial gas mixture is $N_2/O_2/H_2O$ = 85/5/10 with 500 ppm NO at 1 atm, 400 K, and 10 kV. The repetition rate is 10 Hz and the energy deposition is 3 mJ/cc/pulse. The current pulse cannot be resolved in this figure. The NO is primarily converted to N_2 and HNO_3.

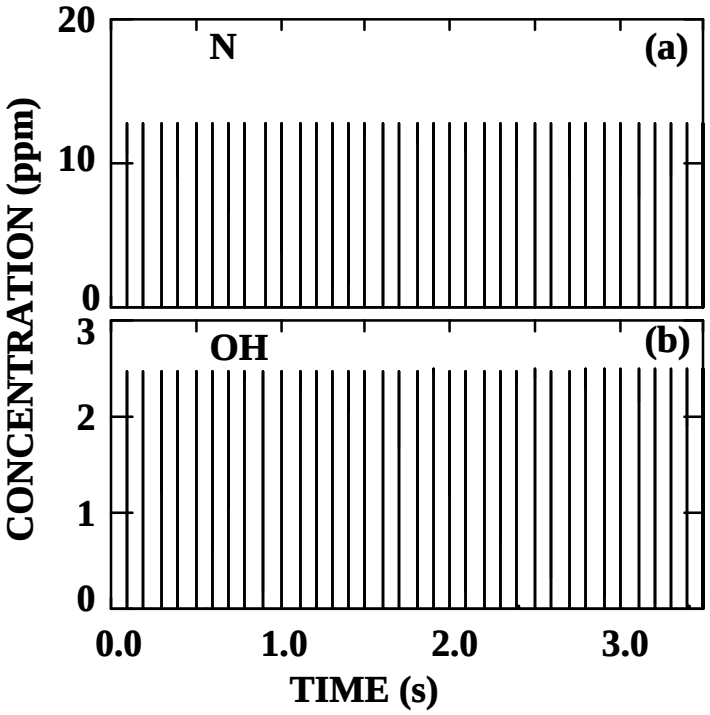

Fig. 4.3. Densities of a) N and b) OH radicals for the conditions of Fig. 4.3. These radicals are produced during the current pulse (not resolved in the figure) and are quickly consumed by radical-radical reactions and reactions in the remediation pathway.

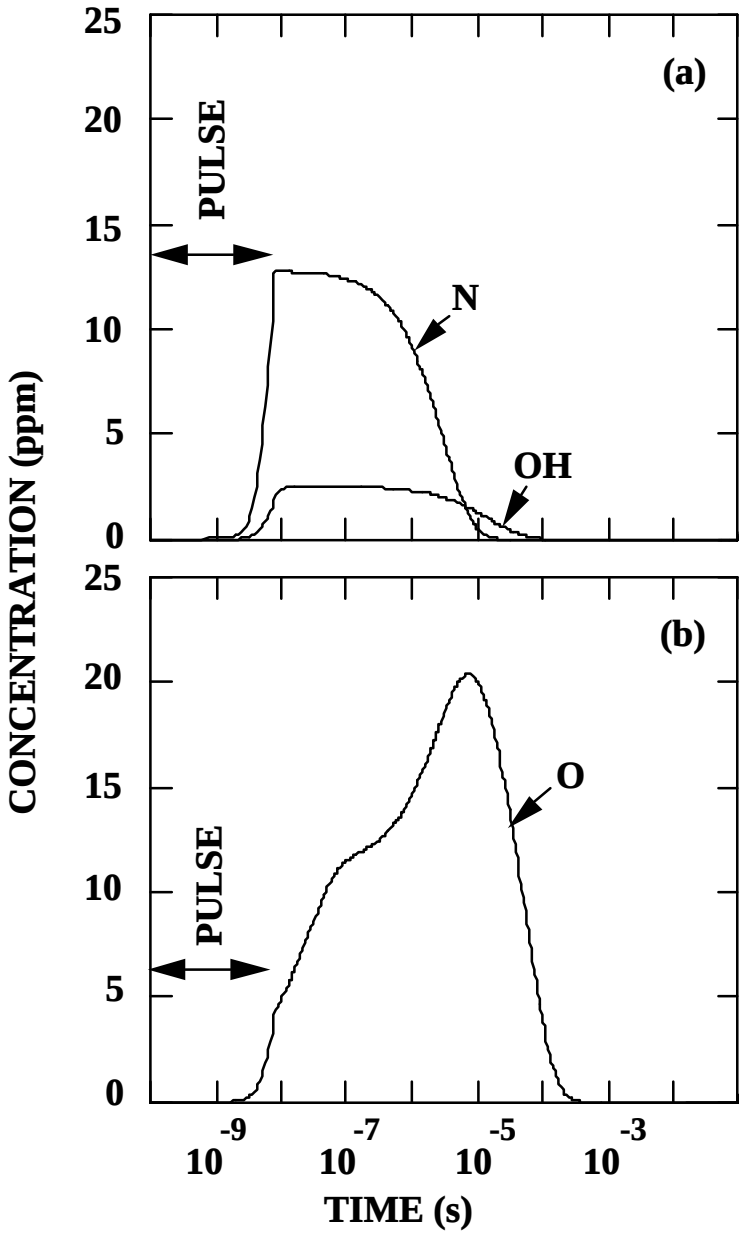

Fig. 4.4. Concentrations of primary radicals during and after a current pulse. a) N and OH; b) O. The conditions are the same as those for Fig 4.2. The N and OH radicals are predominantly produced during the current pulse by electron impact processes. O is produced during the pulse by electron impact processes and after the pulse by the reduction reaction NO + N —> N_2 + O.

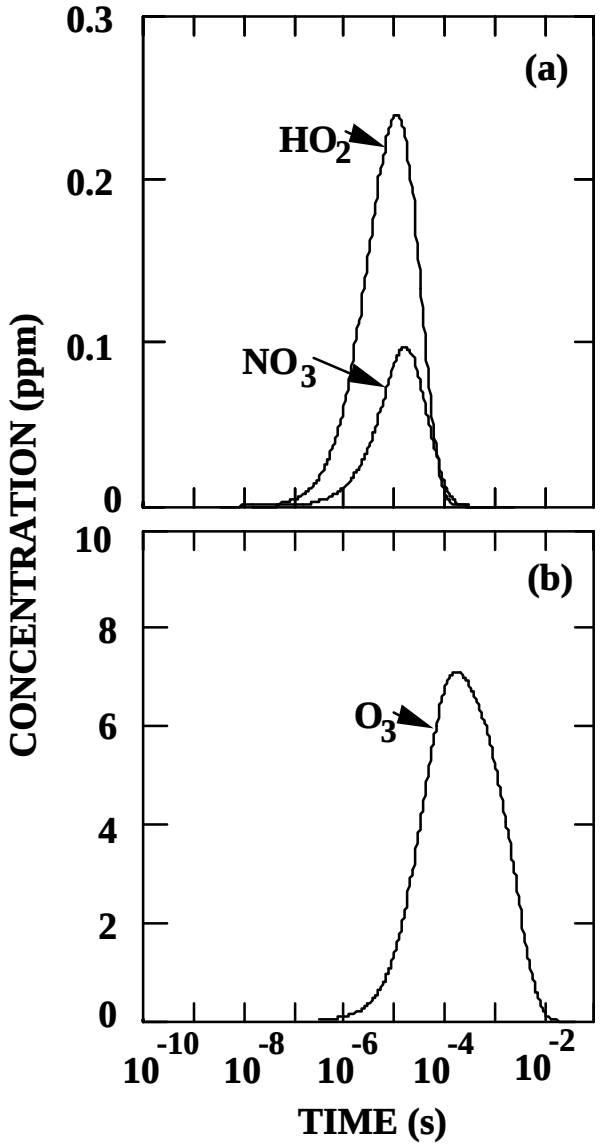

Fig. 4.5. Concentrations of secondary radicals which assist in the remediation of N_xO_y for the conditions of Fig 4.2. a) HO_2 and NO_3; b) O_3. The production of NO_3 and O_3 is predominantly by reaction of O atoms with NO_2 and O_2 respectively.

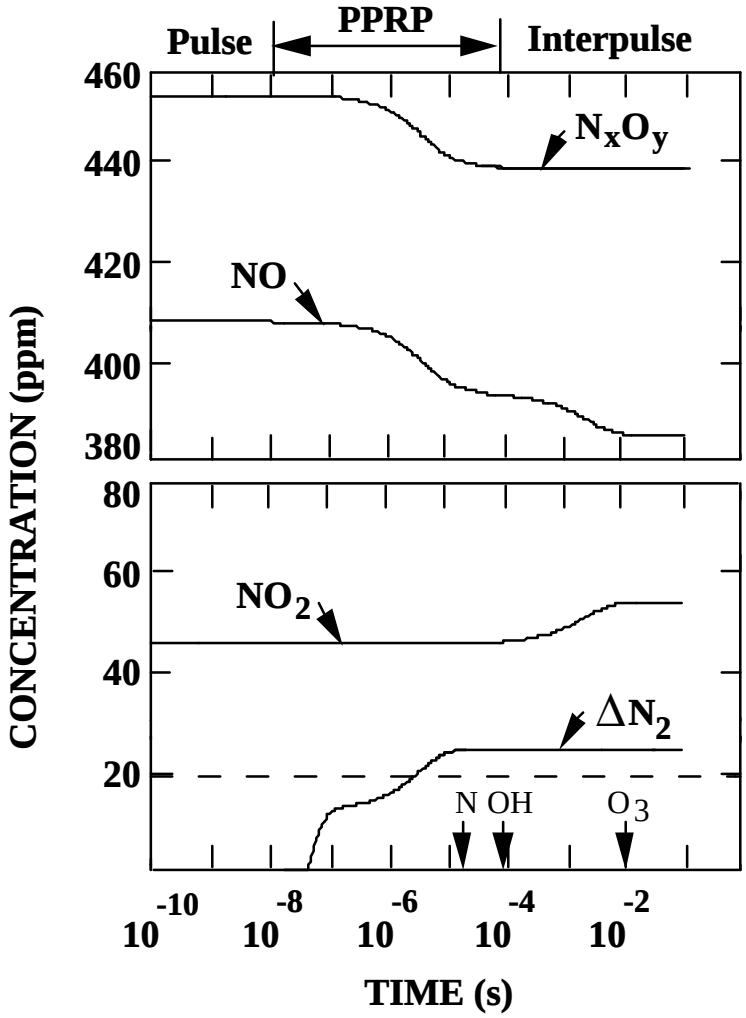

Fig. 4.6. Concentrations of NO, N_xO_y, NO_2, and ΔN_2 for the 4th pulse of Fig 4.2. The durations of the Pulse, PPRP, and IP are shown at the top of the figure. The depletion times for the radicals N, OH, and O_3 which assist in the remediation are indicated on the axis. Although the density of NO decreases throughout the PPRP and IP, the total density of N_xO_y decreases only during the PPRP. During the IP the inventory of N_xO_y is reapportioned amongst the various nitrogen oxides - in particular NO —> NO_2.

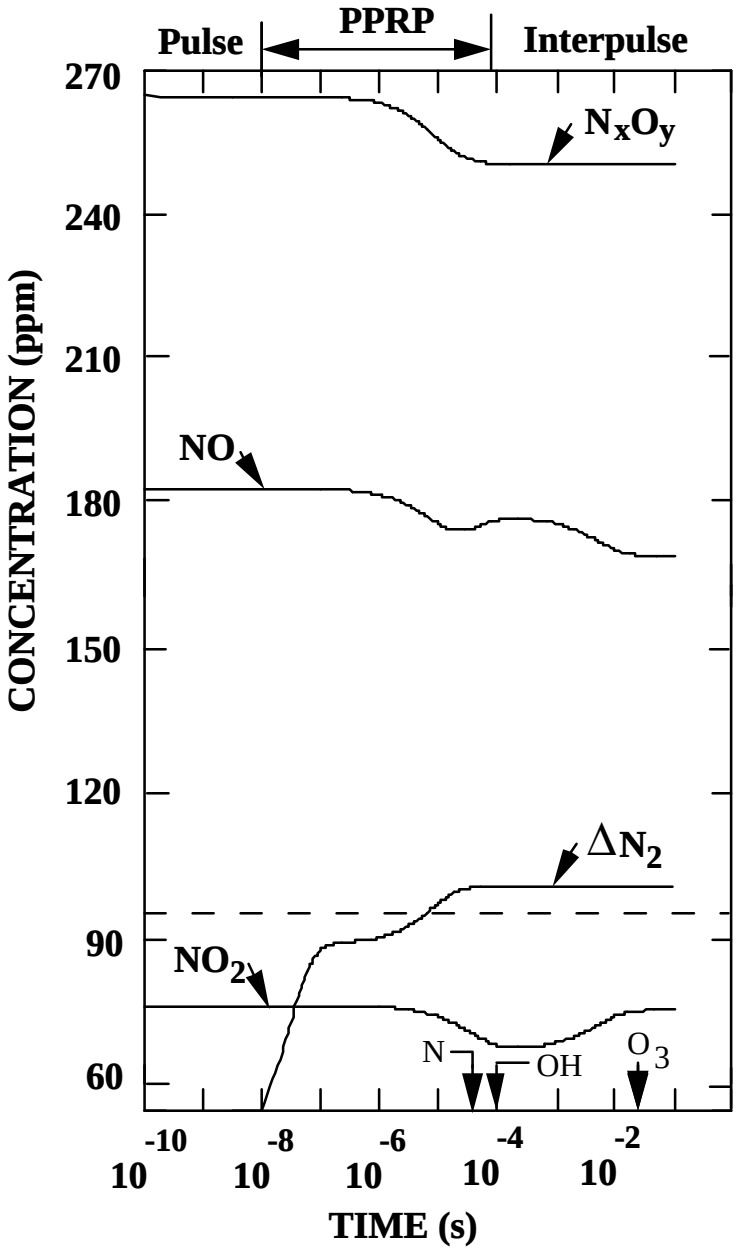

Fig. 4.7. Concentrations of NO, N_xO_y, NO_2, and ΔN_2 for the 17th pulse of Fig 4.2 Depletion times for the radicals N, OH, and O_3 which assist in the remediation are indicated on the axis. Unlike the earlier pulse, the density of NO_2 decreases during the PPRP as a result of the "back reaction".

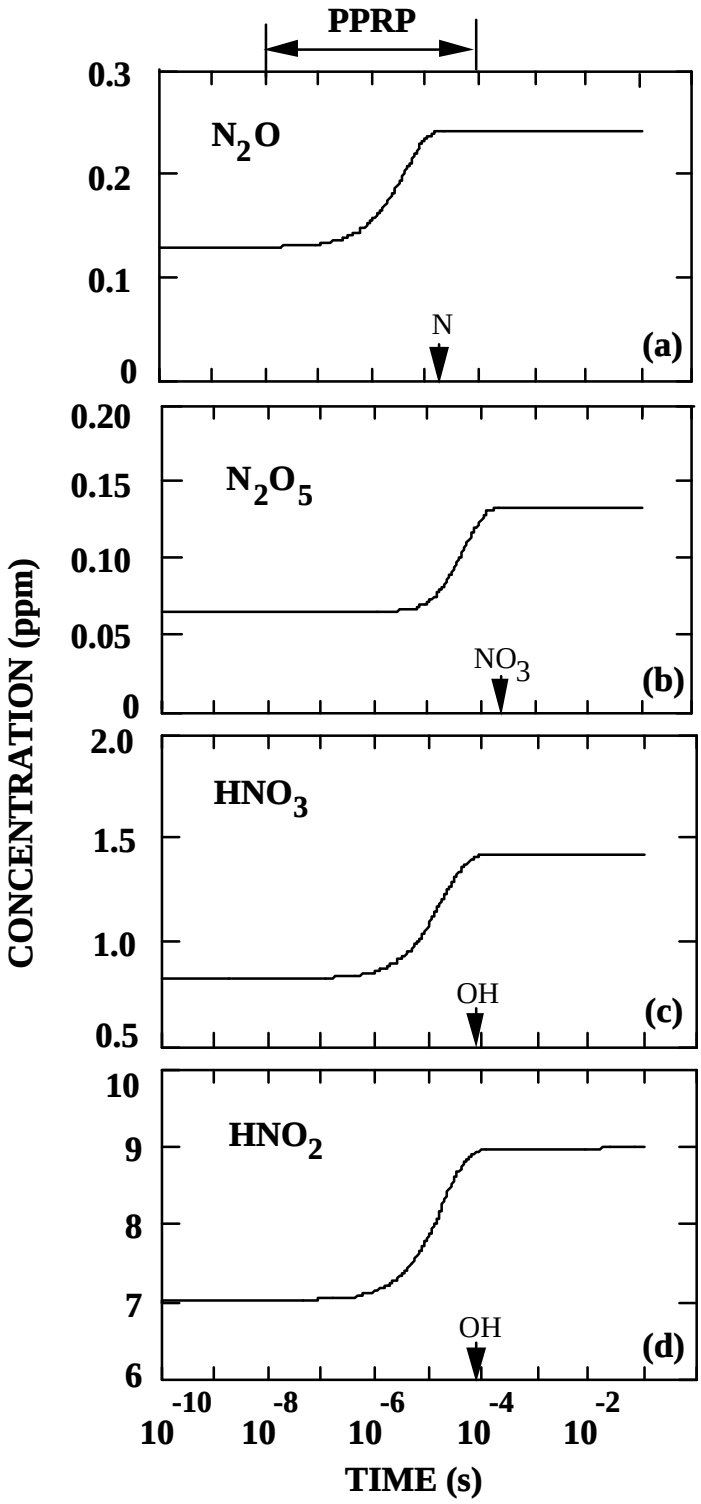

Fig. 4.8. Concentrations of major products. a) N_2O, b) N_2O_5, c) HNO_3, and d) HNO. The generation of these products terminates when the assisting radicals are depleted. The time at which the assisting radical is depleted is marked on that product's time axis.

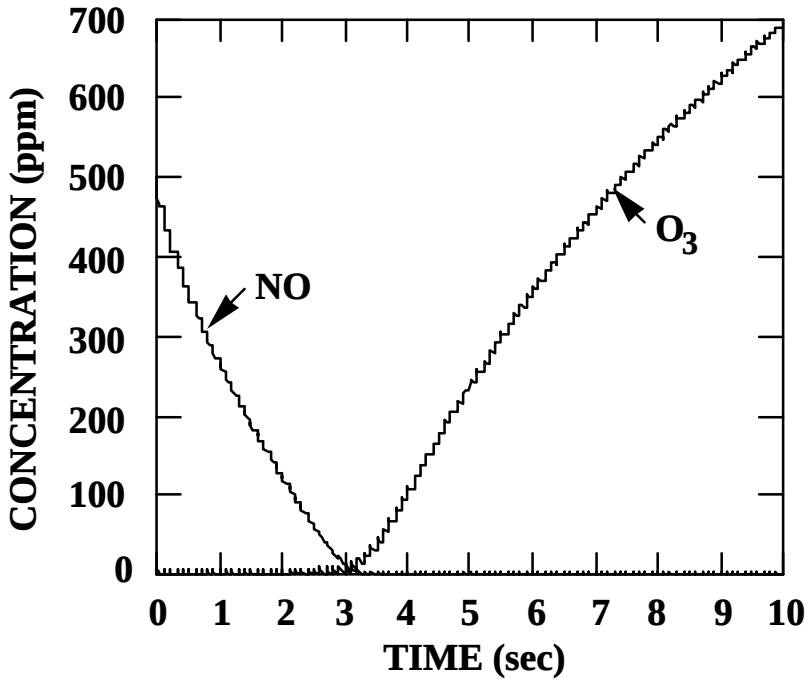

Fig. 4.9. Concentrations of NO and ozone for a sequence of current pulses exceeding that required to remediate the NO. The production of O_3 increases after NO is depleted due to the elimination of its loss to reactions with NO.

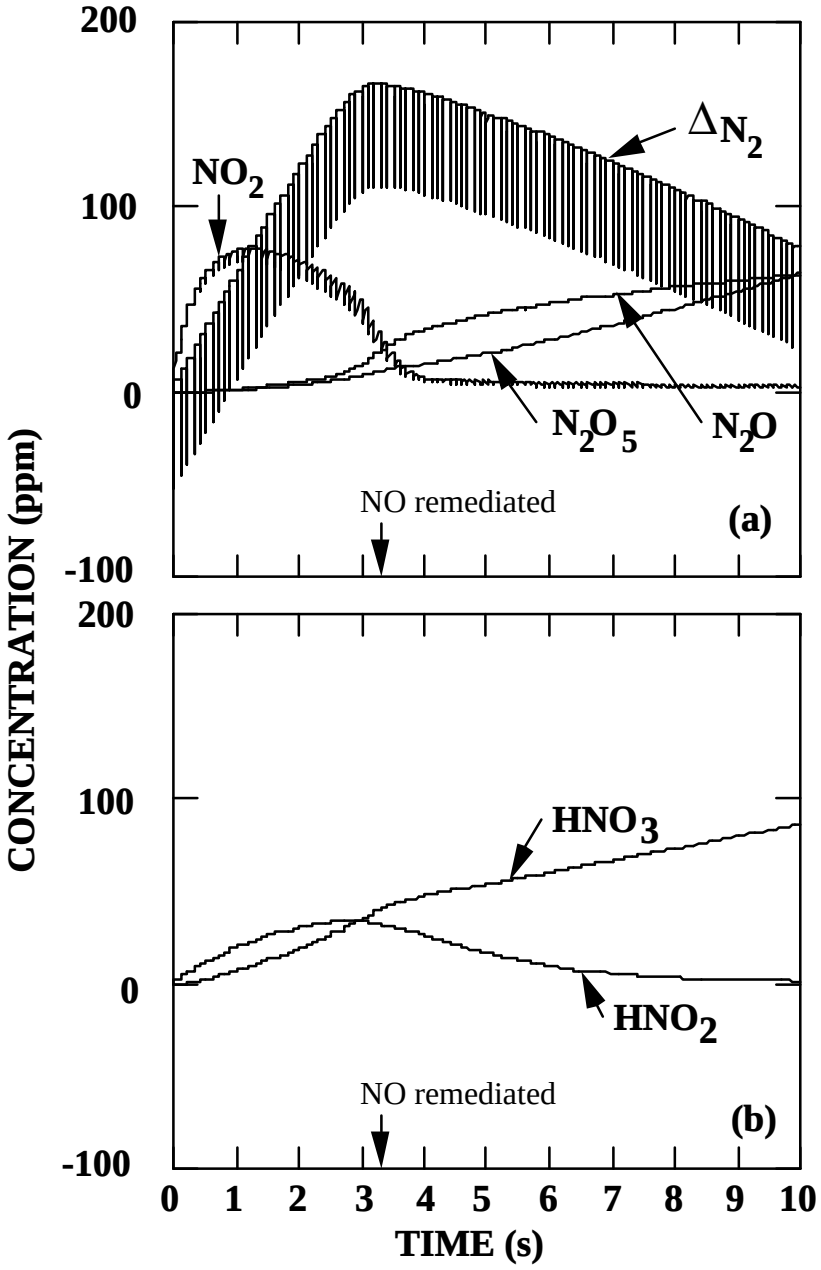

Fig. 4.10. Major end products for a sequence of current pulses exceeding that required to remediate NO. a) N_2 and N_XO_Y products, b) HNO_2 and HNO_3. After depletion of NO, N atoms that would otherwise be depleted by the reduction reaction with NO are available to produce other nitrogen oxides.

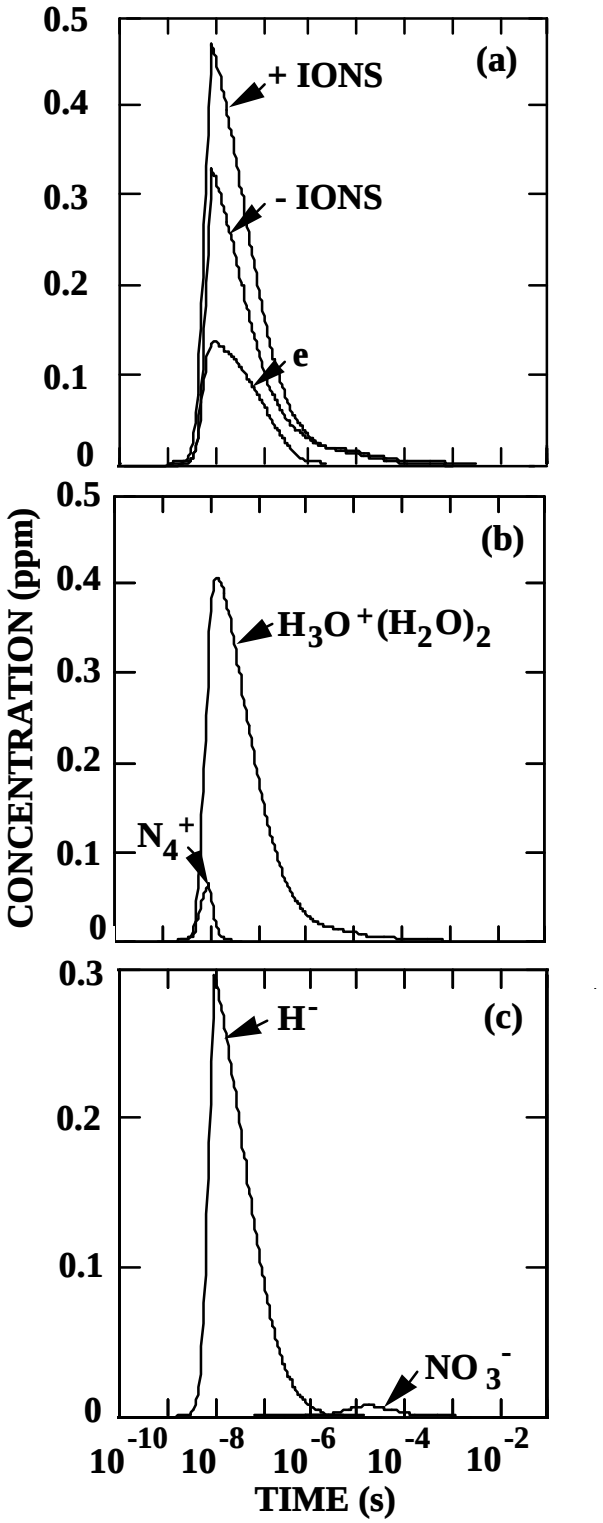

Fig. 4.11. Concentrations of selected charged particles. a) total positive ion, negative ion , and electron densities; b) N_4^+ and cluster ion $H_3O^+(H_2O)_2$; c) H^- and NO_3^-. The total charged species densities have peak values of approximately $1x10^{13}$ cm^{-3}.

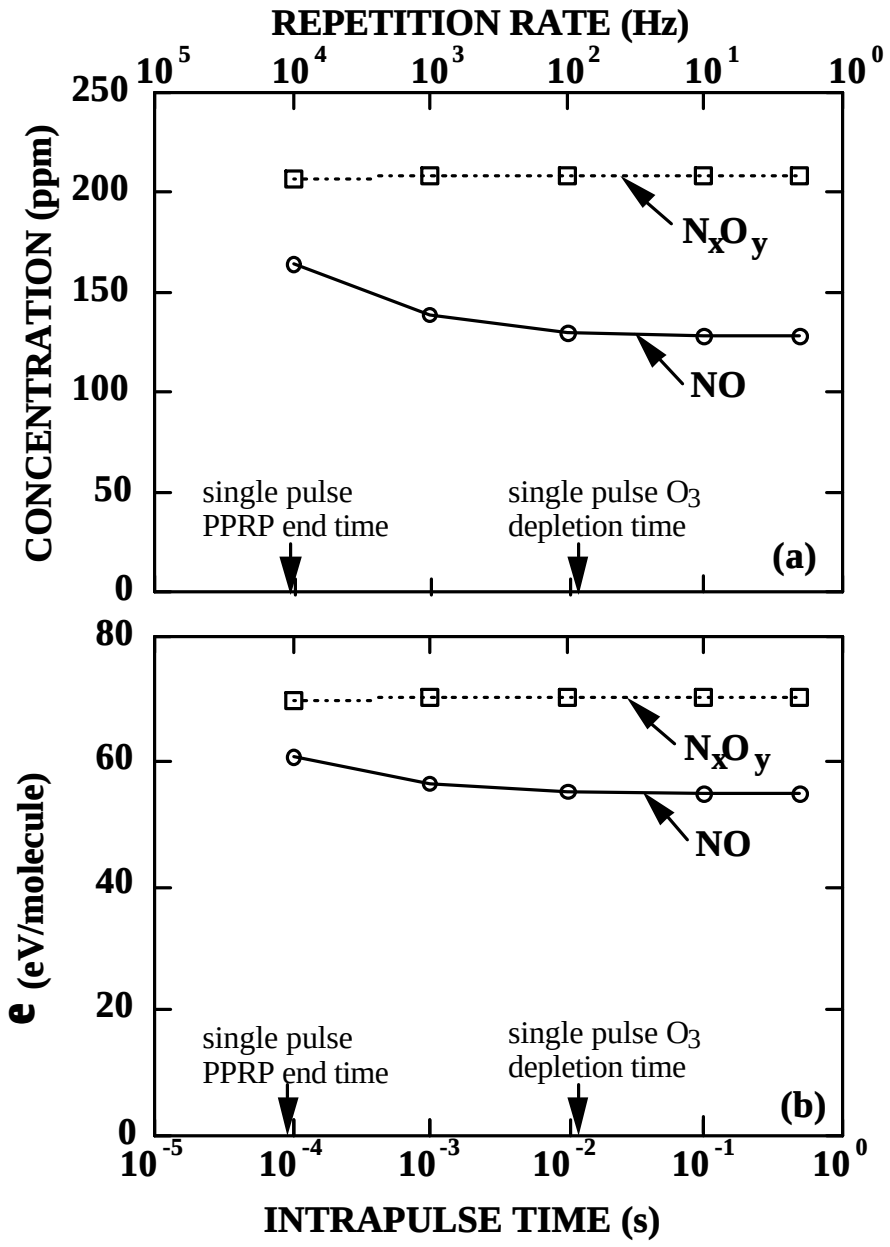

Fig. 4.12. Remediation parameters for NO and N_XO_Y as a function of intrapulse time (or repetition rate). a) concentration and b) efficiency. The length of the PPRP and the O_3 depletion time for a single pulse are indicated on the time axis. N_XO_Y remediation and efficiency are independent of intrapulse time for times greater than the PPRP. NO remediation and efficiency improve until O_3 is depleted.

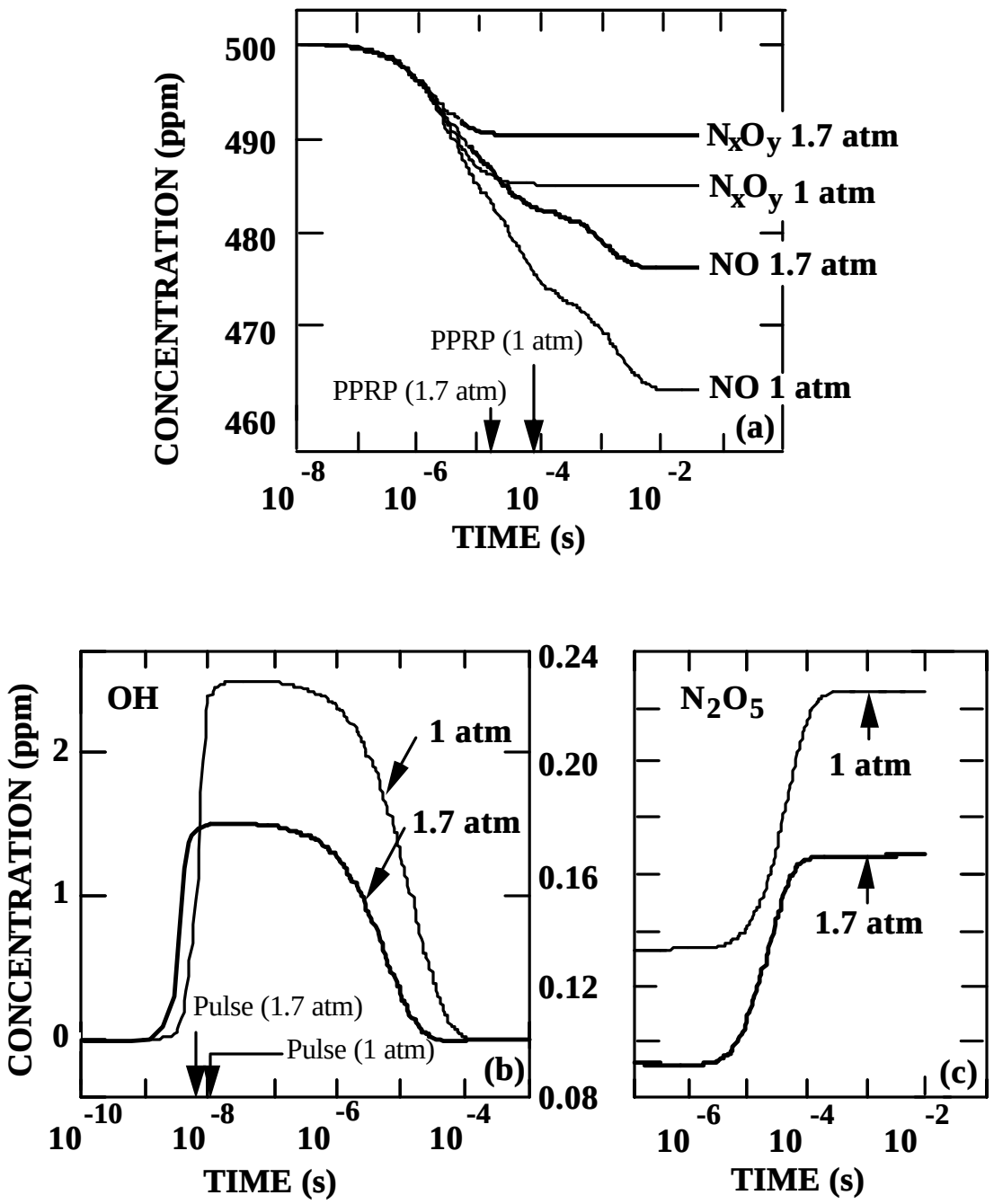

Fig. 4.13. Radical and product concentrations for operation at 1 atm and 1.7 atm as a function of time. a) NO and N_XO_Y; b) OH; c) N_2O_5. The end of the current pulse or PPRP at each pressure are shown on the time axis where significant. Reaction timescales generally decrease with increasing pressure.

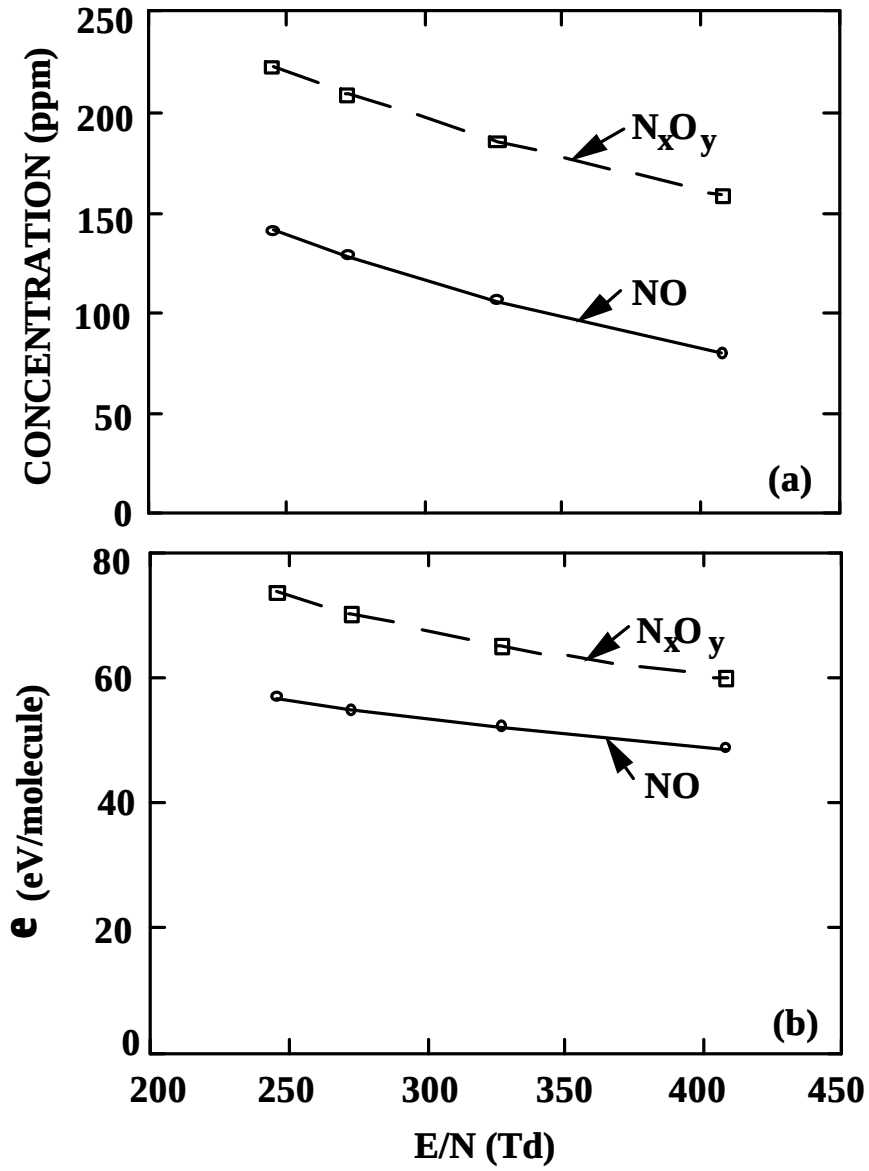

Fig. 4.14. Remediation parameters for NO and N_XO_Y as a function of E/N. a) concentration and b) efficiency. N_XO_Y remediation and efficiency improve with increasing E/N due to more efficient production of N atoms.

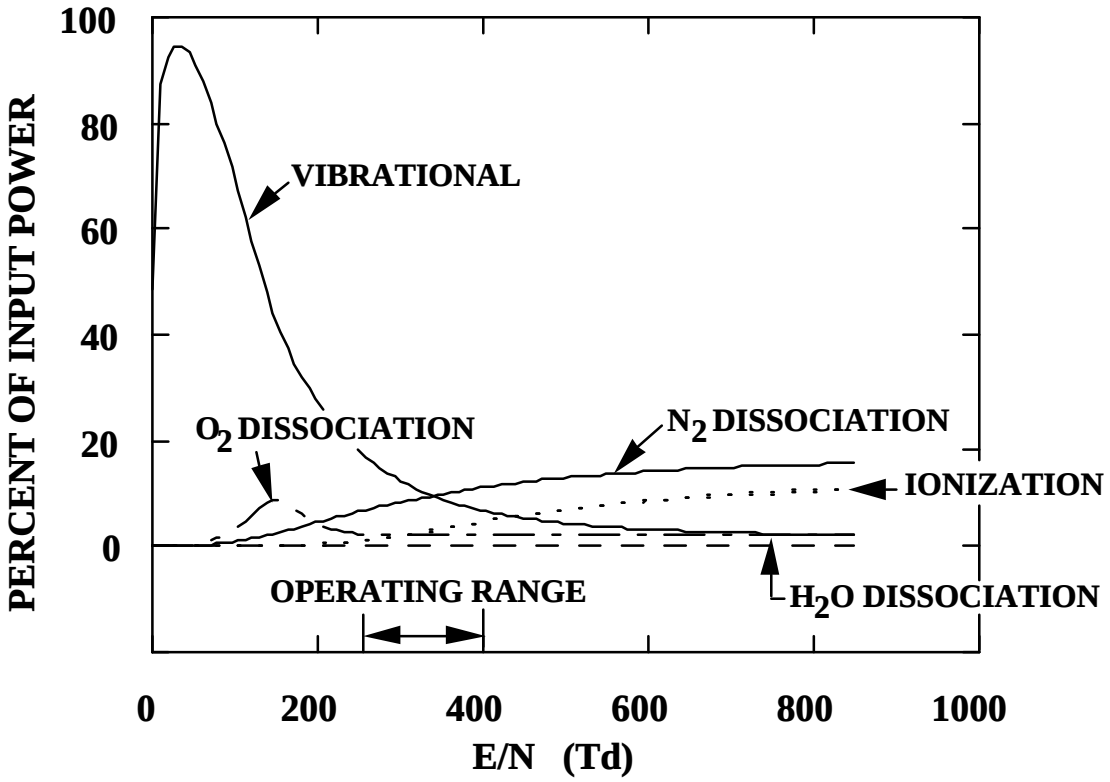

Fig. 4.15. Percent of input power dissipated by electron impact processes as a function of E/N. The fractional power deposition into dissociative and ionizing reactions increases with increasing E/N.

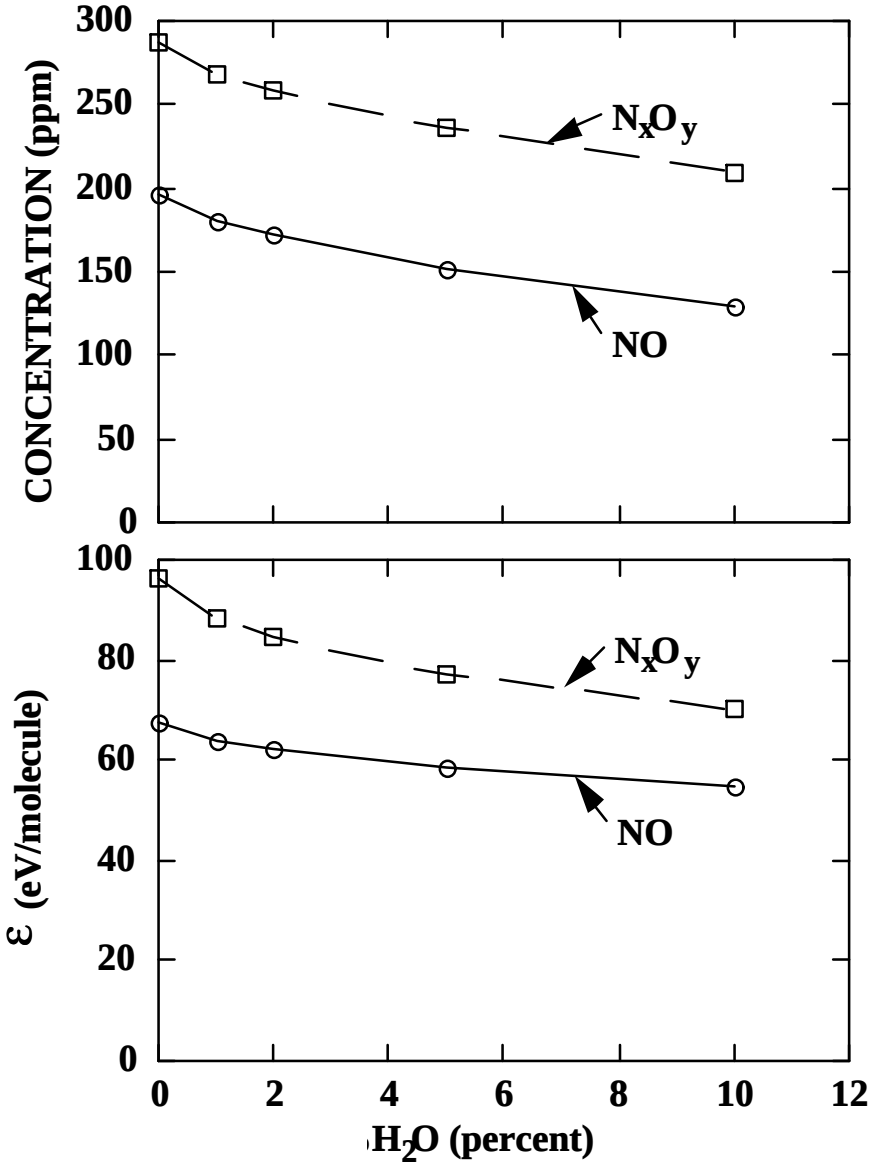

Fig. 4.16. Remediation parameters for NO and N_XO_Y as a function of water content in the gas stream. a) concentration and b) efficiency. N_XO_Y remediation and efficiency improve with increasing H_2O percentage due to the larger contribution of the oxidation channel.

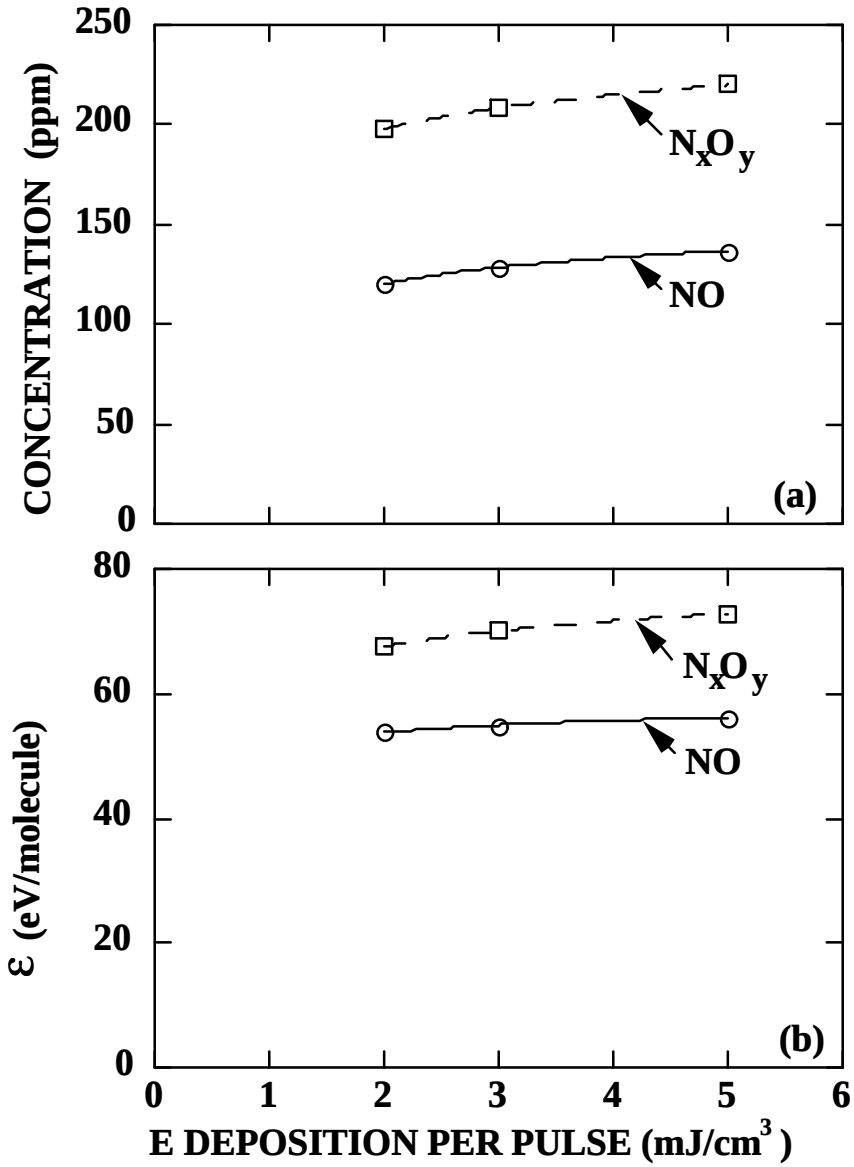

Fig. 4.17. Remediation parameters for NO and N_XO_Y as a function of energy deposition/pulse. a) concentration and b) efficiency. Remediation improves using a larger number of pulses using a smaller specific energy/pulse. At high specific energy deposition, radical-radical reactions compete with the remediation processes for reactants.

5. REMEDIATION OF N_xO_y: DIFFUSIVE TRANSPORT AND RADIALLY DEPENDENT KINETICS

5.1 Introduction

In Chapter 4 we saw that with the 0-D model more efficient removal was obtained with larger applied voltage, faster rising pulses, larger H_2O percentage in the gas stream, and more pulses of lower energy. The general trends that result from voltage and water content will hold in the 1-D case as well, since the underlying physics for these issues will not be affected by spatial dependencies. This does not hold, however, for the case of energy deposition. In this chapter, then, we look for variations from the 0-D results for two reasons. First, the method of energy deposition itself has changed, as the energy is now deposited by a localized streamer. Secondly, the spatial dependencies may affect the reaction kinetics. In the 0-D case we saw that very large concentrations of radicals led to inefficient radical usage as radicals were wasted in recombination reactions as opposed to remediation reactions. In the 1-D case the radical concentrations will change as a result of trade-offs between transport and localized energy deposition. These changes in radical concentration can have effects on radical usage.

We present the effects of spatial dependencies in remediation, specifically the location of radicals and remediation, in Section 5.2. Throughout this chapter, we consider only diffusive transport, using the model described in Section 2.3.1. Additional transport effects due to advection will be discussed in Chapter 6. We discuss the effects of diffusive transport and localized energy deposition on efficiency in Sections 5.3 and 5.4, respectively. We then compare 0-D and 1-D results for the scalings of efficiency with energy deposition per pulse in Section 5.5.

The spatial effects that arise in the 1-D model can have significant effects on the resulting chemistry of certain systems. To highlight these effects, we look at remediation in

$N_2/O_2/H_2O/CO_2$ systems, which are also more realistic in simulating diesel exhaust, in Section 5.6. We conclude this chapter with remarks in Section 5.7.

5.2 Spatial Dependencies in Remediation

Using the radially dependent model of Section 2.3.1, we find that the major chemical processes are the same as those obtained by the 0-D model described in Chapter 4. The species are now subject to diffusive transport, however, and so their densities can vary from region to region. We can still consider the three time regimes introduced in Section 4.3 of the Pulse, Post Pulse Remediative Period (PPRP), and Interpulse (IP). If one considers the volume averaged densities of NO and N_xO_y the same general behavior for the dependencies of NO and N_xO_y is observed using the 1-D model as in the 0-D model, as shown in Fig. 5.1. Profiles for NO and N_xO_y in individual regions will, of course, show different characteristics. The initial conditions for Fig 5.1, as well as for the subsequent figures, are the same as those of the standard case of Chapter 4 ($N_2/O_2/H_2O$ = 85/5/10, 500 ppm NO, 400 K, 1 atm, 10 kV, and 10 Hz) with the exception that the energy deposition has been decreased from 3 mJ/cm^3/pulse to 1 mJ/cm^3/pulse on a volume averaged basis. This is done to keep the contribution to the species densities due to the advective terms small so that densities are determined primarily by the 0-D kinetics and diffusion only. Some higher energy deposition cases presented later in this chapter may, in fact, require inclusion of the advection effects to more accurately capture the behavior of the system under those conditions. These cases are included here without the advective contributions to better compare the effects that are due only to diffusion. Spatial dependencies due to both diffusion and advection and their effects will be discussed in Chapter 6.

As in the 0-D case, primary radicals are produced during the Pulse, with secondary radicals created later. The reaction scheme is again shown in Fig 5.2 with the reactions

which are pertinent to this discussion highlighted as described below. The major PPRP reactions consist of those that are product generating, shown in bold, and the "back reaction"

$$NO_2 + N \rightarrow NO + NO \qquad (5.1)$$

shown in gray. The IP reaction

$$NO + O_3 \rightarrow NO_2 + O_2 \qquad (5.2)$$

is shown by the dashed arrow.

We now consider the species behavior in more detail, noting the spatial dependencies with time. An initial non-uniform electron distribution is defined in the streamer region

$$n_e(r) = 10^9 \exp(-r/r_o)^3 + 10^{-10} \ cm^{-3} \qquad (5.3)$$

where $n_e(r)$ is the electron density at radius r and r_o defines the extent of the streamer, typically 10 μms. Electron avalanches during the current pulse then produce a non-uniform distribution with time. This is shown in Fig 5.3 where the electron profiles are plotted as a function of radius at various times. Here, the edge of the streamer is indicated by the dashed line, and the edge of the block containing the streamer is at 10^{-2} cm. Sequential profiles drop off with increasing time as indicated by the arrow. Since ambipolar diffusion is slow, the electrons do not diffuse far beyond the streamer region.

The electron avalanche leads to a substantial formation of the primary radicals N, OH, and O during the Pulse in and near the streamer. These radicals diffuse out to small but non-negligible densities during their reactive times. As discussed in Section 4.3 these are

times up until the end of the PPRP, roughly 10^{-4} s. Rapid consumption of radicals by the radical-radical recombination reactions and remediative reactions prevents them from traveling far beyond the streamer edge. This behavior is shown in Fig. 5.4a for N. The other primary radicals behave similarly. We concentrate here on N, since much of the remediation progresses through the reduction reaction involving N

$$NO + N \rightarrow N_2 + O. \qquad (5.4)$$

Unlike the primary radicals, the secondary radical O_3 is uniformly distributed at the time of its major remediation reaction (Eq. 5.2) which occurs during the IP, roughly after 10^{-4} s. This is shown in Fig. 5.4b where species density profiles for times leading up to the IP are shown. The O_3 concentration initially builds up in the streamer region due to the large concentration of O atoms resulting from electron impact reactions. The O_3 density then continues to increase and O_3 molecules diffuse out. As the O atoms are depleted, production of O_3 slows down and diffusion levels out the profile. Since the O concentration is substantially reduced by the end of the PPRP, O_3 production is also substantially reduced by this time. Once the production of O_3 has decreased, spatial inhomogeneities induced by the non-uniform source are smoothed out by diffusion. Thus, the leveling out of the profile occurs soon after a substantial amount of O has been depleted near the beginning of the IP.

Since the radicals are responsible for remediation, the radical profiles determine the location and amount of remediation with time. Here we will show the resulting spatial dependencies of NO, N_xO_y, and NO_2. Note that in all of these figures, the minimum density on the y-axis is not zero. NO and N_xO_y densities are shown for the first pulse. NO_2 densities are shown for a later pulse (pulse 5) once NO_2 has accumulated.

The behavior of NO during remediation is shown in Fig. 5.5. The sequence of NO plots is divided up into 3 time scales, during each of which NO shows a distinctly different behavior. In Fig. 5.5a, remediation of NO begins in the streamer region due to the high density of primary radicals there. The concentration of NO drops with time as the rate of remediation exceeds the rate of diffusion during this period. This behavior occurs from roughly 10^{-9} to 10^{-6} s. The second time period from 10^{-6} to 10^{-4} s (the PPRP end) is shown in Fig. 5.5b. The densities during this time are shown in gray. The previous densities are shown in black for contrast. (This coloring scheme will be used throughout this section for any sequential set of profiles.) During this time remediation continues and diffusion from outer regions fills in the NO profile until a uniform distribution is reached. As in the case of the O_3 profile, the NO profile will become level soon after the source of the non-uniformity is removed. For NO, this source is the primary radicals responsible for the remediation. Thus, the NO profile becomes uniform at roughly the end of the PPRP. Finally a uniform decrease in NO due to the IP reaction (Eq. 5.2) is shown in Fig. 5.5c. This decrease is uniform because both the NO and O_3 profiles are uniform at this time.

The N_xO_y profile is similar to that of NO, but without any change during the IP. In Fig. 5.6a, N_xO_y is remediated in and near the streamer, largely due to the NO remediation. As in the NO case, this occurs for roughly 10^{-9} to 10^{-6} s. Then, as shown in Fig. 5.6b, the remediated region fills in as NO diffuses in from larger radii and N_xO_y products are created. As with NO, the N_xO_y profile levels off at about the end of the PPRP. Finally, in Fig. 5.6c, the N_xO_y profile does not change during the IP since there is no change in net N_xO_y due to the IP reaction (Eq. 5.2).

The behavior of the NO_2 density is largely due to reactions involving NO. In Fig. 5.7a, NO_2 initially decreases in the streamer region. This is due to the “back reaction” (Eq. 5.1) which removes NO_2 and generates NO. This reaction is more significant at earlier pulses than for the 0-D case, because the density of the primary radical N is higher

since it is concentrated in and near the streamer. This larger local density greatly increases the reaction rate for this process. For this pulse, such behavior occurs from roughly 10^{-9} to 10^{-6} s. Eventually NO_2 production from NO outweighs its destruction from the "back reaction". NO_2 is then produced primarily in and near the streamer region due to the high density of radicals there. This fills out the initial drop in the NO_2 profile that occurred during the earlier time. As NO_2 continues to be produced it diffuses outward. This is shown in Fig. 5.7b for times up to $5x10^{-5}$ s. Next, diffusion levels out the profile, as seen in Fig. 5.7c. For the same reasons as for NO, and N_xO_y, this occurs at the end of the PPRP. Finally, in Fig. 5.7d, there is a uniform increase during the IP due to Eq. 5.2 since both NO and O_3 are uniform at this time.

5.3 Diffusive Transport and Efficiency

We saw in Section 4.4 that a large concentration of radicals can decrease the efficiency of remediation. The specific issue is the concentration of the remediative radicals relative to the concentration of the species to be remediated. Since the conditions we are operating under favor reduction, these species are primarily N and NO, respectively. In the streamer region where the density of N is high, if the ratio N/NO is large, recombination reactions, such as

$$N + N + M \rightarrow N_2 + M \qquad (5.5)$$

dominate over remediation reactions such as Eq. 5.4 and the efficiency will be low. As N/NO decreases, increasing percentages of N will be used in remediation and the efficiency will increase.

We consider this ratio then for the 0 and 1-D cases. In the 0-D case, this ratio is straightforward. However, spatial and time dependencies make the 1-D case more

complex. A high density of radicals is created in the streamer region and the radicals do not diffuse out far from the streamer before reacting. At first, this would seem to imply a large N/NO ratio. However, NO from regions beyond the edge of the streamer diffuses in on this same time scale, keeping the NO density in the streamer region high as well. These events are shown in Fig. 5.8 for times from 10^{-7} to 10^{-6} s. Here we see that N remains located in and near the streamer region with its concentration dropping off rapidly, while on the same time scale NO diffuses in from locations further out. Rapid consumption of N limits the ability of N to diffuse too far outward. This makes diffusion of NO inward, as opposed to diffusion of N outward, the important factor. This supersedes the fact that NO is physically larger than N and would in general diffuse more slowly. Thus, NO diffusion decreases the N/NO ratio in the streamer region. This effect will be most significant for lower energy depositions, for which fewer radicals are produced, and for early pulses, during which the net NO density is still large.

We contrast 0-D and 1-D remediation, then, for a low energy deposition (1 mJ/cm^3/pulse) and over early (the first five) pulses in Figs. 5.9a and b, respectively. NO and N_XO_Y concentrations shown in the 0-D case are their uniform values. Volume averaged quantities are shown for the 1-D case. Under these conditions, remediation, and thus efficiency, is greater for the 1-D case than for the 0-D. Note that for later pulses in the 1-D case, as the net NO decreases and N/NO increases, the total remediation/efficiency of NO drops significantly. This is indicated by the arrows for pulses 1 and 5 in Fig. 5.9b.

5.4 Localized Energy Deposition and Efficiency

We saw in Section 5.2 that the localized energy deposition resulted in high radical densities localized in the streamer region. Localized energy deposition also results in high gas temperatures in the streamer region. These two factors can affect the efficiency. Gas temperature and N radical profiles are shown for 10^{-8} s < t < 2 x 10^{-7} s in Figs. 5.10a and

b, respectively, for energy depositions of 3 mJ/cm^3 and 1 mJ/cm^3. Both temperature and radical densities increase with increasing energy deposition. Both profiles peak in the streamer center, with most of the drop-off occurring across the streamer region.

Higher temperatures and radical densities increase the rate of radical involved reactions with high activation energies. Of particular interest is

$$N + O_2 \rightarrow NO + O \qquad (5.6)$$

which provides an additional source of NO. This additional production of NO decreases the net amount of remediation. Since the higher temperature and densities occur for higher energy deposition, this effect will be greater for that case. Similarly, since temperature and density profiles peak in the center of the streamer, this effect will be greatest there. This is shown in Fig. 5.11a-c, where NO profiles are shown during the decrease in NO density in and near the streamer region for 1, 2, and 3 mJ/cm^3 respectively. In Fig. 5.11a, where the temperatures and densities are relatively low, the greatest amount of remediation occurs in the streamer center where the radical density is highest. In Fig. 5.11c, reactions such as (Eq. 5.6) become significant during and shortly after the pulse when temperatures and densities are very high, with the greatest effect in the streamer center. This results in greater net remediation outward from the streamer center at early times. For this particular case, the point of greatest remediation occurs nearly at the streamer edge. At later times, once the temperature and radical densities have decreased, net remediation eventually becomes greatest in the streamer center.

5.5 Energy Deposition and Efficiency: 1-D vs. 0-D

As mentioned in Section 5.1, we expect the scaling of efficiency with energy deposition per pulse to be particularly sensitive when considering transport of species. We

now contrast the 0-D and 1-D (diffusion only) efficiencies for NO and N_xO_y remediation after a fixed number of pulses (3). This comparison is shown in Fig. 5.12. We see that as in the 0-D case, remediation is less efficient with increasing energy deposition. (Note that for a fixed number of pulses total remediation will be greater, but the efficiency will be less). The 1-D case is generally more efficient than the 0-D due to diffusive transport affecting the N/NO ratio as described in Section 5.3. This advantage in efficiency decreases at higher energy depositions. This occurs because of the increase in non-remediative processes such as radical-radical recombination (Eq. 5.3), "back reaction" production of NO (Eq. 5.1) due to increased radical densities, and production of NO from high activation energy processes now made accessible (Eq. 5.6).

5.6 Effects of CO_2 on N_xO_y Remediation

The issues of radical production, usage, and spatial dependencies of remediation that arise in the 1-D model can have quite complicated effects on the resulting chemistry. In order to highlight these effects, we consider N_xO_y remediation in the presence of CO_2.

We look at systems of $N_2/O_2/H_2O/CO_2$ = 77/15-X/8/X. The O atom balance is kept by increasing the CO_2 percentage at the expense of O_2. Conditions otherwise are the same as in the previous sections. The only new major reactions are electron impact dissociation of CO_2:

$$e + CO_2 \rightarrow CO + O^- \qquad E_{thresh} = 3.85 \text{ eV} \qquad (5.7)$$

$$e + CO_2 \rightarrow CO + O + e \qquad E_{thresh} = 6.1 \text{ eV} \qquad (5.8)$$

and the analogous reaction to Eq. 5.6:

$$N + CO_2 \rightarrow NO + CO \qquad (5.9)$$

New products are only produced to small amounts. For the case of 12% CO_2, after 10 pulses there is approximately 10 ppm of CO produced. Various cyanides, such as HCN and CN, are produced to less than 10^{-6} ppm total. As a measure of comparison, the top three remediation products are produced to a combined total of 85 ppm.

The inclusion of CO_2 does affect the amount of radicals produced in two ways. First, the resulting decrease in initial O_2 to accommodate the CO_2 affects the production of both O and O_3. The O production is decreased, however, this change is relatively unimportant since the total amount of O is still large. O_2, CO_2 dissociation, and the reduction reaction (Eq. 5.4) are still producers of O. Furthermore, since the primary radical O is highly concentrated in and near the streamer region when it reacts, the density of O in these regions during its reactive times is much larger than the volume averaged density. This results in a large "effective" density of O. The production of O_3 is also decreased, but in a more important way. The total amount of O_3 available is small, even without the presence of CO_2. Additionally, the "effective" density of the secondary radical O_3 is small, since it is spread out uniformly over the discharge when it reacts. The presence of CO_2 also affects the radical production more directly. The low energy threshold for CO_2 dissociation and vibrational excitation changes the electron energy distribution, decreasing the frequency of high energy processes. This is most important for OH production since the H_2O dissociation thresholds are high:

$$e + H_2O \rightarrow OH + H^- \qquad E_{thresh} = 5.526 \text{ eV} \qquad (5.9)$$

$$e + H_2O \rightarrow OH + H + e \qquad E_{thresh} = 13.5 \text{ eV} \qquad (5.10)$$

The effects that the changes in radical production have on the reaction mechanism are shown in Fig. 5.13. For the non-N_xO_y products, the reactions with OH producing

HNO_X (shown by the gray dashed arrow) decrease due to the decrease in OH. The reduction channel (bold dashed) increases commensurately. For the N_XO_Y products, the PPRP production is relatively unaffected, since the effective amount of O is still large and there are multiple pathways available for these products (bold). However, the IP exchange $NO \rightarrow NO_2$ (Eq. 5.1) (dashed) decreases because the effective amount of O_3 has decreased.

The resulting changes in product concentrations for varying amounts of CO_2 are shown in Fig. 5.14 after 10 pulses. Increasing CO_2 decreases the amount of HNO_X produced and increases the amount of N_2 produced (Fig. 5.14a). Increasing CO_2 also decreases the conversion of NO to NO_2 so that NO remediation decreases, but the total N_XO_Y concentration changes only slightly. Variation in the N_XO_Y concentration is primarily due to variations in the rates of Eqs. 5.6 and 5.9 affecting N usage and NO production by these reactions. However, the changes in HNO_X production and $NO \rightarrow NO_2$ conversion are more significant effects.

5.7 Concluding Remarks

Including spatial dependencies in the model allows for localized energy deposition that leads to spatially varying radical concentrations and remediation. The timescales of the Pulse, PPRP, and IP can still be considered in terms of the volume averaged densities for the streamer and surrounding region. Profiles for quantities in individual regions vary, however, as a result of the spatial dependence of the generated radicals. Primary radicals are created in and near the streamer and are concentrated in those regions when they react. These radicals do not diffuse far beyond the streamer. Unlike the primary radicals, the secondary radical O_3 is diffuse over the discharge when it reacts.

Spatial effects lead to changes in the energy efficiency. Diffusion of NO into the streamer region early in the intrapulse times lowers the N/NO ratio there. This leads to

greater remediation efficiency for the 1-D case above the 0-D case, especially for early pulses and low energy depositions. Localized energy deposition leads to higher radical densities and temperatures in the center of the streamer. Reactions with high activation energies that lead to the production of NO are enhanced under these conditions, thus moving the maximum of remediation out from the streamer center, especially for high energy depositions.

As a result of these diffusive transport and localized energy deposition effects, the scaling for efficiency with energy deposition/pulse changes from that obtained in Chapter 4. As in the 0-D case, efficiency still is better for more pulses of lower energy deposition. However, this trend is enhanced for the 1-D case due to the increased detrimental effects that result from the spatial dependencies at higher energy depositions.

Although the spatial dependencies do not significantly change the chemistry for $N_2/O_2/H_2O$ mixtures, they do for mixtures including CO_2. In these cases, reactions involving the primary radicals are generally more important since the "effective" amount of these radicals remain high because they are localized when they react. Reactions involving the secondary radical O_3 are of significantly lesser importance since O_3 is diffuse when it reacts. As a result of these spatial effects and the decrease in OH due to reduced H_2O dissociation, increasing CO_2 decreases the amount of HNO_x produced, increases the amount of N_2 produced, and decreases the conversion of $NO \rightarrow NO_2$. Only a few ppm of CO are produced and cyanides are not produced to any significant amount .

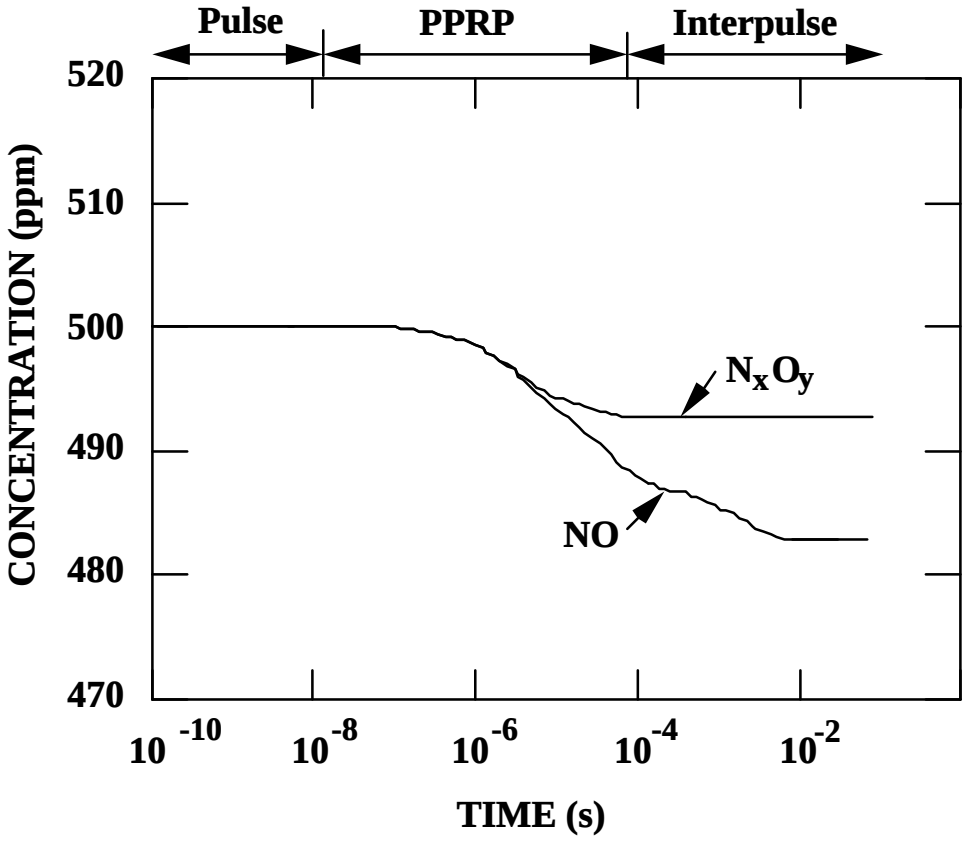

Fig. 5.1. Time regimes in the remediation of N_XO_Y in the 1-D model. Conditions are the same as those of Fig. 4.2 with the exception of the energy deposition/pulse which is now 1 mJ/cc. Time regimes are the same as those in the 0-D case, with the same general behavior occuring for the total area weighted densities of NO and N_XO_Y over the entire streamer and surrounding area.

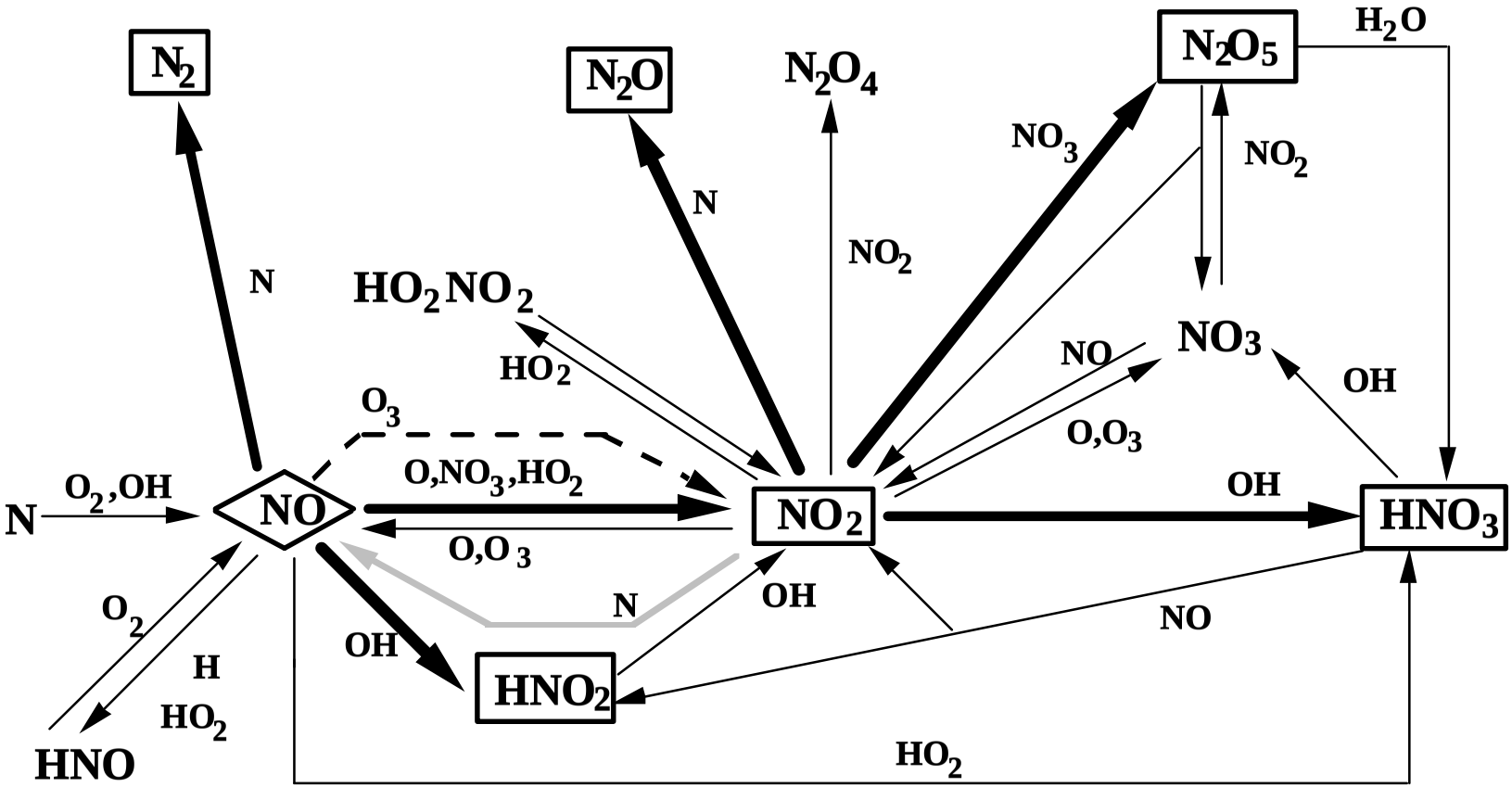

Fig. 5.2. Dominant processes in the remediation of N_x O_y . During the Pulse primary radicals are created. Secondary radicals are produced later. Major PPRP reactions are product producing (shown in bold) and the "back reaction" (Eq. 5.1) (gray). The major IP reaction converts NO to NO_2 (dashed).

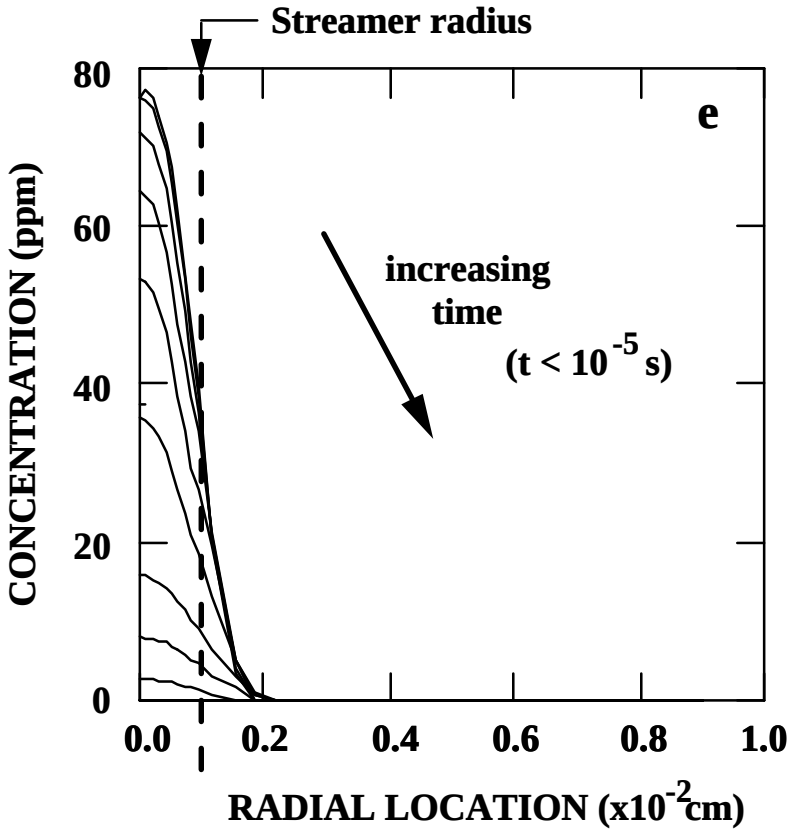

Fig. 5.3. Electron concentration vs. radical location. Conditions are the same as those for Fig. 5.1. Profiles drop off with increasing time as shown by the arrow. The electrons do not diffuse far beyond the streamer region (indicated by the dashed line).

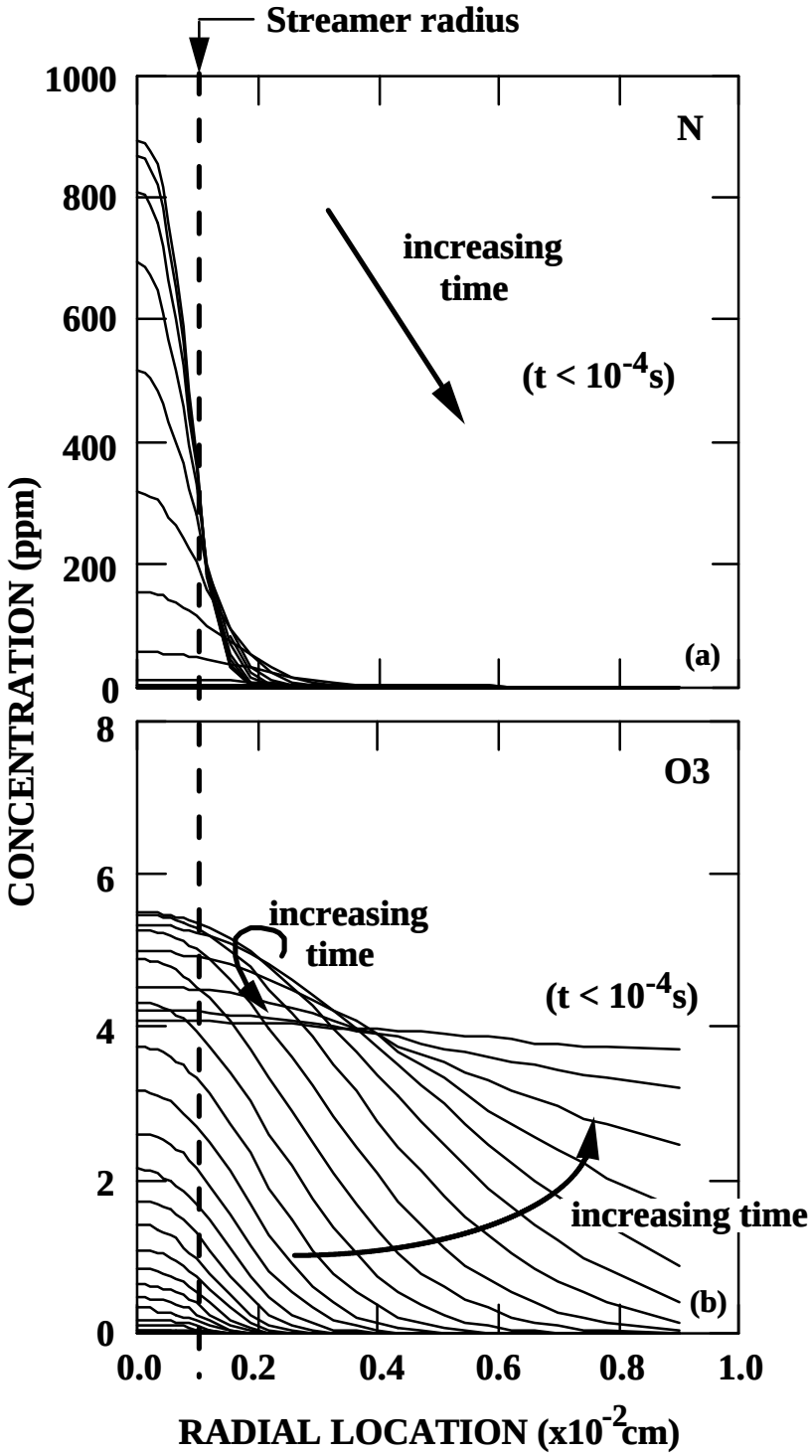

Fig. 5.4. Radical concentration vs. radial location. Conditions are the same as those in Fig. 5.1. a) primary radical N is formed in and near the streamer during the Pulse. Primary radicals diffuse out to small but not negligible densities during their reactive times (t < PPRP end). b) Secondary radical O_3 builds in and near the streamer region and diffuses out. O_3 is uniformly distributed at the time its major reaction ($NO_2 + O_3$ —> NO + NO) occurs (t during the IP).

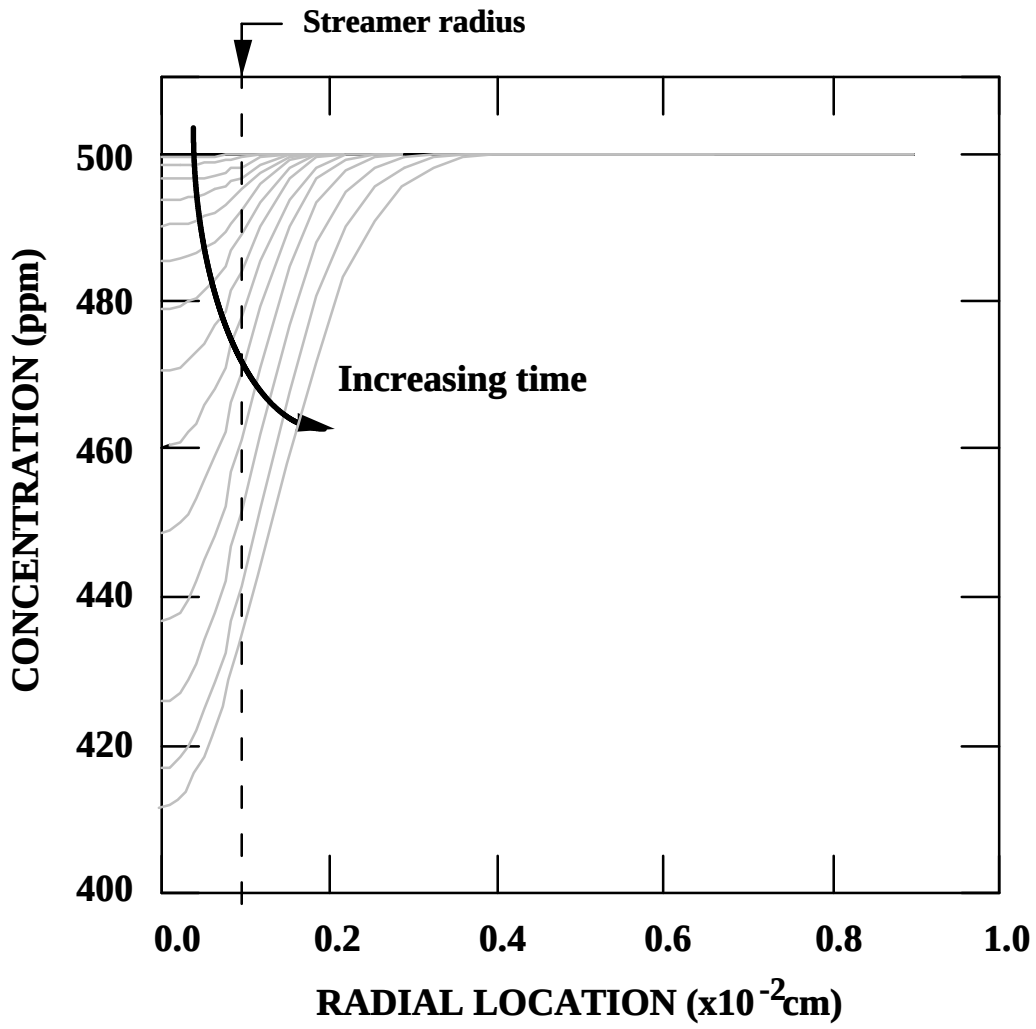

Fig. 5.5a. Behavior of NO during the first pulse for the conditions of Fig. 5.1. First figure in a series of 3. Curves in gray correspond to 10-9 s < t < 10-6 s. Remediation begins in the streamer region due to the high density of radicals there. Remediation exceeds diffusion during this time.

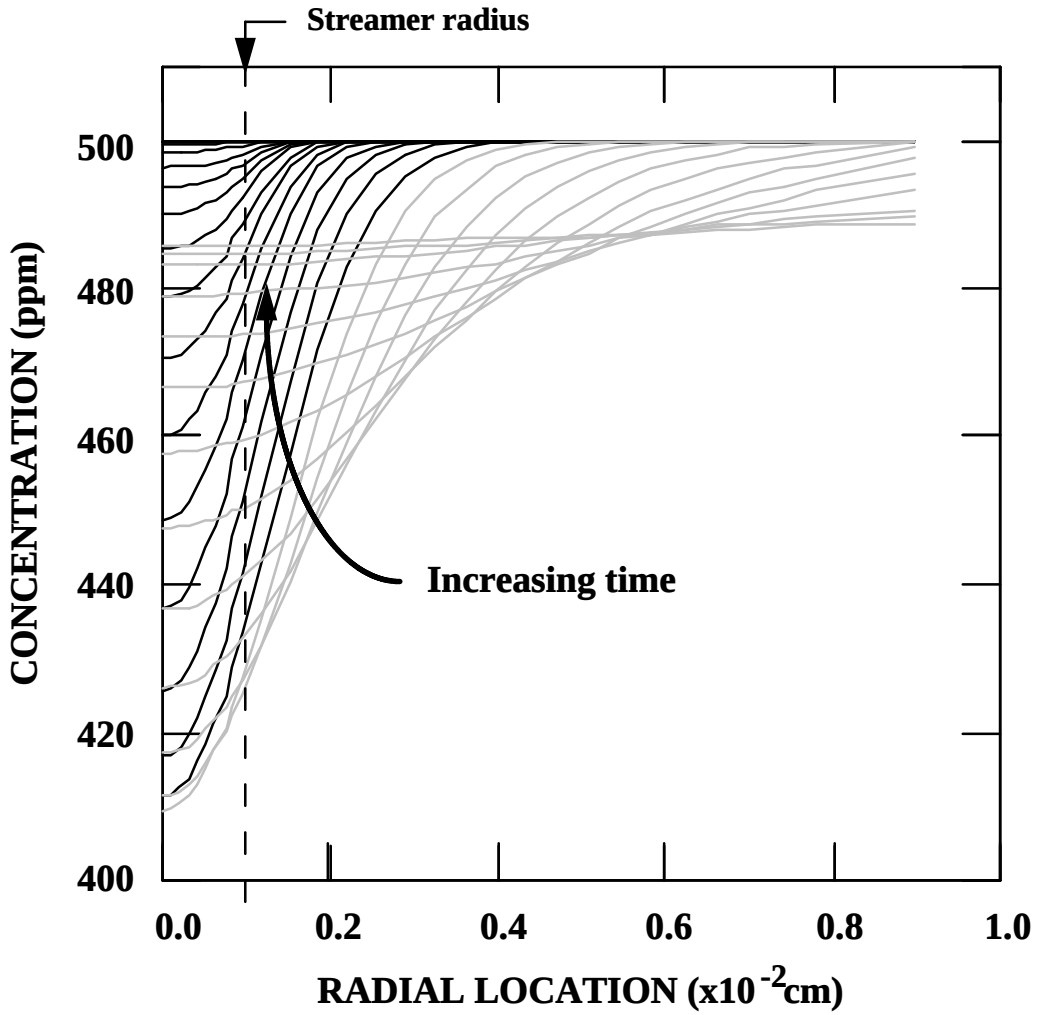

Fig. 5.5b. Behavior of NO during the first pulse for the conditions of Fig 5.1. Second figure in a series of 3. Curves in gray correspond to 10^{-6} s < t < 10^{-4} s (i.e., PPRP end); curves in black correspond to the preceeding time period. Remediation continues; diffusion from the outer regions fills in the profile until a uniform NO distribution is reached.

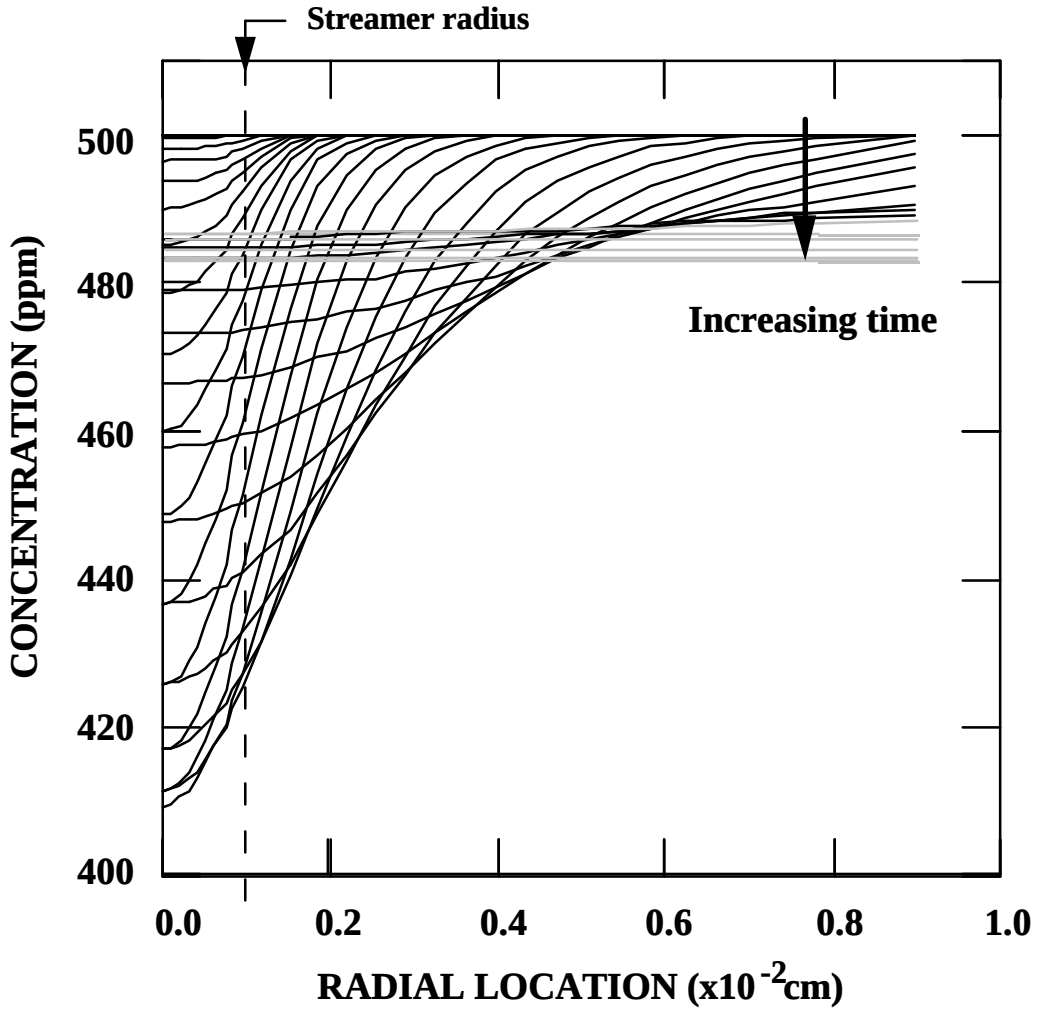

Fig. 5.5c. Behavior of NO during the first pulse for the conditions of Fig 5.1. Third figure in a series of 3. Curves in gray correspond to t $>10^{-4}$ s (i.e., IP); curves in black correspond to all preceeding times. NO drops uniformly during the IP due to the uniform distribution of NO and O_3 during this time.

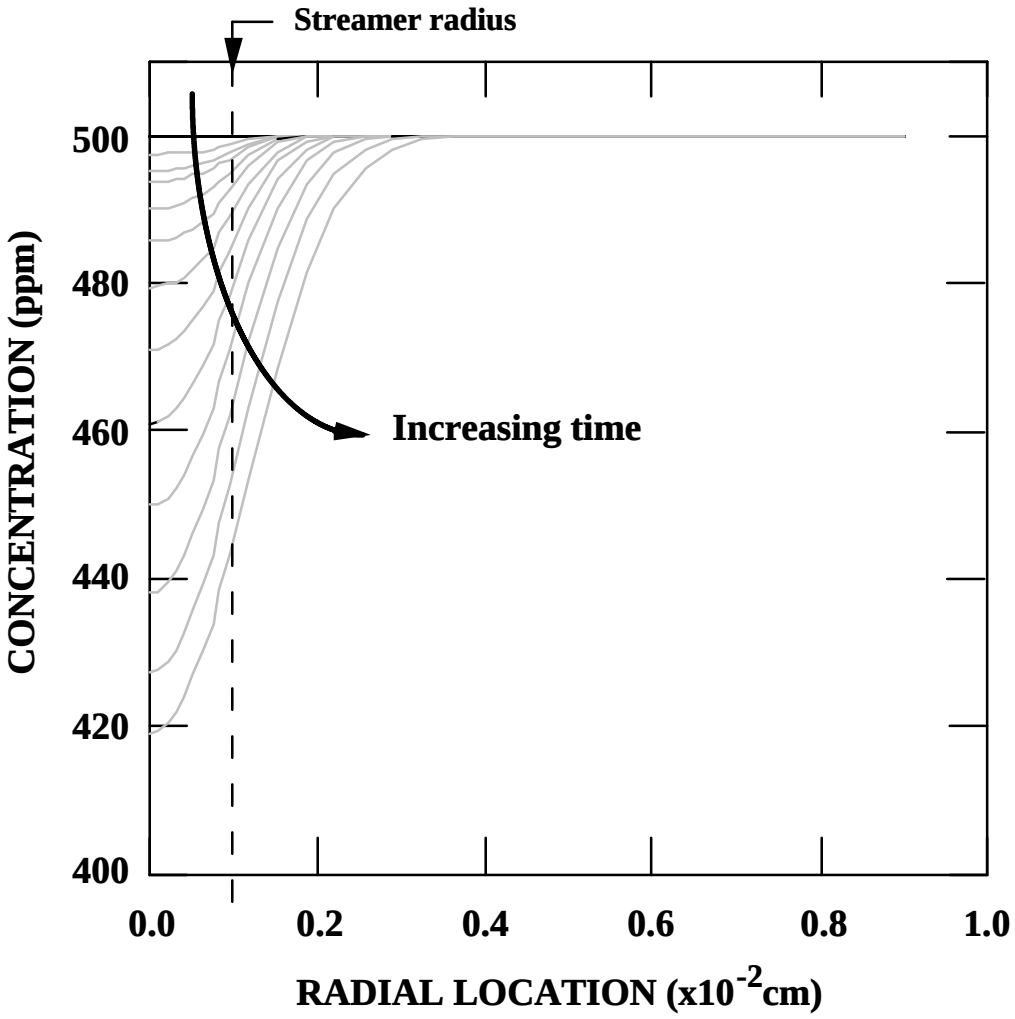

Fig. 5.6a. Behavior of N_XO_Y during the first pulse for the conditions of Fig 5.1. First figure in a series of 3. Curves in gray correspond to 10^{-9} s < t < 10^{-6} s. N_XO_Y is preferentially remediated in and near the streamer region due to NO remediation.

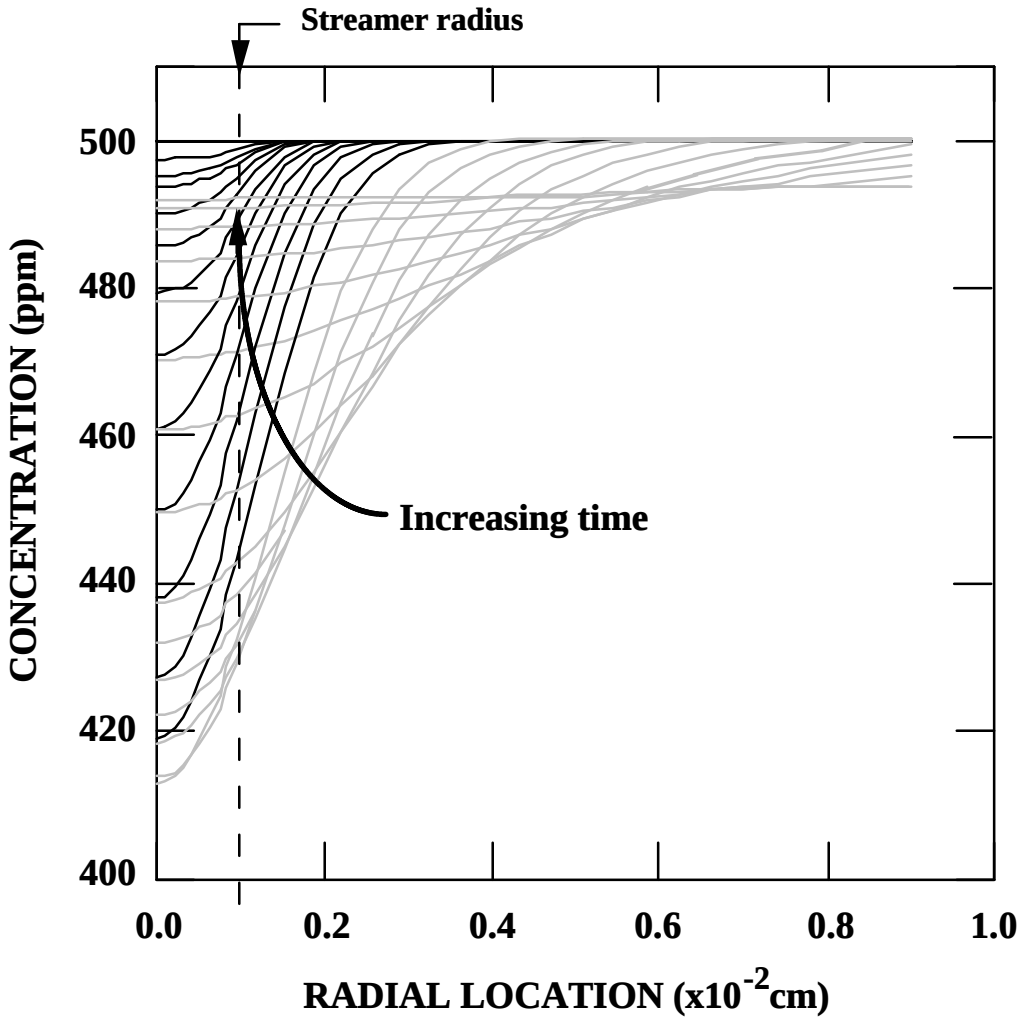

Fig. 5.6b. Behavior of N_XO_Y during the first pulse for the conditions of Fig 5.1. Second figure in a series of 3. Curves in gray correspond to 10^{-6} s < t < 10^{-4} s (i.e., PPRP end); curves in black correspond to the preceeding time period. Remediated region fills in as NO diffuses in and N_XO_Y products are created. N_XO_Y profile becomes level at PPRP end.

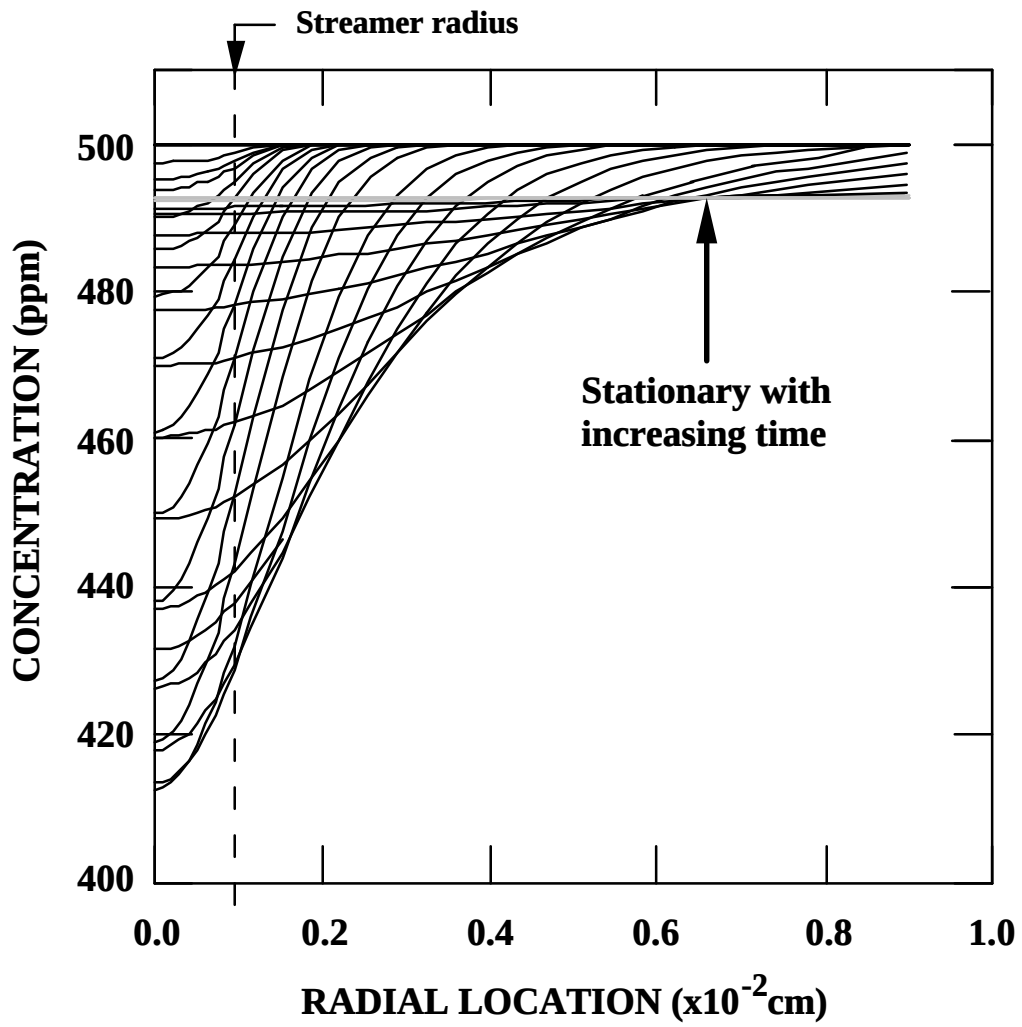

Fig. 5.6c. Behavior of N_XO_Y during the first pulse for the conditions of Fig 5.1. Third figure in a series of 3. Curves in gray correspond to t $>10^{-4}$ s (i.e., IP); curves in black correspond to all preceeding times. N_XO_Y profile is stationary since IP reaction does not change the total N_XO_Y concentration.

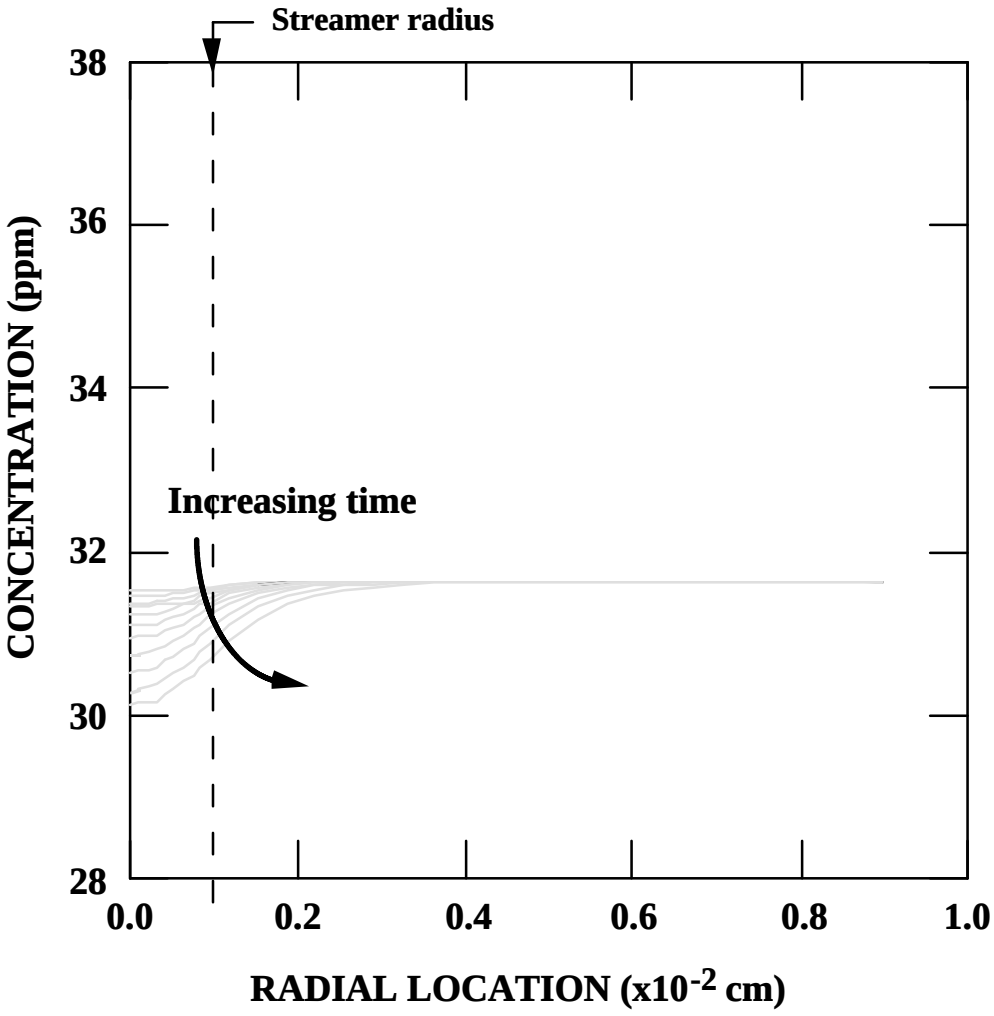

Fig. 5.7a. Behavior of NO_2 during the fifth pulse for the conditions of Fig 5.1. First figure in a series of 4. Curves in gray correspond to $t < 10^{-6}$ s. NO_2 initially decreases in the streamer region due to the "back reaction" Eq. 5.1. This reaction contributes significantly earlier in the 1-D case than in the 0-D since the primary radical N is located densely in and near the streamer region during its reactive times.

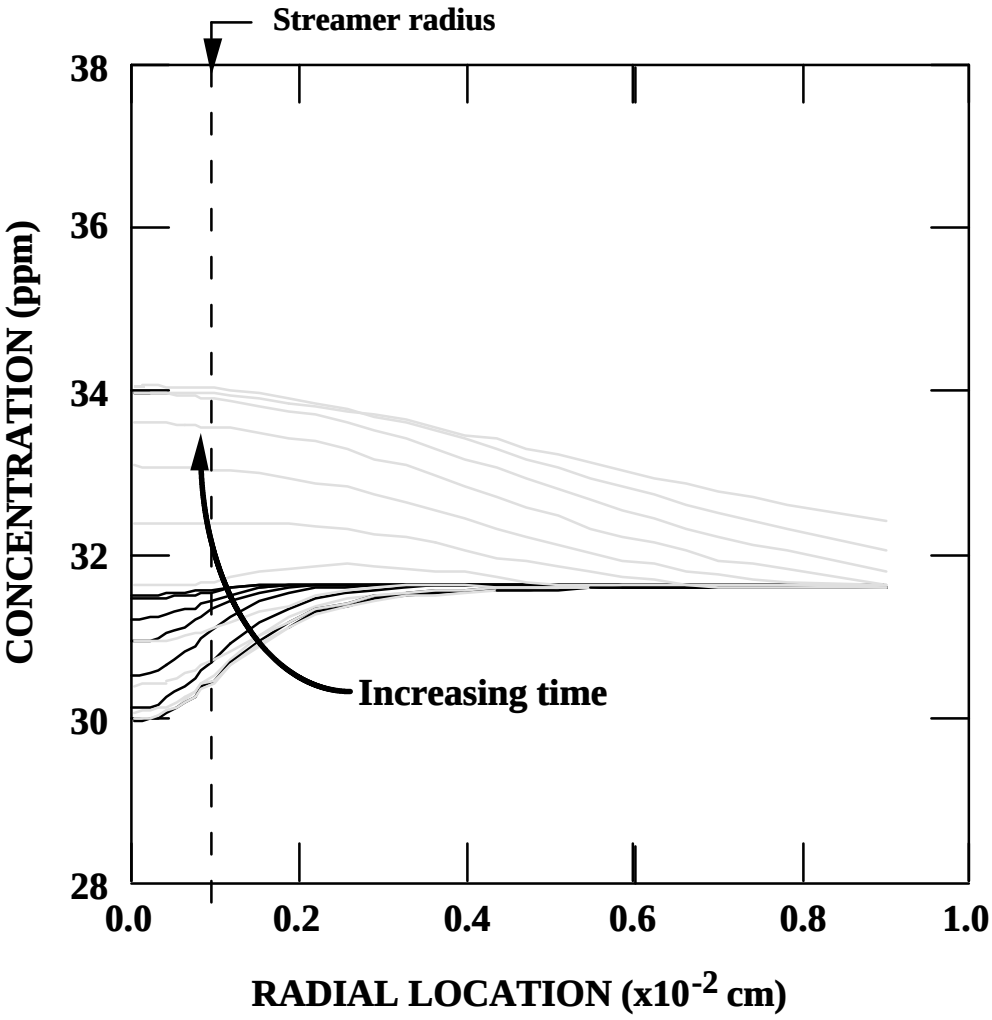

Fig. 5.7b. Behavior of NO_2 during the fifth pulse for the conditions of Fig 5.1. Second figure in a series of 4. Curves in gray correspond to 10^{-6} s < t < $5x10^{-5}$ s; curves in black correspond to the preceeding time period. NO_2 production from NO outweighs its destruction from the "back reaction". NO_2 accumulates and diffuses out.

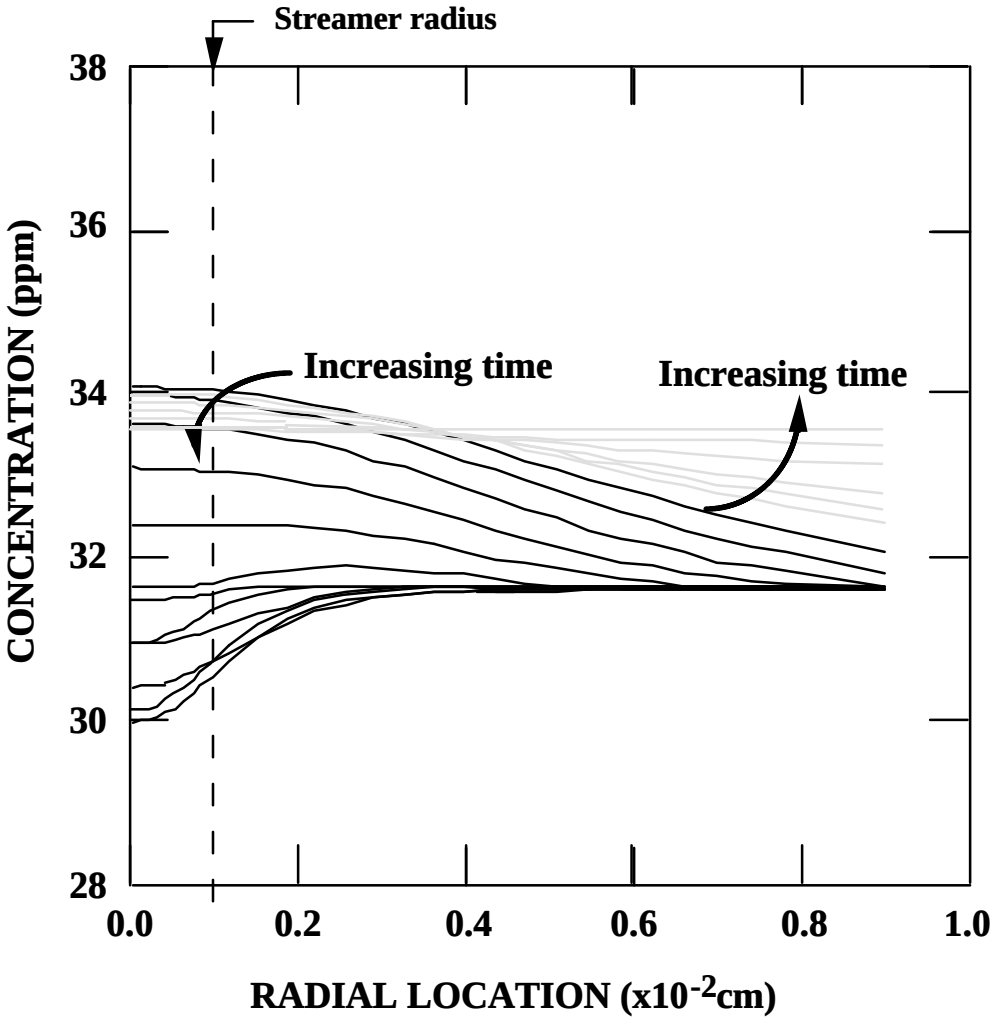

Fig. 5.7c. Behavior of NO_2 during the fifth pulse for the conditions of Fig 5.1. Third figure in a series of 4. Curves in gray correspond to $5x10^{-5}$ s < t < 10^{-4} s (i.e., PPRP end); curves in black correspond to all preceeding times. Diffusion levels out the profile.

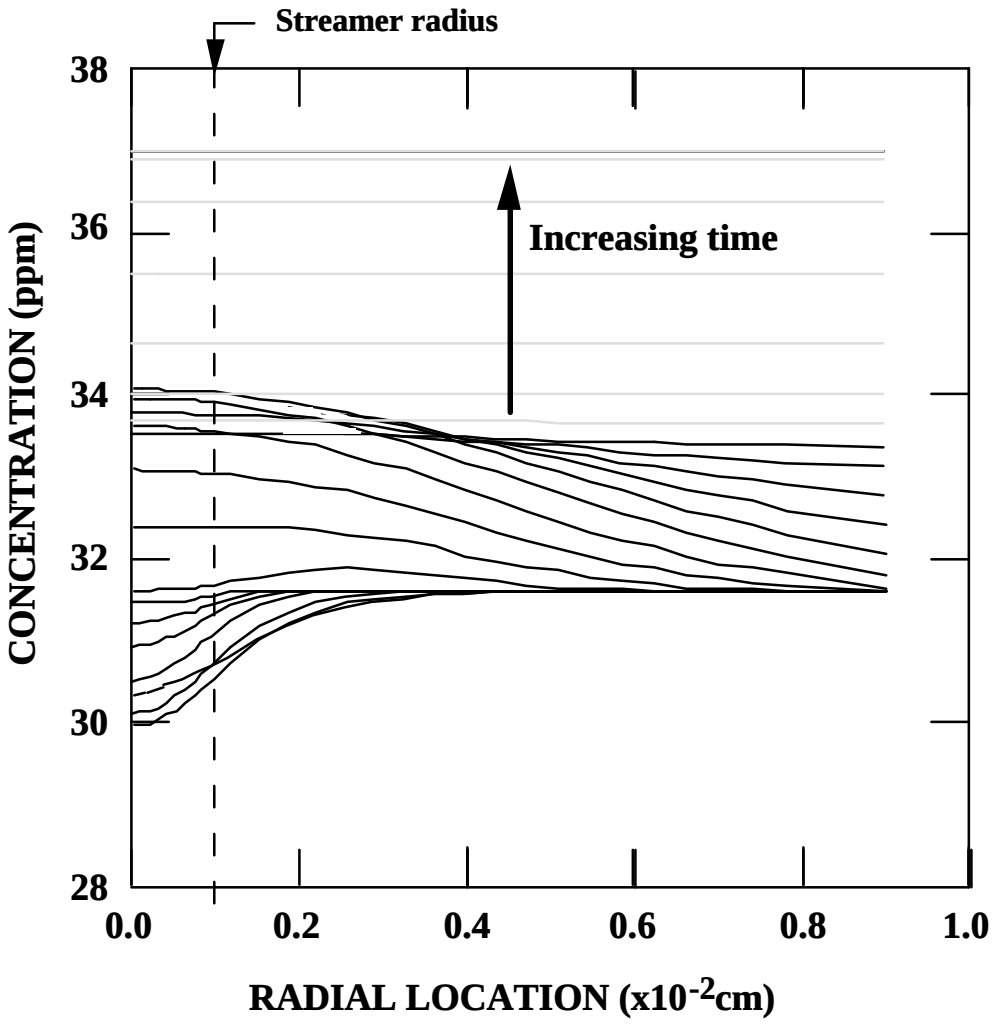

Fig. 5.7d. Behavior of NO_2 during the fifth pulse for the conditions of Fig. 5.1. Fourth figure in a series of 4. Curves in gray correspond to t $>10^{-4}$ s (i.e., IP); curves in black correspond to all preceeding times. NO_2 increases uniformly due to NO and O_3.

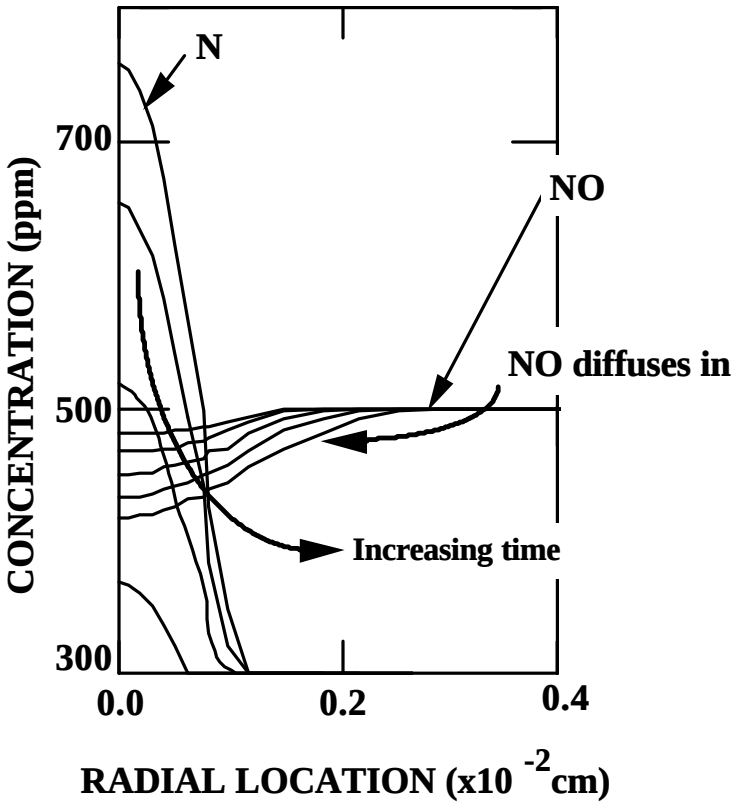

Fig. 5.8. 1-D contributions of N and NO to the N/NO ratio for 10^{-7} s < t < 10^{-6} s. N remains located in and near the streamer region with its concentration dropping off rapidly. Although NO is remediated in and near the streamer region, NO diffusion in during the same time period can keep the N/NO ratio small.

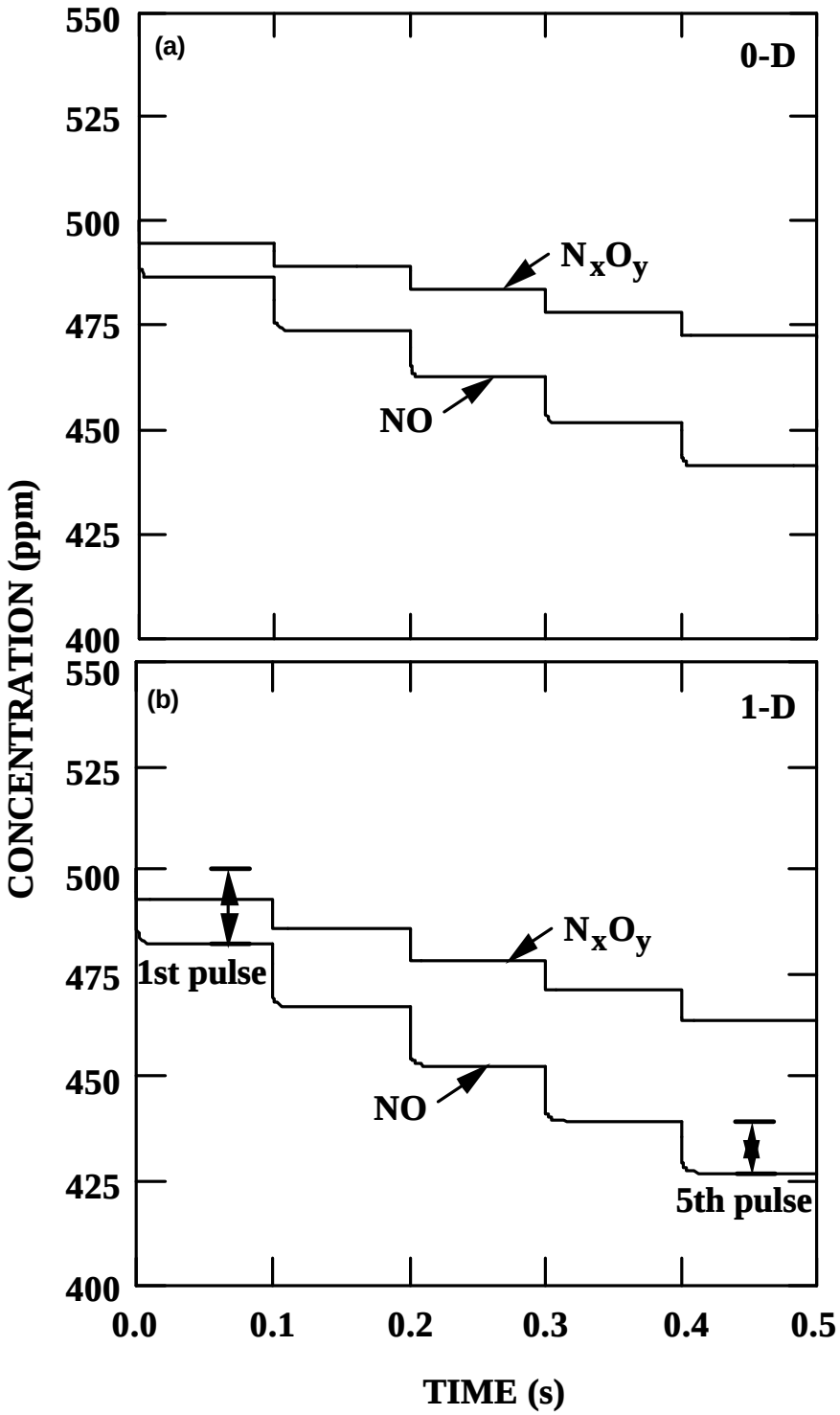

Fig. 5.9. NO and N_xO_y remediation. a) 0-D uniform densities, b) 1-D area weighted average densities. Remediation is greater for 1-D than for 0-D at low energy deposition and early pulses. 1-D remediation drops off with later pulses as net NO decreases and N/NO increases.

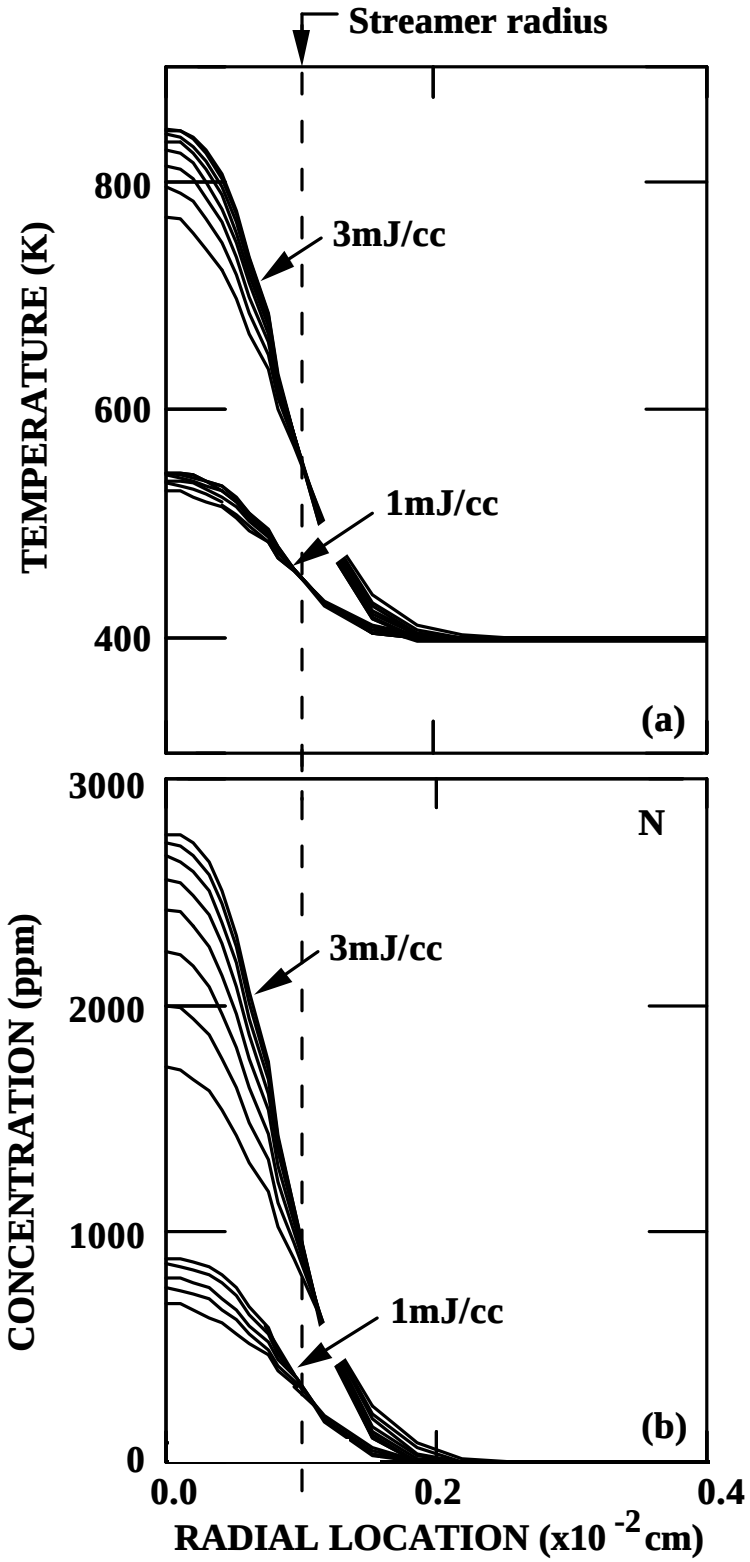

Fig. 5.10. Effects of localized energy deposition on a) temperature and b) N radical density (10^{-8} s < t < $2x10^{-7}$ s). Values are high in the streamer region. Both profiles are greater for higher energy deposition and peak in the streamer center with most of the drop-off occuring across the streamer.

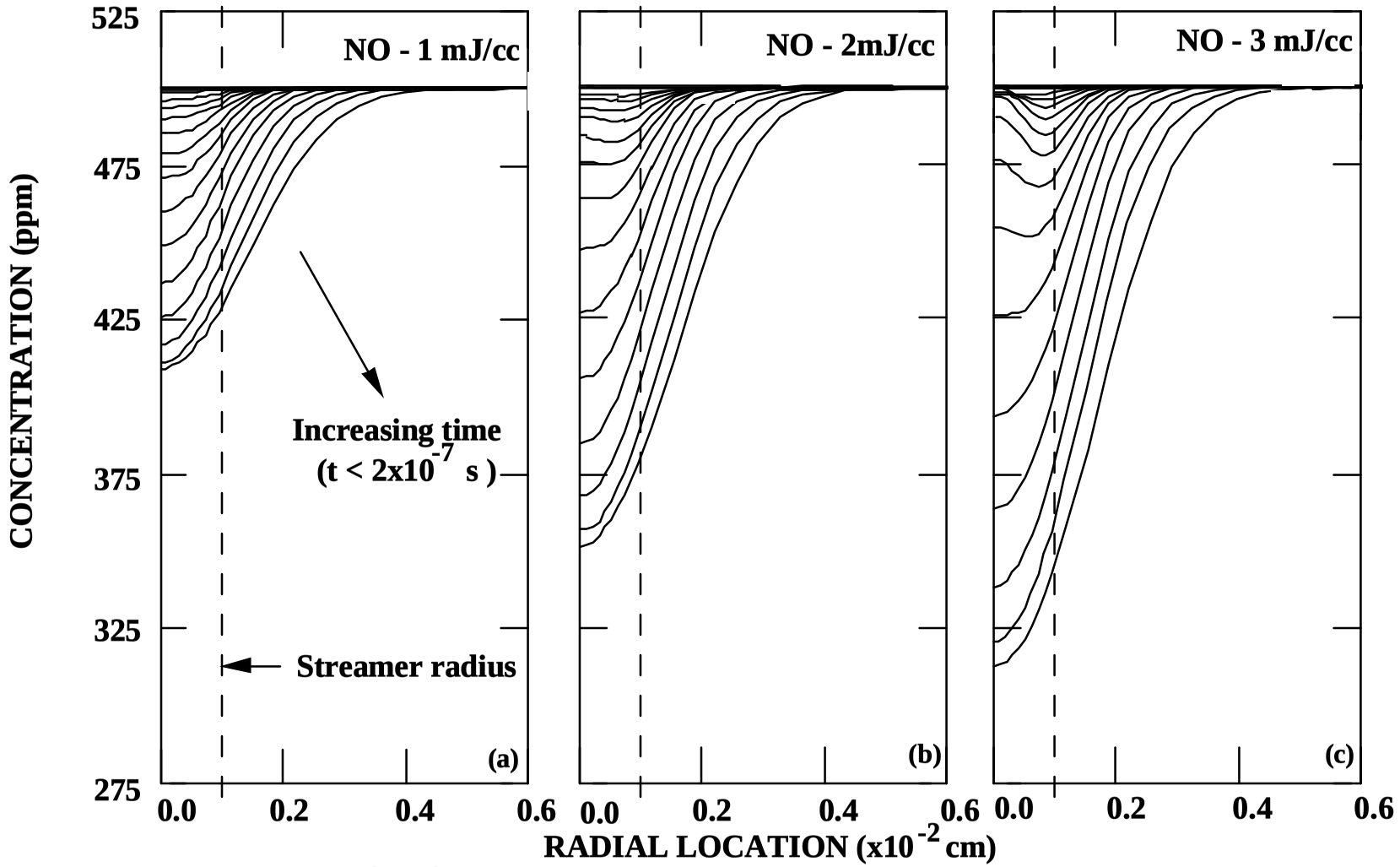

Fig 5.11 Early pulse remediation of NO for a) 1, b) 2, and c) 3 mJ/cc energy deposition. Higher temperatures and radical densities that result from larger energy deposition increase the rate of NO producing reactions with high activation energies. These effects are greatest in the streamer center, moving the point of greatest net remediation outward from at higher energy depositions.

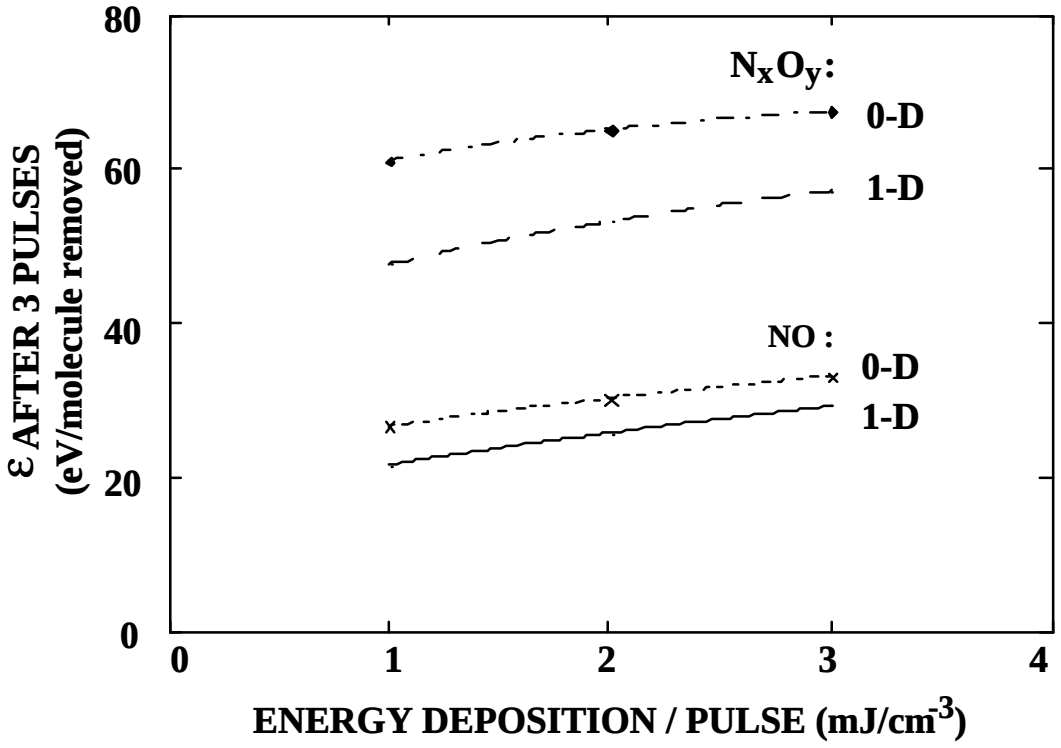

Fig. 5.12. 0-D and 1-D energy efficiency vs. energy deposition/pulse. For both 0-D and 1-D efficiency is lower with increasing energy deposition. 1-D is generally more efficient than 0-D due to transport (N/NO). This advantage in efficiency decreases at higher energy deposition due to enhanced non-remediative processes such as N + N —> N_2 and the "back reaction" N + NO_2 —> NO + NO (high localized radical concentrations), as well as N + O_2 —> NO + O (high activation energy).

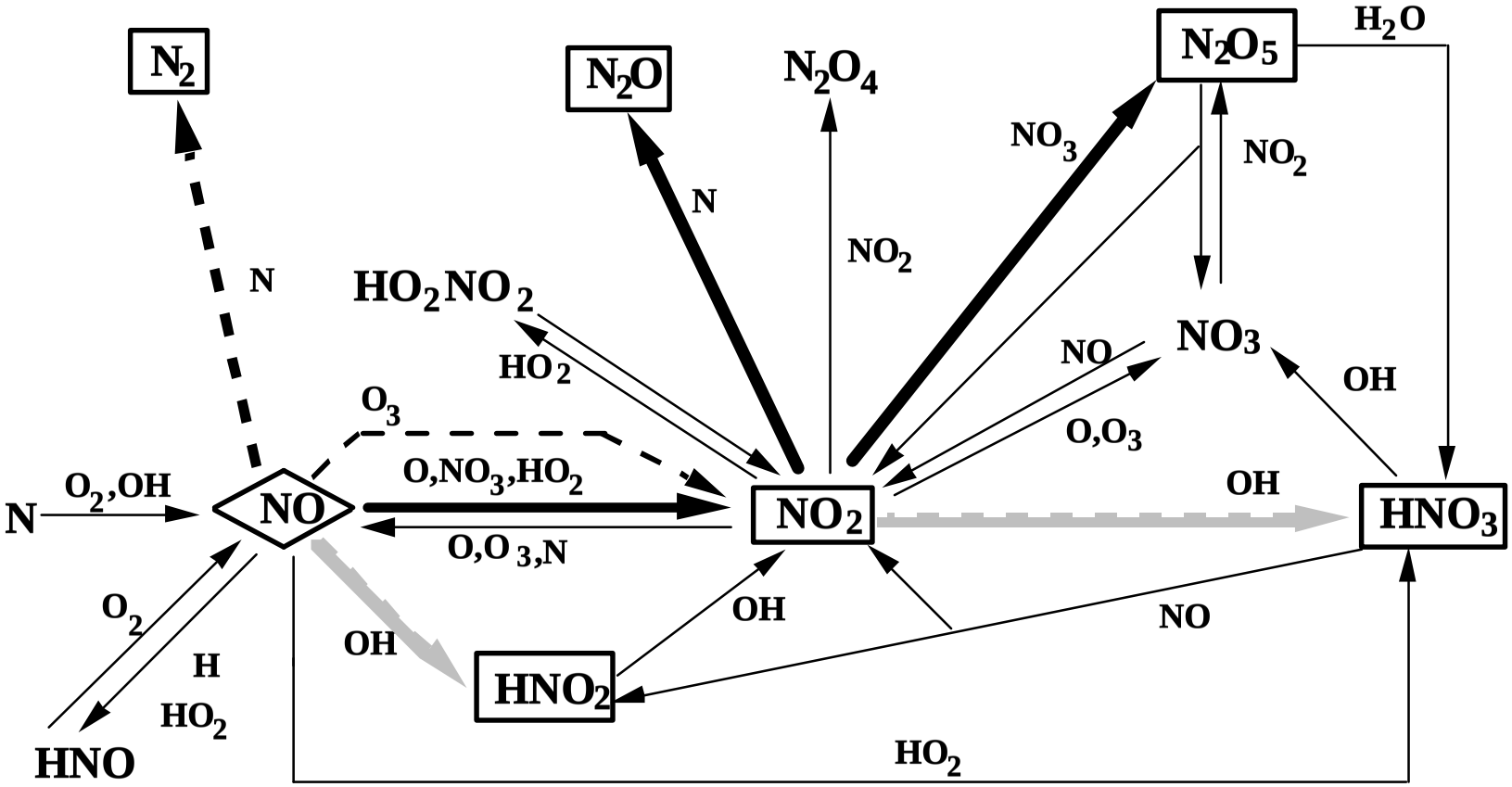

Fig. 5.13. Changes in the reaction scheme due to the addition of CO_2 . Of the non-N_xO_y producing reactions, those with OH producing HNO_x decrease (gray dashed); that with N producing N_2 increases commensurately (bold dashed). Of the N_xO_y product producing reactions, PPRP reactions are relatively unaffected because the effective amount of O is still large, and there are multiple available pathways (bold); the IP reaction converting NO to NO_2 decreases because the effective amount of O_3 is small (dashed).

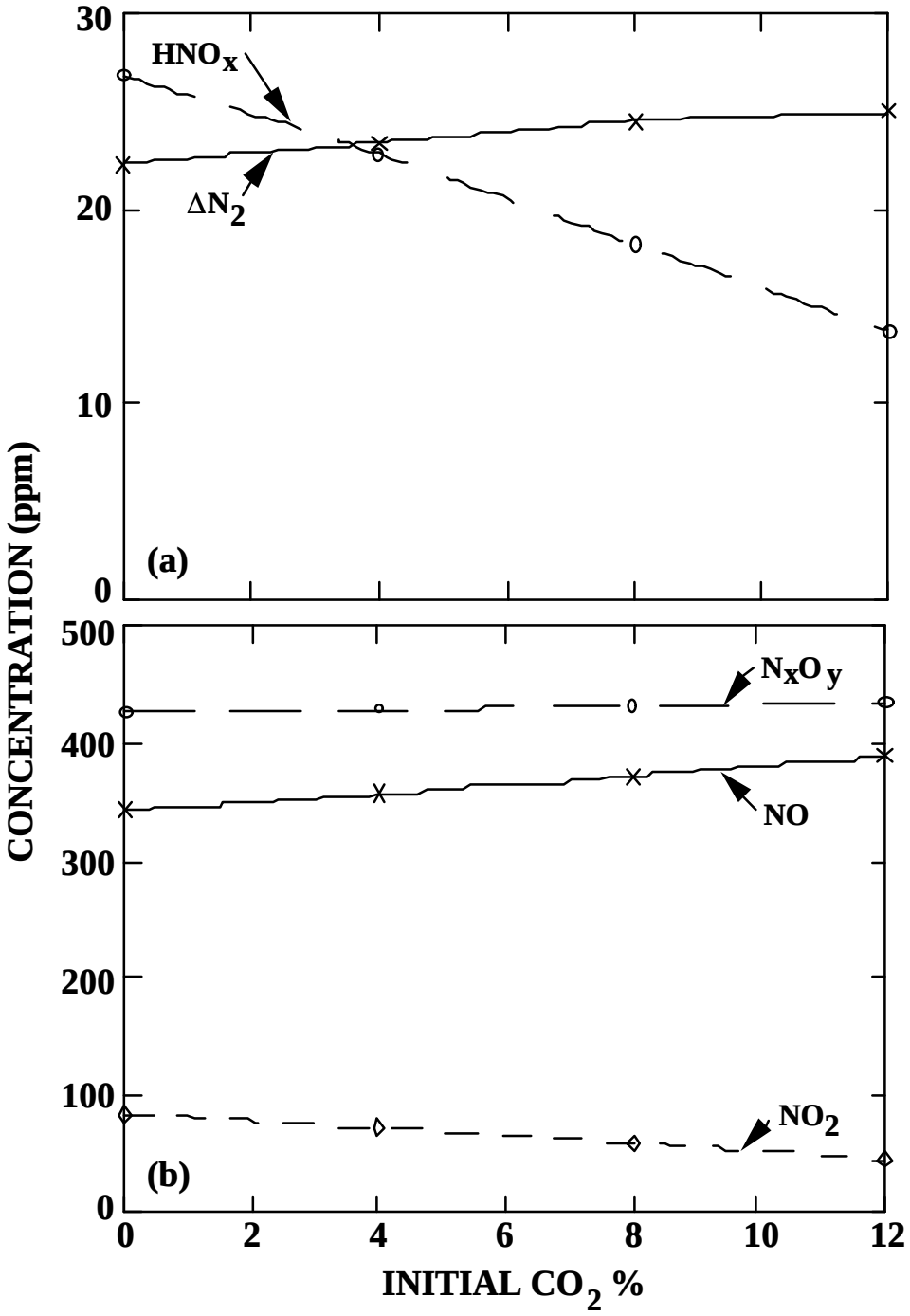

Fig. 5.14. Changes in product concentration with initial CO_2 concentration. a) increasing CO_2 decreases HNO_X produced and increases N_2 produced. b) NO —> NO_2 conversion decreases with increasing CO_2 so that NO remediation decreases, but total N_XO_Y changes only slightly.

6. REMEDIATION OF N_xO_y: DIFFUSIVE AND ADVECTIVE TRANSPORT

6.1 Introduction

In Chapter 5, we saw that spatial dependencies in remediation can affect the processes that occur during remediation, and, hence, affect the energy efficiencies obtained. In particular, high N/NO in the streamer region where the absolute density of N is large and high temperatures can lead to decreasing efficiencies since N will be increasingly used in non-remediative channels. It is therefore of interest to examine cases having high energy depositions, in which N radical formation and the temperature rise are large.

In Chapter 5, we investigated the spatial dependencies in remediation which resulted from including only diffusive transport. This simplification is appropriate only for low energy depositions where pressure gradients are small enough that advection is not important. In this chapter, then, we consider the effects of including both diffusive and advective transport using the model described in Section 2.3.

In Section 6.2, we discuss the general dynamics that occur as a result of high energy depositions, focusing on the mass density and temperature during and after the current pulse. In Section 6.3.1, we then examine the dynamics of the individual species densities that occur due to inclusion of the advective transport and compare them to those obtained from the lower energy deposition, diffusive transport only case of Chapter 5. In Section 6.3.2, we show that advective transport is necessary to more accurately represent the dynamics of the system by examining the behavior of a high energy deposition case artificially constrained to diffusive transport only. We examine the effects of energy deposition on efficiency as a result of including the advective transport in Section 6.4. Concluding remarks are in Section 6.5.

6.2 Mass Density and Temperature

In this section, we consider the general dynamics of the system, focusing on the mass density and the temperature. Temporal and spatial dependencies of these quantities due to the inclusion of advective transport will result in significant changes to the remediation process as compared to that obtained from considering diffusive transport only.

To better resolve the processes occurring during the pulse, we have expanded the streamer radius from 10 μm, used in Chapter 5, to 30 μm. In order to avoid any complications of edge effects that might arise due to the larger streamer radius, we have increased the block radius from 0.01 cm to 0.4 cm. The standard case used in this chapter is the same as that used in Chapter 5 ($N_2/O_2/H_2O$ = 85/5/10, 500 ppm NO, 400 K initial, 10 kV, and 10 Hz) with the exception that the energy deposition has been changed from 1 mJ/cm^3/pulse to 5 x 10^{-2} mJ/cm^3/pulse. The change in volumes of the streamer and the block prohibits a direct comparison between these figures. A more useful figure for comparison is the energy deposition into the streamer volume. For the standard case of Chapter 5, this corresponds to 127 mJ/cm^3/pulse, and for the standard case of this chapter, 1131 mJ/cm^3/pulse.

For computational stability, the number of mesh points is larger and the time steps smaller when including advection. Due to the resulting increased computational time required, we have decreased the number of species in the model to include only those directly involved in the major remediation pathways, by-products from those pathways, and by-products from the radical production. A list of the species in this reduced set is given in Table 6.1. Furthermore, we limit the discussion to the first pulse only.

During the pulse, the temperature increases in the streamer region. The resulting pressure gradient generates an advective velocity which forces mass out of the streamer region. This conversion of the thermal energy of the gas into kinetic energy results in a peak

temperature rise roughly the same as that obtained in the standard case of Chapter 5, despite the increased energy deposition into the streamer region. The temperature, mass density, and mass flux (mass density x velocity) during the pulse (roughly 2 x 10^{-8} s) are shown in Fig. 6.1a-c, respectively. Unlike the diffusion-only cases, the movement of the hot mass out of the streamer region, results in significantly increased temperature at regions noticeably outside of the streamer region. Mass moving out of the streamer region forms a front of increased density outside of the streamer. The mass flux becomes greatest just outside of the streamer edge due to a combination of the larger temperature gradient there and the increased mass density. During these times, all mass movement is out of the streamer.

These same quantities are shown in Figs. 6.2a-c for times shortly after the cessation of the pulse. Quantities from the pulse end to 5 x 10^{-8} s are shown in gray. Quantities during the pulse are shown in black, for contrast. Once the energy deposition has stopped at the end of the pulse, the temperature begins to decrease. Mass continues to move radially outward due to both inertia and the still negative pressure gradient. The end result is a rarefaction wave.

Once the temperature has decreased sufficiently by conduction and expansion, the behavior of the system changes notably. Gas temperature, mass density, and mass flux are shown in Fig. 6.3a-c from 5 x 10^{-8} s to 2 x 10^{-7} s. The decrease in temperature and reversal of the pressure gradient cause mass in and near the streamer region to move radially inward. The mass density in the streamer region reaches a minimum at 1 x 10^{-7} s and then begins to rise. Backward movement of the mass into the streamer region causes the mass flux at larger radii to decrease. Mass in the wave nearest the streamer beings to move backward, while that in the front of the wave continues to move outward. The finite propagation time of the backward movement of the mass density during these times can be

seen in Fig. 6.3c. This results in a local minimum in the mass density and temperature profiles at the near edge of the wave.

The backward motion of the mass into the streamer region, the viscosity of the gas acting on the forward motion of the streamer, and the differential in temperature, and thus internal energy, across the wave widen and flatten the wave. The outward motion and dissipation of the wave is shown in Fig. 6.4 for times between 5×10^{-8} s and 2×10^{-6} s. The streamer region fills in due to diffusion and the remaining cooling of the core and backstreaming of the gas. This is shown from 3×10^{-6} s to 1×10^{-1} s in Fig. 6.5a. Advective motion at long times is mainly limited to small acoustic waves which propagate back and forth throughout the gas. These are shown for distances far from the streamer region from 1×10^{-5} s to 1×10^{-3} s in Fig. 6.5b. The amplitude of these waves is small compared to the absolute density of the gas and they do not contribute significantly to changes in the gas density at these times.

6.3 Spatial Dependencies in Remediation due to Inclusion of Advective Transport

In Chapters 4 and 5, we showed that the remediative process can be discussed in terms of three time regimes: Pulse, Post Pulse Remediative Period (PPRP), and Interpulse (IP). Primary radicals are produced during the Pulse. NO and N_xO_y are remediated during the PPRP. NO is converted to NO_2 during the IP. The major reactions in the remediative process that determine the energy efficiency of remediation are:

PPRP reduction reaction:

$$NO + N \rightarrow N_2 + O \qquad (6.1)$$

N-N reassociation reaction:

$$N + N + M \rightarrow N_2 + M \qquad (6.2)$$

IP reaction:

$$NO + O_3 \rightarrow NO_2 + O_2 \quad (6.3)$$

"back reaction":

$$NO_2 + N \rightarrow NO + NO \quad (6.4)$$

NO producing, high activation energy reaction:

$$N + O_2 \rightarrow NO + O \quad (6.5)$$

The PPRP reduction reaction (Eq. 6.1) is the major NO remediation pathway. The N-N reassociation reaction (Eq. 6.2) is the major competing process for N atoms. For large values of N/NO, N will largely reassociate; for small N/NO values significant percentages of N will be used in reduction. The IP reaction (Eq. 6.3) converts NO to NO_2 by reaction with the long lived secondary radical O_3 after the primary radicals (N, O, and OH) are depleted. After much of the NO has been remediated so that the NO and NO_2 densities are roughly of the same order of magnitude, this reaction combined with the "back reaction" (Eq. 6.4) can lead to the production of NO. At the high temperatures encountered during the pulse, NO can also be produced by the high activation energy reaction (Eq. 6.5).

Since the inclusion of advective transport affects both the temperature and the species densities, the times and locations at which each of these reactions are important can be different from those obtained when considering only diffusive transport. This will affect the resulting energy efficiency. We will therefore discuss the changes in the spatial dependencies in remediation that arise from including advective transport. In Section 6.3.1 we compare the full transport case with the standard case of Chapter 5 which has a lower energy deposition but roughly the same temperature rise. In Section 6.3.2 we will show that at high energy depositions inclusion of advective transport is necessary to accurately portray the dynamics.

6.3.1 Details of Remediation and Comparison with Diffusive Transport Only Remediation at Lower Energy Deposition

During the pulse electrons are formed in and near the streamer region (Fig. 6.6). Unlike the diffusion only cases discussed in Chapter 5, the electron density is significant outside of the streamer region. The increased energy deposition and longer pulse result in more ionization. Electrons move outside of the streamer as a result of both the advective transport of the ions and greater diffusion outward during the longer pulse. This results in production of N outside as well as inside the streamer. This is shown in Fig. 6.7a. NO decreases in and near the streamer region due to reactions with N as well as its advective motion outward (Fig. 6.7b).

For a short time after the pulse, N and NO decrease due to depleting reactions and advective motion outward. This is shown in Fig. 6.8, where densities during the pulse are shown in black and those from the end of the pulse to 8×10^{-8} s are shown in dark gray. Next, N consumption in the streamer region slows and the NO concentration rises due to the backward flux of mass into the streamer regions. Outside of the streamer region, a local minimum in the NO occurs for reasons similar to those for the mass density described above. N and NO during this time, from 8×10^{-8} s to 2×10^{-7} s, are shown in light gray in Fig. 6.8.

Despite the increase in the mass density in and near the streamer region after 2×10^{-7} s, the NO density continues to decrease until 1×10^{-5} s, principally due to reactions with the radicals. Reactions with the secondary radical O_3 as well as the primary radicals contribute to the decrease of NO during this time. Since the reactions with N and O_3 are significant in determining the efficiency, the details of their reactions with NO will be discussed in more detail below. Concentrations of N and NO during this time are shown in gray in Fig. 6.9. Previous densities are shown in black. Unlike the diffusion-only case of Chapter 5, NO is almost entirely removed from the streamer region during these times. This

near depletion of NO is due to the advective transport outward as well as to reaction with N. As a result, N radicals in the streamer region are not consumed as quickly by reactions with NO and can diffuse out to greater distances from the streamer region. Therefore N is no longer quite as localized in the streamer region as it was in the diffusion-only case. The significant N density outside the streamer region, due both to this greater diffusion as well as its initial creation there during the pulse, leads to greater remediation outside of the streamer than in the diffusion-only case.

After 1 x 10^{-5} s, NO fills back in and near the streamer region. This is shown in Fig 6.10 from times from 1 x 10^{-5} s until the end of the pulse. Details of the conversion of NO to NO_2 by the IP reaction (Eq. 6.3) are not discernible in the figure. However, evidence of this reaction can be seen in the behavior of the volume averaged densities of NO and N_xO_y, shown in Fig. 6.11. NO decreases on the same timescale previously attributed to the IP reaction, with no change in N_xO_y. (The increased volume of the gas results in fewer total ppm removed than in those cases considered in previous chapters and so a comparison of the absolute numbers is misleading. A more useful comparison is that of energy efficiencies and will be discussed in Section 6.4.) Since removal of NO during this time occurs over a large volume (as will be discussed in more detail below), the local removal is slight and therefore not apparent in Fig. 6.10.

The substantial depletion of NO in and near the streamer region between 1 x 10^{-6} s and 1 x 10^{-5} s leads to changes in the behavior of the density of NO_2 from that in the diffusion-only case. The density of NO_2 up until 1 x 10^{-6} s is shown in Fig. 6.12. At early times, NO_2 is predominantly produced from NO in and near the streamer region due to the high density of radicals there. By 1 x 10^{-6} s, NO is sufficiently depleted in the streamer region so that NO_2 production becomes greater at regions outside the streamer edge than within the streamer region. Eventually enough NO_2 is produced in the streamer region for it to compete with the reduced amount of NO for the N atoms. Thus, the “back reaction”

(Eq. 6.4) consumes NO_2 in the streamer region. This is shown in Fig. 6.13 where the density from 1 x 10^{-6} s to 1 x 10^{-5} s is shown in gray. The density of NO_2 for times less than 1 x 10^{-6} s is shown in black in this figure for contrast. Eq. 6.4 thus becomes significant even during the first pulse in the full transport case. This is different than the lower energy deposition, diffusion-only case of Chapter 5 where accumulation of NO_2 over several pulses is required for this reaction to be important.

During the same times, enough NO still remains outside of the streamer region to produce NO_2 there. Production occurs both through reaction with O by

$$NO + O + M \rightarrow NO_2 + M \qquad (6.6)$$

as well as with reaction with O_3 (Eq. 6.3). Densities of O and O_3 are shown in Fig. 6.14a and b, respectively. The density of O is shown for times between 1 x 10^{-6} s to 1 x 10^{-5} s. The density of O_3 is shown for times less than 1 x 10^{-5} s. As with N, a large density of O is produced during the pulse. The depletion of NO in the streamer region allows significant O_3 to build up without being consumed in and near the streamer region. Thus, Eq. 6.3 is seen to contribute to the production of NO_2 earlier than in the diffusion only case.

After 1 x 10^{-5} s, as NO begins to increase in the streamer region, the NO_2 is then produced in the streamer region again. Production by NO with the increasing O_3 density at larger radii increases the density of NO_2 farther out. NO_2 and O_3 from 1 x 10^{-5} s to 1 x 10^{-4} s are shown in Figs. 6.15 a and b, respectively.

Details of the production of NO_2 after this time are not well illustrated in the NO_2 profiles since the diffusive motion outward and the production are not easily separately distinguished. Once again, Fig. 6.11 provides evidence for the contribution of the IP reaction during this time. The O_3 concentration from 1 x 10^{-4} s to 1 x 10^{-1} s is shown in Fig. 6.16a. O_3 during this time is spread over a large region, resulting in small local

production of NO_2. (O_3 is not uniform across the discharge at these times as it was in the diffusion only case largely due to the increased volume.) The total amount of NO_2 produced is however, significant, as the volume averaged density of O_3 reaches its maximum during this time (Fig. 6.16b).

N_xO_y behaves much like NO since the conversion of NO to other N_xO_y products during the PPRP is slight and during the IP is locally small.

Despite the differences in the times and locations in the details of the remediation process for the full transport case as compared to the diffusion only case, the volume averaged NO and N_xO_y densities (Fig. 6.11) show the same general shape as that obtained in Chapters 4 and 5. The time scales for the PPRP and the IP are the same for all cases. Although the conversion of NO to NO_2 by Eq. 6.3 occurs early in the streamer region, conversion of NO_2 back to NO by Eq. 6.4 occurs early near the streamer region as well. Thus, the earlier onset of the IP reaction does not change the characteristics of the PPRP or cause the IP to start sooner. The PPRP end is still set by the primary radical lifetimes. These lifetimes are still approximately the same as those given in Chapter 4, since they are primarily determined by radical reassociation reactions and not remediation reactions. The vast majority of the conversion of NO to NO_2 still occurs during the IP by the long lived O_3.

The changes in the dynamics in remediation from the full transport case as compared to the lower energy deposition, diffusion-only case that will most likely affect energy efficiency are the peak temperature rise, through Eq. 6.5, and the increased motion of N outward and the depletion of NO in the streamer region through Eqs. 6.1 and 6.2.

In order to determine the extent of these changes that is due to advective transport, we next compare the full transport case to a case of identical conditions artificially constrained to diffusive transport only.

6.3.2 Comparison with Diffusive Transport Only Remediation for Equivalent Energy Deposition

In order to highlight the behavior that is due to the advection alone, we now consider a case for the equivalent geometry and energy deposition as above, but include only diffusive transport in the model. We will see that high energy deposition requires inclusion of the advective transport in order to accurately capture the dynamics of the system.

The temperature increase during the pulse for the diffusion-only case is shown in Fig. 6.17. Without the inclusion of advection allowing conversion of thermal energy into motion of the gas, the temperature increase is much higher. Thus NO is produced at early times in the streamer region by Eq. 6.5. The densities of N and NO for times less than 8 x 10^{-8} s are shown in Fig. 6.18. The rise of N during the pulse is suppressed in the figure for clarity.

After the pulse ends and the temperature has cooled sufficiently, significant amounts of NO are removed from the streamer region. N and NO are shown for times less than 1 x 10^{-5} s in Fig. 6.19. The rise of N during the pulse is again suppressed. Although the NO depletion appears similar to the decrease in density in the full transport case, here NO is not subject to advective transport out of the high temperature region. Thus the decrease in the streamer region is entirely due to reactions with the radicals. The N density profile has a slightly greater width in the full transport case (Fig. 6.9a) and drops off more quickly at early times due to the advective motion outward. Likewise, more NO is removed from regions outside the streamer in the full transport case (Fig. 6.9b) than in the diffusion-only case due to the advective transport of NO outward and consumption with the greater N density there. (The production of NO during the pulse of the diffusion-only case also contributes to this effect.) This behavior is more significant at early times when the advective transport is greatest.

Inclusion of advective transport is thus necessary to obtain accurate representation of the temperature rise and the motion of N outward at high energy depositions. The depletion of NO in the streamer region is exhibited in both the diffusion-only and the full transport cases since it is largely due to the remediation reactions with the high density of radicals produced in the streamer region. However, it is necessary to include advective transport to capture the early motion of NO and the radial extent over which NO is depleted. Correct representation of the temperature and the behavior of N and NO is important in determining the energy efficiency as will be discussed in more detail in the next section.

6.4 Energy Deposition and Efficiency

As was discussed in Chapter 5, spatial dependencies in remediation will affect the energy efficiency. Of particular interest were the increase in temperature due to the localized energy deposition increasing production of NO by Eq. 6.4 and the local N/NO ratio in the gas determining the N radical usage through the competing processes of Eqs. 6.1 and 6.2. We examine how these quantities change for varying energy depositions in the full transport case, and how they vary from the diffusion-only case.

The temperature increase for an energy deposition of 7.5×10^{-2} mJ/cm^3/pulse is shown in Fig. 6.20. N and NO during the pulse time ($t < 2.7 \times 10^{-8}$ s) are shown in Fig. 6.21. The increase in temperature and N production over the lower energy deposition case of Section 6.3.1 result in production of NO in the streamer region.

After this initial NO production, the system behaves much the same as the standard case, with the details being somewhat enhanced. That is, N moves farther out of the streamer region and NO is depleted more in the streamer region. Thus, more N is available to react with NO in regions outside the streamer where the NO is not as significantly depleted so that NO is removed over a larger area. N and NO for times less than 1×10^{-5} s

are shown in Fig. 6.22. The rise in N during the pulse time has been suppressed. Remediation is thus increased with *increasing* N/NO in the bulk gas since the absolute density of N there is small, and so reassociation of N (Eq. 6.2) is slight, and with *decreasing* N/NO in the streamer region since the absolute density of N there is large, favoring reassociation.

The increased temperature producing NO and the more favorable N/NO ratio as N moves farther out from the streamer region into the bulk gas are competing processes in remediation that affect the energy efficiency. This is shown in Fig. 6.23. The efficiency parameter, ε, is defined as in previous chapters as (energy deposition in eV) / (NO or N_xO_y molecule removed). Thus, lower ε is more efficient. As in Chapters 4 and 5, removal is generally less efficient at higher energy depositions. However, the instantaneous rate of change of ε with energy deposition is less at higher energy depositions due to the increased transport. This outweighs the production of NO due to the increased temperature.

The efficiency for the standard case of this chapter is, of course, worse than that obtained for the Chapter 5 case since this case has a higher energy deposition in the streamer region. However, the efficiency for this case is higher than that obtained for the diffusion-only, equivalent energy deposition case of Section 6.3.2. For that case, ε is 55 eV/molecule for NO and 116 eV/molecule for N_xO_y. The higher temperature rise and lack of transport of N outward decrease the efficiency obtained for that case.

6.5 Concluding Remarks

Inclusion of advective transport is necessary to more accurately portray the dynamics of remediation for cases of higher energy deposition. In such cases, conversion

of thermal energy to kinetic energy restrains the temperature in the streamer region. Motion of mass out of the streamer allows for significant N density outside of the streamer. NO is nearly depleted in the streamer region due to the advective motion outward and its reaction with radicals. The lower temperature and more favorable N/NO ratio in the bulk gas result in greater energy efficiencies for the full transport case than for an equivalent case with inclusion of diffusive transport only.

Despite the changes in the location of radicals and NO in the full transport case from the diffusion-only cases of lower energy deposition, volume averaged profiles of NO and N_xO_y show generally the same behavior on the same timescales as in the diffusion-only case. Radical lifetimes that determine the PPRP and IP timescales are roughly the same as in the diffusion-only cases. NO to NO_2 conversion by O_3 at early times is small compared to that occurring over larger distances during the IP.

Energy efficiency decreases with increasing energy deposition. The instantaneous rate of change of efficiency decreases at higher energy depositions due to the increased transport improving the N/NO ratio. This offsets the increased production of NO at higher temperatures.

H	HNO_3	$N_2(A)$	O^-
H^+	HO_2	N_4^+	$O(^1D)$
H^-	HO_2NO_2	N_2O	OH
H_2	N	N_2O_5	O_2
H_2^+	$N(^2D)$	NO	O_2^+
H_2O	N^+	NO_2	$O_2^+ \cdot H_2O$
H_2O^+	NH	NO_3	O_2^-
HNO	N_2	O	O_3
HNO_2	N_2^+	O^+	

Table 6.1. List of species used in the reduced reaction set. Reactions are used are those in Appendix B pertaining to these species.

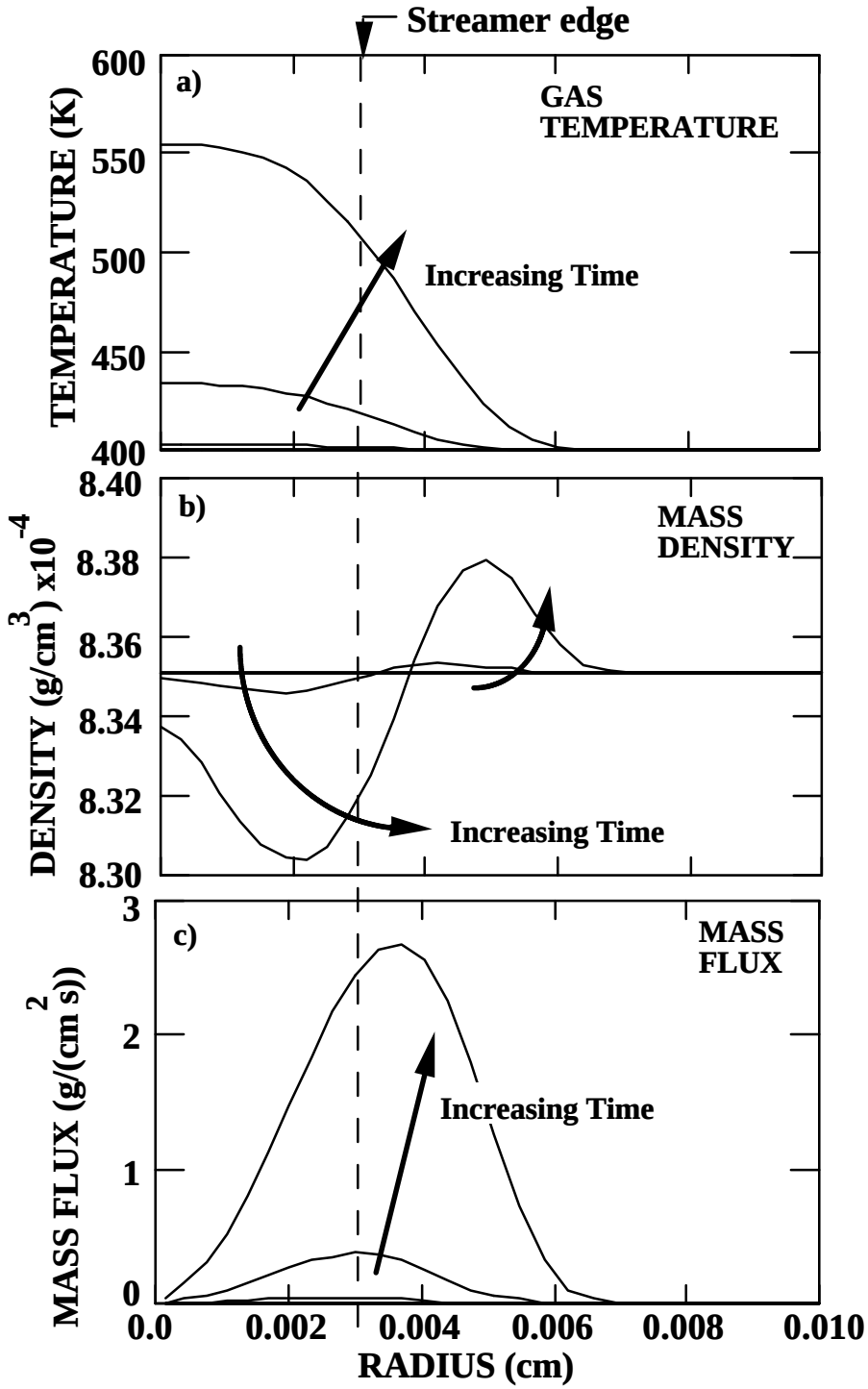

Fig. 6.1a) Temperature, b) mass density, and c) mass flux during the pulse. Initial conditions are the same as those of Chapter 5 with the exception of the energy deposition/pulse which is now 5 x 10^{-2} mJ/cm^3 averaged over the entire volume and 1131 mJ/cm^3 (as opposed to 127 mJ/cm^3) averaged over the streamer. The temperature is increased outside the streamer region due to the motion of mass outward. A front of high mass density forms outside the streamer region. The mass flux is greatest outside the streamer edge due to the larger temperature gradient and increased mass density there.

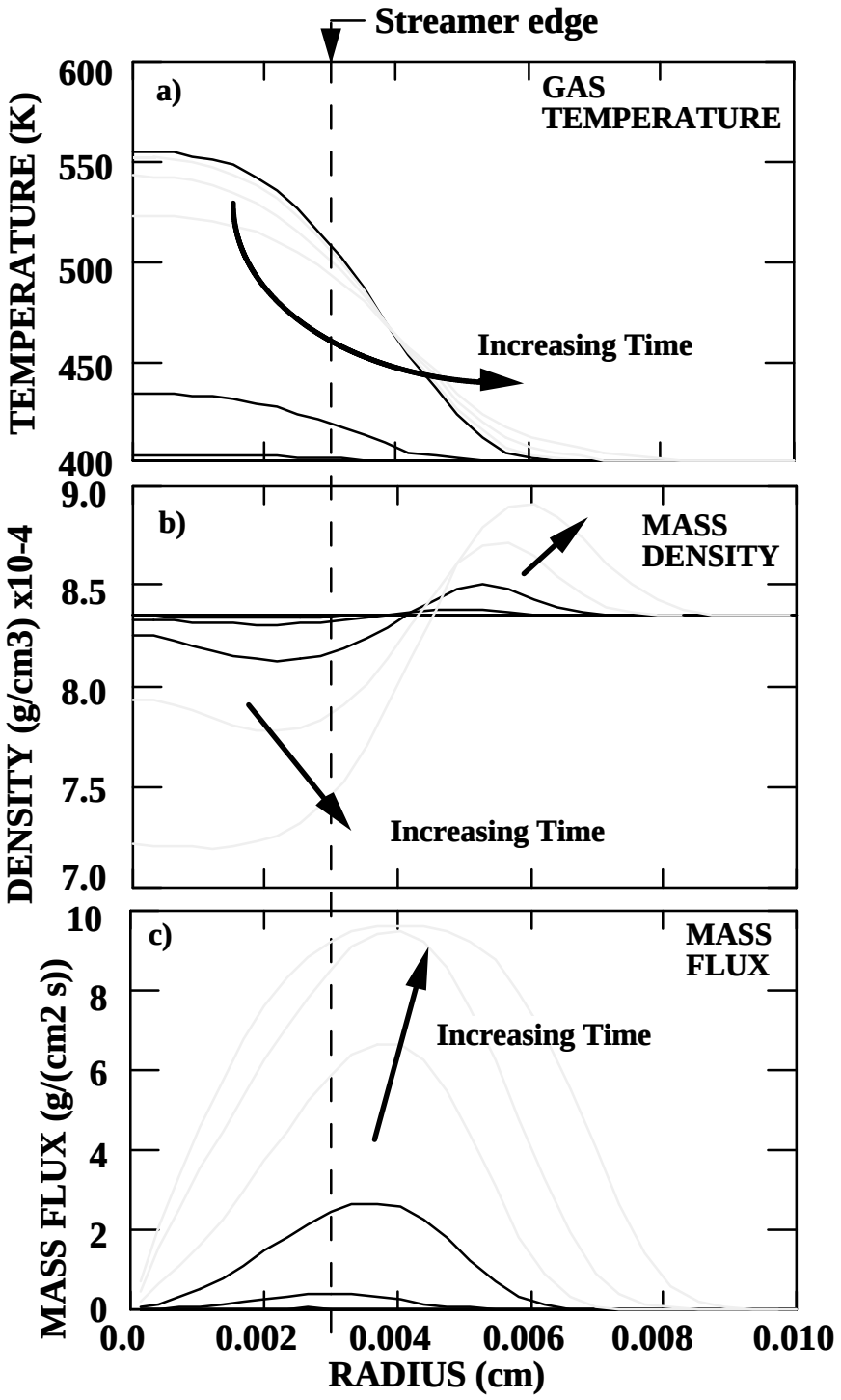

Fig. 6.2 a) Temperature, b) mass density, and c) mass flux. Behavior during the pulse is shown in black. Behavior from the pulse end to 5 x10^{-8} s is shown in gray. The temperature begins to drop after the energy deposition has stopped. Mass continues to move outside the higher temperature regions. The mass flux of the mass front is positive, resulting in motion of the front outward from the streamer center producing a rarefaction wave.

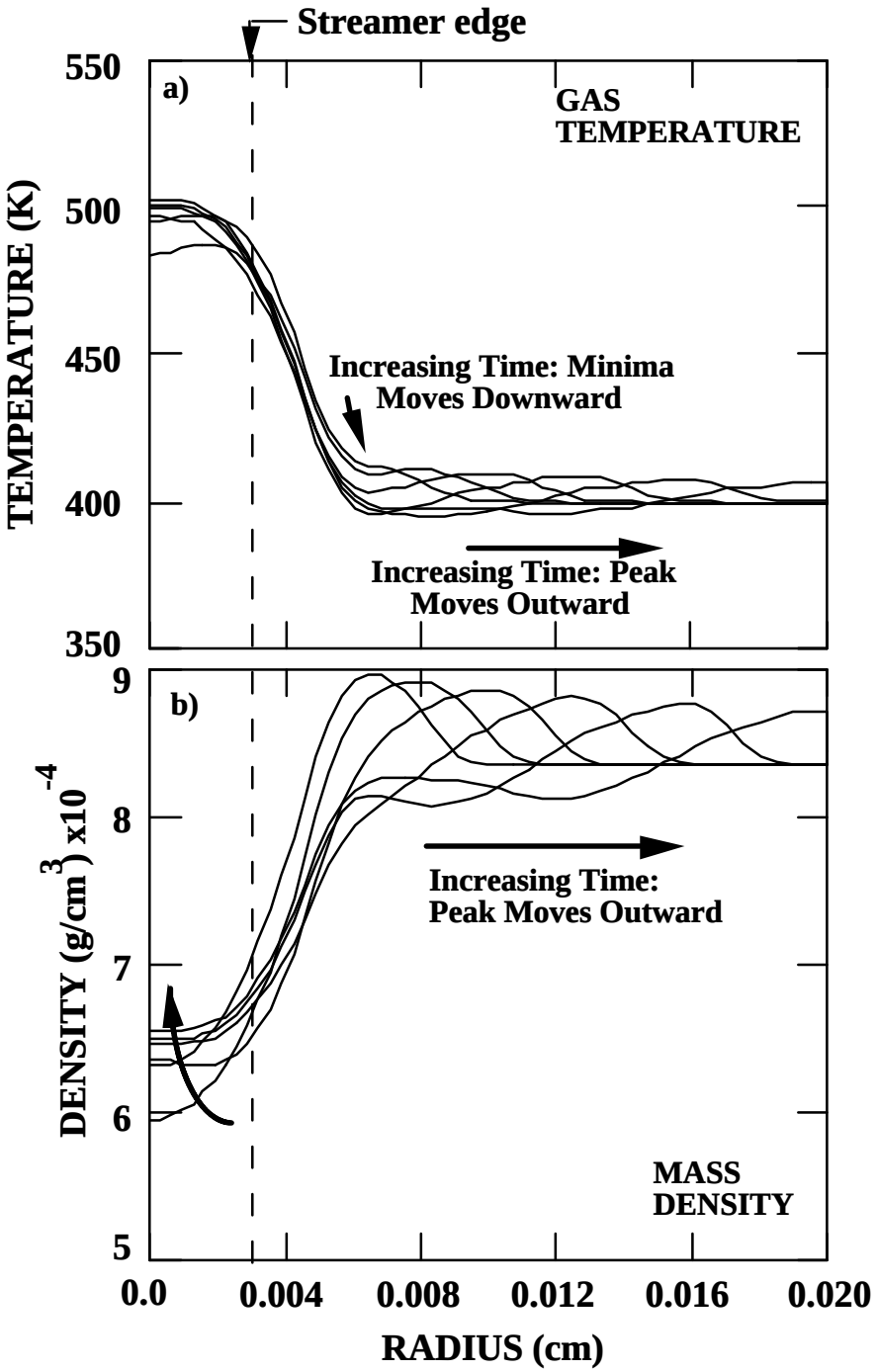

Fig. 6.3 a) Temperature and b) mass density shown from 5 x 10^{-8} s to 2 x 10^{-7} s for the conditions of Fig. 6.1. The decrease in temperature and reversal of the pressure gradient cause mass to move radially inward. The mass density in the streamer region reaches a minimum at 1 x 10^{-7} s. Backward motion of the mass causes a local minimum to form in the mass density and temperature at the near edge of the wave.

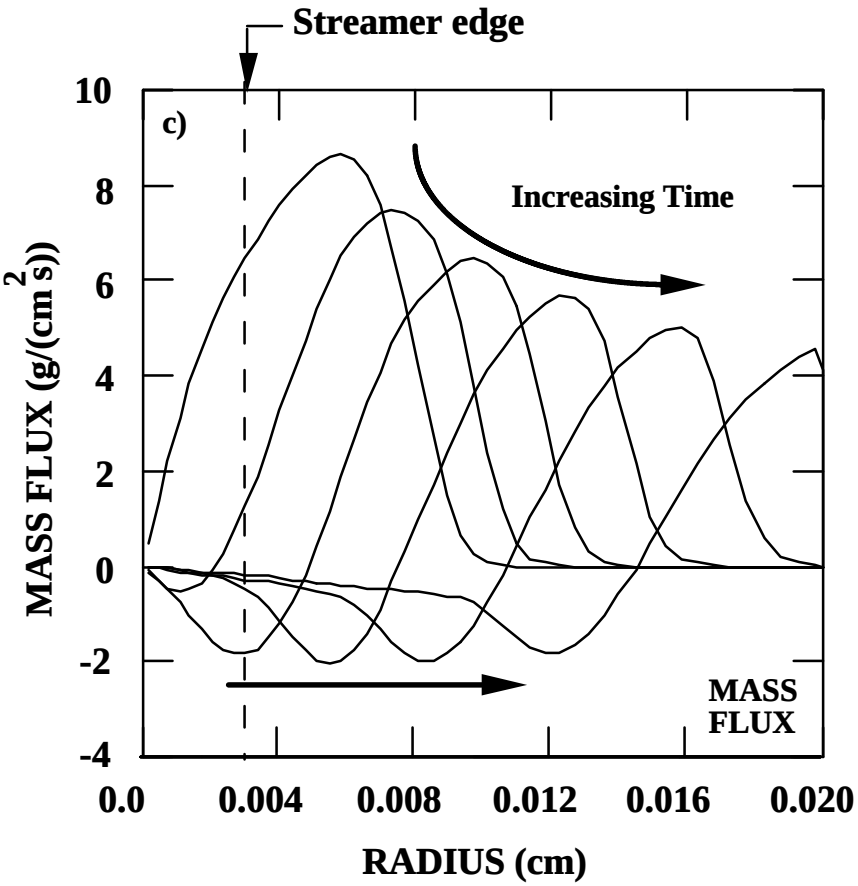

Fig. 6.3c. Mass flux shown from 5 x 10^{-8} s to 2 x 10^{-7} s for the conditions of Fig. 6.1. The decrease in temperature and the reversal of the pressure gradient result in mass flux back into the streamer region . Negative values of the mass flux at the edge of the wave cause the local minimum in the wave at the near edge of the streamer.

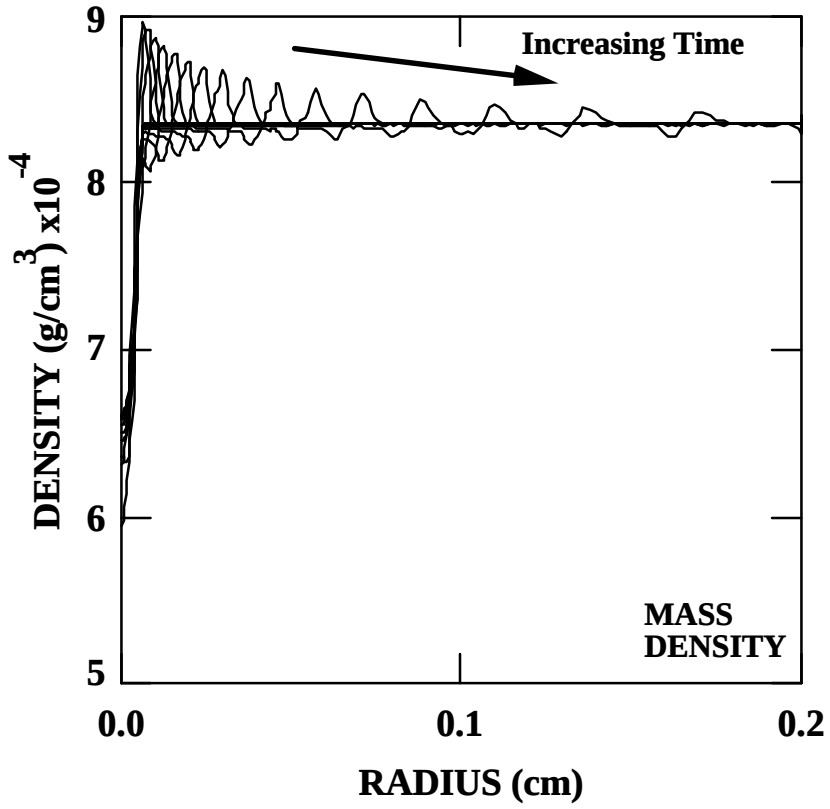

Fig. 6.4. Mass density from 5 x 10^{-8} s to 2 x10^{-6} s for the conditions of Fig. 6.1. The rarefaction wave moves out and dissipates.

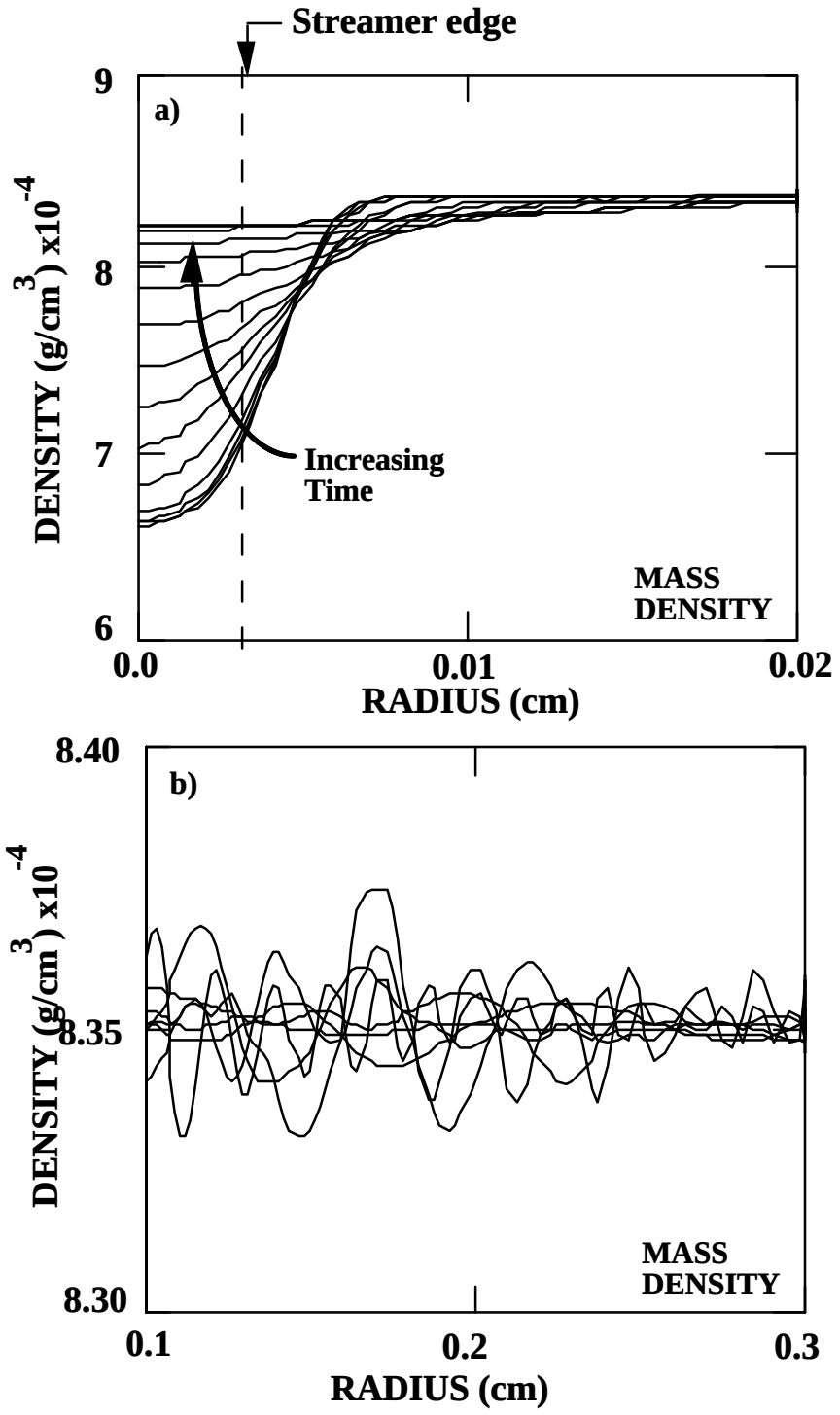

Fig. 6.5 a) Mass density from 3 x 10^{-6} s to 1 x10^{-1} s for the conditions of Fig. 6.1. Mass density in the streamer region fills in. b) Mass density from 1 x 10^{-5} s to 1 x 10^{-3} s at regions far from the streamer. Advective motion at long times is limited to small acoustics waves which propagate back and forth throughout the gas.

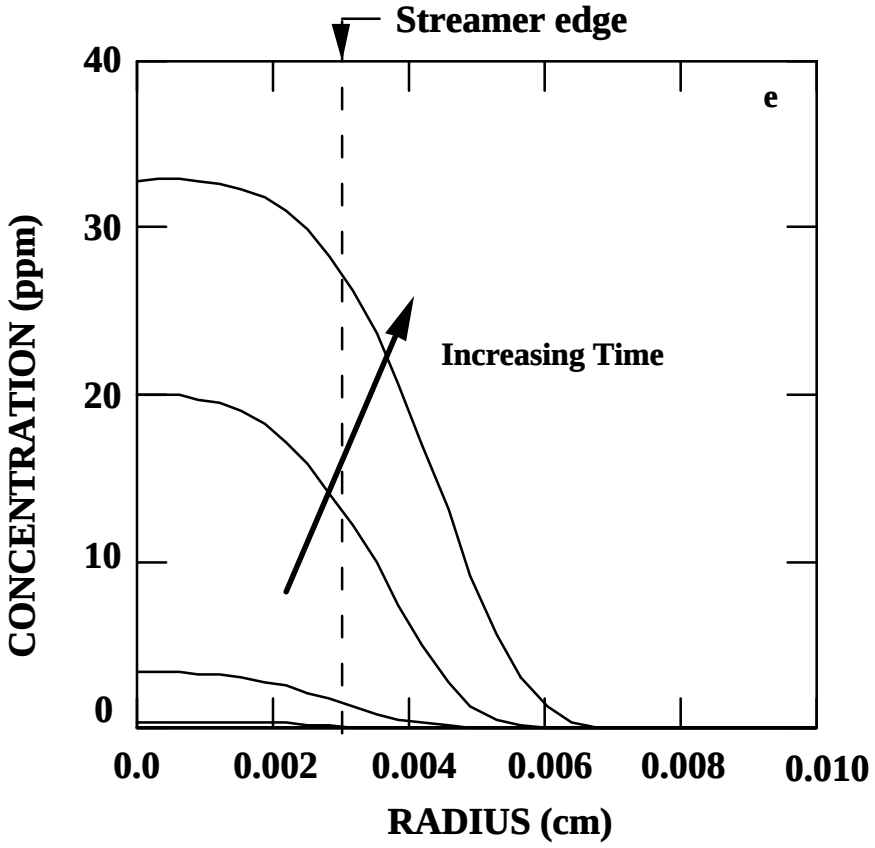

Fig. 6.6. Electron concentration vs. radial location. Conditions are the same as those of Fig. 6.1. Electrons are formed during the pulse in and near the streamer region.

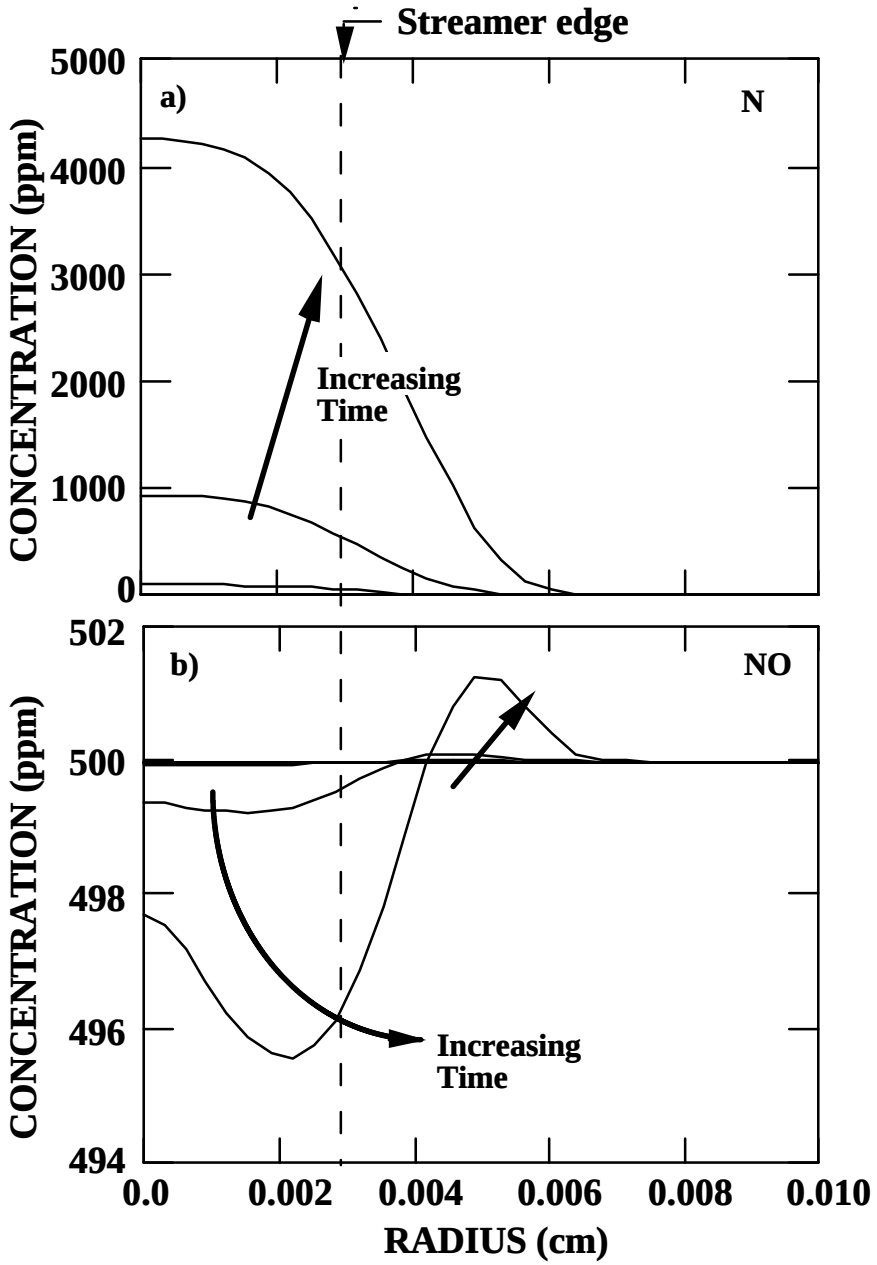

Fig. 6.7 a) N and b) NO during the pulse for the conditions of Fig. 6.1. N is produced in and near the streamer. NO decreases in and near the streamer due to its reactions with N and advective transport outward. A front of NO is formed outside of the streamer.

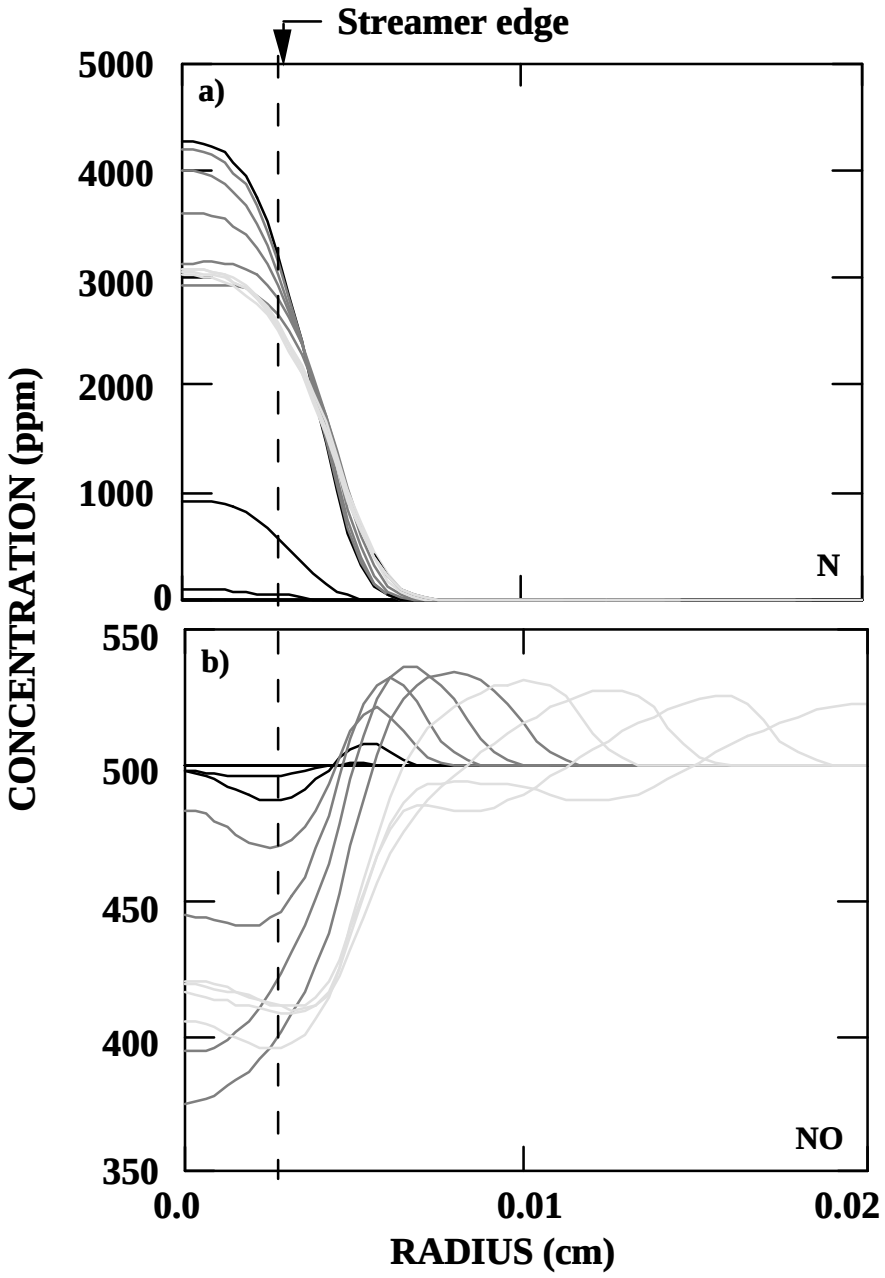

Fig. 6.8 a) N and b) NO for the conditions of Fig. 6.1. Densities during the pulse are shown in black. Densities from the pulse end until 8 x 10^{-8} s are shown in dark gray. During this time N consumption in the streamer region slows down and NO concentration rises due to the backward flux of mass. Densities from 8 x 10^{-8} s to 2 x 10^{-7} s are shown in light gray. During this time a local minimum forms in the near edge of the NO front.

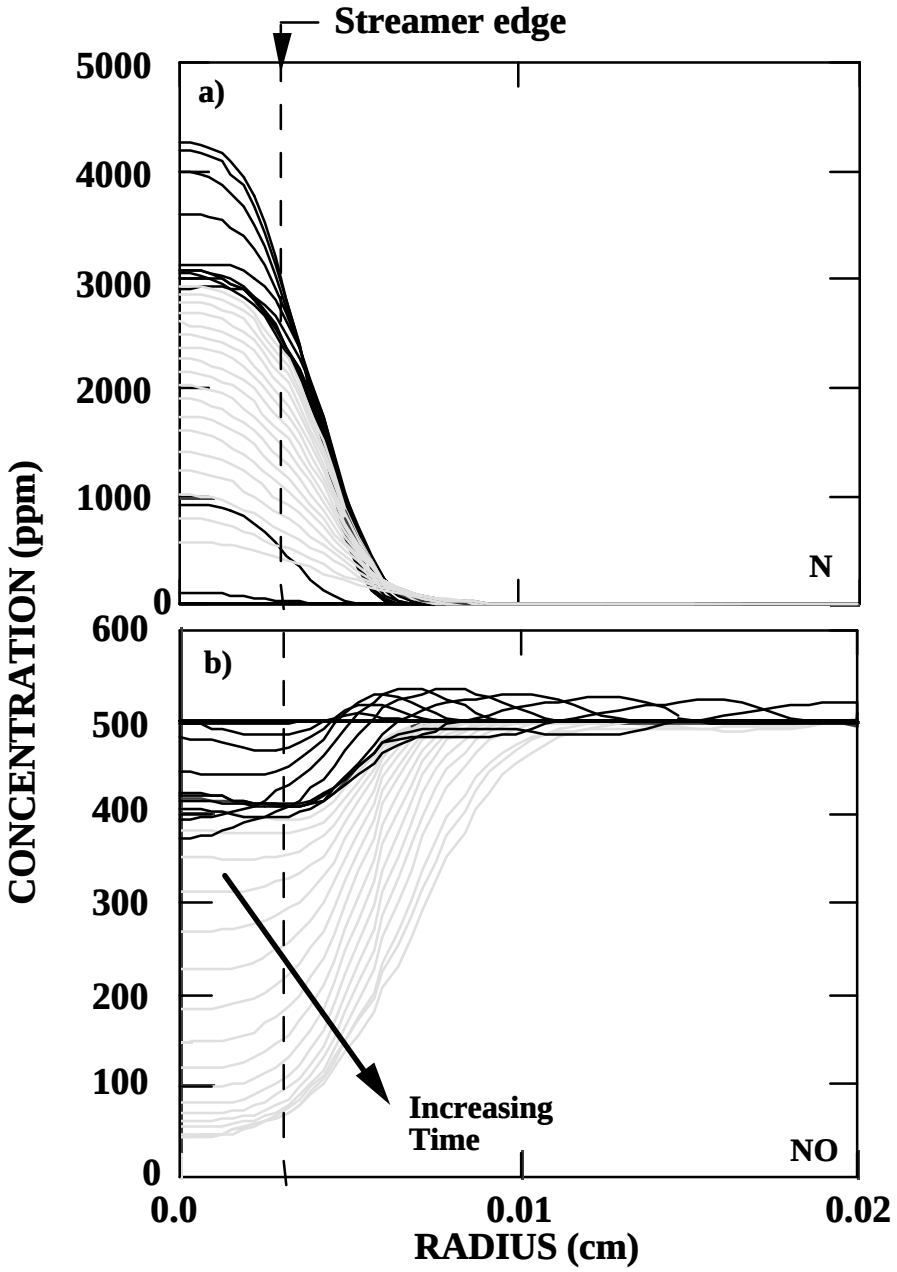

Fig. 6.9 a) N and b) NO for the conditions of Fig. 6.1. Densities from 2 x 10^{-7} s to 1 x 10^{-5} s are shown in gray. Previous densities are shown in black. NO continues to decrease until 1 x 10^{-5} s, due to advective transport outward as well as to reaction with N. Unlike the diffusion-only case of Chapter 5, NO is almost entirely removed from the streamer region. N diffuses out to greater distances from the streamer than in the diffusion-only case.

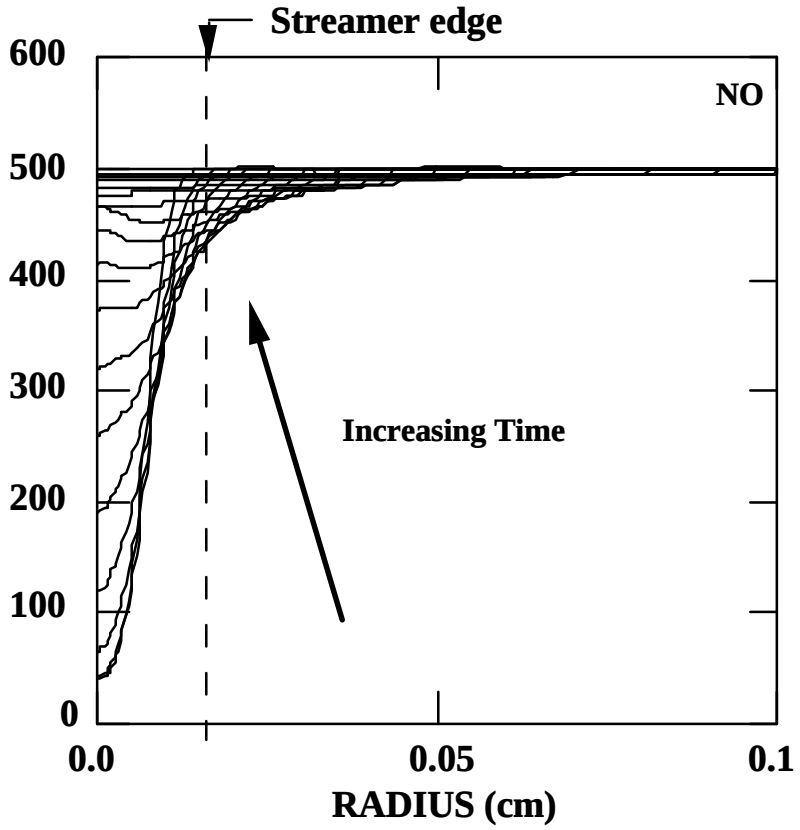

Fig. 6.10. NO for t > 1 x 10^{-5} s for the conditions of Fig. 6.1 NO fills back into the streamer region. Details of NO removal due to the IP reaction are not discernable in the figure since removal occurs over a sufficiently large region that local removal is slight.

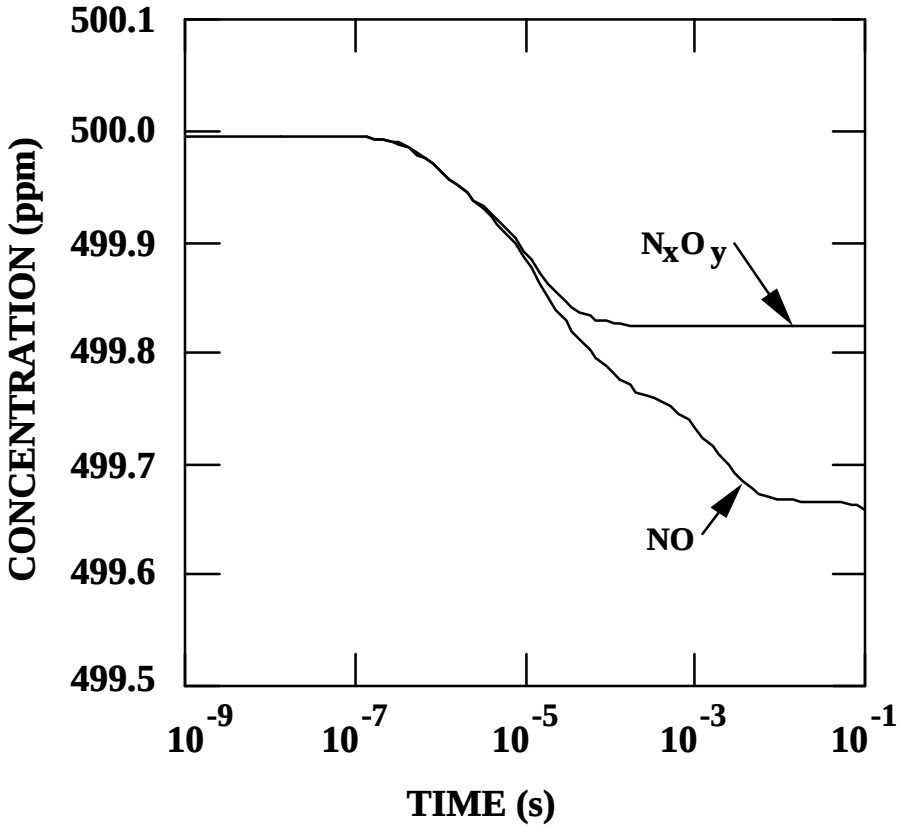

Fig. 6.11. Volume averaged densities of NO and N_XO_Y. The general timescales in remediation are the same as those obtained for the diffusion-only case.

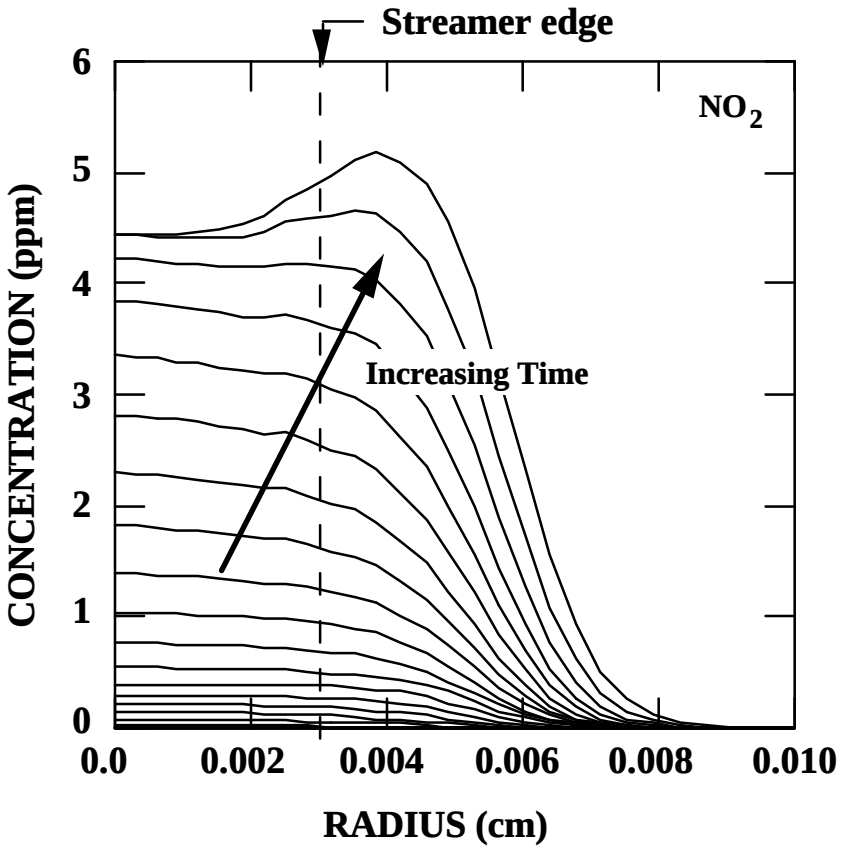

Fig. 6.12. NO_2 for t > 1 x 10^{-6} s for the conditions of Fig. 6.1. NO_2 is produced from NO in and near the streamer due to the high density of radicals there. By 1 x 10^{-6} s, NO is sufficiently depleted in the streamer that NO_2 production is greater outside the streamer region than within.

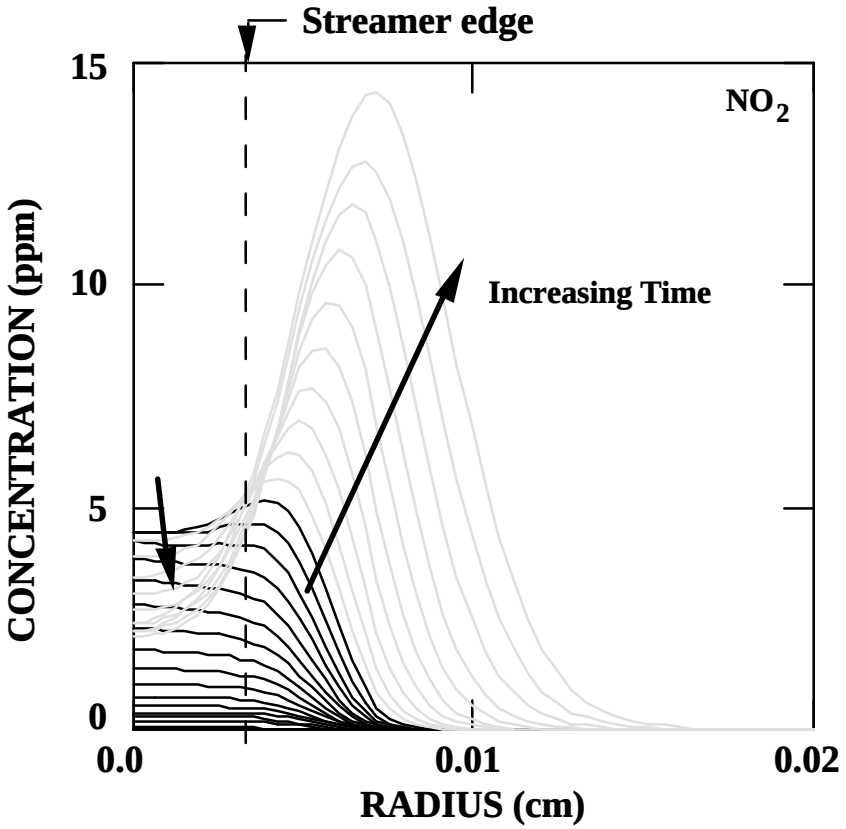

Fig. 6.13. NO_2 for the conditions of Fig. 6.1 ($t > 1 \times 10^{-5}$ s) . Density from 1×10^{-6} s to 1×10^{-5} s is shown in gray. Previous density is shown in black. NO_2 competes with the nearly depleted NO in the streamer region for N radicals. NO_2 decreases there due to the "back reaction" (Eq. 6.4). NO_2 continues to be produced outside of the streamer region due to reaction with O (Eq. 6.6) and O_3 (Eq. 6.3).

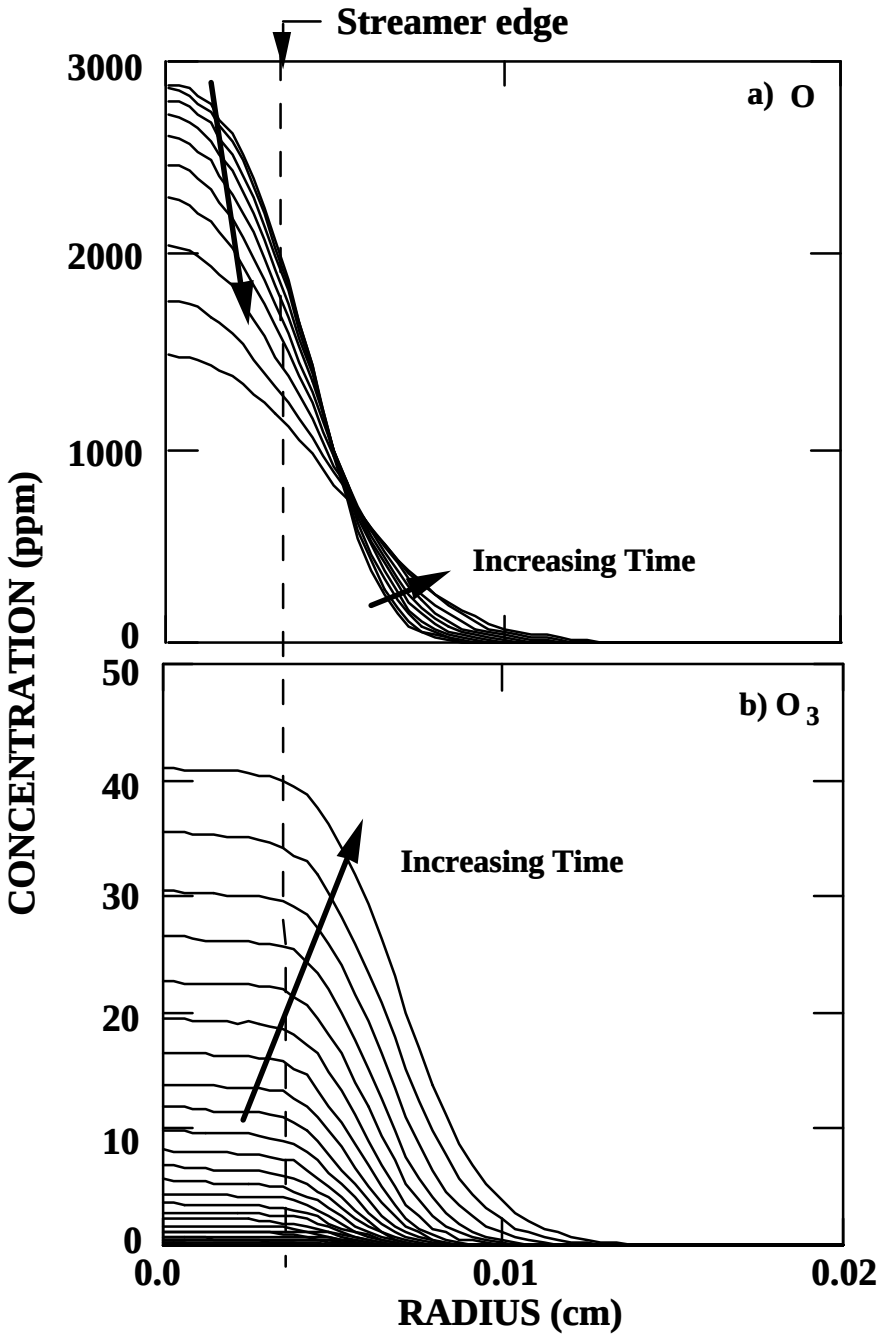

Fig. 6.14 a) O for 1 x 10^{-6} s < t < 1 x 10^{-5} s and b) O_3 for t < 1 x 10^{-5} s for the conditions of Fig. 6.1. O_3 is produced in and near the streamer region due to the large amount of O. O_3 accumulates due to the near depletion of NO in and near the streamer region. O_3 outside the streamer region reacts with NO to produce NO_2 at larger radii.

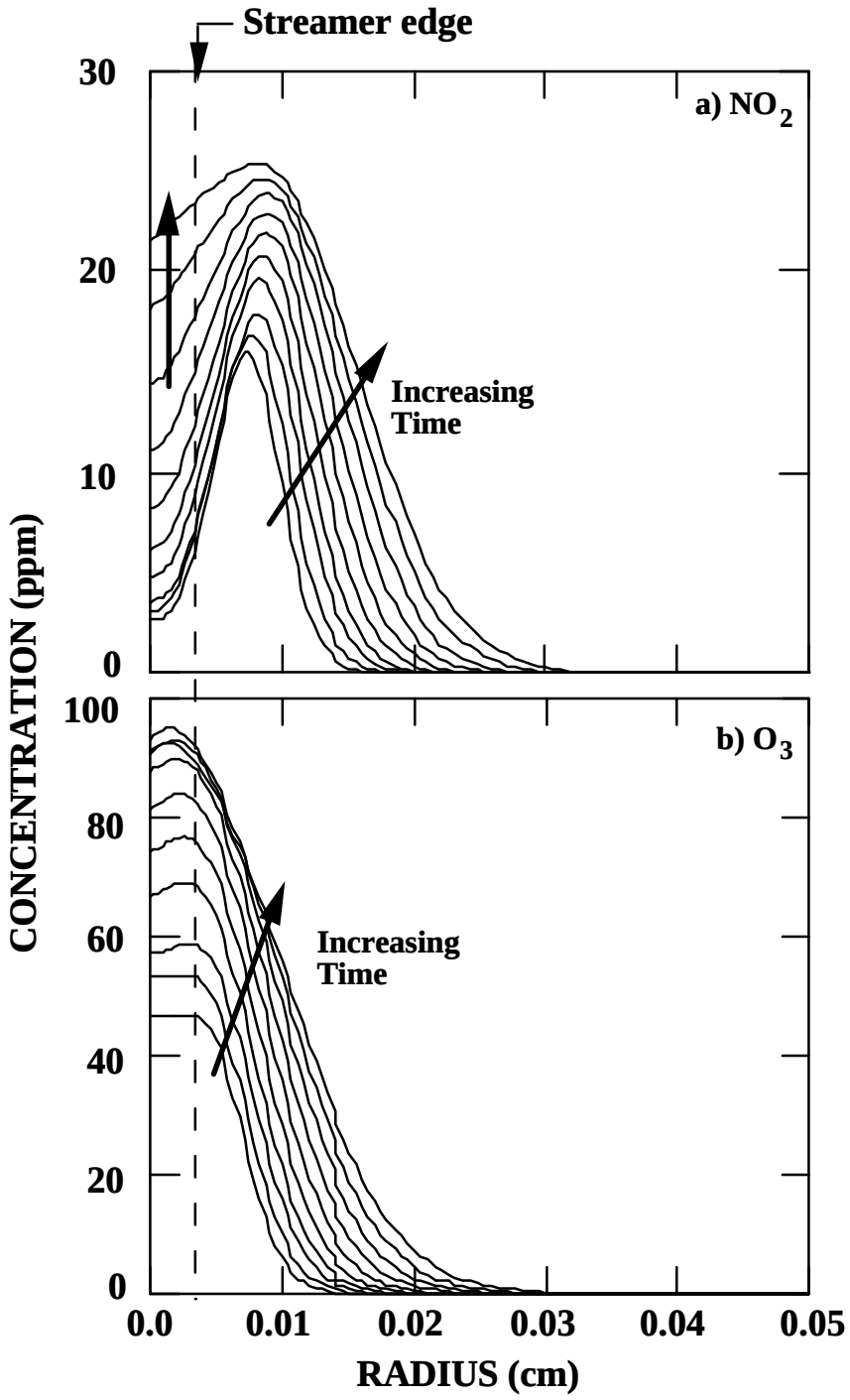

Fig 6.15 a) NO_2 and b) O_3 for 1×10^{-5} s < t < 1×10^{-4} s for the conditions of Fig. 6.1. NO_2 is produced in the streamer region as NO reaccumulates there. NO_2 is also produced at larger radii due to the increasing O_3 density there.

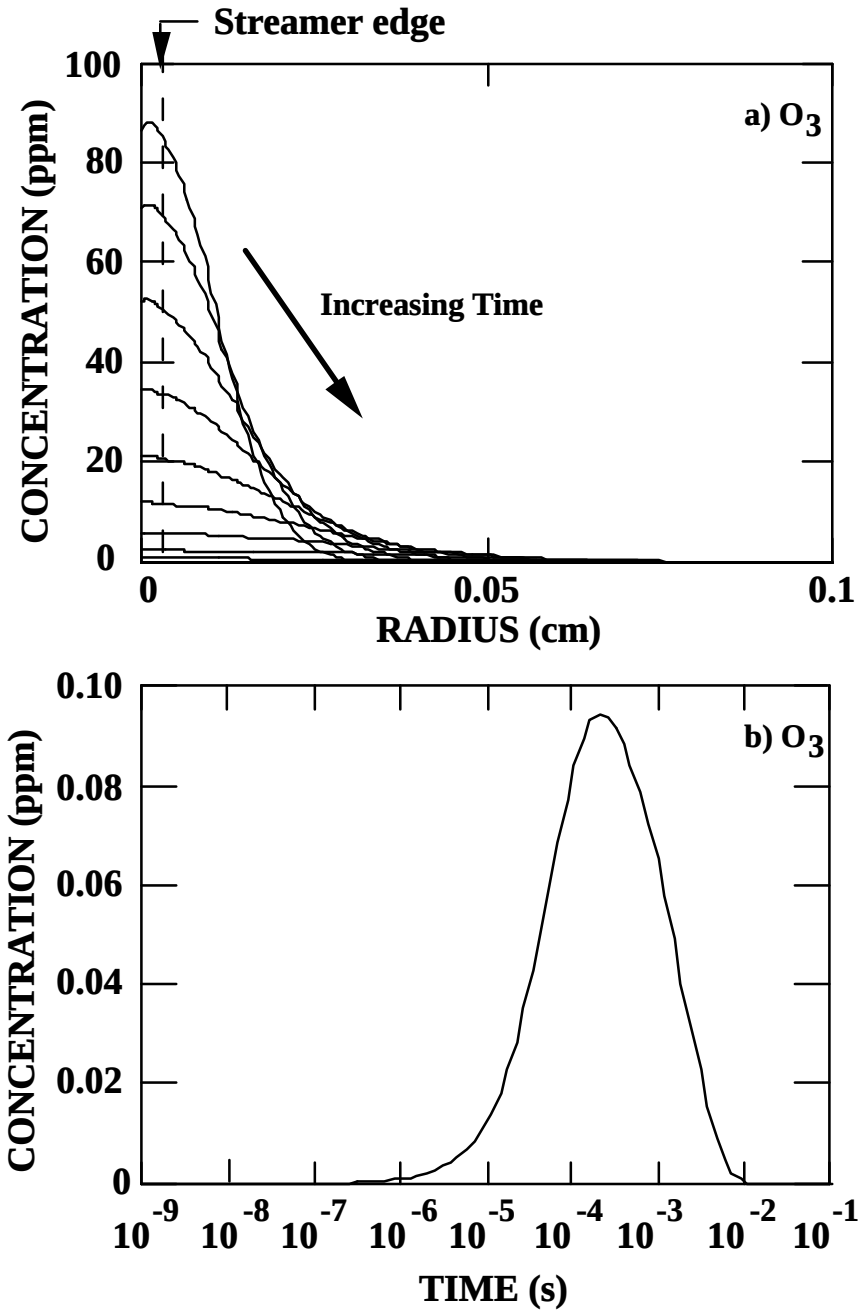

Fig. 6.16 a) O_3 density for 1 x 10^{-4} s < t < 1 x 10^{-1}s for the conditions of Fig. 6.1. b) Volume averaged O_3 density. O_3 is spread over a large region, resulting in small local production of NO_2 by reaction 6.3. The total amount of NO_2 produced during this time is large since the volume averaged density of O_3 reaches its maximum during this time.

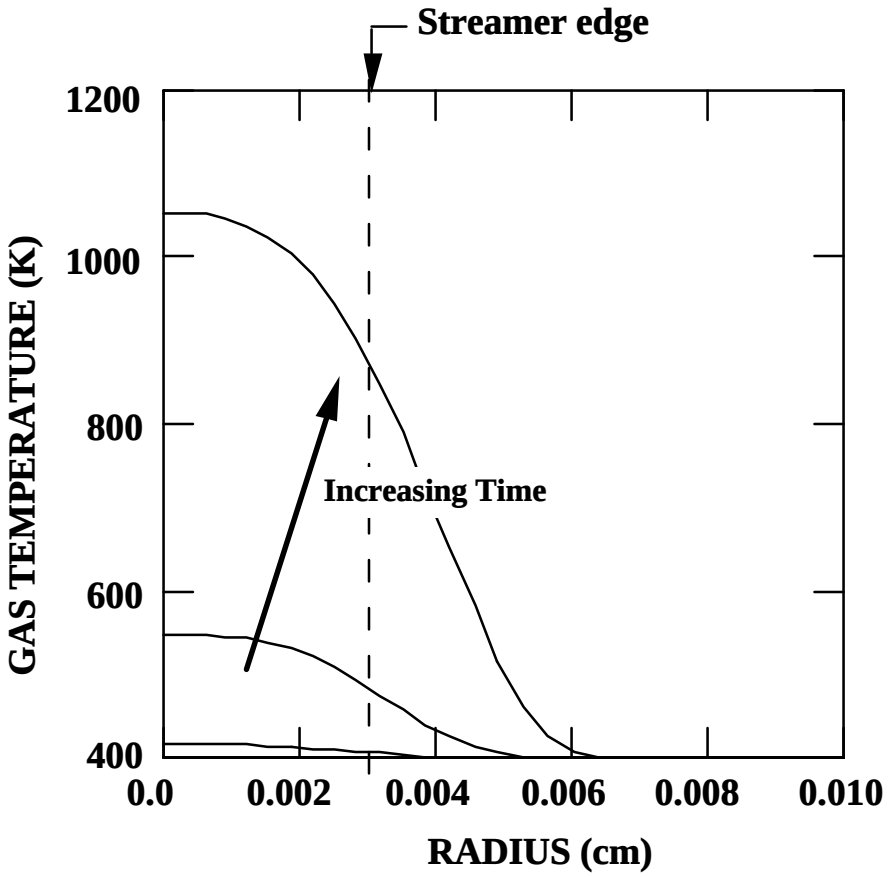

Fig. 6.17. Temperature rise for a case of equivalent energy deposition to that of Fig. 6.1 artificially constrained to diffusive transport only. Without the inclusion of advection allowing conversion of thermal energy into motion of the gas, the temperature increase is much higher than in the full transport case.

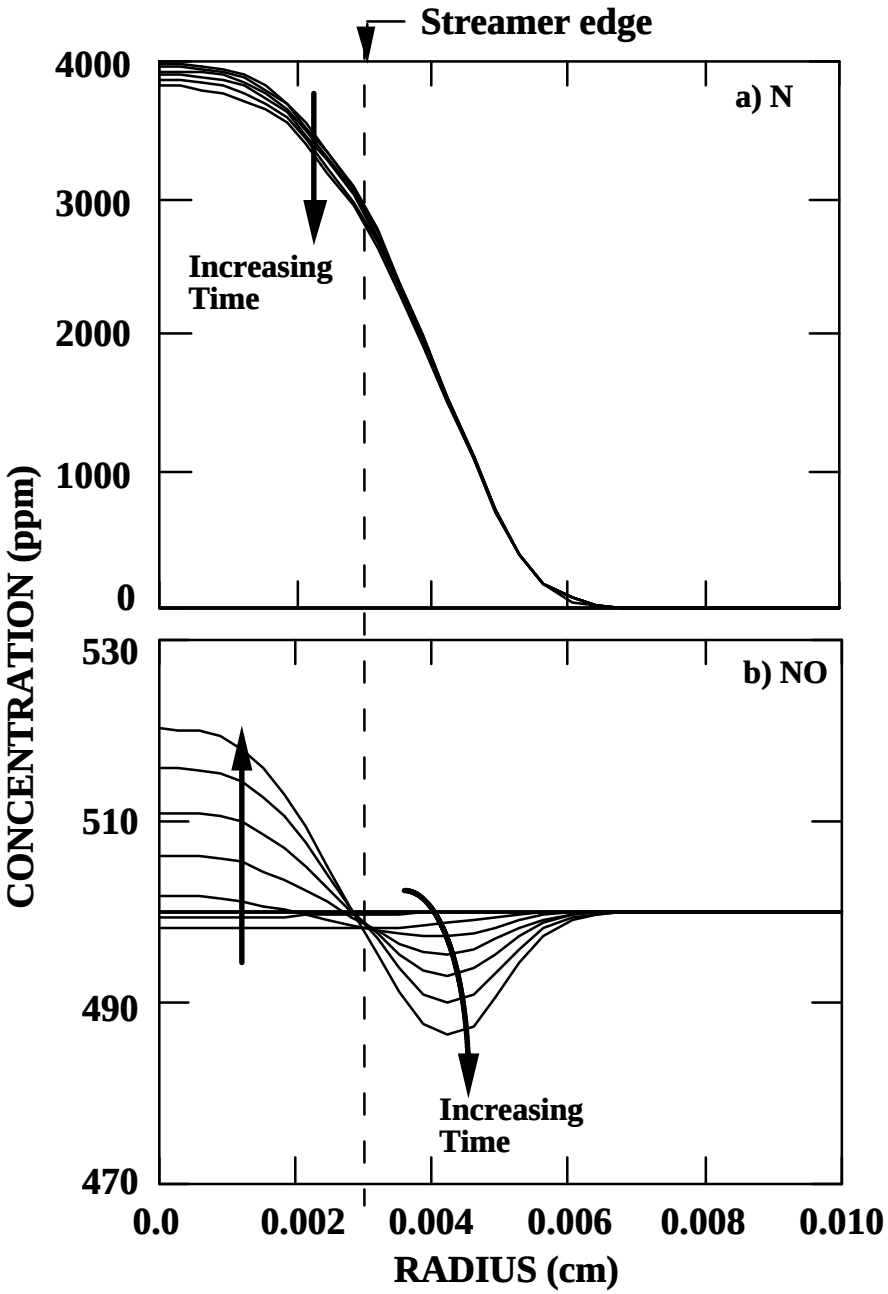

Fig. 6.18 a) N and b) NO for $t < 8 \times 10^{-8}$ s for the conditions of Fig. 6.17. The rise in N during the pulse has been suppressed in the figure. NO is produced in the streamer region by Eq. 6.5 due to the high temperature and N density there.

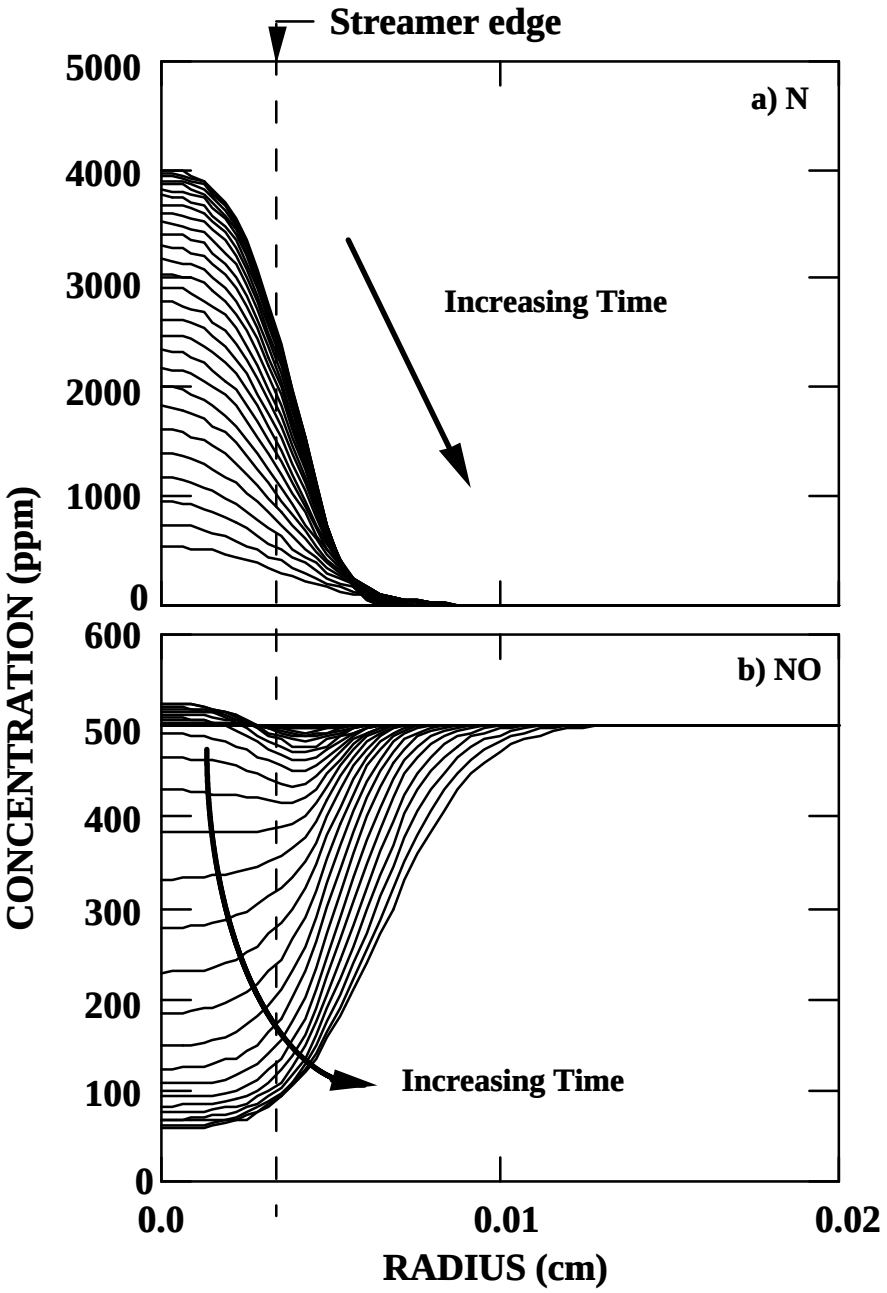

Fig. 6.19 a) N and b) NO for $t < 1 \times 10^{-5}$ s for the conditions of Fig. 6.17. The rise of N during the pulse has been suppressed in the figure. The N density profile has a slightly smaller width than the full transport case. Less NO is removed from regions outside the streamer than in the full transport case due to the advective transport of NO outward and consumption by the greater N density outside the streamer in that case.

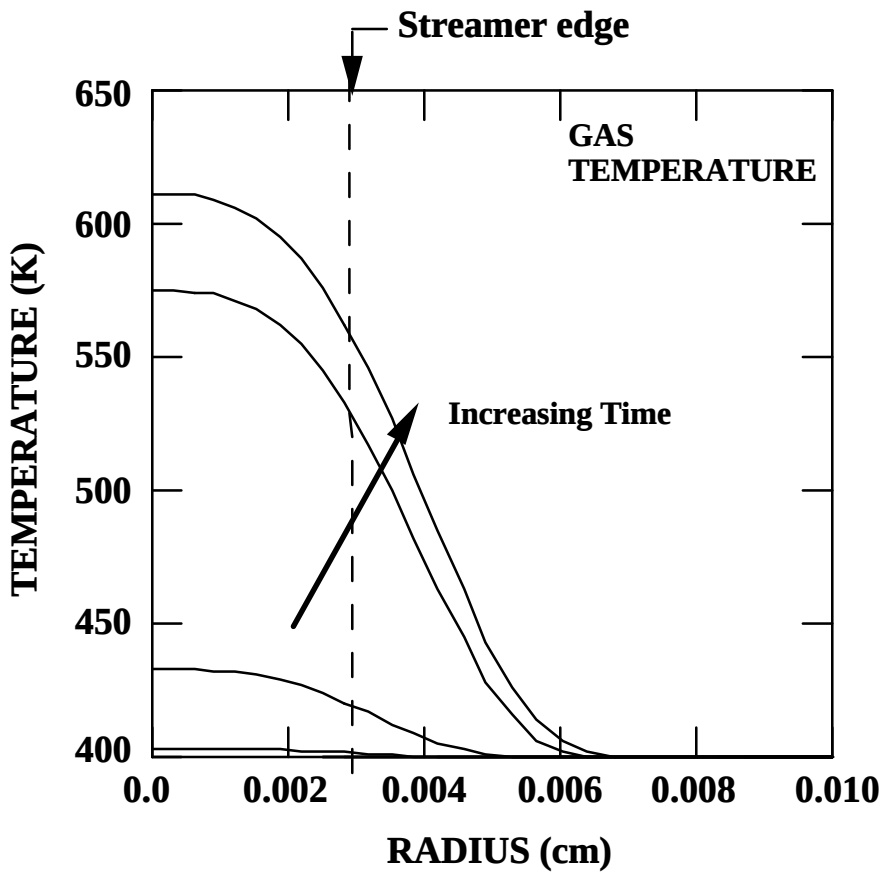

Fig. 6.20. Temperature rise during the pulse ($t < 2.7 \times 10^{-8}$ s) of the full transport case with a volume averaged energy deposition of 7.5×10^{-2} mJ/cm^3. Conditions are otherwise the same as those of Fig. 6.1. The temperature rise is greater with greater energy deposition.

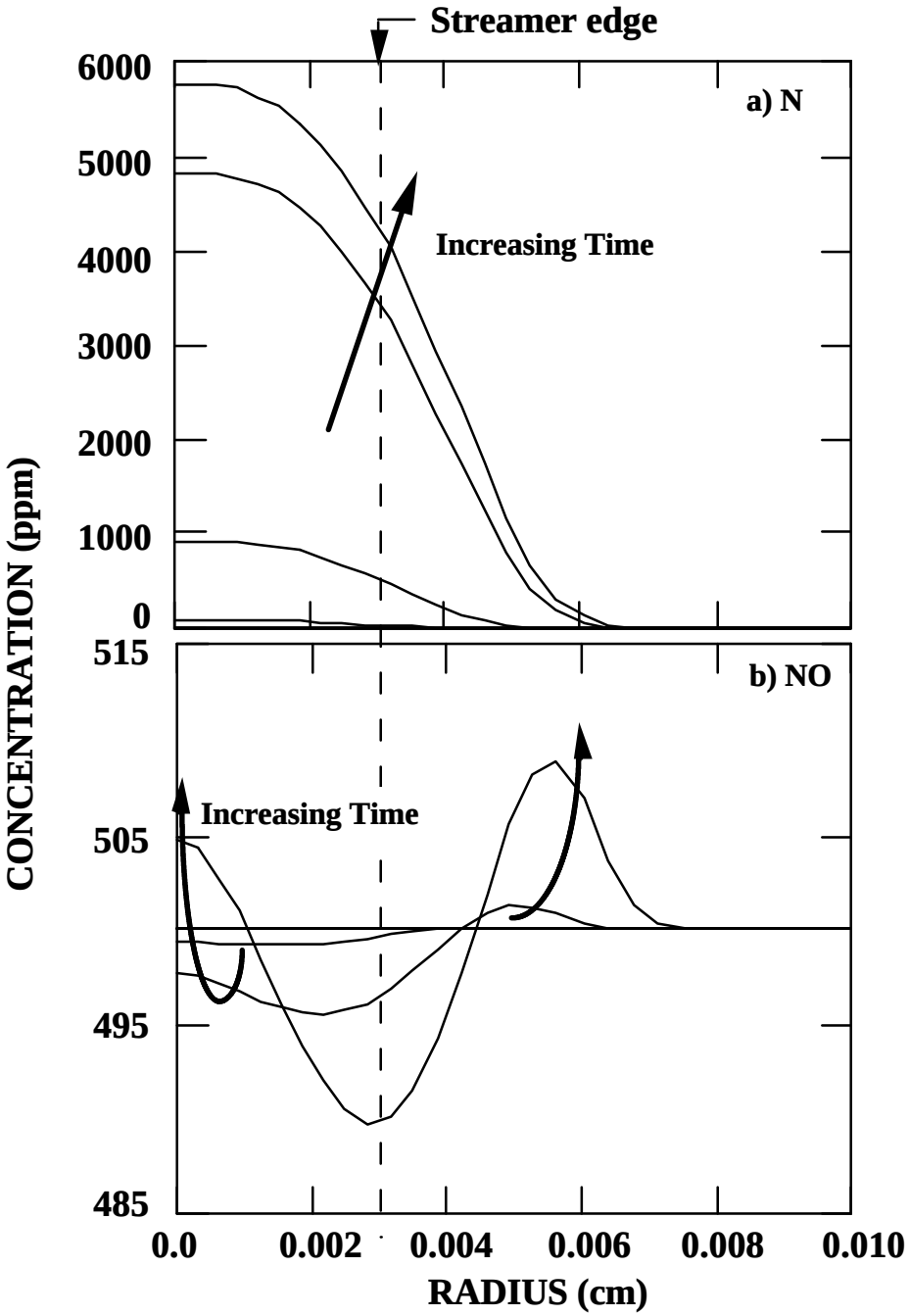

Fig. 6.21 a) N and b) NO during the pulse for the conditions of Fig. 6.20. The increase in temperature and N production over the lower energy deposition case of Figs. 6.1 - 6.16 result in production of NO in the streamer region by Eq. 6.5.

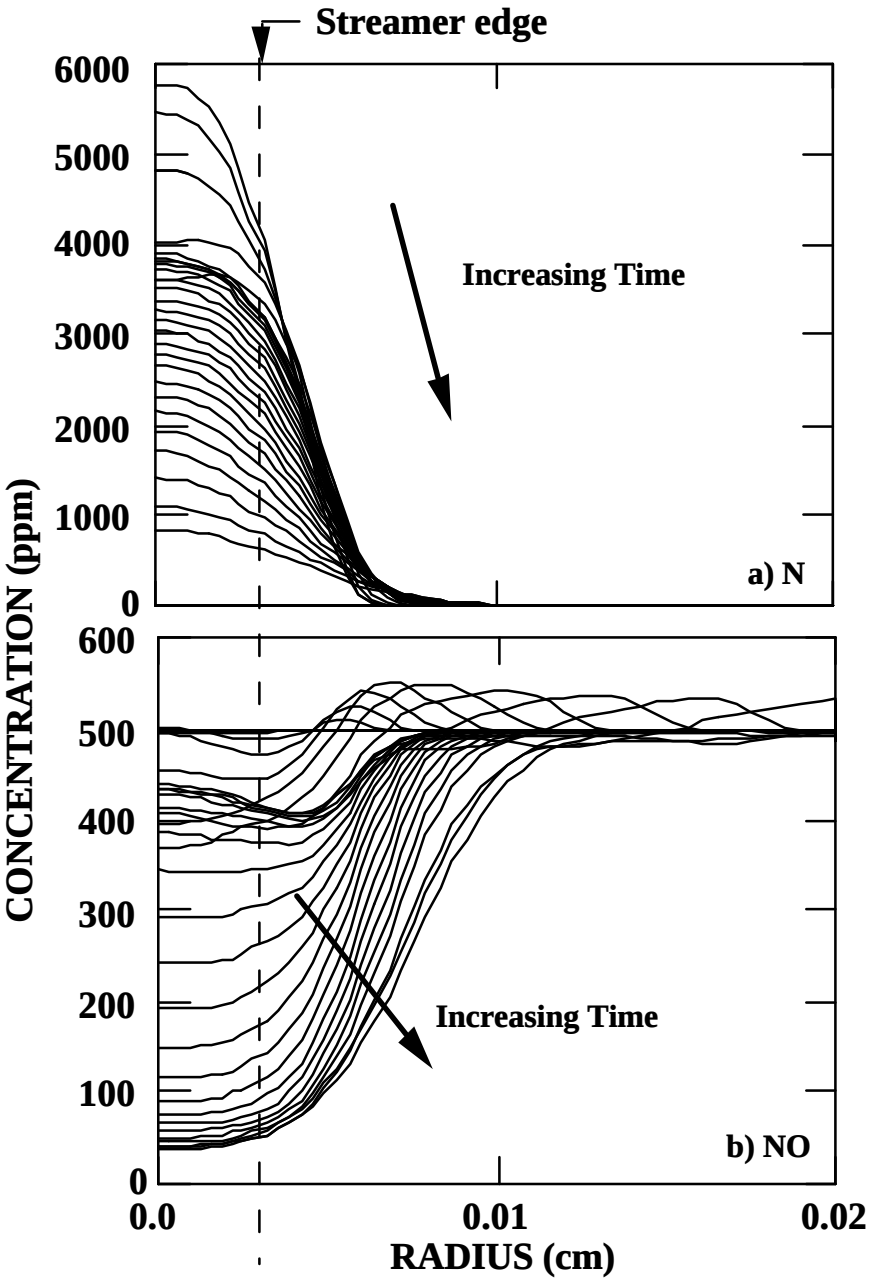

Fig. 6.22 a) N and b) NO for $t < 1 \times 10^{-5}$ s for conditions of Fig. 6.20. The rise of N during the pulse has been suppressed in the figure. N moves farther out of the streamer region and more NO is removed from the streamer region than in the lower energy deposition case of Figs. 6.1 - 6.16. Thus, more N is available to react with NO in regions outside the streamer where the NO is not as depleted.

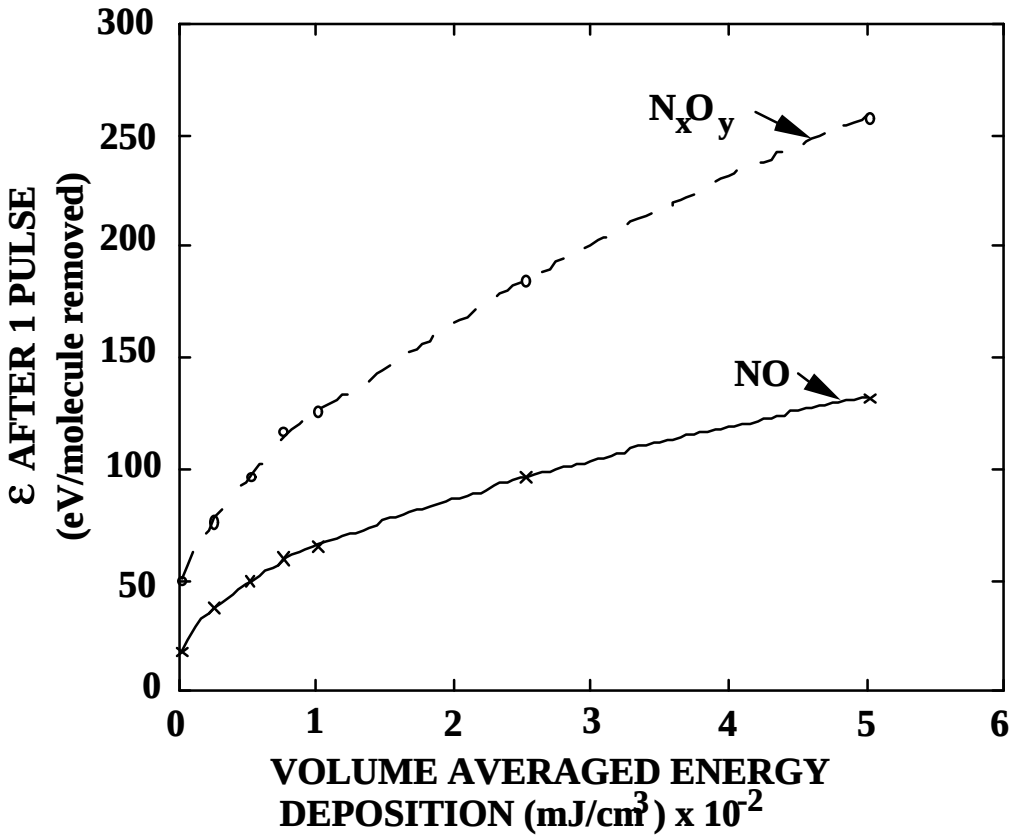

Fig. 6.23. Energy efficiency vs. volume averaged energy deposition. The range corresponds to 57 mJ/cm^3 to 1.1 x 10^4 mJ/cm^3 in the streamer. Over this range, removal is generally less efficient with increasing energy deposition. The instantaneous rate of change of ε with energy deposition is less at higher energy depositions due to the increased transport of N improving the N/NO ratio. This outweighs the increased production of NO due to the increased temperature.

7. CONCLUDING REMARKS

We have developed 0-D and 1-D (radially dependent) computer models for Dielectric Barrier Discharge processing of atmospheric pressure gas streams to be applied to the specific case of toxic gas remediation. The models allow for a detailed analysis of the plasma induced chemical reactions that occur during the remediation process. The goal of the analysis is to optimize the energy efficiency of the remediation and to control the end products obtained.

Remediation of perchloroethylene (PCE) progresses by a chain chemistry. Remediation reactions with OH are primarily responsible for the initiation of production of ClO. Remediation by ClO is self propagating and becomes the dominant pathway. The large densities of O_3 produced by the discharge aid in the production of ClO by reaction with Cl. Production of ClO is slow in the absence of H_2O, making remediation in dry mixtures less efficient than in humid mixtures. Products of remediation, while still toxic, can be further treated by more conventional methods and disposed.

Processes during N_xO_y remediation can be considered in terms of three time regimes. During the Pulse, primary radicals N, O, and OH are produced. The secondary radical O_3 is produced on a longer timescale by reaction of O with O_2. During the Post Pulse Remediative Period (PPRP), NO and N_xOy are remediated. During the Interpulse Period (IP) NO is converted to NO_2 by O_3 with no net change in N_xO_y. Remediation of NO progresses through radical assisted reactions with the ions largely uninvolved. The end products of remediation are primarily N_2 and HNO_3. Only small amounts of restricted nitrogen oxides or ozone are formed as long as the discharge is not operated at power levels beyond that required for total NO remediation.

Remediation is more efficient with higher applied voltage, faster rising pulses, more H_2O in the gas stream, and more pulses of lower energy. The optimum intrapulse time for remediation is at least as long as the O_3 depletion time.

Spatial dependencies can affect the chemistry of remediation. CO_2 in the gas stream decreases the amount of OH, O, and O_3 produced. Reactions with the localized O in the streamer region are less affected than those with the diffuse O_3. As a result, increasing CO_2 decreases the amount of HNO_x produced, increases the amount of N_2 produced, and decreases the conversion of $NO \rightarrow NO_2$.

Spatial dependencies can affect the energy efficiencies of remediation as well. Localized energy deposition in the streamer can result in high temperatures, facilitating production of NO. At low energy depositions, diffusion of NO into the streamer region where the density of N is large increases remediation. At high energy depositions, advective and diffusive transport of N into the bulk gas where the density of NO is large increases remediation. The increased temperature in the streamer region and the increased advective motion are competing processes in determining the energy efficiency at very large energy depositions. Efficiency generally decreases with increasing energy deposition. At very high energy depositions, transport decreases the instantaneous rate of change of efficiency with energy deposition, despite the increased temperature.

The major sources of inaccuracy in the models come from the simplifications in the streamer behavior and the inherent uncertainties in the reaction rates and sets and electron impact cross sections.

Future work should address the sources of inaccuracy. The streamer can be made more realistic by including its axial variations. Non-uniformities will affect radical production, and thus remediation. Inclusion of the dielectric to shut off the streamer more realistically will change E/N and affect radical production as well. Consideration of many streamers in the discharge, with variable spacing and formation times will change the distribution of species at any location, and thus change the chemistry.

Changes due to more accurate representation of the gas mixture would, however, be far more significant than changes due to more accurate representation of the device. Inclusion of even a single additional highly reactive species, or at least highly reactive

with any of the major species, could significantly alter the chemical pathways and the energy efficiencies. Of particular concern in this regard for the study of vehicle exhaust are unburned or partially burned hydrocarbons. Many of the hydrocarbons in vehicle exhaust are not in ring from, but in chain, and react with NO_X to form peroxoacetyl nitrate (PAN) [1]. They also react with the radicals that would otherwise react with NO_X. Thus, inclusion of hydrocarbons in the model could possibly affect the chemistry and the energy efficiency significantly. Limitations on the accuracy and availability of hydrocarbon reactions may, however, add additional uncertainties to the results.

7.1 References

1. J. Durant, private communication (1995).

APPENDIX A. LIST OF CHEMICAL SPECIES USED IN THE REMEDIATION OF PCE IN AR/O_2/H_2O AND N_XO_Y IN N_2/O_2/H_2O/CO_2

Ar	Ar^+	Ar^*	Ar_2^+	Ar_2^*
C	C^+	C_6Cl_6	C_6Cl_7	C_6Cl_8
C_4Cl_5	C_4Cl_6	C_4Cl_7	C_3Cl_5	C_3Cl_6
C_3Cl_7	C_2Cl	C_2Cl_2	C_2Cl_3	C_2Cl_4
C_2Cl_5	C_2Cl_6	C_2Cl_2O	C_2HCl_4	C_2HCl_5
CCN	C_2O	CCl	CCl^+	CCl_2
CCl_2^+	CCl_2^{+2}	CCl_2COCl	CCl_3	CCl_3^+
CCl_3^{+2}	CCl_3CO	CCl_3COCl	CCl_4	CCl_4(v)
CCl_3O	CCl_3O_2	CHCl	CH_2O	$CHCl_2$
$CHCl_2CO$	$CHCl_2COCl$	$CHCl_3$	CHOCl	CN
CNN	CO	COCl	$COCl_2$	CO_2
CO_2^+	Cl	Cl^+	Cl^-	Cl_2
Cl_2^+	Cl_3	Cl_2O	ClO	ClOO
H	H^+	H^-	HCN	HCO HCOOH
	HCl	H_2	H_2^+	H_3O
H_3O^+	$H_3O^+ \cdot H_2O$	$H_3O^+ \cdot (H_2O)_2$	H_2O	$(H_2O)_3$
H_2O_2	HNCO	HNO	HNO_2	HNO_3
HOCN	$HOCO^*$	HOCl	HO_2	HO_2NO_2
N	N^+	$N(^2D)$	NCCN	NCO
NH	NH_2	NH_3	NH_3^+	NH_4^+
N_2	N_2^+	N_2(A)	N_3	N_3^+
N_4	N_4^+	N_2O	N_2O_4	N_2O_5
NO	NO^+	$NO^+ \cdot H_2O$	$NO^+ \cdot (H_2O)_2$	$NO^+ \cdot (H_2O)_3$
$NO^+ \cdot O_2$	NO_2	NO_2^+	NO_2^-	NO_3
NO_3^-	O	O^+	O^-	$O(^1D)$
OH	O_2	O_2^+	$O_2^+ \cdot H_2O$	O_2-
O_3				

APPENDIX B. LIST OF REACTIONS USED IN THE REMEDIATION OF PCE IN AR/O_2/H_2O AND N_XO_Y IN N_2/O_2/H_2O/CO_2

Electron impact reactions resulting in the production of new species

Reaction	Rate Coefficient [a]	Ref.
$e + N_2 \rightarrow N_2^+ + e + e$	6.664×10^{-11}	1
$e + N_2 \rightarrow N_2(A) + e$	8.524×10^{-9}	1
$e + N_2 \rightarrow N + N + e$	7.05×10^{-10}	1
$e + O_2 \rightarrow O^- + O$	5.276×10^{-11}	1
$e + O_2 \rightarrow O_2^+ + e + e$	1.961×10^{-10}	2
$e + O_2 \rightarrow O + O + e$	1.434×10^{-9}	2
$e + O_2 \rightarrow O(^1D) + O + e$	4.8×10^{-9}	2
$e + N_2^+ \rightarrow N(^2D) + N$	$2 \times 10^{-7} Te^{-0.5}$	34
$e + H_2O \rightarrow H_2O^+ + e + e$	6.525×10^{-11}	3
$e + H_2O \rightarrow H + OH + e$	5.322×10^{-11}	3
$e + H_2O \rightarrow H^- + OH$	2.512×10^{-10}	3
$e + N_3^+ \rightarrow N + N_2$	$2 \times 10^{-7} Te^{-0.5}$	b
$e + H_3O^+ \cdot (H_2O)_2 \rightarrow H + (H_2O)_3$	$2 \times 10^{-7} Te^{-0.5}$	b
$e + NO_2^+ \rightarrow NO + O$	$2 \times 10^{-7} Te^{-0.5}$	b
$e + NO_2^+ \rightarrow NO + O(^1D)$	$2 \times 10^{-7} Te^{-0.5}$	4
$e + H_2NO^+ \rightarrow H_2O + N$	$2 \times 10^{-7} Te^{-0.5}$	b
$e + NO^+ \rightarrow N(^2D) + O$	$2 \times 10^{-7} Te^{-0.5}$	4
$e + NO^+ \rightarrow N + O(^1D)$	$2 \times 10^{-7} Te^{-0.5}$	34
$e + O_2 + M \rightarrow O_2^- + M$	$1 \times 10^{-31} Te^{-0.5}$	4
$e + NO^+ \cdot O_2 \rightarrow NO + O_2$	$2 \times 10^{-7} Te^{-0.5}$	b
$e + NO_2 \rightarrow NO_2^-$	4×10^{-11}	4
$e + N_4^+ \rightarrow N_2 + N_2$	$2 \times 10^{-7} Te^{-0.5}$	b

$e + NO^+\cdot(H_2O)_2 \rightarrow NO + H_2O + H_2O$	$2x10^{-7}Te^{-0.5}$	b
$e + H_2O^+ \rightarrow OH + H$	$6.6x10^{-6}Te^{-0.5}$	5
$e + H_2O^+ \rightarrow O + H + H$	$2.88x10^{-6}Te^{-0.5}$	5
$e + H_2O^+ \rightarrow O + H_2$	$2.52x10^{-6}Te^{-0.5}$	5
$e + H_3O^+ \rightarrow H_2O + H$	$2x10^{-7}Te^{-0.5}$	b
$e + O_2^+ \rightarrow O(^1D) + O$	$2x10^{-7}Te^{-0.5}$	b
$e + H_2^+ \rightarrow H_2$	$2x10^{-7}Te^{-0.5}$	b
$e + O_2^+\cdot H_2O \rightarrow O_2 + H_2O$	$2x10^{-7}Te^{-0.5}$	b
$e + H_3O^+\cdot H_2O \rightarrow H + H_2O + H_2O$	$2x10^{-7}Te^{-0.5}$	b
$e + NH_3^+ \rightarrow NH_2 + H$	$2x10^{-7}Te^{-0.5}$	b
$e + NH_4^+ \rightarrow NH_3 + H$	$2x10^{-7}Te^{-0.5}$	b
$e + NO^+\cdot H_2O \rightarrow NO + H_2O$	$2x10^{-7}Te^{-0.5}$	b
$e + NO^+\cdot(H_2O)_3 \rightarrow NO + H_2O + H_2O + H_2O$	$2x10^{-7}Te^{-0.5}$	b
$e + N_2(A) \rightarrow N_2^+ + e + e$	$2.2x10^{-7}$ x (exp(-9.33/Te)/($Te^{-0.5}$ (1+9.33)/Te)) x ((20+9.33/Te)$^{-1}$ + log (1.25(1+Te/9.33)))	35
$e + O_3 \rightarrow e + O_2 + O(^1D)$	$5x10^{-10}$	b
$e + CO_2 \rightarrow O + CO + e$	$1.195x10^{-9}$	6
$e + CO_2 \rightarrow CO_2^+ + e + e$	$1.693x10^{-10}$	6
$e + CO_2 \rightarrow O^- + CO$	$6.565x10^{-12}$	6
$e + CO_2^+ \rightarrow CO + O$	$2x10^{-7}Te^{-0.5}$	b
$e + CCl_4 \rightarrow CCl_3^+ + Cl + e + e$	$2.053x10^{-9}$	7
$e + CCl_4 \rightarrow CCl_2^+ + Cl_2 + e + e$	$4.611x10^{-11}$	7
$e + CCl_4 \rightarrow CCl^+ + Cl_3 + e + e$	$1.259x10^{-11}$	7
$e + CCl_4 \rightarrow Cl_2^+ + CCl_2 + e + e$	$1.029x10^{-14}$	7
$e + CCl_4 \rightarrow Cl^+ + CCl_3 + e + e$	$4.631x10^{-13}$	7

$e + CCl_4 \rightarrow C^+ + Cl_2 + Cl + Cl + e + e$	$7.024x10^{-15}$	7
$e + CCl_4 \rightarrow CCl_3^{+2} + Cl + e + e + e$	$1.712x10^{-16}$	7
$e + CCl_4 \rightarrow CCl_2^{+2} + Cl_2 + e + e + e$	$1.252x10^{-18}$	7
$e + CCl_4 \rightarrow CCl_3 + Cl^-$	$1.622x10^{-9}$	7
$e + CCl_4 \rightarrow CCl_2 + Cl + Cl + e$	$3.393x10^{-8}$	7
$e + CCl_3^+ \rightarrow CCl_2 + Cl$	$2x10^{-7}Te^{-0.5}$	34
$e + CCl_2^+ \rightarrow CCl + Cl$	$2x10^{-7}Te^{-0.5}$	34
$e + CCl^+ \rightarrow C + Cl$	$2x10^{-7}Te^{-0.5}$	34
$e + Cl_2^+ \rightarrow Cl + Cl$	$2x10^{-7}Te^{-0.5}$	34
$e + Cl^+ \rightarrow Cl$	$2x10^{-7}Te^{-0.5}$	34
$e + C^+ \rightarrow C$	$2x10^{-7}Te^{-0.5}$	34
$e + CCl_3^{+2} \rightarrow CCl_2^+ + Cl$	$2x10^{-7}Te^{-0.5}$	34
$e + CCl_2^{+2} \rightarrow CCl^+ + Cl$	$2x10^{-7}Te^{-0.5}$	34
$e + Ar \rightarrow Ar^* + e$	$1.172x10^{-10}$	8
$e + Ar \rightarrow Ar^{**} + e$	$4.351x10^{-10}$	8
$e + Ar \rightarrow Ar^+ + e + e$	$1.296x10^{-10}$	9
$e + Ar^* \rightarrow Ar^{**} + e$	$8.14x10^{-7}$	36
$e + Ar^* \rightarrow Ar^+ + e + e$	$7.335x10^{-8}$	10
$e + Ar^{**} \rightarrow Ar^+ + e + e$	$1x10^{-30}$	b
$e + Ar^* \rightarrow Ar + e$	$3.187x10^{-9}$	36
$e + Ar^{**} \rightarrow Ar + e$	$1x10^{-30}$	b
$e + Ar_2^* \rightarrow Ar + Ar + e$	$1x10^{-7}$	b
$e + Ar_2^+ \rightarrow Ar^* + Ar$	$1x10^{-7}$	b
$e + CCl_4 \rightarrow CCl_4(v) + e$	$1.766x10^{-9}$	3
$e + CCl_4 \rightarrow CCl_4(v) + e$	$2.008x10^{-10}$	3
$e + CCl_4 \rightarrow CCl_4(v) + e$	$7.335x10^{-8}$	3
$e + CCl_4 \rightarrow CCl_4(v) + e$	$2.134x10^{-9}$	3

$e + CCl_4(v) \rightarrow CCl_3^+ + Cl + e + e$	2.053×10^{-9}	7
$e + CCl_4(v) \rightarrow CCl_2^+ + Cl_2 + e + e$	4.611×10^{-11}	7
$e + CCl_4(v) \rightarrow CCl^+ + Cl_3 + e + e$	1.259×10^{-11}	7
$e + CCl_4(v) \rightarrow Cl_2^+ + CCl_2 + e + e$	1.029×10^{-14}	7
$e + CCl_4(v) \rightarrow Cl^+ + CCl_3 + e + e$	4.631×10^{-13}	7
$e + CCl_4(v) \rightarrow C^+ + Cl_2 + e + e$	7.024×10^{-15}	7
$e + CCl_4(v) \rightarrow e + CCl4(v) + Cl + Cl$	7.024×10^{-15}	7
$e + CCl_4(v) \rightarrow CCl_3^{+2} + Cl + e + e + e$	1.712×10^{-16}	7
$e + CCl_4(v) \rightarrow CCl_2^{+2} + Cl_2 + e + e + e$	1.252×10^{-18}	7
$e + CCl_4(v) \rightarrow CCl_3 + Cl^-$	1.622×10^{-9}	7
$e + CCl_4(v) \rightarrow CCl_2 + Cl + Cl + e$	3.393×10^{-8}	7

Reactions of $N_2/O_2/H_2O/NO$

Reaction	Rate Coefficient [c]	Ref.
$O + O_2 + M \rightarrow O_3 + M$	$6.9 \times 10^{-34}(T/300)^{-1.25}$	30
$H + OH + M \rightarrow H_2O + M$	4.3×10^{-31}	4
$N_2O_5 \rightarrow NO_2 + NO_3$	$5.49 \times 10^{14} T^{0.1} \exp(-11080/T)$	30
$NO + O_2 + NO \rightarrow NO_2 + NO_2$	1.4×10^{-38}	b
$NO + HO_2 \rightarrow NO_2 + OH$	$3.7 \times 10^{-12} \exp(240/T)$	11
$N(^2D) + N_2 \rightarrow N + N_2$	2.4×10^{-14}	4
$NO + O + O_2 \rightarrow NO_2 + O_2$	$2.44 \times 10^{-27} T^{-1.8}$	11

$N(^2D) + O_2 \rightarrow NO + O$	$6.8x10^{-12}$	4
$NO + OH + M \rightarrow HNO_2 + M$	$7.4x10^{-31}(T/300)^{-2.4}$	11
$N(^2D) + NO \rightarrow N_2 + O$	$6.3x10^{-11}$	4
$NO + H + M \rightarrow HNO + M$	$3.4x10^{-32}$	4
$N(^2D) + N_2O \rightarrow NO + N_2$	$2.6x10^{-12}$	4
$NO + NO_3 \rightarrow NO_2 + NO_2$	$1.6x10^{-11}exp(150/T)$	11
$HO_2 + NO + M \rightarrow HNO_3 + M$	$5.6x10^{-33}$	b
$HO_2 + NO \rightarrow O_2 + HNO$	$9.0x10^{-19}exp(2819/T)$	12
$N(^2D) + NO_2 \rightarrow N_2O + O$	$1.5x10^{-12}$	4
$NO + O_3 \rightarrow NO_2 + O_2$	$2.0x10^{-12}exp(-1400/T)$	13
$N(^2D) + NO_2 \rightarrow NO + NO$	$1.5x10^{-12}$	4
$NO + N \rightarrow N_2 + O$	$3.1x10^{-11}$	4
$H + O_2 + M \rightarrow HO_2 + M$	$5.64x10^{-28}T^{-1.6}$	14
$H + H + M \rightarrow H_2 + M$	$4.8x10^{-33}$	4
$H + NO_2 \rightarrow OH + NO$	$8x10^{-11}$	4
$H + HO_2 \rightarrow OH + OH$	$2.8x10^{-10}exp(-440/T)$	15
$N_2(A) + N_2 \rightarrow N_2 + N_2$	$1.9x10^{-13}$	37
$H + O_3 \rightarrow OH + O_2$	$1.4x10^{-10}exp(-480/T)$	11
$N_2(A) + NO \rightarrow NO + N_2$	$3.6x10^{-10}$	37
$H + HNO \rightarrow H_2 + NO$	$1x10^{-11}$	4
$N_2(A) + O_2 \rightarrow O + O + N_2$	$1.5x10^{-12}$	37
$N + NO_2 \rightarrow N_2O + O$	$2.4x10^{-12}$	4
$N_2(A) + O_2 \rightarrow O_2 + N_2$	$2.8x10^{-11}$	37
$N + NO_2 \rightarrow NO + NO$	$6x10^{-13}$	4
$N_2(A) + N_2O \rightarrow N_2 + N_2 + O$	$1.4x10^{-11}$	37
$N_2(A) + N_2O \rightarrow N_2 + N_2O$	$1.7x10^{-10}$	37
$N + N + M \rightarrow N_2 + M$	$3.9x10^{-33}$	4

$N_2(A) + NO_2 \rightarrow NO + O + N_2$	$1x10^{-12}$	37
$N_2(A) + H_2 \rightarrow N_2 + H_2$	$2.6x10^{-11}$	37
$N + OH \rightarrow NO + H$	$3.8x10^{-11}exp(85/T)$	11
$O(^1D) + N_2 \rightarrow O + N_2$	$1.8x10^{-11}exp(107/T)$	11
$N + O + M \rightarrow NO + M$	$5.46x10^{-33}exp(155/T)$	16
$O(^1D) + O_2 \rightarrow O + O_2$	$3.8x10^{-11}$	4
$N + O_2 \rightarrow NO + O$	$4.4x10^{-12}exp(-3220/T)$	11
$N + O_3 \rightarrow NO + O_2$	$5x10^{-16}$	4
$O(^1D) + H_2O \rightarrow O + H_2O$	$1.2x10^{-11}$	4
$O(^1D) + H_2O \rightarrow OH + OH$	$2.2x10^{-10}$	4
$O + HO_2 \rightarrow OH + O_2$	$2.9x10^{-11}exp(200/T)$	11
$O + O3 \rightarrow O2 + O2$	$8.0x10^{-12}exp(-2060/T)$	11
$O + NO_2 + M \rightarrow NO_3 + M$	$9.0x10^{-32}(T/300)^{-2.0}$	11
$NO_3 + NO_3 \rightarrow NO_2 + NO_2 + O_2$	$1.2x10^{-15}$	4
$OH + OH \rightarrow O + H_2O$	$3.5x10^{-16}T^{1.4}exp(200/T)$	15
$N_2O_5 + H_2O \rightarrow HNO_3 + HNO_3$	$5x10^{-21}$	4
$NH + NO \rightarrow N_2O + H$	$1.3x10^{-12}$	4
$OH + NO_2 + N_2 \rightarrow HNO_3 + N_2$	$2.2x10^{-30}exp(T/300)^{-2.9}$	11
$NH + O_2 \rightarrow HNO + O$	$2.3x10^{-13}$	4
$OH + HNO_3 \rightarrow NO_3 + H_2O$	$1.5x10^{-14}exp(650/T)$	24
$OH + HNO \rightarrow H_2O + NO$	$2.15x10^{-17}T^{1.88}exp(481/T)$	21
$OH + HO_2 \rightarrow H_2O + O_2$	$8x10^{-11}$	b
$H_2O^+ + H_2O \rightarrow H_3O^+ + OH$	$1.7x10^{-9}$	4
$OH + HNO_2 \rightarrow NO_2 + H_2O$	$1.8x10^{-11}exp(-390/T)$	11
$H_2O^+ + O_2 \rightarrow O_2^+ + H_2O$	$4.3x10^{-10}$	4

$OH + O_3 \rightarrow HO_2 + O_2$	$1.9x10^{-12}exp(-1000/T)$	24
$N_3^+ + O_2 \rightarrow NO^+ + N_2O$	$3.6x10^{-11}$	4
$OH + N_2O \rightarrow HNO + NO$	$3.8x10^{-17}$	4
$N_3^+ + O_2 \rightarrow NO_2^+ + N_2$	$1.5x10^{-11}$	4
$HO_2 + NO_2 + N_2 \rightarrow HO_2NO_2 + N_2$	$1.5x10^{-31}(T/300)^{-3.2}$	11
$N_3^+ + NO \rightarrow NO^+ + N + N_2$	$1.4x10^{-10}$	4
$HO_2 + O_3 \rightarrow OH + O_2 + O_2$	$1.4x10^{-14}exp(-600/T)$	24
$N_3^+ + NO_2 \rightarrow NO^+ + NO + N_2$	$7x10^{-11}$	4
$NO_2 + O_3 \rightarrow NO_3 + O_2$	$1.2x10^{-13}exp(-2450/T)$	11
$N_3^+ + NO_2 \rightarrow NO_2^+ + N + N_2$	$7x10^{-11}$	4
$N_3^+ + N_2O \rightarrow NO^+ + N_2 + N_2$	$5x10^{-11}$	4
$O + NO_2 \rightarrow NO + O_2$	$6.5x10^{-12}exp(120/T)$	11
$O + NO_3 \rightarrow O_2 + NO_2$	$1x10^{-11}$	4
$N_3^+ + NO_2^- \rightarrow N + N_2 + NO_2$	$2x10^{-6}(T/300)^{-0.5}$	4
$O + OH \rightarrow H + O_2$	$2.3x10^{-11}exp(110/T)$	15
$O^+ + N_2 \rightarrow NO^+ + N$	$1.2x10^{-12}$	4
$OH + OH + O_2 \rightarrow H_2O_2 + O_2$	$6.9x10^{-31}(T/300)^{-0.8}$	11
$O^+ + NO \rightarrow NO^+ + O$	$1.7x10^{-12}$	4
$OH + H_2O_2 \rightarrow H_2O + HO_2$	$2.9x10^{-12}exp(-160/T)$	24
$O^+ + O_2 \rightarrow O_2^+ + O$	$1.9x10^{-11}$	4
$H + HO_2 \rightarrow H_2 + O_2$	$1.1x10^{-10}exp(-1070/T)$	15
$O^+ + NO_2 \rightarrow NO_2^+ + O$	$1.6x10^{-9}$	4
$HO_2NO_2 + O_2 \rightarrow HO_2 + NO_2 + O_2$	$3.6x10^{-6}exp(-10000/T)$	24
$O^+ + NO_2^- \rightarrow O + NO_2$	$2x10^{-6}(T/300)^{-0.5}$	4
$O_2^+ + NO \rightarrow NO^+ + O_2$	$4.4x10^{-10}$	4

$O_2^+ + NO_2 \rightarrow NO_2^+ + O_2$	8.8×10^{-9}	4
$O_2^+ \cdot H_2O + H_2O \rightarrow H_3O^+ + OH + O_2$	1.2×10^{-9}	4
$H_3O^+ + H_2O + M \rightarrow H_3O^+ \cdot H_2O + M$	5×10^{-27}	4
$O_2^+ + NO_2^- \rightarrow O_2 + NO_2$	$2 \times 10^{-6}(T/300)^{-0.5}$	4
$H_3O^+ \cdot H_2O + H_2O \rightarrow H_3O^+ \cdot (H_2O)_2$	1×10^{-9}	4
$NO_2^+ + NO \rightarrow NO^+ + NO_2$	2.9×10^{-10}	4
$H_3O^+ \cdot (H_2O)_2 + NO_2^- \rightarrow H + (H_2O)_3 + NO_2$	$2 \times 10^{-7}(T/300)^{-0.5}$	4
$H_3O^+ \cdot (H_2O)_2 + NO_3^- \rightarrow H + (H_2O)_3 + NO_3$	$2 \times 10^{-7}(T/300)^{-0.5}$	4
$NO_2^+ + NO_2^- \rightarrow NO_2 + NO_2$	$3 \times 10^{-6}(T/300)^{-0.5}$	4
$NO_2^+ + NO_3^- \rightarrow NO_2 + NO_3$	$3 \times 10^{-6}(T/300)^{-0.5}$	4
$N_2^+ + NO \rightarrow NO^+ + N_2$	3.3×10^{-10}	4
$N_3^+ + H_2O \rightarrow H_2NO^+ + N_2$	3.3×10^{-10}	4
$N_2^+ + NO_2 \rightarrow NO_2^+ + N_2$	3.3×10^{-10}	4
$N_2^+ + NO_2 \rightarrow NO^+ + N_2O$	5.0×10^{-11}	4
$H_2NO^+ + NO_2^- \rightarrow H_2O + N + NO_2$	$2 \times 10^{-6}(T/300)^{-0.5}$	4
$H_2NO^+ + NO_3^- \rightarrow H_2O + N + NO_3$	$2 \times 10^{-6}(T/300)^{-0.5}$	4
$NO_2^- + HNO_3 \rightarrow NO_3^- + HNO_2$	1.6×10^{-9}	4
$N_2^+ + NO_2^- \rightarrow N_2 + NO_2$	$3 \times 10^{-6}(T/300)^{-0.5}$	4
$NO_2^- + NO_2 \rightarrow NO_3^- + NO$	1×10^{-13}	4
$N_2^+ + NO_3^- \rightarrow N_2 + NO_3$	$3 \times 10^{-6}(T/300)^{-0.5}$	4
$NO_2^- + N_2O \rightarrow NO_3^- + N_2$	5×10^{-13}	4
$NO_2^- + N_2O_5 \rightarrow$	7×10^{-10}	4

$NO_3^- + NO_2 + NO_2$		
$NO_2^- + O_3 \rightarrow NO_3^- + O_2$	1.2×10^{-10}	4
$NO_3^- + NO \rightarrow NO_2^- + NO_2$	5×10^{-13}	4
$NO^+ + NO_2^- \rightarrow NO + NO_2$	$3 \times 10^{-6}(T/300)^{-0.5}$	4
$NO^+ + NO_3^- \rightarrow NO + NO_3$	$3 \times 10^{-6}(T/300)^{-0.5}$	4
$O_2^- + NO_2 \rightarrow NO_2^- + O_2$	7×10^{-10}	4
$NO^+ + O_2 + M \rightarrow NO^+ \cdot O_2 + M$	3×10^{-31}	26
$O_2^- + N_2^+ \rightarrow N_2 + O_2$	$2 \times 10^{-6}(T/300)^{-0.5}$	4
$NO^+ \cdot O_2 + NO_2^- \rightarrow NO + O_2 + NO_2$	$3 \times 10^{-6}(T/300)^{-0.5}$	4
$N(^2D) + NH_3 \rightarrow NH + NH_2$	5×10^{-11}	4
$NO^+ \cdot O_2 + NO_2^- \rightarrow NO_3 + NO_2$	$2 \times 10^{-7}(T/300)^{-0.5}$	4
$NO^+ \cdot O_2 + NO_3^- \rightarrow NO + O_2 + NO_3$	$3 \times 10^{-6}(T/300)^{-0.5}$	4
$OH + NH_3 \rightarrow NH_2 + H_2O$	$3.5 \times 10^{-12}\exp(-925/T)$	11
$O(^1D) + NH_3 \rightarrow NH_2 + OH$	2.5×10^{-10}	4
$NH_2 + NO \rightarrow N_2 + H_2O$	$1.6 \times 10^{-11}(T/300)^{-1.5}$	11
$N^+ + N_2 + M \rightarrow N_3^+ + M$	5.2×10^{-30}	4
$NH_2 + NO_2 \rightarrow N_2O + H_2O$	$1.9 \times 10^{-11}(T/300)^{-2.2}$	11
$N^+ + O_2 \rightarrow NO^+ + O$	2.6×10^{-10}	4
$O_2^+ + NH_3 \rightarrow NH_3^+ + O_2$	1×10^{-9}	26
$N^+ + O_2 \rightarrow O_2^+ + N$	3.1×10^{-10}	4
$NH_3^+ + NH_3 \rightarrow NH_4^+ + NH_2$	2.2×10^{-9}	4
$N^+ + O_2 \rightarrow O^+ + NO$	3.6×10^{-11}	4
$H_3O^+ + NH_3 \rightarrow NH_4^+ + H_2O$	2.5×10^{-9}	4
$N^+ + NO \rightarrow NO^+ + N$	9×10^{-10}	4
$N^+ + NH_3 \rightarrow NH_3^+ + N$	2.4×10^{-9}	4

$N_2^+ + N_2 + M \rightarrow N_4^+ + M$	$1.1x10^{-29}$	4
$N_3^+ + NH_3 \rightarrow NH_3^+ + N + N_2$	$2.1x10^{-9}$	4
$N_2^+ + O_2 \rightarrow O_2^+ + N_2$	$5.1x10^{-11}$	4
$N_2^+ + NH_3 \rightarrow NH_3^+ + N_2$	$1.9x10^{-9}$	4
$N_4^+ + NO \rightarrow NO^+ + N_2 + N_2$	$1.8x10^{-9}$	4
$N_4^+ + NO_2 \rightarrow NO_2^+ + N_2 + N_2$	$2.5x10^{-10}$	4
$NH_3^+ + NO_3^- \rightarrow NH_3 + NO_3$	$5x10^{-6}(T/300)^{-0.5}$	b
$N_4^+ + NO_2 \rightarrow NO^+ + N_2O + N_2$	$5x10^{-11}$	4
$NH_4^+ + NO_3^- \rightarrow NH_3 + H + NO_3$	$3x10^{-6}(T/300)^{-0.5}$	4
$N_4^+ + O_2 \rightarrow O_2^+ + N_2 + N_2$	$2.5x10^{-10}$	4
$NO^+ + H_2O + M \rightarrow NO^+\cdot H_2O + M$	$1.6x10^{-28}$	4
$NO^+\cdot H_2O + H_2O + M \rightarrow NO^+\cdot (H_2O)_2 + M$	$1x10^{-27}$	4
$N_4^+ + NO_2^- \rightarrow NO_2 + N_2 + N_2$	$3x10^{-6}(T/300)^{-0.5}$	4
$NO^+\cdot (H_2O)_2 + M \rightarrow NO^+\cdot H_2O + H_2O + M$	$1.3x10^{-12}$	4
$N_4^+ + NO_3^- \rightarrow NO_3 + N_2 + N_2$	$3x10^{-6}(T/300)^{-0.5}$	4
$NO^+\cdot (H_2O)_2 + H_2O \rightarrow NO^+\cdot (H_2O)_3$	$1x10^{-9}$	4
$O_2^+ + H_2O + M \rightarrow O_2^+\cdot H_2O + M$	$2.5x10^{-28}$	4
$NO^+\cdot (H_2O)_3 + H_2O \rightarrow H_3O^+\cdot (H_2O)_2 + HNO_2$	$8x10^{-11}$	4
$NH_2 + O \rightarrow NH + OH$	$1.2x10^{-11}$	26
$NH_2 + O \rightarrow HNO + H$	$7.6x10^{-11}$	26
$HO_2NO_2 + N_2 \rightarrow HO_2 + NO_2 + N_2$	$5x10^{-6}\exp(-10000/T)$	11
$OH + NO_2 + O_2 \rightarrow HNO_3 + O_2$	$2.6x10^{-30}(T/300)^{-2.9}$	11

$OH + H_2 \rightarrow H_2O + H$	$7.7x10^{-12}exp(-2100/T)$	15
$O(^1D) + H_2O \rightarrow H_2 + O_2$	$2.3x10^{-12}$	24
$O(^1D) + H_2 \rightarrow OH + H$	$1.1x10^{-10}$	24
$O + H_2O_2 \rightarrow OH + HO_2$	$1.4x10^{-12}exp(-2000/T)$	15
$O+ H_2 \rightarrow OH + H$	$1.6x10^{-11}exp(-4570/T)$	24
$H + HO_2 \rightarrow H_2O + O$	$9.4x10^{-13}$	24
$O + O_2 + N_2 \rightarrow O_2 + O + N_2$	$6.2x10^{-34}(T/300)^{-2.0}$	30[b]
$HO_2 + HO_2 + M \rightarrow H_2O_2 + O_2 + M$	$1.9x10^{-33}exp(980/T)$	11
$O + NO + N_2 \rightarrow NO_2 + N_2$	$9.1x10^{-28}T^{-1.6}$	11
$NO_2 + NO_3 + M \rightarrow N_2O_5 + M$	$2.7x10^{-30}(T/300)^{-3.4}$	11
$N^+ + H_2O \rightarrow H_2O^+ + N$	$5.55x10^{-8}T^{-0.52}$	5
$H_2O^+ + NO_2^- \rightarrow H_2O + NO_2$	$2x10^{-6}(T/300)^{-0.5}$	32
$H_2O^+ + NO_3^- \rightarrow H_2O + NO_3$	$2x10^{-6}(T/300)^{-0.5}$	32
$H_2O^+ + O_2^- \rightarrow H_2O + O_2$	$2x10^{-6}(T/300)^{-0.5}$	32
$H_3O^+ + NO_2^- \rightarrow H_2O + H + NO_2$	$2x10^{-6}(T/300)^{-0.5}$	32
$H_3O^+ + NO_3^- \rightarrow H_2O + H + NO_3$	$2x10^{-6}(T/300)^{-0.5}$	32
$H_3O^+ + O_2^- \rightarrow H_2O + H + O_2$	$2x10^{-6}(T/300)^{-0.5}$	32
$O_2^+ + NO_3^- \rightarrow O_2 + NO_3$	$2x10^{-6}(T/300)^{-0.5}$	32
$O_2^+ + O_2^- \rightarrow O_2 + O_2$	$2x10^{-6}(T/300)^{-0.5}$	32
$N_3^+ + NO_3^- \rightarrow N_2 + N + NO_3$	$2x10^{-6}(T/300)^{-0.5}$	b
$N_3^+ + O_2^- \rightarrow N_2 + N + O_2$	$2x10^{-6}(T/300)^{-0.5}$	b
$NO^+ + O_2^- \rightarrow NO + O_2$	$2x10^{-6}(T/300)^{-0.5}$	32
$NO_2^+ + O_2^- \rightarrow NO_2 + O_2$	$2x10^{-6}(T/300)^{-0.5}$	32
$O^+ + NO_3^- \rightarrow O+ NO_3$	$2x10^{-6}(T/300)^{-0.5}$	32
$O^+ + O_2^- \rightarrow O+ O_2$	$2x10^{-6}(T/300)^{-0.5}$	32
$NO^+ \cdot O_2 + O_2^- \rightarrow NO + O_2 + O_2$	$2x10^{-6}(T/300)^{-0.5}$	b

$N^+ + O_2^- \rightarrow N + O_2$	$2x10^{-6}(T/300)^{-0.5}$	32
$N^+ + NO_2^- \rightarrow N + NO_2$	$2x10^{-6}(T/300)^{-0.5}$	32
$N^+ + NO_3^- \rightarrow N + NO_3$	$2x10^{-6}(T/300)^{-0.5}$	32
$N_4^+ + O_2^- \rightarrow N_2 + N_2 + O_2$	$2x10^{-6}(T/300)^{-0.5}$	b
$O_2^+ \cdot H_2O + O_2^- \rightarrow O_2 + O_2 + H_2O$	$2x10^{-6}(T/300)^{-0.5}$	b
$O_2^+ \cdot H_2O + NO_3^- \rightarrow O_2 + NO_3 + H_2O$	$2x10^{-6}(T/300)^{-0.5}$	b
$O_2^+ \cdot H_2O + NO_2^- \rightarrow O_2 + H_2O + NO_2$	$2x10^{-6}(T/300)^{-0.5}$	b
$H_3O^+ \cdot H_2O + NO_2^- \rightarrow H + H_2O + H_2O + NO_2$	$2x10^{-6}(T/300)^{-0.5}$	b
$H_3O^+ \cdot H_2O + NO_3^- \rightarrow H + H_2O + H_2O + NO_3$	$2x10^{-6}(T/300)^{-0.5}$	b
$H_3O^+ \cdot H_2O + O_2^- \rightarrow H + H_2O + H_2O + O_2$	$2x10^{-6}(T/300)^{-0.5}$	b
$H_3O^+ \cdot (H_2O)_2 + O_2^- \rightarrow (H_2O)_3 + O_2$	$2x10^{-6}(T/300)^{-0.5}$	b H +
$H_2NO^+ + O_2^- \rightarrow H_2O + N + O_2$	$2x10^{-6}(T/300)^{-0.5}$	b
$NH_3^+ + NO_2^- \rightarrow NH_3 + NO_2$	$2x10^{-6}(T/300)^{-0.5}$	32
$NH_3^+ + O_2^- \rightarrow NH_3 + O_2$	$2x10^{-6}(T/300)^{-0.5}$	32
$NH_4^+ + NO_2^- \rightarrow NH_3 + H + NO_2$	$2x10^{-6}(T/300)^{-0.5}$	b
$NH_4^+ + NO_3^- \rightarrow NH_3 + H + NO_3$	$2x10^{-6}(T/300)^{-0.5}$	b
$NH_4^+ + O_2^- \rightarrow NH_3 + H + O_2$	$2x10^{-6}(T/300)^{-0.5}$	b
$NO^+ \cdot H_2O + NO_2^- \rightarrow NO + H_2O + NO_2$	$2x10^{-6}(T/300)^{-0.5}$	b
$NO^+ \cdot H_2O + NO_3^- \rightarrow NO + H_2O + NO_3$	$2x10^{-6}(T/300)^{-0.5}$	b

$NO^+ \cdot H_2O + O_2^- \rightarrow$ $NO + H_2O + O_2$	$2x10^{-6}(T/300)^{-0.5}$	b
$NO^+ \cdot (H_2O)_2 + NO_3^- \rightarrow$ $NO + H_2O + H_2O + NO_3$	$2x10^{-6}(T/300)^{-0.5}$	b
$NO^+ \cdot (H_2O)_3 + NO_3^- \rightarrow$ $NO + H_2O + H_2O + H_2O + NO_3$	$2x10^{-6}(T/300)^{-0.5}$	b
$NO^+ \cdot (H_2O)_2 + NO_2^- \rightarrow$ $NO + H_2O + H_2O + NO_2$	$2x10^{-6}(T/300)^{-0.5}$	b
$NO^+ \cdot (H_2O)_3 + NO_2^- \rightarrow$ $NO + H_2O + H_2O + H_2O + NO_2$	$2x10^{-6}(T/300)^{-0.5}$	b
$NO^+ \cdot (H_2O)_2 + O_2^- \rightarrow$ $NO + H_2O + H_2O + O_2$	$2x10^{-6}(T/300)^{-0.5}$	b
$NO^+ \cdot (H_2O)_3 + O_2^- \rightarrow$ $NO + H_2O + H_2O + H_2O + O_2$	$2.00x10^{-6}(T/300)^{-0.5}$	b
$O + H + M \rightarrow OH + M$	$1.62x10^{-32}$	28
$H + H_2O_2 \rightarrow H_2O + OH$	$4x10^{-11}\exp(-2000/T)$	15
$NO_2 + NO_2 + N_2 \rightarrow$ $N_2O_4 + N_2$	$1.4x10^{-33}(T/300)^{-3.8}$	17
$N_2O_4 + N_2 \rightarrow$ $NO_2 + NO_2 + N_2$	$1.29x10^{-5}(T/300)^{-3.8}$ $*\exp(-6460/T)$	17
$NH_2 + H_2 \rightarrow NH_3 + H$	$5.98x10^{-12}\exp(-2290/T)$	27
$NH_3 + H \rightarrow NH_2 + H_2$	$1.35x10^{-10}\exp(-3660/T)$	27
$OH + NO_3 \rightarrow HO_2 + NO_2$	$2.6x10^{-11}$	29
$HO_2 + NO_3 \rightarrow OH + NO_2 + O_2$	$3.6x10^{-12}$	29
$HO_2 + NO_3 \rightarrow HNO_3 + O_2$	$9.2x10^{-13}$	29
$H + H_2O_2 \rightarrow HO_2 + H_2$	$8x10^{-11}\exp(-4000/T)$	15
$HNO_3 + NO \rightarrow HNO_2 + NO_2$	$7.37x10^{-21}$	25
$H_2 + O_2 \rightarrow H + HO_2$	$2.4x10^{-10}\exp(-28500/T)$	15
$H + O_2 \rightarrow OH + O$	$2.8x10^{-7}T^{-0.9}\exp(-8750/T)$	15
$OH + M \rightarrow O + H + M$	$4x10^{-9}\exp(-50000/T)$	15

$OH + O_2 \rightarrow O + HO_2$	$3.7x10^{-11}exp(-26500/T)$	15
$OH + H \rightarrow O + H_2$	$1.14x10^{-12}T^{0.67}exp(-518/T)$	5
$HO_2 + M \rightarrow H + O_2 + M$	$2x10^{-5}T^{-1.18}exp(-24363/T)$	15
$HO_2 + H_2 \rightarrow H_2O_2 + H$	$5x10^{-11}exp(-13100/T)$	15
$H_2O_2 + O_2 \rightarrow HO_2 + HO_2$	$9x10^{-11}exp(-20000/T)$	15
$H_2O + H \rightarrow H_2 + OH$	$1.03x10^{-16}T^{1.9}exp(-9265/T)$	15
$H_2O + O \rightarrow OH + OH$	$7.6x10^{-15}T^{1.3}exp(-8605/T)$	15
$H^- + N_2^+ \rightarrow H + N_2$	$3x10^{-6}(T/300)^{-0.5}$	b
$O^- + N_2^+ \rightarrow O + N_2$	$3x10^{-6}(T/300)^{-0.5}$	b
$O^- + H_2^+ \rightarrow O + H_2$	$3x10^{-6}(T/300)^{-0.5}$	32
$O_2^- + H_2^+ \rightarrow O_2 + H_2$	$3x10^{-6}(T/300)^{-0.5}$	32
$H^- + H_2^+ \rightarrow H + H_2$	$3x10^{-6}(T/300)^{-0.5}$	32
$H^- + H_2O^+ \rightarrow H + H_2O$	$3x10^{-6}(T/300)^{-0.5}$	32
$O^- + H_2O^+ \rightarrow O + H_2O$	$3x10^{-6}(T/300)^{-0.5}$	32
$H^- + H_3O^+ \rightarrow H_2 + H_2O$	$3x10^{-6}(T/300)^{-0.5}$	b
$O^- + H_3O^+ \rightarrow OH + H_2O$	$3x10^{-6}(T/300)^{-0.5}$	b
$H^- + O_2^+ + M \rightarrow H_2O + M$	$1.2x10^{-25}$	b
$O^- + O_2^+ \rightarrow O + O_2$	$3x10^{-6}(T/300)^{-0.5}$	32
$H^- + N_3^+ \rightarrow NH + N_2$	$3x10^{-6}(T/300)^{-0.5}$	b
$O^- + N_3^+ \rightarrow NO + N_2$	$3x10^{-6}(T/300)^{-0.5}$	b
$H^- + NO^+ + M \rightarrow HNO + M$	$1.2x10^{-25}$	b
$O^- + NO^+ \rightarrow NO + O$	$3x10^{-6}(T/300)^{-0.5}$	b
$H^- + NO_2^+ + M \rightarrow HNO_2 + M$	$1.2x10^{-25}$	b
$O^- + NO_2^+ \rightarrow NO_2 + O$	$3x10^{-6}(T/300)^{-0.5}$	32
$H^- + O^+ + M \rightarrow OH + M$	$1.2x10^{-25}$	b
$O^- + O^+ + M \rightarrow O_2 + M$	$1.2x10^{-25}$	b
$H^- + NO^+ \cdot O_2 \rightarrow HNO + O_2$	$3x10^{-6}(T/300)^{-0.5}$	b

$O^- + NO^+ \cdot O_2 \rightarrow NO_2 + O_2$	$3x10^{-6}(T/300)^{-0.5}$	b
$H^- + N^+ + M \rightarrow NH + M$	$1.2x10^{-25}$	b
$O^- + N^+ + M \rightarrow NO + M$	$1.2x10^{-25}$	b
$H^- + N_4^+ \rightarrow H + N_2 + N_2$	$3x10^{-6}(T/300)^{-0.5}$	b
$O^- + N_4^+ \rightarrow O + N_2 + N_2$	$3x10^{-6}(T/300)^{-0.5}$	b
$H^- + O_2^+ \cdot H_2O \rightarrow HO_2 + H_2O$	$3x10^{-6}(T/300)^{-0.5}$	b
$O^- + O_2^+ \cdot H_2O \rightarrow O + O_2 + H_2O$	$3x10^{-6}(T/300)^{-0.5}$	b
$H^- + H_3O^+ \cdot H_2O \rightarrow H_2 + H_2O + H_2O$	$3x10^{-6}(T/300)^{-0.5}$	b
$O^- + H_3O^+ \cdot H_2O \rightarrow OH + H_2O + H_2O$	$3x10^{-6}(T/300)^{-0.5}$	b
$H^- + H_3O^+ \cdot (H_2O)_2 \rightarrow H_2 + (H_2O)_3$	$3x10^{-6}(T/300)^{-0.5}$	b
$O^- + H_3O^+ \cdot (H_2O)_2 \rightarrow OH + (H_2O)_3$	$3x10^{-6}(T/300)^{-0.5}$	b
$H^- + H_2NO^+ \rightarrow H_2 + HNO$	$3x10^{-6}(T/300)^{-0.5}$	b
$O^- + H_2NO^+ \rightarrow OH + HNO$	$3x10^{-6}(T/300)^{-0.5}$	b
$H^- + NH_3^+ \rightarrow H + NH_3$	$3x10^{-6}(T/300)^{-0.5}$	b
$O^- + NH_3^+ \rightarrow O + NH_3$	$3x10^{-6}(T/300)^{-0.5}$	b
$H^- + NH_4^+ \rightarrow H_2 + NH_3$	$3x10^{-6}(T/300)^{-0.5}$	b
$O^- + NH_4^+ \rightarrow OH + NH_3$	$3x10^{-6}(T/300)^{-0.5}$	b
$H^- + NO^+ \cdot H_2O \rightarrow H + NO + H_2O$	$3x10^{-6}(T/300)^{-0.5}$	b
$O^- + NO^+ \cdot H_2O \rightarrow O + NO + H_2O$	$3x10^{-6}(T/300)^{-0.5}$	b
$H^- + NO^+ \cdot (H_2O)_2 \rightarrow HNO + H_2O + H_2O$	$3x10^{-6}(T/300)^{-0.5}$	b
$O^- + NO^+ \cdot (H_2O)_2 \rightarrow NO_2 + H_2O + H_2O$	$3x10^{-6}(T/300)^{-0.5}$	b
$H^- + NO^+ \cdot (H_2O)_3 \rightarrow HNO + H_2O + H_2O + H_2O$	$3x10^{-6}(T/300)^{-0.5}$	b
$O^- + NO^+ \cdot (H_2O)_3 \rightarrow$	$3x10^{-6}(T/300)^{-0.5}$	b

$NO_2 + H_2O + H_2O + H_2O$		
$(H_2O)_3 \rightarrow H_2O + H_2O + H_2O$	$1x10^{-7}$	b
$OH + NO_2 + H_2O \rightarrow HNO_3 + H_2O$	$2.2x10^{-30}(T/300)^{-2.9}$	30
$N_2^+ + H_2O \rightarrow H_2O^+ + N_2$	$2x10^{-9}$	b
$O + OH + M \rightarrow HO_2 + M$	$2.76x10^{-31}$	30
$O(^1D) + O_3 \rightarrow O_2 + O + O$	$1.2x10^{-10}$	31
$O(^1D) + NO \rightarrow O_2 + N$	$8.5x10^{-11}$	31
$NH + NO \rightarrow N_2 + OH$	$4.5x10^{-11}$	31
$N_3 + NO \rightarrow N_2O + N_2$	$1.19x10^{-12}$	31
$NH_2 + O \rightarrow H_2 + NO$	$8.3x10^{-12}$	31
$OH + NO_2 \rightarrow HO_2 + NO$	$3.03x10^{-11}exp(-3360/T)$	31
$NO_3 + NO_2 \rightarrow NO + NO_2 + O_2$	$8.21x10^{-14}exp(-1480/T)$	31
$O(^1D) + NO_2 \rightarrow O_2 + NO$	$2.5x10^{-10}$	31
$O(^1D) + N_2O \rightarrow NO + NO$	$6.7x10^{-11}$	31
$NO_2 + O_3 \rightarrow O_2 + O_2 + NO$	$1.0x10^{-18}$	22
$O + N_3 \rightarrow NO + N_2$	$1.12x10^{-11}$	31
$O + HNO \rightarrow OH + NO$	$1.82x10^{-11}$	31
$HNO + O_2 \rightarrow NO + HO_2$	$5.25x10^{-12}exp(-1510/T)$	23
$O + O + M \rightarrow O_2 + M$	$5.21x10^{-35}exp(900/T)$	31

Additional reactions of $N_2/O_2/H_2O/CO_2$

Reaction	Rate Coefficient [c]	Ref.
$N_2(A) + CO_2 \rightarrow N_2 + CO_2$	$2.5x10^{-11}$	37
$N_2(A) + CO \rightarrow N_2 + CO$	$1.1x10^{-10}$	37
$O(^1D) + CO_2 \rightarrow O + CO_2$	$7.4x10^{-11}$	b
$OH + CO \rightarrow CO_2 + H$	$1.12x10^{-13}exp(-9.1x10^{-4} \times T)$	15
$CO_2^+ + NO \rightarrow NO^+ + CO_2$	$1.2x10^{-10}$	4

$CO_2^+ + O_2 \rightarrow O_2^+ + CO_2$	$5.6x10^{-11}$	4
$CO_2^+ + NO_2^- \rightarrow CO_2 + NO_2$	$2x10^{-6}(T/300)^{-0.5}$	32
$CO_2^+ + NO_3^- \rightarrow CO_2 + NO_3$	$2x10^{-6}(T/300)^{-0.5}$	32
$CO_2^+ + O_2^- \rightarrow CO_2 + O_2$	$2x10^{-6}(T/300)^{-0.5}$	32
$OH + CO \rightarrow HOCO^*$	$1.55x10^{-13}$	b
$CO_2 + H \rightarrow CO + OH$	$2.5x10^{-10}\exp(-13300/T)$	15
$CO_2 + O \rightarrow CO + O_2$	$2.8x10^{-11}\exp(-26500/T)$	15
$CO + O_2 \rightarrow CO_2 + O$	$4.2x10^{-12}\exp(-24000/T)$	15
$CO + O + M \rightarrow CO_2 + M$	$1.7x10^{-33}\exp(-1510/T)$	15
$CO + HO_2 \rightarrow OH + CO_2$	$2.5x10^{-10}\exp(-11900/T)$	15
$HCO + M \rightarrow H + CO + M$	$8.5x10^{-3}T^{-2.14}\exp(-10278/T)$	15
$HCO + H_2 \rightarrow CH_2O + H$	$3x10^{-18}T^{2.0}\exp(-8972/T)$	15
$HCO + O_2 \rightarrow HO_2 + CO$	$8.5x10^{-11}\exp(-850/T)$	15
$HCO + H \rightarrow H_2 + CO$	$2x10^{-10}$	15
$HCO + O \rightarrow H + CO_2$	$5x10^{-11}$	15
$HCO + O \rightarrow OH + CO$	$5x10^{-11}$	15
$HCO + OH \rightarrow H_2O + CO$	$5x10^{-11}$	15
$HCO + HO_2 \rightarrow OH + H + CO_2$	$5x10^{-11}$	15
$HCO + H_2O_2 \rightarrow CH_2O + HO_2$	$1.7x10^{-13}\exp(-3486/T)$	15
$HCO + H_2O \rightarrow CH_2O + OH$	$3.9x10^{-16}T^{1.35}\exp(-13146/T)$	15
$HCO + HCO \rightarrow CH_2O + CO$	$3x10^{-11}$	15
$HCO + HCO \rightarrow H_2 + CO + CO$	$5x10^{-12}$	15
$H^- + CO_2^+ \rightarrow H + CO_2$	$3x10^{-6}(T/300)^{-0.5}$	b
$O^- + CO_2^+ \rightarrow O + CO_2$	$3x10^{-6}(T/300)^{-0.5}$	b
$CH_2O + OH \rightarrow H + HCOOH$	$2x10^{-13}$	31
$HCOOH + OH \rightarrow H_2O + CO_2 + H$	$4.8x10^{-13}$	31

$CN + O \rightarrow CO + N$	$1.7x10^{-11}$	31
$CN + N \rightarrow N_2 + C$	$3x10^{-10}$	b
$CN + N + M \rightarrow CNN + M$	$2.76x10^{-32}$	31
$CN + NO \rightarrow N_2 + CO$	$1.2x10^{-13}$	31
$CN + N_2O \rightarrow CNN + NO$	$6.40x10^{-21}T^{2.6}exp(-1860/T)$	31
$CN + HCN \rightarrow NCCN + H$	$6.31x10^{-17}T^{1.57}exp(-50/T)$	31
$CN + H_2O \rightarrow HCN + OH$	$1.33x10^{-11}exp(-3752/T)$	31
$CN + H_2 \rightarrow HCN + H$	$1.13x10^{-10}exp(-2700/T)$	31
$CN + O_2 \rightarrow NCO + O$	$1.1x10^{-11}exp(205/T)$	31
$CN + CO_2 \rightarrow NCO + CO$	$2x10^{-15}$	31
$HCN + O \rightarrow OH + CN$	$4.5x10^{-15}T^{1.58}exp(-13386/T)$	31
$HCN + O \rightarrow H + NCO$	$3.3x10^{-16}T^{1.47}exp(-3774/T)$	31
$HCN + O \rightarrow CO + NH$	$9.0x10^{-16}T^{1.21}exp(-3824/T)$	31
$HCN + OH \rightarrow H_2O + CN$	$1.28x10^{-11}exp(-4161/T)$	31
$HCN + OH \rightarrow HOCN + H$	$2.01x10^{-11}exp(-8516/T)$	31
$HCN + OH \rightarrow HNCO + H$	$2.84x10^{-13}exp(-4397/T)$	31
$HCN + OH \rightarrow NH_2 + CO$	$1.07x10^{-13}exp(-5892/T)$	31
$HCN + H \rightarrow CN + H_2$	$6.31x10^{-10}exp(-12400/T)$	31
$NCO + H_2 \rightarrow H + HNCO$	$1.26x10^{-21}T^{3}exp(-2012/T)$	31
$NCO + O \rightarrow NO + CO$	$1.48x10^{-11}$	31
$NCO + O_2 \rightarrow NO + CO_2$	$1.32x10^{-12}$	31
$NCO + NO \rightarrow CO + N_2 + O$	$7.61x10^{-12}$	31
$NCO + NO \rightarrow CO_2 + N_2$	$1.45x10^{-11}$	31
$NCO + NO \rightarrow N_2O + CO$	$1.09x10^{-11}$	31
$NCCN + O \rightarrow CN + NCO$	$4.15x10^{-11}exp(-5500/T)$	31
$NCCN + H \rightarrow NCN + CN$	$8.59x10^{-16}$	31
$CO + H + M \rightarrow HCO + M$	$1.99x10^{-33}exp(-842/T)$	31

$CO + NO_2 \rightarrow CO_2 + NO$	$1.48x10^{-10}exp(-17009/T)$	31
$CO + O_3 \rightarrow O_2 + CO_2$	$4x10^{-25}$	31
$C + CO + M \rightarrow C_2O + M$	$6.3x10^{-32}$	31
$C_2O + O \rightarrow CO + CO$	$9.51x10^{-11}$	31
$C_2O + O_2 \rightarrow C_2O + CO$	$3.3x10^{-13}$	31
$C_2O + N \rightarrow CO + CN$	$5.5x10^{-10}$	31
$C + N + M \rightarrow CN + M$	$9.41x10^{-33}$	31
$C + NCCN \rightarrow CN + CCN$	$3x10^{-11}$	31
$C + NO \rightarrow CN + O$	$4.8x10^{-11}$	31
$C + N_2 + M \rightarrow CNN + M$	$3.1x10^{-33}$	31
$C + N_3 \rightarrow CN + N_2$	$1.10x10^{-10}$	31
$C + O_2 \rightarrow CO + O$	$2.6x10^{-11}$	31
$CCN+ O \rightarrow CO + CN$	$6x10^{-12}$	31
$CCN+ N \rightarrow CN + CN$	$1x10^{-10}$	31
$CO_2 + N \rightarrow CO + NO$	$3.2x10^{-13}exp(-1710/T)$	31

Additional reactions of $Ar/O_2/H_2O$/PCE

Reaction	Rate Coefficient [c]	Ref.
$Cl^- + H_2^+ \rightarrow Cl + H_2$	$3x10^{-6}\ (T/300)^{-0.5}$	32
$CCl_4 + O \rightarrow ClO + CCl_3$	$4.98x10^{-13}exp(-2200/T)$	30
$ClO + H_2 \rightarrow HCl + OH$	$4.98x10^{-16}$	30
$ClO + H_2 \rightarrow HOCl + H$	$1.1x10^{-20}$	31
$ClO + O \rightarrow Cl + O_2$	$3x10^{-11}exp(-6.995/T)$	30
$ClO + ClO \rightarrow Cl_2 + O_2$	$4.9x10^{-15}$	30
$CCl_4 + OH \rightarrow HOCl + CCl_3$	$1x10^{-12}exp(-2320/T)$	30
$HOCl + O \rightarrow OH + ClO$	$1x10^{-11}exp(-2200/T)$	30
$HOCl + OH \rightarrow H_2O + ClO$	$3x10^{-12}exp(-500.2/T)$	30

$CCl_3 + H_2 \rightarrow CHCl_3 + H$	$8.32x10^{-12}exp(-7196/T)$	31
$CCl_3 + O \rightarrow Cl + COCl_2$	$4.15x10^{-11}$	30
$CCl_3 + O_2 + M \rightarrow CCl_3O_2 + M$	$3.244x10^{-23}T^{-3}$ exp$(2.922x10^{-8}/T)$*0.02	30
$CHCl_3 + O \rightarrow OH + CCl_3$	$4.98x10^{-12}exp(-2500/T)$	30
$CHCl_3 + OH \rightarrow H_2O + CCl_3$	$4.064x10^{-12}exp(-1088/T)$	30
$CHCl_3 + Cl \rightarrow HCl + CCl_3$	$5.69x10^{-12}$	30
$COCl_2 + O \rightarrow ClO + COCl$	$9.96x10^{-15}$	30
$COCl_2 + O(^1D) \rightarrow ClO + COCl$	$1x10^{-10}$	30[b]
$ClO + ClO \rightarrow Cl + ClOO$	$3.4x10^{-15}$	30
$O + HCl \rightarrow OH + Cl$	$9.784x10^{-12}exp(-3308/T)$	30
$OH + HCl \rightarrow H_2O + Cl$	$2.999x10^{-12}exp(-414.5/T)$	30
$H + HCl \rightarrow H_2 + Cl$	$1.32x10^{-11}exp(-1710/T)$	30
$Cl + H_2O \rightarrow OH + HCl$	$2.79x10^{-11}exp(-8670/T)$	31
$Cl + H_2 \rightarrow HCl + H$	$3.7x10^{-11}exp(-2300/T)$	30
$Cl + O_2 + M \rightarrow ClOO + M$	$8.996x10^{-30}T^{-1.45}$ x exp$(2.911x10^{-8}/T)$	30
$OH + Cl \rightarrow O + HCl$	$9.8x10^{-12}exp(-2860/T)$	30
$Cl + O_3 \rightarrow ClO + O_2$	$2.609x10^{-11}exp(-236.9/T)$	30
$Cl + CCl_3 \rightarrow CCl_4$	$5x10^{-11}$	30
$Cl + HOCl \rightarrow Cl_2 + OH$	$3x10^{-12}exp(-129.8/T)$	30
$Cl + HOCl \rightarrow HCl + ClO$	$3x10^{-12}exp(-129.8/T)$	30
$Cl + ClO \rightarrow O + Cl_2$	$1.74x10^{-12}exp(-4590/T)$	b
$CCl_3^+ + H^- \rightarrow CCl_3 + H$	$5x10^{-8}$ $(T/300)^{-0.5}$	32
$CCl_3^+ + O^- \rightarrow CCl_3 + O$	$5x10^{-8}$ $(T/300)^{-0.5}$	32
$CCl_3^+ + O_2^- \rightarrow CCl_3 + O_2$	$5x10^{-8}$ $(T/300)^{-0.5}$	32
$CCl_3^+ + Cl^- \rightarrow CCl_3 + Cl$	$5x10^{-8}$ $(T/300)^{-0.5}$	32

$CCl_2^+ + H^- \rightarrow CCl_2 + H$	$5x10^{-8} (T/300)^{-0.5}$	32
$CCl_2^+ + O^- \rightarrow CCl_2 + O$	$5x10^{-8} (T/300)^{-0.5}$	32
$CCl_2^+ + O_2^- \rightarrow CCl_2 + O_2$	$5x10^{-8} (T/300)^{-0.5}$	32
$CCl_2^+ + Cl^- \rightarrow CCl_2 + Cl$	$5x10^{-8} (T/300)^{-0.5}$	32
$CCl^+ + H^- \rightarrow CCl + H$	$5x10^{-8} (T/300)^{-0.5}$	32
$CCl^+ + O^- \rightarrow CCl + O$	$5x10^{-8} (T/300)^{-0.5}$	32
$CCl^+ + O_2^- \rightarrow CCl + O_2$	$5x10^{-8} (T/300)^{-0.5}$	32
$CCl^+ + Cl^- \rightarrow CCl + Cl$	$5x10^{-8} (T/300)^{-0.5}$	32
$Cl_2^+ + H^- \rightarrow Cl_2 + H$	$5x10^{-8} (T/300)^{-0.5}$	32
$Cl_2^+ + O^- \rightarrow Cl_2 + O$	$5x10^{-8} (T/300)^{-0.5}$	32
$Cl_2^+ + O_2^- \rightarrow Cl_2 + O_2$	$5x10^{-8} (T/300)^{-0.5}$	32
$Cl_2^+ + Cl^- \rightarrow Cl_2 + Cl$	$5x10^{-8} (T/300)^{-0.5}$	32
$Cl^+ + H^- \rightarrow Cl + H$	$5x10^{-8} (T/300)^{-0.5}$	32
$Cl^+ + O^- \rightarrow Cl + O$	$5x10^{-8} (T/300)^{-0.5}$	32
$Cl^+ + O_2^- \rightarrow Cl + O_2$	$5x10^{-8} (T/300)^{-0.5}$	32
$Cl^+ + Cl^- \rightarrow Cl + Cl$	$5x10^{-8} (T/300)^{-0.5}$	32
$C^+ + H^- \rightarrow C + H$	$5x10^{-8} (T/300)^{-0.5}$	32
$C^+ + O^- \rightarrow C + O$	$5x10^{-8} (T/300)^{-0.5}$	32
$C^+ + O_2^- \rightarrow C + O_2$	$5x10^{-8} (T/300)^{-0.5}$	32
$C^+ + Cl^- \rightarrow C + Cl$	$5x10^{-8} (T/300)^{-0.5}$	32
$CCl_3^{+2} + H^- \rightarrow CCl_3^+ + H$	$5x10^{-8} (T/300)^{-0.5}$	32
$CCl_3^{+2} + O^- \rightarrow CCl_3^+ + O$	$5x10^{-8} (T/300)^{-0.5}$	32
$CCl_3^{+2} + O_2^- \rightarrow CCl_3^+ + O_2$	$5x10^{-8} (T/300)^{-0.5}$	32
$CCl_3^{+2} + Cl^- \rightarrow CCl_3^+ + Cl$	$5x10^{-8} (T/300)^{-0.5}$	32
$CCl_2^{+2} + H^- \rightarrow CCl_2^+ + H$	$5x10^{-8} (T/300)^{-0.5}$	32
$CCl_2^{+2} + O^- \rightarrow CCl_2^+ + O$	$5x10^{-8} (T/300)^{-0.5}$	32
$CCl_2^{+2} + O_2^- \rightarrow CCl_2^+ + O_2$	$5x10^{-8} (T/300)^{-0.5}$	32

$CCl_2^{+2} + Cl^- \rightarrow CCl_2^+ + Cl$	$5x10^{-8}\ (T/300)^{-0.5}$	32
$H_2O + Cl^- \rightarrow H_2O + Cl$	$5x10^{-8}\ (T/300)^{-0.5}$	32
$H_3O + Cl^- \rightarrow H_3O + Cl$	$5x10^{-8}\ (T/300)^{-0.5}$	32
$O_2^+ + Cl^- \rightarrow O_2 + Cl$	$5x10^{-8}\ (T/300)^{-0.5}$	32
$O^+ + Cl^- \rightarrow O + Cl$	$5x10^{-8}\ (T/300)^{-0.5}$	32
$O_2^+ \cdot H_2O + Cl^- \rightarrow O_2 + H_2O + Cl$	$5x10^{-8}\ (T/300)^{-0.5}$	b
$H_3O^+ \cdot H_2O + Cl^- \rightarrow H_3O + H_2O + Cl$	$5x10^{-8}\ (T/300)^{-0.5}$	b
$CO_2^+ + Cl^- \rightarrow CO_2 + Cl$	$5x10^{-8}\ (T/300)^{-0.5}$	b
$H_3O^+ \cdot (H_2O)_2 + Cl^- \rightarrow H + (H_2O)_3 + Cl$	$5x10^{-8}\ (T/300)^{-0.5}$	b
$ClOO + M \rightarrow Cl + O_2 + M$	$1.5x10^{-8}exp(-3286/T)$	31
$H + ClOO \rightarrow OH + ClO$	$5.64x10^{-11}$	30
$Cl + ClOO \rightarrow Cl_2 + O_2$	$1.4x10^{-10}$	30
$Cl + ClOO \rightarrow ClO + ClO$	$8x10^{-12}$	30
$Cl + CCl_2 \rightarrow CCl_3$	$5x10^{-11}$	b
$H_2O + CCl_4 \rightarrow CCl_3^+ + Cl + H_2O$	$1x10^{-9}$	b
$O_2 + CCl_4 \rightarrow CCl_3^+ + Cl + O_2$	$1x10^{-9}$	b
$O^+ + CCl_4 \rightarrow CCl_3^+ + Cl + O$	$1x10^{-9}$	b
$CCl_3O_2 \rightarrow CCl_3 + O_2$	$4.485x10^{20}T^{-1.0}exp(-11070/T)$	30
$CCl_3O_2 + CCl_3 \rightarrow CCl_3O + CCl_3O$	$1x10^{-12}$	30
$CCl_3O_2 + CCl_3O_2 \rightarrow CCl_3O + CCl_3O + O_2$	$4.24x10^{-5}T^{-3}$	30
$CCl_3O \rightarrow COCl_2 + Cl$	$1x10^{+5}$	30
$Ar^+ + O_2 \rightarrow O_2^+ + Ar$	$4x10^{-11}$	b
$Ar^+ + O_3 \rightarrow O_2^+ + Ar + O$	$4x10^{-11}$	b

$Ar^+ + H_2 \rightarrow H_2^+ + Ar$	$1x10^{-9}$	b
$Ar^+ + CCl_4 \rightarrow CCl3^+ + Cl + Ar$	$1x10^{-9}$	b
$Ar^* + CCl_4 \rightarrow CCl_2 + Cl_2 + Ar$	$1x10^{-10}$	b
$Ar^{**} \rightarrow Ar^*$	$1x10^{+6}$	b
$Ar^{**} + CCl_4 \rightarrow CCl_2 + Cl_2 + Ar$	$1x10^{-10}$	b
$Ar^{**} + Ar + M \rightarrow Ar_2^* + M$	$3x10^{-33}$	b
$Ar_2^* \rightarrow Ar + Ar$	$6x10^{+7}$	b
$Ar^+ + Ar + M \rightarrow Ar_2^+ + M$	$2x10^{-31}$	b
$Ar_2^+ + O_2 \rightarrow O_2^+ + Ar + Ar$	$1.2x10^{-10}$	38
$Ar^+ + H_2O \rightarrow H_2O^+ + Ar$	$1.6x10^{-9}$	38
$Ar_2^+ + H_2O \rightarrow H_2O^+ + Ar + Ar$	$2x10^{-9}$	38
$Ar_2^+ + CCl_4 \rightarrow CCl_3^+ + Ar + Ar$	$1x10^{-9}$	b
$Ar^+ + Cl^- \rightarrow Ar + Cl$	$1x10^{-7}$	32b
$Ar_2^+ + Cl^- \rightarrow Ar + Ar + Cl$	$1x10^{-7}$	32b
$Ar^+ + O^- \rightarrow Ar + O$	$1x10^{-7}$	32b
$Ar_2^+ + O^- \rightarrow Ar + Ar + O$	$1x10^{-7}$	b
$Ar_2^* + Ar_2^* \rightarrow Ar_2^+ + e + Ar + Ar$	$3x10^{-10}$	b
$Cl + HO_2 \rightarrow HCl + O_2$	$3x10^{-11}$	20
$CCl_4 + O(^1D) \rightarrow CCl_3 + ClO$	$3.54x10^{-10}$	20
$CCl_3 + OH \rightarrow HCl + COCl_2$	$1x10^{-11}$	b
$CCl_2 + O \rightarrow COCl + Cl$	$1x10^{-11}$	b
$CCl_2 + OH \rightarrow HCl + COCl$	$1x10^{-11}$	b
$CCl + O \rightarrow COCl$	$1x10^{-12}$	b
$CCl + O_2 \rightarrow COCl + O$	$2.9x10^{-12}$	30
$CCl + OH \rightarrow HCl + CO$	$4x10^{-11}$	b
$CCl + O \rightarrow ClO + C$	$1.380x10^{-10}exp(-16048/T)$	31
$COCl + Cl \rightarrow CO + Cl_2$	$2.16x10^{-9}exp(-1.670x10^3/T)$	30

$COCl + O_2 \rightarrow CO_2 + ClO$	$1x10^{-11}$	18[b]
$COCl + O \rightarrow CO + ClO$	$1x10^{-11}$	b
$Cl_2 + OH \rightarrow HOCl + Cl$	$1.7x10^{-12}exp(-900/T)$	31
$Ar^* + O_2 \rightarrow O(^1D) + O + Ar$	$2.1x10^{-10}$	33
$Ar^{**} + O_2 \rightarrow O(^1D) + O + Ar$	$2.1x10^{-10}$	33
$Ar^* + O_3 \rightarrow O(^1D) + O_2 + Ar$	$2.1x10^{-10}$	b
$Ar^{**} + O_3 \rightarrow O(^1D) + O_2 + Ar$	$2.1x10^{-10}$	b
$Ar^* + H_2O \rightarrow H + OH + Ar$	$2.1x10^{-10}$	33
$Ar^{**} + H_2O \rightarrow H + OH + Ar$	$2.1x10^{-10}$	33
$CH_2O + O \rightarrow HCO + OH$	$2.99x10^{-11}exp(-1543/T)$	31
$CH_2O + OH \rightarrow HCO + H_2O$	$1.600x10^{-11}exp(-110/T)$	31
$CH_2O + OH \rightarrow H + HCOOH$	$2x10^{-13}$	31
$CH_2O + H \rightarrow HCO + H_2$	$3.64x10^{-16}T^{1.77}exp(-1510/T)$	31
$CCl_4(v) + M \rightarrow CCl_4 + M$	$1.495x10^{-11}$	d
$CCl_4(v) + O \rightarrow ClO + CCl_3$	$4.98x10^{-13}exp(-2200/T)$ x $exp(771.962/T)$	30[b]
$CCl_4(v) + OH \rightarrow HOCl + CCl_3$	$1.00x10^{-12}exp(-2320/T)$ x $exp(771.962/T)$	30[b]
$HCOOH + OH \rightarrow H_2O + CO_2 + H$	$4.8x10^{-13}$	31
$H_2O^+ + CCl_4(v) \rightarrow CCl_3^+ + Cl + H_2O$	$1x10^{-9}$	b
$O2^+ + CCl_4(v) \rightarrow CCl_3^+ + Cl + O_2$	$1x10^{-9}$	b
$O^+ + CCl_4(v) \rightarrow CCl_3^+ + Cl + O$	$1x10^{-9}$	b
$Ar^+ + CCl_4(v) \rightarrow CCl_3^+ + Cl + Ar$	$1x10^{-9}$	b
$Ar^* + CCl_4(v) \rightarrow$	$1x10^{-10}$	b

$CCl_2 + Cl_2 + Ar$		
$Ar^{**} + CCl_4(v) \rightarrow CCl_2 + Cl_2 + Ar$	$1x10^{-10}$	b
$Ar_2^+ + CCl_4(v) \rightarrow CCl_3^+ + Ar + Ar$	$1x10^{-9}$	b
$CCl_4(v) + O(^1D) \rightarrow CCl_3 + ClO$	$3.54x10^{-10}$	b
$C_2Cl_4 + OH \rightarrow CHCl_2COCl + Cl$	$9.34x10^{-12}exp(-1212/T)$	18
$C_2Cl_4 + O \rightarrow COCl_2 + CCl_2$	$1.66x10^{-13}exp(-2525/T)$	18
$C_2Cl_4 + ClO \rightarrow CCl_3COCl + Cl$	$1.66x10^{-13}exp(-2525/T)$	18
$C_2Cl_4 + Cl \rightarrow C_2Cl_5$	$4.37x10^{+11}T^{-7.71} exp(-2.677x10^3/T)$	18
$C_2Cl_3 + Cl_2 \rightarrow C_2Cl_4 + Cl$	$4.17x10^{-12}exp(-1515/T)$	18
$C_2HCl_5 + Cl \rightarrow HCl + C_2Cl_5$	$3.31x10^{-12}exp(-1667/T)$	18
$C_2Cl_5 \rightarrow C_2Cl_4 + Cl$	$2.51x10^{+13}exp(-7800/T)$	31
$C_2HCl_5 + Cl \rightarrow Cl_2 + C_2HCl_4$	$1.66x10^{-11}exp(-8384/T)$	18
$C_2Cl_6 + Cl \rightarrow Cl_2 + C_2Cl_5$	$1.05x10^{-10}exp(-9242/T)$	18
$C_2HCl_2 + Cl \rightarrow C_2Cl_2 + HCl$	$1.2x10^{-8}T^{-0.97}exp(-959.6/T)$	18
$C_2HCl_2 + O_2 \rightarrow CHOCl + COCl$	$1.66x10^{-13}exp(-2525/T)$	18
$C_2Cl_3 + Cl \rightarrow C_2Cl_4$	$7.42x10^{9}T^{-7.21}exp(-2879/T)$	18
$C_2Cl_3 + Cl \rightarrow C_2Cl_2 + Cl_2$	$8.72x10^{-7}T^{-1.66}exp(-2576/T)$	30
$C_2Cl_3 + O_2 \rightarrow COCl_2 + COCl$	$1.66x10^{-13}exp(-2525/T)$	18
$C_2Cl_3 + O_2 \rightarrow C_2Cl_2O + ClO$	$5.25x10^{-13}exp(-2525/T)$	18
$C_2Cl_2O + Cl \rightarrow CO + CCl_3$	$1.66x10^{-11}$	18
$C_2Cl_3 + O \rightarrow CO + CCl_3$	$1.66x10^{-11}$	18
$C_2Cl_3 + ClO \rightarrow CO + CCl_4$	$1.66x10^{-11}$	18
$C_2HCl_4 + O_2 \rightarrow CHCl_2COCl + ClO$	$1.66x10^{-13}exp(-2525/T)$	18
$CHCl_2COCl + Cl \rightarrow CCl_2COCl + HCl$	$1.66x10^{-11}exp(-2525/T)$	18

$CHCl_2COCl + Cl \rightarrow CHCl_2CO + Cl_2$	$1.66x10^{-10}exp(-8889/T)$	18
$CCl_2COCl \rightarrow CO + CCl_3$	$1x10^{12}exp(-2525/T)$ *0.02	18[b]
$CHCl_2CO \rightarrow CHCl_2 + CO$	$5.25x10^{-11}exp(-6818/T)$	18
$C_2HCl_4 + Cl \rightarrow CHCl_2 + CCl_3$	$1.02x10^{-3}T^{-1.75}exp(-8333/T)$	18
$C_2Cl_5 + Cl \rightarrow CCl_3 + CCl_3$	$2.82x10^{3}T^{-4.01}exp(-6111/T)$	18
$C_2Cl_5 + Cl \rightarrow C2Cl_4 + Cl_2$	$6.61x10^{-9}$ exp(-603/T)	31
$C_2Cl_5 + O_2 \rightarrow CCl_3COCl + ClO$	$1.66x10^{-12}exp(-6061/T)$	18
$CCl_3COCl + Cl \rightarrow CCl_3CO + Cl_2$	$1.66x10^{-10}exp(-8889/T)$	18
$CCl_3CO \rightarrow CCl_3 + CO$	$3.16x10^{+13}exp(-4040/T)$ *0.02	18[b]
$C_2Cl_2 + O_2 \rightarrow COCl + COCl$	$1.66x10^{-13}exp(-2525/T)$	18
$C_2Cl_3 + M \rightarrow C_2Cl_2 + Cl + M$	$1.32x10^{-9}exp(-14140/T)$	18
$C_2Cl_2 + ClO \rightarrow CO + CCl_3$	$1.66x10^{-12}$	18
$C_2Cl_2 + OH \rightarrow CO + CHCl_2$	$1.66x10^{-12}$	18
$CHCl_3 + O \rightarrow COCl_2 + HCl$	$1.66x10^{-13}exp(-2020/T)$	18
$CHCl_3 + O \rightarrow CCl_3 + OH$	$4.79x10^{-12}exp(-2525/T)$	18
$CHCl_3 + Cl \rightarrow CHCl_2 + Cl_2$	$1.66x10^{-10}exp(-10610/T)$	18
$CHCl_3 + Cl \rightarrow CCl_3 + HCl$	$1.15x10^{-11}exp(-1667/T)$	18
$CCl_3 + O_2 \rightarrow COCl_2 + ClO$	$1.66x10^{-11}exp(-14140/T)$	18
$CCl_3 + Cl_2 \rightarrow CCl_4 + Cl$	$4.17x10^{-12}exp(-3030/T)$	18
$CCl_3 + CCl_3 \rightarrow C_2Cl_6$	$2.35x10^{12}T^{-7.48}$ exp(-3384/T)	18
$CCl_3 + CCl_3 \rightarrow C_2Cl_4 + Cl_2$	$3.72x10^{12}T^{-4.43}$ exp(-4545/T)	18
$CCl_3 + CHCl_2 \rightarrow C_2HCl_5$	$2.76x10^{10}T^{-6.79}$ exp(-3030/T)	18
$CCl_3 + CHCl_2 \rightarrow C_2Cl_4 + HCl$	$3.89x10^{-4}T^{-2.45}$ exp(-3232/T)	18

$CHCl_2 + O_2 \rightarrow CHOCl + ClO$	$1.66x10^{-11}exp(-14140/T)$	18
$CHCl_2 + O \rightarrow CHOCl + Cl$	$1.66x10^{-10}$	18
$CCl_2 + O_2 \rightarrow ClO + COCl$	$1.66x10^{-11}exp(-505.1/T)$ *0.02	18[b]
$CCl_2 + Cl_2 \rightarrow CCl_3 + Cl$	$8.33x10^{-12}exp(-1515/T)$	18
$CHOCl + M \rightarrow CO + HCl + M$	$1.66x10^{-7}exp(-20200/T)$	18
$CHOCl + Cl \rightarrow COCl + HCl$	$3.31x10^{-11}exp(-1515/T)$	18
$CCl_3 + C_2Cl_2 \rightarrow C_3Cl_5$	$5.25x10^{-13}exp(-2677/T)$	18
$C_3Cl_6 + Cl \rightarrow C_3Cl_5 + Cl_2$	$5.25x10^{-11}exp(-10100/T)$	18
$C_3Cl_7 \rightarrow C_3Cl_6 + Cl$	$1x10^{13}exp(-9394/T)$	18
$CCl_3 + C_2Cl_4 \rightarrow C_3Cl_7$	$5.25x10^{-13}exp(-2172/T)$	30
$C_2Cl_3 + C_2Cl_2 \rightarrow C_4Cl_5$	$1.05x10^{-12}exp(-2121/T)$	18
$C_2Cl_2 + C_4Cl_5 \rightarrow C_6Cl_7$	$3.31x10^{-12}exp(-2020/T)$	18
$C_6Cl_7 \rightarrow C_6Cl_6 + Cl$	$1x10^{+7}$	b
$C_4Cl_6 + Cl \rightarrow C_4Cl_5 + Cl_2$	$8.33x10^{-12}exp(-10100/T)$	18
$C_2Cl_3 + C2Cl_4 \rightarrow C_4Cl_7$	$3.02x10^{-13}exp(-2071/T)$	18
$C_4Cl_7 \rightarrow C_4Cl_6 + Cl$	$1x10^{13}exp(-9091/T)$	18
$C_4Cl_6 + C_2Cl_3 \rightarrow C_6Cl_8 + Cl$	$8.33x10^{-13}exp(-505.1/T)$	18
$C_6Cl_8 \rightarrow C_6Cl_6 + Cl_2$	$1x10^{+7}$	b
$ClO + CO \rightarrow CO_2 + Cl$	$1x10^{-12}exp(-3737/T)$	18
$COCl + M \rightarrow CO + Cl + M$	$3.31x10^{-10}exp(-3283/T)$	18
$COCl + H \rightarrow CO + HCl$	$1.66x10^{-10}$	18
$COCl + OH \rightarrow CO + HOCl$	$1.66x10^{-10}$	18
$COCl + O \rightarrow CO_2 + Cl$	$1.66x10^{-11}$	18
$H + Cl_2 \rightarrow HCl + Cl$	$1.41x10^{-10}exp(-606.1/T)$	18
$O + Cl_2 \rightarrow ClO + Cl$	$2.09x10^{-11}exp(-1414/T)$	19
$Cl + HO_2 \rightarrow OH + ClO$	$1.05x10^{-10}exp(-858.6/T)$	18

$H + HOCl \rightarrow HCl + OH$	$1.66x10^{-11}exp(-505.1/T)$	18
$ClOO + CO \rightarrow CO_2 + ClO$	$1.66x10^{-10}exp(-10100/T)$	18
$O + ClOO \rightarrow ClO + O_2$	$5.25x10^{-11}exp(-252.2/T)$	18
$COCl_2 + Cl \rightarrow COCl + Cl_2$	$5.25x10^{-11}T^{0.5}\ exp(-10100/T)$	18
$COCl_2 + OH \rightarrow COCl + HOCl$	$1.66x10^{-12}exp(-5051/T)$	18
$COCl_2 + H \rightarrow COCl + HCl$	$1.66x10^{-11}exp(-1010/T)$	18
$C_2Cl_4 + OH \rightarrow C_2Cl_3 + HOCl$	$1.66x10^{-11}exp(-6061/T)$	18
$C_2Cl_4 + OH \rightarrow CHCl_2 + COCl_2$	$1.66x10^{-11}exp(-1010/T)$	18
$C_2Cl_4 + ClO \rightarrow CCl_3 + COCl_2$	$1.66x10^{-11}exp(-1010/T)$	18
$C_2Cl_4 + Cl \rightarrow C_2Cl_3 + Cl_2$	$1.66x10^{-11}exp(-9091/T)$	18
$C_2Cl_3 + M \rightarrow C_2Cl_2 + Cl + M$	$8.31x10^{-9}exp(-14140/T)$	18
$C_2Cl_3 + O_2 \rightarrow COCl_2 + COCl$	$1.66x10^{-13}exp(-2525/T)$	18
$C_2Cl_2 + Cl \rightarrow C_2Cl + Cl_2$	$3.32x10^{-10}exp(-7576/T)$	18
$C_2Cl_2 + ClO \rightarrow C_2Cl + Cl_2O$	$1.66x10^{-10}exp(-20200/T)$	18
$C_2Cl_2 + OH \rightarrow C_2Cl + HOCl$	$1.66x10^{-10}exp(-5051/T)$	18
$C_2Cl + O_2 \rightarrow COCl + CO$	$1.66x10^{-11}exp(-2525/T)$	18
$CHCl + Cl_2 \rightarrow CHCl_2 + Cl$	$1.66x10^{-11}exp(-505.1/T)$	18
$CHCl + O_2 \rightarrow COCl + OH$	$1.66x10^{-11}exp(-505.1/T)$	18
$ClO + OH \rightarrow HCl + O_2$	$8.77x10^{-13}exp(173/T)$	30[b]
$COCl + ClO \rightarrow CO + Cl_2O$	$1.66x10^{-10}$	18
$COCl + ClO \rightarrow CO_2 + Cl_2$	$1.66x10^{-10}$	18
$H_2O_2 + Cl \rightarrow HO_2 + HCl$	$3.32x10^{-12}exp(-1010/T)$	30
$Cl_2O + O \rightarrow ClO + ClO$	$3.11x10^{-11}exp(-700/T)$	30
$Cl_2O + OH \rightarrow HOCl + ClO$	$6.5x10^{-12}$	30
$CHOCl + O \rightarrow OH + COCl$	$5x10^{-13}$	b
$CHCl_2COCl + O \rightarrow CCl_2COCl + OH$	$5x10^{-13}$	b

$CHCl_2COCl + O \rightarrow$ $CHCl + ClO + COCl$	$5x10^{-13}$	b
$CHOCl + O(^1D) \rightarrow OH + COCl$	$1x10^{-10}$	b
$CHCl_2COCl + O(^1D) \rightarrow$ $CCl_2COCl + OH$	$1x10^{-10}$	b
$CHCl_2COCl + O(^1D) \rightarrow$ $ClO + COCl + CHCl$	$1x10^{-10}$	b
$ClO + O_3 \rightarrow ClOO + O_2$	$1x10^{-12}exp(-4000/T)$	30
$CCl_3 + O_3 \rightarrow CCl_3O + O_2$	$5x10^{-13}$	b

a Rate coefficients have units of cm^3s^{-1}. Electron impact reactions without specific electron temperature dependencies are given for typical values of E/N.

b Estimated.

c Rate coefficients have units of s^{-1} for 1 body reaction, cm^3s^{-1} for 2 body reactions, and cm^6s^{-1} for 3 body reactions. Activation energies have equivalent units of K. T is the gas temperature. Two body reactions which do not have specific temperature dependencies were scaled by $(T/300)^{1/2}$ to account for changes in the reaction rate due to thermal speeds. Three body reactions were similarly scaled by $(T/300)^{-3/2}$.

d Estimated based on Lennard-Jones parameters. Value shown for T = 300K.

B.1 References

1. Y. Itikawa, M. Hayashi, A. Ichimura, K. Onda, K. Sakimoto, K. Takayanagi, M. Nakamura, H. Nishimura, and T. Takayanagi, "Cross Sections for Collisions of Electrons and Photons with Nitrogen Molecules" J. Phys. Chem. Ref. Data Reprint Number 299, **15** (3), 985 (1986).
2. A. V. Phelps, "Tabulations of Collision Cross Sections and Calculated Transport and Reaction Coefficients for Electron Collisions with O_2", JILA Information Center Report Number 28, University of Colorado, Boulder, CO (1985).
3. M. Hayashi, "Electron Collision Cross Sections for Molecules Determined from Beam and Swarm Data" Nagoya Institute of Technology, Gokiso-Cho, Showa-Ku, Nagoya, 466, Japan. Printed in "Swarm Studies and Inelastic Electron-Molecular Collisions" Eds. L. C. Pitchford, B. V. McKoy, A. Chutjian, and S. Tratmar. Proceedings of the Meeting of the 4th International Swarm Seminar and the Inelastic Electron-Molecular Collision Symposium, July 19-23, 1985. Tahoe City, CA. Springer-Verlag, N.Y. 1987.
4. J. C. Person and D. O. Ham, Radiat. Phys. Chem., **31**, 1 (1988).
5. B. R. Rowe, F. Vallée, J. L. Queffelec, J. C. Gomet, and M. Morlais, J. Phys. Chem. **88**, 845 (1988).
6. J. J. Lowke, A. V. Phelps, and B. W. Irwin, J. Appl. Phys. **44**, 4664 (1973).
7. K. Leiter, K.Stephan, E. Märk, and T. D. Märk, "Absolute Partial and Total Electron Ionization Cross Sections for CCl_4 from Threshold up to 180 eV", Plasma Chem. and Plasma Proc., **4** (4), 235 (1984).
8. K. Tachibana, Phys. Rev. A **34**, 1007 (1986).
9. D. Rapp and P. Englander-Golden, J. Chem. Phys. **43**, 1464 (1965).
10. M. Hayashi, "Recommended Values of Transport Cross Sections for Elastic Collision and Total Collision Cross Section for Electrons in Atomic and Molecular Gases", Nagoya Institute of Technology Report No. IPPJ-AM-19, 1991.

11. R. Atkinson, D. L. Baulch, R. A. Cox, R. F. Hampson, Jr., J. A. Kerr, and J. Troe, "Evaluated Kinetic and Photochemical Data for Atmospheric Chemistry: Supplement III", J. Phys. Chem, Ref. Data, 18, 881 (1989).
12. C. J. Howard, J. Chem. Phys. **71**, 2352 (1979).
13. W. B. DeMore, D. M. Golden, R. F. Hampson, C. J. Howard, M. J. Kurylo, M. J. Molina, A. R. Ravishankara, and S. P. Sander, "Chemical Kinetics and Photchemical Data for Use in Stratospheric Modeling: Evaluation Number 8", JPL Publication 87-41, Jet Propulsion Laboratory, California Institute of Technology, Pasadena, California (1987).
14. R. Atkinson, D. L. Baulch, R. A. Cox, R. F. Hampson, Jr., J. A. Kerr, and J. Troe, "Evaluated Kinetic and Photochemical Data for Atmospheric Chemistry: Supplement IV", J. Phys. Chem, Ref. Data, 21, 1125 (1992).
15. W. Tsang and R. F. Hampson, J. Phys. Chem. Ref. Data **15**, 1087 (1986).
16. I. M. Campbell and C. N. Gray, Chem. Phys. Lett. **18**, 607 (1973).
17. P. Borrell, C. J. Cobos, and K. Luther, J. Phys. Chem. **92**, 4377 (1988).
18. W. D. Chang and S. M. Senkan, Environ. Sci. Technol. **23**, 442 (1989).
19. W. D. Chang, S. B. Karra, and S. M. Senkan, Combust. Sci. Technol. **49**, 107 (1986).
20. R. T. Watson, J. Phys. Chem. Ref. Data **6**, 871 (1977).
21. M. R. Soto, M. Page, and M. L. McKee, Chem. Phys. **153**, 415 (1991).
22. J. Hjorth, J. Notholt, and G. Restelli, Int. J. Chem. Kin. **24**, 51 (1992).
23. N. Fujii, H. Miyama, M. Koshi, T. Asuba, Symp. (Int.) Combust., [Proc.] **18**, 873 (1981).
24. S. Mukkavilli, C. K. Lee, K.Varghese, and L. L. Tavlarides, IEEE Trans. Plasma Sci. **16**, 652 (1988).
25. R. Svensson and E. Ljungström, Int. J. Chem. Kin. **20**, 857 (1988).
26. H. Mätzing, Radiat. Phys. Chem. **33**, 81 (1989).

27. W. Hack, P. Rouveirolles, and H. G. Wagner, J. Phys. Chem. **90**, 2505 (1986).

28. R. K. Bera and R. J. Hanrahan, J. Appl. Phys. **62**, 2523 (1987).

29. A. Mellouki, G. Le Bras, and G. Poulet, J. Phys. Chem. **92**, 2229 (1988).

30. F. Westley, J. T. Herron, R. J. Cvetanovic, R. F. Hampson, and W. G. Mallard, NIST Chemical Kinetics Database, NIST Standard Reference Database 17. National Institute of Standards and Technology, Standard Reference Data Program, Gaithersburg, MD 20899.

31. W. G. Mallard, F. Westley, J. T. Herron, and R. F. Hampson, NIST Chemical Kinetics Database - Version 6.0, NIST Standard Reference Database 17. National Institute of Standards and Technology, NIST Standard Reference Data, Gaithersburg, MD (1994).

32. R. E. Olson, J. R. Peterson, and J. Moseley, J. Chem. Phys. **53**, 3391 (1970).

33. L. G. Piper, J. E. Velazco, D. W. Setser, J. Chem. Phys. **59**, 3323 (1973).

34. J. B. A. Mitchell, Phys. Rpts. **186**, 215 (1990).

35. C. Deutch, J. Appl. Phys. **44**, 1142 (1973).

36. F. Kannari, M. Obara, T. Fujioka, J. Appl. Phys. **57**, 4309 (1985).

37. L. G. Piper, J. Chem. Phys. **87**, 1625 (1987).

38. D. Albritton, At. Data. Nucl. Data Tables **22**, 8 (1978).